Open Research Online

The Open University's repository of research publications
and other research outputs

Ecological Impacts of Degassing From Masaya Volcano, Nicaragua

Thesis

How to cite:

Parkes, Bethan Rose Burson (2016). Ecological Impacts of Degassing From Masaya Volcano, Nicaragua. PhD thesis The Open University.

For guidance on citations see FAQs.

© 2016 The Author

https://creativecommons.org/licenses/by-nc-nd/4.0/

Version: Version of Record

Link(s) to article on publisher's website:
http://dx.doi.org/doi:10.21954/ou.ro.0000ef7a

Copyright and Moral Rights for the articles on this site are retained by the individual authors and/or other copyright owners. For more information on Open Research Online's data policy on reuse of materials please consult the policies page.

oro.open.ac.uk

The Open University

Ecological impacts of degassing from Masaya volcano, Nicaragua

A thesis submitted for the degree of Doctor of Philosophy

Bethan R B Parkes
BA (University of Cambridge)

Department of Environment, Earth and Ecosystems,
The Open University,
United Kingdom

DATE OF SUBMISSION: 30 September 2015
DATE OF AWARD: 17 MARCH 2016

ProQuest Number: 13834774

All rights reserved

INFORMATION TO ALL USERS
The quality of this reproduction is dependent upon the quality of the copy submitted.

In the unlikely event that the author did not send a complete manuscript
and there are missing pages, these will be noted. Also, if material had to be removed,
a note will indicate the deletion.

ProQuest 13834774

Published by ProQuest LLC (2019). Copyright of the Dissertation is held by the Author.

All rights reserved.
This work is protected against unauthorized copying under Title 17, United States Code
Microform Edition © ProQuest LLC.

ProQuest LLC.
789 East Eisenhower Parkway
P.O. Box 1346
Ann Arbor, MI 48106 – 1346

Abstract

Persistent degassing is an unusual type of volcanic activity with considerable environmental impacts, although its effects on downwind ecosystems are poorly researched. Up to 1000 tonnes of SO_2 per day are degassed from Masaya Volcano in Nicaragua, and trade winds blow the plume in a WSW direction. A cross-wind transect through this plume provides a natural laboratory for this study on volcanic gases and their impacts on the tropical dry forest.

Measurements of gas concentration and deposition rates of SO_2, HCl and HF along the transect were described by Gaussian profiles. These were linked to gas emission at the crater and the wind direction estimated from the HYSPLIT model. SO_2 concentration profiles were used to investigate the ecological response to exposure to the volcanic plume along the same transect at two scales: the vegetation community and individual plant traits.

The plant community level study found high levels of volcanic SO_2 were associated with low species richness, comprising mostly grasses and herbs, an acidic soil, an open canopy and a thin leaf litter layer. Local feedbacks with these environmental variables have likely slowed succession in this area, indicating long-term impacts of volcanic degassing.

At the species level, *Dalechampia scandens* response to SO_2 was surprising; its largest leaves were found where volcanic pollution was highest. Elevated H_2O, CO_2 or nutrient levels from the plume may have benefited these tolerant plants. Compared with vegetation composition, this likely shows a more short-term response to volcanic gas levels.

As well as informing ecological studies, fitting Gaussian profiles to volcanic gas data has validated our understanding of plume dispersal. The first evidence of vegetation community and plant trait response to volcanic gases presented here may give useful insights into the impacts of other degassing volcanoes or future industrial pollution in the tropics.

Acknowledgements

Firstly, I'd like to thank my supervisors Michael Gillman, Steve Blake and Hazel Rymer for everything they have done for me the past three years- from helping shape this thesis, to being great company on fieldwork and giving me the opportunities to do so much alongside my PhD.

Thanks to Hilary Erenler for all the help and company on field trips and for sharing initial results from her observations of *Dalechampia scandens* and suggesting this would be interesting to study, particularly if paired with volcanic gas measurements.

Thanks to everyone in Nicaragua who helped make fieldwork possible and fun. In particular Carlos and family for their brilliant hospitality and Sergio for driving me everywhere and helping me to navigate Nicaraguan bureaucracy! Thanks to all the people at Parque Nacional Volcan Masaya, in particular Nelson, Erico, Julio, Carlos and Carlos who were a real help with identifying plants. Thanks also to Earthwatch for funding field trips and providing enthusiastic volunteers!

Thanks to everyone in the EGL laboratories, who have always dropped what they were doing to help me find equipment I needed and helped my find the best methods. In particular, a special thanks to Emily who was great at analysing all my sulfation plates and keeping me safe in the lab, and Graham who was always helpful and enthusiastic about my project.

Thanks to Vince Gauci and Saskia van Manen, who although are no longer my supervisors, have both helped me out along the way.

Thanks to everyone else at the OU who has helped to make my time here fun- particularly my lovely office mates and the football, relay and cricket teams which provided welcome breaks from the computer screen!

Finally, I must also thank all my family and friends who have supported me through this. Of course my parents for always wanting to understand what I am up to and to my wonderful husband Tom for making sure I don't get stressed doing it!

Contents

List of Figures

List of Tables

Chapter 1

Introduction

1.1 Volcanoes in the environment

Volcanic emissions are incredibly varied in terms of their composition (e.g. lava, ash, gas) and their spatial and temporal characteristics. Consequently, the environmental impacts of volcanic activity are wide ranging. Lava flows are totally destructive to the area around a volcano, resulting in primary succession (Chevennement, 1990; Bashan *et al.* , 2002; Cutler, 2009; Munguía, 2013). Some plants and the seed bank may survive ash eruptions, including ash clouds and pyroclastic flows, allowing for a faster recovery period (Whittaker *et al.* , 1989; Tsuyuzaki & Del Moral, 1995; Thornton, 1996; Marler & Moral, 2013; Chang & del Moral, 2015). Both of these types of activity are typically considered as discrete events, with local to regional impacts. Volcanic gases can be emitted alongside eruptions of ash and lava, or degassing may occur by itself.

Global and regional impacts of volcanic gases released during large explosive eruptions that reach the stratosphere are well quantified. These are associated with feedbacks with the climate system, as a result of sulfate aerosols in the stratosphere reducing incoming solar radiation (Briffa *et al.* , 1998; Robock, 2000). This causes global cooling and has led to crop failures (Post, 1977). Persistent volcanic degassing is a special type of volcanic activity, because it is a continuous (albeit variable) state, rather than a discrete event, and is associated with strong localized impacts. Unlike large ex-

plosive volcanic eruptions, emissions from persistently degassing volcanoes typically stay within the troposphere, so their impacts are different.

1.2 Volcanic degassing

Volcanoes are estimated to contribute 13 Tg per year of SO_2 to the atmosphere (Andres & Kasgnoc, 1998), including both persistent degassing and explosive eruptions. Persistently degassing volcanoes discharge large amounts of gas from a free magma surface exposed to the atmosphere (Figure 1.1). The rate of emission is sufficient to sustain a gas plume. This plume is typically ash-free and persistently degassing volcanoes infrequently erupt lava or ash. Gases emitted include H_2O, CO_2, SO_2, HCl and HF (Table 1.1). Since H_2O and CO_2 have high and variable atmospheric background levels, volcanic gas emissions are typically quantified in terms of SO_2. Some persistently degassing volcanoes, whose emissions can reach hundreds to thousands of tonnes per day (Table 1.2), have been particularly well monitored, including Masaya (Delmelle *et al.* , 2001, 2002; Martin *et al.* , 2010) and Etna (Bellomo *et al.* , 2007; Floor *et al.* , 2011).

Figure 1.1: Dispersion of gases from Masaya's Santiago crater. Photograph taken looking North towards Masaya volcano on the right, and the gas plume blowing in a SW direction to the left. Taken on the 26th of February 2014.

Gas	mo %
H_2O	94.26
CO_2	3.25
SO_2	1.43
HCl	0.85
HF	0.19

Table 1.1: Molar percentages of the five principal emissions from Masaya volcano in 1999 (Burton *et al.* , 2000)

Volcano	SO_2 flux ($T\ day^{-1}$)
Etna, Italy	4000
Bagana, PNG	3300
Lascar, Chile	2400
Ruiz, Colombia	1900
Sakurajima, Japan	1900
Manam, PNG	920
Yasur, Vanuatu	900
Kilauea, Hawaii	800
Masaya, Nicaragua	790
Stromboli, Italy	730

Table 1.2: Ten degassing volcanoes and their estimated fluxes, from Andres & Kasgnoc (1998). These represent an average flux, typically over a short time period of measurement, and there may be considerable fluctuations on long and short time-scales.

1.2.1 Ecological and environmental impacts

Persistently degassing volcanoes are, therefore, potent sources of pollutant gases into the troposphere with potential for considerable environmental impacts. Volcanic gas plumes are known to acidify the downwind environment, through emissions of SO_2, HCl and HF (Johnson & Parnell, 1986; Delmelle *et al.* , 2002; Bellomo *et al.* , 2007; Kamijo *et al.* , 2008; Floor *et al.* , 2011). Plants are damaged by these acidic emissions which cause leaf necrosis and chlorosis (Wahid, 2006; Nelson & Sewake, 2008). Satellite imagery, including studies using the Normalized Difference Vegetation Index (NDVI), show significant damage to vegetation (Nadeau, 2004). At the community scale, volcanic emissions are associated with a decline in species richness and vegetation cover (Kamijo & Hashiba, 2003; Kamijo *et al.* , 2008; Ting & Poulsen, 2009). Most pronounced is the decline in trees, but this can allow for an expansion of herbaceous plants and grasses (Kamijo *et al.* , 2008). This is because the death or defoliation of trees allows for more light to penetrate to the understory, and this reduces competition for resources for herbs and grasses.

There are potentially competing effects of different mixtures of volcanic gases on the health of an individual plant. The principal constituents of volcanic emissions are H_2O and CO_2, both of which are the key components of photosynthesis and, therefore, vital to plant growth (Abrams, 2011; Jenkins, 2012; McElrone *et al.* , 2013). A study on photosynthesis in *Gunnera insignisis* at Turrialba, a degassing volcano in Costa Rica, suggested that high levels of volcanic CO_2 was able to counteract the negative effects of exposure to SO_2 (Jenkins, 2012). Heavy and trace metals are also emitted by degassing volcanoes and can damage plants. However, their concentrations in plants growing near degassing volcanoes do not typically exceed phytotoxic levels and are, therefore, unlikely to have significant direct implications for plants or their consumers (Grasso *et al.* , 1999; Martin *et al.* , 2009b, 2010; Burson, 2012; van Manen, 2014b).

Some species growing downwind of Masaya are able to neutralise volcanic acid rain caused by degassing using leaf cation exchange (Johnson & Parnell, 1986). How-

ever, functional parts of a plant might respond differently to volcanic gas emissions (Abe *et al.* , 2014). For example, leaf health might not be affected by exposure to volcanic gases, but reproductive success might be decreased. Volcanic emissions are likely to have an overall negative ecological impact, though they may benefit tolerant plants in some ways.

1.3 Industrial pollution

The effects of industrial air pollution on downwind vegetation have been well studied, and these pollutants can provide a useful analogue for volcanic gases. Industrial pollutants principally consist of sulphur (S), nitrogen (N) and ozone based compounds, but may also include heavy metals. S is a key component of volcanic emissions, but chlorine (Cl) and fluorine (F) which are also released from degassing volcanoes (D'Alessandro *et al.* , 2008; Aiuppa *et al.* , 2009), are less associated with industrial pollution (Evans *et al.* , 2011). There is some evidence for volcanic N emissions in the form of HNO_3 (Mather *et al.* , 2004), but these are not as significant as S. Volcanic S, Cl and F are also known for their acidifying effects on the local environment, which is a common consequence of industrial air pollution. Acidification affects terrestrial ecosystems directly as well as through the responses of soils and their microbes (Singh & Agrawal, 2008). Whilst industrial emission rates can be significantly higher than those of volcanic degassing, it is important to remember that volcanic degassing cannot be controlled, so potentially represents a long-term pollutant source. Insights from industrial pollution literature are likely to prove useful in developing an understanding of how volcanic gases might affect local ecosystems, even if there are variations in pollutant composition.

Like volcanic degassing, high levels of industrial SO_2 pollution is linked to decreased species richness and a decline in tree cover supporting the expansion of understory species, including herbs and grasses. Many other industrial pollutants such as nitrogen and ozone have been shown to modify plant communities (Fuhrer *et al.* ,

1997; Bobbink *et al.* , 1998; Stevens *et al.* , 2004; Payne *et al.* , 2011, 2013; Dirnbock *et al.* , 2014). Pollution can, therefore, affect vegetation cover, the number of species and their composition.

The effect of industrial pollutants is well studied for northern hemisphere ecosystems, such as boreal forest (Vávrová *et al.* , 2009). However, at lower latitudes where climatic conditions differ and there are different limiting factors, the impacts of pollution (volcanic or industrial) are less well known (Delmelle *et al.* , 2001). Therefore, the results from this thesis might also be useful for informing predictions of the potential ecological impact of industrial pollution in the tropics.

1.4 Introduction to Masaya Volcano, Nicaragua

In 1979, Nicaragua's first national park *Parque Nacional Volcán Masaya* was formed. It is located approximately 20-25 km south of Managua (Figure 1.2), and lies to the west of the town of Masaya (Figure 1.5). The summit elevation of Masaya volcano is 635 m a.s.l.. Average annual temperatures range from 20 to 28°C and there is 1500 mm of rain per year, mostly during the wet season which runs from May to October (Wermundsen, 1999).

1.4.1 Geological setting

Masaya Volcano is a part of the Central American Volcanic Front (CAVF), which stretches from Guatemala (Tacaná) in the North to Panama (La Yeguada) in the South. This chain is a result of the subduction of the Cocos and Nazca Plates underneath the Caribbean Plate (Carr, 1984). The geological history of Masaya has been well documented by Walker *et al.* (1993), and the large caldera (6 $\times$ 11.5 km) is thought to have been formed by a series of explosive basaltic eruptions (Williams, 1983). Masaya has a low shield volcano shape, unlike the characteristic composite cone shape of many other Nicaragua volcanoes.

Historical records mention the existence of a lava lake within Nindiri crater (Figure 1.3), which produced a lava flow in 1670 (McBirney, 1956). More recently, there was a lava flow from the flanks of the San Fernando crater (Figure 1.3) in 1772. Between 1850 and 1859, a large subsidence event formed the currently active Santiago Crater (Figure 1.3). Since then, there have been many degassing crises lasting years to decades, coupled with occasional very small ash eruptions (McBirney, 1956; Stoiber *et al.*, 1986; Walker *et al.*, 1993; Rymer *et al.*, 1998). Incandescence from the magma can be frequently seen in the Santiago crater.

Dates	Reference
1850-1859	1
1902-1906	1
1919-1927	1
1946-1959	1,2
1979-1988	2,3,4
1993-present	4,5,6

Table 1.3: Dates of recorded degassing crises at Masaya, adapted from Horrocks (2001). 1: McBirney (1956), 2: Stoiber *et al.* (1986), 3: Walker *et al.* (1993), 4: Rymer *et al.* (1998), 5: Delmelle *et al.* (1999), 6: Martin *et al.* (2012).

1.4.2 Recent activity at Masaya Volcano

Masaya is a degassing volcano characterized by periodic phases of degassing that last years to decades, with the latest starting in 1993 and continuing to the present day (Table 1.3). The regional trade winds are north-easterly, blowing the plume to the south-west. The downwind area is polluted with volcanic gases, including SO_2, HCl and HF (Delmelle *et al.* , 2001). The plume also carries water and carbon dioxide, as well as volcanogenic heavy metals and trace elements (Horrocks, 2001; Martin *et al.* , 2010). There have been very infrequent ash eruptions from the Santiago Crater, which might also have temporarily added ash particles to the volcanic plume of gases.

Gas emissions from Masaya have been well studied, with the first measurements of volcanic SO_2 made by Stoiber *et al.* (1986) using COSPEC (Correlation Spectrometer), a UV spectroscopy technique. This has since been advanced and a new instrument, named FLYSPEC, is currently used to measure volcanic SO_2 at Masaya (Horton *et al.* , 2005; Williams-Jones *et al.* , 2005; Nadeau, 2004) as well as a DOAS, Differential Optical Absorption Spectroscopy, (Mather *et al.* , 2006). Other studies have used similar remote sensing techniques, such as open-path Fourier Transform Infrared spectroscopy (Horrocks, 2001), allowing for the measurement of a wider range of gases, including CO_2, H_2O, HCl and HF. Others have directly quantified gas emissions from Masaya using diffusion tubes (Allen, 2002), sulfation plates (Delmelle *et al.* , 2001, 2002) and direct measurement of aerosols have been made using impactors (Mather *et al.* , 2003;

Martin *et al.* , 2012) and filter packs (Mather *et al.* , 2006; Martin *et al.* , 2009a).

The degassing history of Masaya is well-studied compared with other volcanoes, making it a good candidate location for the study of the ecological impacts of volcanic degassing.

1.4.3 Environmental impacts

The ambient SO_2 concentrations downwind of Masaya regularly exceed the WHO health recommendations of above 500 μg m^{-3} for periods of more than 10 minutes, or above 20 μg m^{-3} over a 24 hour period (Delmelle *et al.* , 2002; WHO, 2011; van Manen, 2014a). S, as well as Cl and F compounds are dry-deposited on the local downwind environment (Delmelle *et al.* , 2001, 2002). During the wet season, these gases mix with moisture in the atmosphere and produce acid rain (Johnson & Parnell, 1986). Both dry and wet deposition of these volcanic plume constituents are known to acidify the soil (Delmelle *et al.* , 2003). Downwind of Masaya, volcanic andosols have the capacity to sequester aluminum-hydroxy- sulfate minerals, which reduces to some extent the impacts of acidification (Delfosse *et al.* , 2005).

1.4.4 Ecological setting

The climax community at Masaya is tropical dry forest. This is a forest ecosystem found at tropical and sub-tropical latitudes where rainfall is seasonal and there is a dry period of no or little rainfall, during which many plant species lose their leaves. Tropical dry forest is an endangered ecosystem in Central America and only 0.1% of its original extent remains (Gillespie & Walter, 2001). Tropical dry forests are a biodiversity hotspot and so are priorities for conservation (Myers *et al.* , 2000).

Secondary tropical dry forest succession is well studied in response to both human disturbances (e.g. forest cutting for cultivation- Hartter *et al.* (2008); Williams-Linera *et al.* (2010), grazing- Larkin *et al.* (2012), invasive species- Johnson & Wedin (1997)) and natural disturbances (e.g. landslide- Shiels & Walker (2003); Velázquez

& Gómez-Sal (2009), hurricane- Willig *et al.* (2011)). Recovery or regeneration from these types of disturbances can be observed on relatively short timescales (years to decades). However, processes and patterns in primary succession of tropical dry forest, which take much longer due to the requirement of soil formation, are less well understood. There are no studies of the ecological impacts of volcanic degassing on any tropical dry forest ecosystems.

Masaya Volcano National Park is very dry and has lower plant species richness compared with other dry forest reserves in Costa Rica and Nicaragua (Gillespie & Walter, 2001). As a result of volcanic activity, there are a variety of habitats covering different successional stages. This ranges from two recent lava flows emplaced in 1772 and 1670 CE that are barely colonized (lichens and ferns, with some pioneer trees becoming established e.g. *Plumeria rubra*) to parts of the park that appear to have reached a tropical dry forest climax community. Additionally, although not permitted outside of the designated agricultural area, grazing by local farmers livestock and firewood removal are not uncommon. Like other dry forests, Masaya is also vulnerable to natural disturbances such as fire. This means that although a large area of the park is forested, very little of it can be defined as primary forest.

1.4.5 Ecological impacts of degassing from Masaya

Due to volcanic activity in the early 1950s, coffee plantations several kilometres downwind of the volcano became infertile (McBirney, 1956). Significant damage to plants and crops has also been observed since 1993, the beginning of the latest degassing period (Delmelle *et al.* , 2001, 2002). Normalized Difference Vegetation Index (NDVI) imagery of the volcano and its surroundings shows areas of high vegetation damage within the first few kilometres downwind of the active vent (Nadeau, 2004), which is also evident on Google Earth satellite imagery (Figure 1.3).

High accumulations of major and trace elements have been found in grasses growing downwind of degassing volcanoes, including Masaya (Martin *et al.* , 2010) and

Turrialba (Burson, 2012). Whilst these have been shown to act as useful tracers of volcanic emissions, they do not typically reach phytotoxic levels for the plants. Additionally, a study of cultivated foods growing downwind of Masaya, including pineapple and pitaya, found heavy metal concentrations did not exceed the threshold for human consumption (van Manen, 2014a). This suggests that it is acid species such as SO_2, HCl and HF, which are released in much larger quantities, that are responsible for the most damage to vegetation. These acid species are known to directly damage leaves for example, through necrosis and chlorosis (Nelson & Sewake, 2008).

However, there is evidence that some plants, *Melanthera* sp. and *Lantana* sp. (Johnson & Parnell, 1986), have the capacity to neutralize acid rain allowing them to persist in the most affected areas. Additionally, despite the influence of the volcano, Pacific Parakeets have been observed inhabiting the crater (Wermundsen, 1999) and solitary bees nest in the ash at the crater edge where volcanic gas concentrations are extremely high (H. Erenler, pers. comm., 21 November 2013). However, to date there has been no research into how volcanic degassing is affecting plant communities downwind of the volcano. Additionally, at the plant scale it is not known how plant growth and traits respond to exposure to volcanic gases.

Figure 1.2: Map of Central America showing the location of Masaya Volcano National Park marked with a green dot. The capital of Nicaragua, Managua, is marked with a red dot

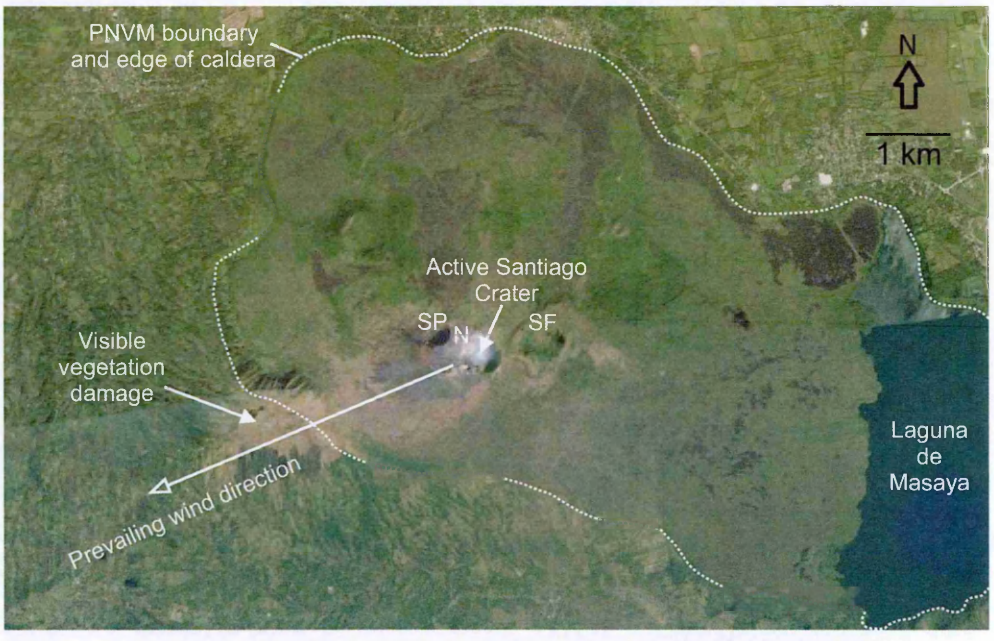

Figure 1.3: Google Earth satellite imagery of the area surrounding Masaya Volcano from the 29th March 2014 and the 8th December 2014. An area of damaged vegetation is evident to the SW of the active crater. SP= San Pedro Crater, N= Nindiri Crater and SF= San Fernando Crater.

Figure 1.4: Plume of gases emerging from Santiago Crater

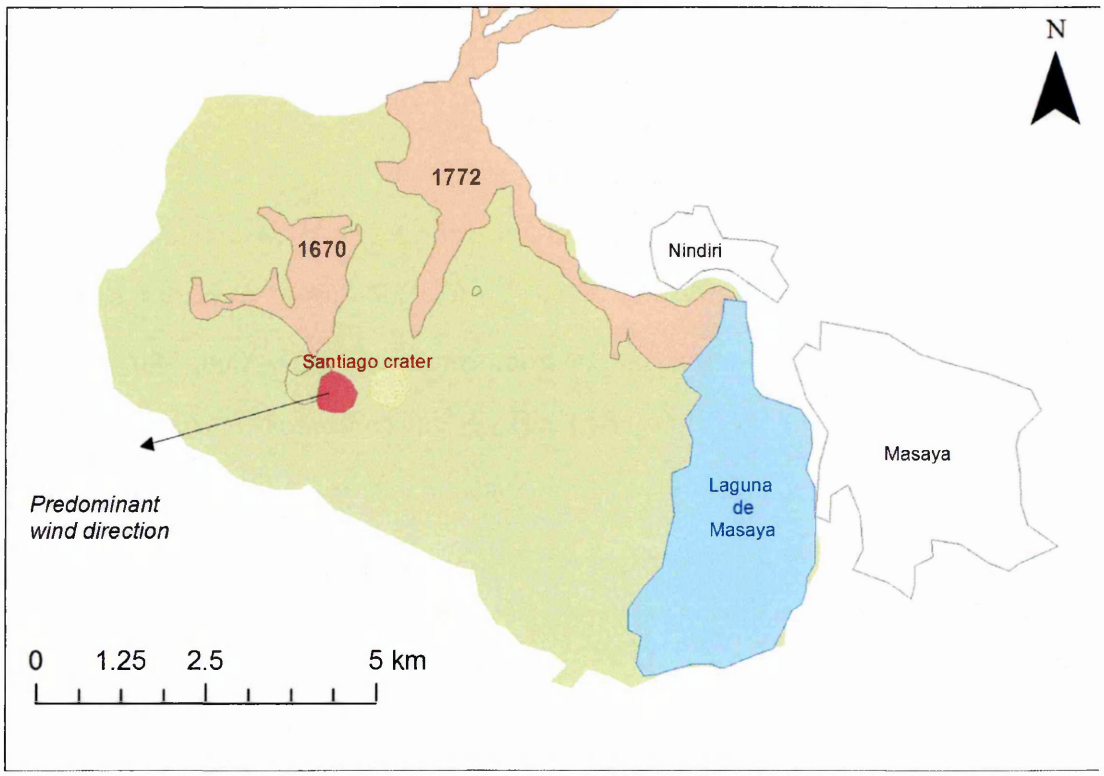

Figure 1.5: Map of Masaya Volcano National Park (PNVM). The active Santiago Crater is marked in red, and the predominant wind direction is shown with an arrow. The two most recent lava flows (in 1670 and 1772, which extends beyond the park boundary) are shown, as is the lava flow underlying the main sampling area, named Chocoyos. Nearby towns of Masaya and Nindiri are also marked, as is the lake, Laguna de Masaya.

1.5 Thesis outline

Persistent volcanic plumes provide natural laboratories for studying the environmental and ecological effects of gas fumigation and acid deposition. Downwind and crosswind variation in gas concentrations and deposition rates produce a strong and short gradient along which ecological and environmental data can be collected. Persistent degassing from Masaya Volcano in Nicaragua has been recorded for several decades, making it an ideal candidate for a study of the long-term ecological and environmental impacts. Additionally, it is situated in a well-populated area, making it both easy to access and of relevance for the health and livelihoods of local people.

The focus of this thesis is a cross-wind transect, several kilometres downwind of the actively degassing Santiago Crater at Masaya Volcano, where data were collected on volcanic gases and ecological and environmental variables. Along this transect, measurements of ground level SO_2, HCl and HF gas concentrations and deposition rates were used to characterize the pollution load and exposure to the volcanic plume. These measurements covered a large area across five different sampling periods. This combination of spatial and temporal detail has not yet been previously studied downwind of Masaya.

Gas concentrations along a cross-wind transect are expected to follow a Gaussian distribution. Fitting a Gaussian model to gas concentration and deposition rate data would allow for the plume profile to be characterized in terms of its centreline, width and peak concentration. These data revealed variations through time in the composition and dispersal of volcanic gases from Masaya, demonstrating the relevance of volcanic and meteorological factors in influencing the downwind distribution of volcanic gases and their deposition. Additionally, using a Gaussian model to describe the cross-wind distribution of volcanic gases would allow for estimated volcanic gas levels at any point along the transect, where measurements were not taken. This was applied in the following chapters, where is was possible to estimate SO_2 concentrations where ecological data were collected along the transect.

Results from the Gaussian fit were taken at sites where ecological (plant community) and environmental (soil pH, EC, leaf litter layer depth and canopy cover) data were collected. The variation in these ecological and environmental data were linked to the gradient of exposure to volcanic gases. This provides the first study of the impact of volcanic degassing alone on plant community composition. Additionally, it contributes to the small body of literature on the effects of environmental disturbance on tropical dry forest ecosystems, and might help inform predictions of the ecological impacts of industrial pollution in tropical regions.

To complement the plant community data, the trait response of individual species was also studied, providing the first evidence of plant morphological response to volcanic degassing. The response of *Dalechampia scandens* leaf and blossom traits to variation in exposure to volcanic gases was tested, and compared to a second species with a similar distribution, *Byrsonima crassifolia*. Additionally, this provides the first field evidence for the Berg Hypothesis using *D. scandens*. This species is known from greenhouse studies to have a strong response in leaf traits, but not blossom traits, to variation in environmental conditions.

The diversity of responses at the plant scale to volcanic gases can be linked to the variation in plant community composition along the transect. Additionally, plant trait data provide a contrasting assessment of the ecological response to volcanic gases to a study at the plant community level. Plant traits are likely to respond more rapidly to short term variations in volcanic gas levels, whereas the plant community likely represents the long term impacts of volcanic degassing.

1.5.1 Aims

The aims of this thesis are to answer the following questions:

- Volcanic gas concentrations and their deposition rates downwind of Masaya
  - What are the atmospheric concentrations and deposition rates of volcanic SO_2, HCl and HF along a cross-wind transect downwind of Masaya, and can they be described using a Gaussian model?
  - Is there any temporal variation in these gas concentrations and deposition rates?
  - Can this be attributed to variation in volcanic degassing levels or in meteorological conditions for dispersal of the gas plume?
- Plant communities downwind of Masaya
  - How does the exposure gradient affect some environmental variables along the transect?
  - How does this gradient affect plant species richness and composition?
  - What evidence is there for ecological feedbacks in response to volcanic gases?
- *Dalechampia scandens* response to volcanic gases
  - Is there evidence in support of the Berg Hypothesis using *Dalechampia scandens* in a field setting?
  - Does volcanic degassing produce unfavourable conditions for *Dalechampia scandens* growth?
  - Does another plant, *Byrsonima crassifolia* respond in the same way as *Dalechampia scandens*?

1.5.2 Structure

The aims of this thesis, as described above, will be addressed in Chapters 2-4. A cross-wind transect that represents an environmental gradient in exposure to the plume forms the basis for the data presented in these chapters. Chapter 2 contains the data collected on volcanic gas concentrations and deposition rates along the transect, collected over five sampling periods. This data is discussed in the context of changing emissions from Masaya volcano and variation in meteorological conditions for dispersal of the gas plume. Chapters 3 and 4 use the gradient produced by volcanic degassing along this transect to identify the ecological response. The plant community response along this environmental gradient is the subject of Chapter 3. This chapter also includes a discussion of ecological feedback mechanisms that might also influence the plant species composition along the transect. Chapter 4 focuses on the plant scale response, and tests the Berg Hypothesis in a field setting using the response of *Dalechampia scandens* to this gradient.

Chapter 2

Volcanic gas concentrations and deposition rates downwind of Masaya

Results from diffusion tubes and sulfation plates that were deployed along a cross-wind transect during five sampling periods are presented alongside meteorological data obtained from the HYSPLIT model. It will be shown that both volcanic degassing and meteorological conditions play an important role in determining downwind atmospheric pollutant concentrations and their deposition rates.

2.1 Introduction

Degassing volcanoes release a range of gases including H_2O, CO_2, SO_2, HCl and HF. Although most volcanic emissions are made up of H_2O and CO_2, detecting these is more difficult because their background levels are high and variable (Oppenheimer, 2003). Therefore, volcanic gas plumes are typically monitored in terms of the amount of SO_2, the next most abundant gas. SO_2, is of particular interest because it can have significant impacts on the nearby environment and human populations. Similarly, HCL and HF are also acid gases that can produce considerable impacts so are often used as tracers for volcanic emissions. Away from industrialized areas, SO_2, HCl and HF typically have a negligible background concentration. Therefore, a study of the distribution of volcanic gas concentrations in the atmosphere and the rate of their deposition onto the surrounding environment would be useful in determining an exposure gradient to the volcanic plume.

In order to better understand the distribution of the atmospheric concentrations of these gases around a volcano, two important factors must be considered: the emission rate of these gases from the volcano and the meteorological conditions for the dispersal of and deposition from the resulting volcanic plume. The deposition rate is calculated by:

$$D = V * C \tag{2.1}$$

where D, the deposition rate of a gas, is a product of the deposition velocity for that gas (V) and its atmospheric concentration at the same location (C). Therefore, the deposition rate will also depend on the factors influencing gas concentration, as well as the deposition velocity of the gas, which is determined by the properties of the gas, meteorological conditions and the type of surface it is being deposited on. Under high deposition velocities, more gas is transferred to the environment, thus reducing its concentration in the atmosphere.

The emission rate from a volcano may vary on both short and long time-scales.

Masaya is known for having cycles of degassing activity (McBirney, 1956; Johnson & Parnell, 1986; Horrocks, 2001; Williams-Jones *et al.* , 2003), with large changes in emission rates of SO_2 and other gases over time-scales of decades. Gas emissions are also variable on hourly and daily time-scales (Stoiber *et al.* , 1986; Nadeau, 2004). Additionally, there may also be small changes in the composition of emissions, i.e. ratios between the different gas constituents, which is often used to forecast eruptions or changes in a volcano's behaviour (Burton *et al.* , 2000; Horrocks, 2001; Mather *et al.* , 2006).

The dispersal of a volcanic plume, once it has been emitted, is controlled primarily by meteorological factors. The wind velocity, i.e. its speed and direction, will determine the area most affected by the volcanic plume (Vallero, 2007). Additionally, atmospheric stratification will also control the height of the plume, and therefore the extent to which the ground is fumigated (Delmelle *et al.* , 2001). Under 'ideal' atmospheric conditions, the dispersal of a volcanic (or other pollutant) plume is expected to follow a Gaussian distribution in both the horizontal (x) and vertical axes (z), (Vallero, 2007) and this spread grows downwind, diluting the plume. Data collected along a cross section through urban, industrial and volcanic plumes have demonstrated that a Gaussian model can provide an appropriate fit to the dispersal of gases and their deposition (Weil & Jepsen, 1977; Harrison & McCartney, 1980; Mehdizadeh & Rifai, 2004; Martin *et al.* , 2010).

Meteorological factors also play an important role in modifying a volcanic plume's composition. Changes to the plume may arise from chemical processes such as the oxidization of sulfur dioxide to sulfuric acid, which is dependant on the presence of cloud water and high humidity (Langmann *et al.* , 2009). Additionally, both wet and dry deposition will change the plume composition, and the rate of these is controlled by atmospheric conditions such as humidity, temperature and wind speed. Deposition velocities vary between chemical species depending on size characteristics; larger particles will be sedimented out more rapidly, whilst finer particles will have a longer atmospheric residence time and will be deposited further downwind.

At a small spatial scale, downwind gas concentrations and deposition rates are locally controlled by geographical factors such as topography and the presence of vegetation which might cause mechanical turbulence. Meteorological conditions for deposition, as well as dispersal, change through seasons and days (Langmann *et al.* , 2009) therefore, the importance of wet and dry deposition is likely to be both spatially and temporally variable. It is both dry and wet deposition mechanisms that are responsible for the deposition of acid species (including S, Cl and F), which have significant impacts on ecosystems (Singh & Agrawal, 2008). Since there are potentially large variations through time in gas emission rates from a volcano, as well as meteorological conditions for the dispersal, this is an important consideration for the methodology of this study. This is of particular significance when considering the environmental and ecological impacts, as these will respond to long term variation in exposure to volcanic emissions.

Previous studies on the spatial distribution of volcanic or industrial gases typically use passive sampling devices such as diffusion tubes or sulphation plates. Since these are small, inexpensive and do not require power they are particularly useful tools for assessing spatial variability as a large number can be deployed over a large area (Nash & Leith, 2010). Other methods for measuring such gases such as spectroscopy provide more precise measurements through time for a given location (Williams-Jones *et al.* , 2005). However, these provide an indication of the variation in emission rate only with less information on the potential dispersal of the plume. For the purposes of the study, which considers the environmental and ecological impacts in later chapters, passive samplers which allow for a large spatial coverage are more appropriate. Diffusion tubes (Delmelle *et al.* , 2001; Allen, 2002; Delmelle *et al.* , 2002; Bellomo *et al.* , 2007; Staszewski *et al.* , 2011; Godoi *et al.* , 2013; van Manen, 2014a,b) and sulfation plates (Lynch *et al.* , 1978; Bourque & Arp, 1996; Delmelle *et al.* , 2001, 2002; Ta *et al.* , 2005; Tasdemir & Gunez, 2006) have been previously used in many studies of both industrial and volcanic gases . Typically, maximum gas concentrations and deposition rates were much higher in studies downwind of volcanoes than in industrial

regions.

At Masaya, studies of the downwind spatial distribution of volcanic gas concentrations and their deposition rates have only been undertaken during the dry season, in February and March (Delmelle *et al.* , 2001, 2002; van Manen, 2014b). Downwind rain samples were collected in August and October 1981, which were found to be acidified by volcanic sulfur and chloride, though this was not linked to volcanic gas data such as concentration, deposition rate or emission rate (Johnson & Parnell, 1986). Although measurements of plume composition have been undertaken across a variety of seasons (Burton *et al.* , 2000; Allen, 2002; Witt *et al.* , 2008; Martin *et al.* , 2009a, 2012), these studies have been conducted at the crater rim only, so have focused on characterizing the composition of volcanic emissions, and not their ultimate fate in the environment. Therefore, to fully understand the potential environmental and ecological impacts of degassing from Masaya, it is necessary to have well constrained data from different seasons.

2.1.1 Aims

The aim of this chapter is to characterize volcanic gas concentrations and deposition rates along a downwind transect that provides an approximate cross-section through the plume. These data are compared with a Gaussian distribution. Five sampling periods, at different times of the year, are used to investigate the influence of variation in volcanic gas emission levels and meteorological conditions on the dispersal profile of the plume. Data on volcanic gas concentrations and deposition rates are used to estimate total exposure to the plume along the transect. The results from this chapter provide an essential data set for the following two chapter on the ecological impacts of these gases at the plant community and individual plant scale.

2.2 Methods

2.2.1 Sampling

2.2.1.1 Sampling locations

Preliminary data were collected in February 2013, and three sampling areas were established: an upwind zone, the volcano crater edge and a downwind transect (Figure 2.1). The downwind transect was selected based on the typical wind direction (WSW), and upwind sites were chosen in the opposite direction. Data were collected across four sampling periods (December 2013, February 2014, May 2014 and June 2014) using these sampling areas, though the exact locations of sampling sites were not always the same. Some diffusion tubes and sulfation plates placed in visible locations were missing on return. It is likely that these were stolen by local passers-by, so a more hidden location at the same site was used in following sampling seasons. Additionally, in May 2014 and June 2014 a longer transect was used, given that NW winds were known to be more common during these months (Figures 2.21 and 2.22). The 3 km long transect followed a path at the base of the caldera wall, which provides an approximate cross section through the plume, which lies about 2 km downwind of the actively degassing Santiago Crater. The exact shape of the transect was restricted in places by access due to the caldera wall to the West and an agricultural area to the North where many samplers had been likely stolen as more people pass through this part of the park.

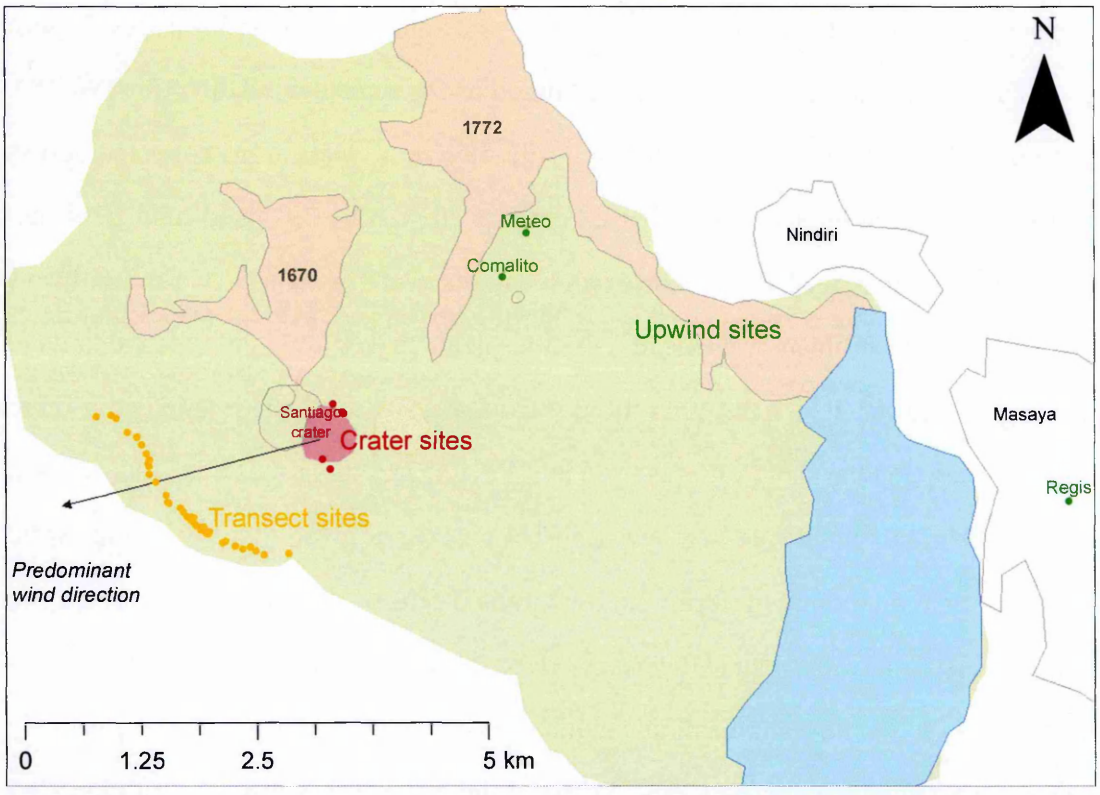

Figure 2.1: Map of the the sampling sites. Upwind sites are in dark green, crater sites are in red and the transect sites are in orange. Precise locations for the crater are shown in Figure 2.8 and for the transect a map for each field season is displayed below (Figures 2.2, 2.3, 2.4, 2.5). The actively degassing Santiago Crater is marked in red and the black arrow shows the typical prevailing wind direction. For the location of Parque Nacional Volcan Masaya within Nicaragua see Figure 1.2.

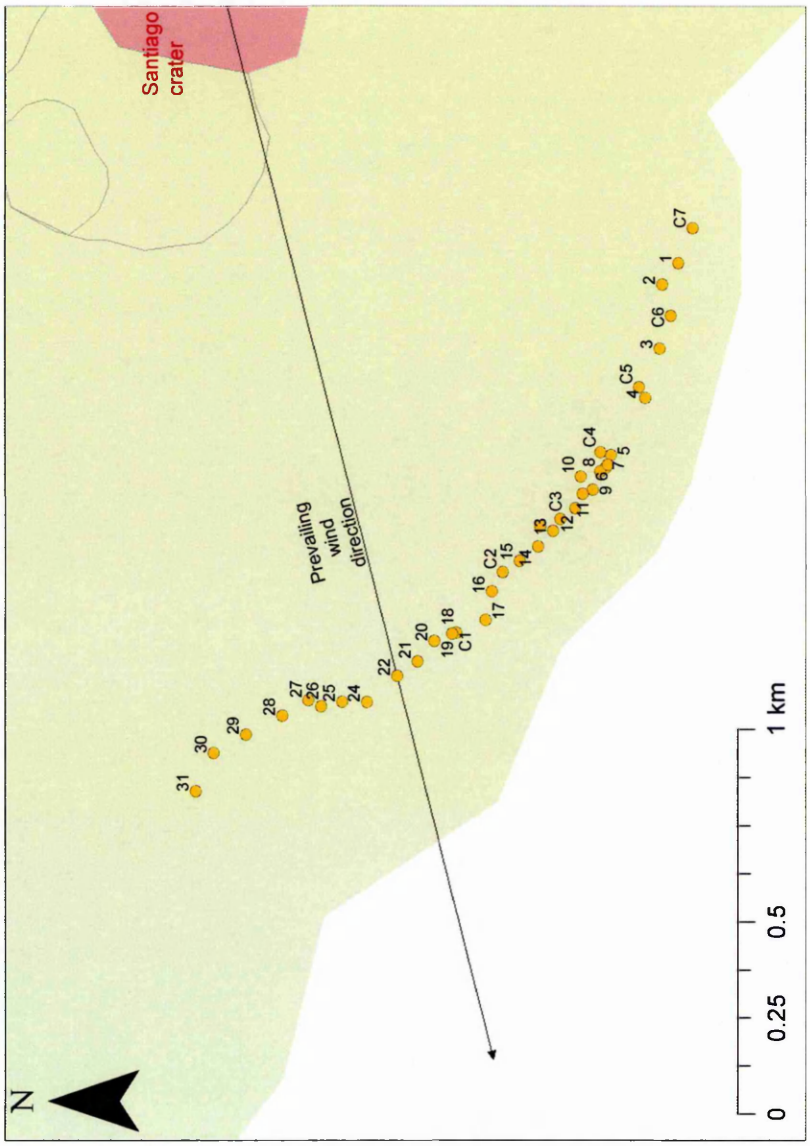

Figure 2.2: Location map of transect sites for February 2013.

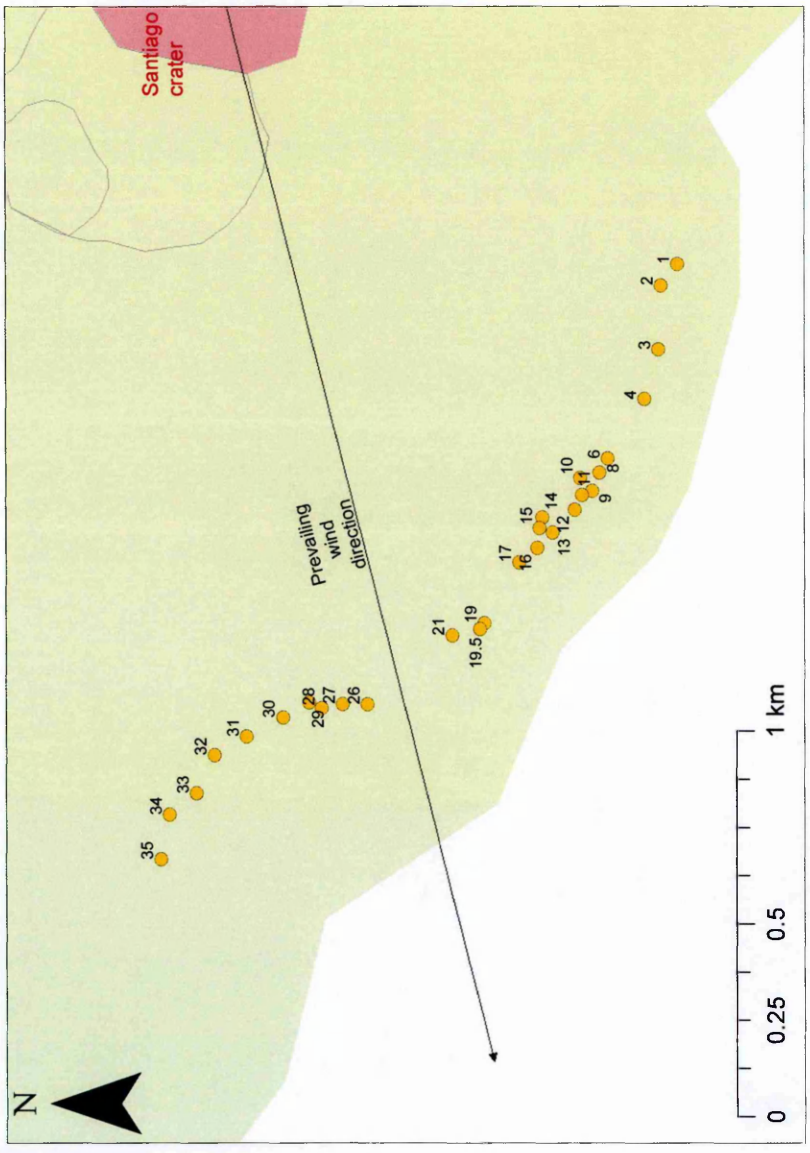

Figure 2.3: Location map of transect sites for December 2013.

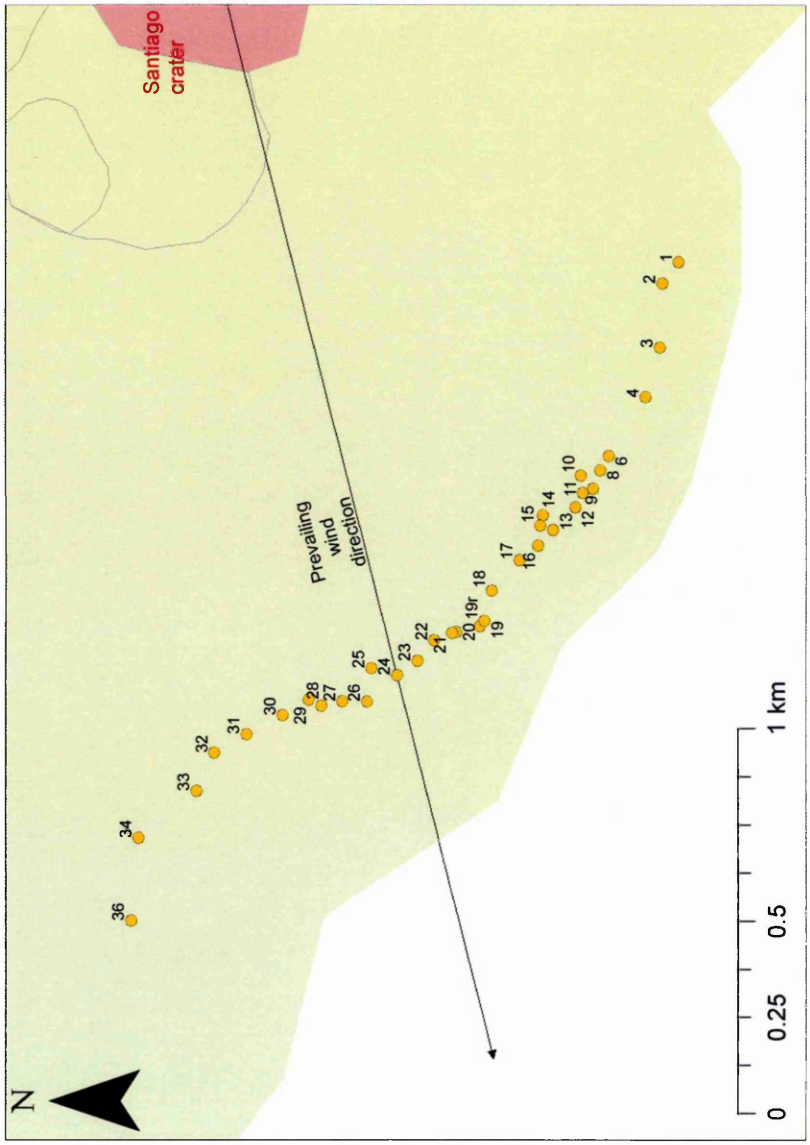

Figure 2.4: Location map of transect sites for February 2014.

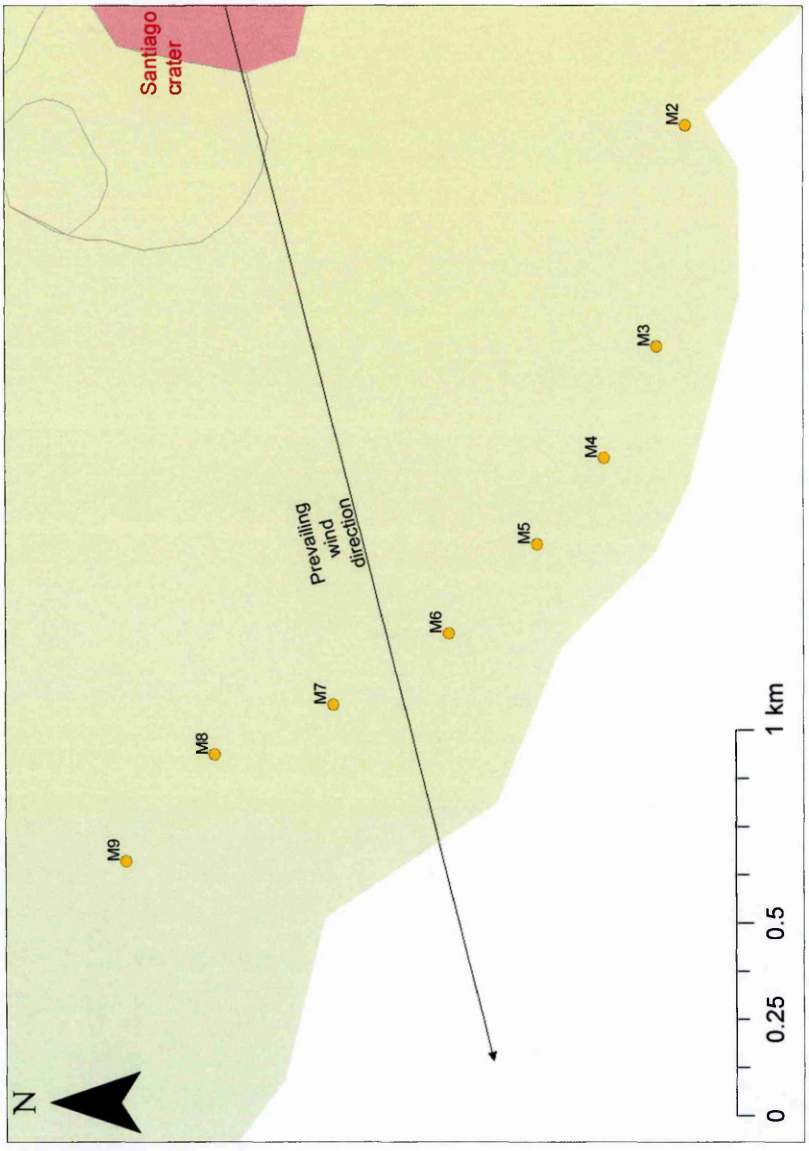

Figure 2.5: Location map of transect sites for May and June 2014. M6 is the same location as Site 21 in previous sampling seasons.

2.2.1.2 Sampling periods

Data were collected for five periods (February 2013, December 2013, February 2014, May 2014 and June 2014). At Upwind sites only for May and June 2014, one exposure period (May-June 2014) was used to cover both these sampling periods, as more accurate measurements can be obtained from longer sampling periods when concentrations are thought to be low, which was found to be the case during the previous sampling periods. Having multiple sampling periods was useful to constrain variation in volcanic gas emissions, and also variation in meteorological conditions which would affect plume dispersal and gas deposition rate.

2.2.2 Diffusion tubes

Diffusion tubes are used for measuring atmospheric gas concentrations and have previously been used to detect indoor (Godoi *et al.*, 2013) and outdoor pollutants (Staszewski *et al.*, 2011), including volcanic emissions (Delmelle *et al.*, 2001; Mather *et al.*, 2006; van Manen, 2014a). They are passive sampling devices that comprise a small plastic tube with a filter at one end and an absorbent at the other that collects the target gases e.g. SO_2 (Gradko Environmental, 2012) and acid gases including HCl, HF, H_2SO_4, NO_3, HBr, NH_3 and H_3PO_4 (Gradko Environmental, 2014b). Diffusion tubes function on the principle that a compound will diffuse through the filter from an area of high concentration (outside the tube) to an area of low concentration (inside the tube) and then collect on the absorbent (Gradko Environmental, 2014a). The absorption of the compounds maintains the diffusion gradient between the inside of the tube and its surroundings. The tubes are exposed for a known length of time, during which the absorbent collects the target gas. The absorbent is then analysed for its chemical composition, using Ion Chromatography (IC) to determine atmospheric gas concentrations, accounting for the time exposed.

Two types of diffusion tubes were purchased from and analysed by Gradko Environmental to measure volcanic gas concentrations. They were attached to trees (Figure

2.6) or structures (e.g. a hut) and exposed for 1-2 weeks, before being sealed in larger tubes and returned to Gradko Environmental for analysis.

Volcanic gases measured by diffusion tubes included SO_2, H_2SO_4, HCl and HF. The H_2SO_4 data correlated well with the other volcanic gas data (SO_2, HCl and HF). However, there is uncertainty in the potential overlap between SO_2 and H_2SO_4 as the methods for sampling both of these are very similar. This means that SO_2 diffusion tubes might also be recording H_2SO_4 and vice-versa. SO_2 typically had a stronger correlation with HCl and HF, as well as deposited S, Cl and F, when compared with H_2SO_4, and had a better NRMSE (Normalized Root Mean Squared Error) for the Gaussian fits (Table A.4). Therefore, only the SO_2 data will be used to represent sulfuric gas concentration levels. Using SO_2 rather than H_2SO_4 will also allow for a comparison of atmospheric SO_2 concentrations with other studies of volcanic and industrial pollution, as this gas has been more commonly measured than H_2SO_4.

Other acid gases were measured in December 2013 and February 2014 (NO_3, HBr, NH_3 and H_3PO_4) but these have not been included as they did not show any relationship with volcanic degassing. In December 2013, HBr and H_3PO_4 were below the limit of detection for all sites with the exception of one for HBr (9.94 μg m^{-3}) and another for H_3PO_4 (15.56 μg m^{-3}). Variable concentrations of NO_3 were found during this sampling season, with some high concentrations found at the beginning (south) of the transect but low or below the limit of detection elsewhere including at the crater. These have not been presented in this study as they are thought to have been caused by the fertilization of nearby farmland, outside the national park. In February 2014 NO_3, HBr, NH_3 and H_3PO_4 were all below the limit of detection. Therefore, results presented in this thesis include SO_2, HCl and HF only.

Diffusion tubes were analysed by Gradko Environmental using Ion Chromatography (IC) following their standard in-house method GLM1 for SO_2 (Gradko Environmental, 2012) and GLM3 for acid gases (Gradko Environmental, 2014b). All data (upwind, crater and transect) have been blank corrected, i.e. the raw blank values (Table 2.1) for that season and gas were subtracted from the raw values for exposed tubes,

before calculation of atmospheric concentration based on exposure time. The limit of detection was 0.03 μg for SO_2, 0.14 μg for HCl and 0.05 μg for HF. One batch of acid gas tubes, exposed in December 2013, was suspected to have been affected by a chloride contamination during the manufacturing process. However, this was only identified by Gradko Environmental after the tubes had been installed. Since other gases recorded by the tubes (e.g. HF) were expected to be unaffected, sampling proceeded as planned. Although upwind sites recorded higher levels of HCl than in other sampling periods, it is thought that correcting the transect and crater sites data with blank and background (upwind) would account for this.

Gas	Feb 2013	Dec 2013	Feb 2014	May-June 2014
SO_2	0.01	0.002	0.02	0.01
HCl	0.55	0.33	0.12	0.43
HF	0.09	0.08	0.07	0.11

Table 2.1: Blank diffusion tube results in μg.

To assess variation between individual tubes, a pair of tubes was exposed at the same site in each sampling season. The mean relative deviation was 5.8% for SO_2, 3.2% for HCl and 8% for HF. Similarly, to test whether there was an upper saturation limit to the tubes, during the May-June 2014 sampling period one tube was exposed for the entire duration (2 weeks), alongside one in May (1 week) and one in June (1 week) at the crater rim (site OCP) where high gas concentrations had been previously measured. It was possible to add the total concentrations detected in each tube, prior to time corrections, and the mean relative deviation was 7.6% for SO_2, 19.4% for HCl and 0.3% for HF (see results in Table 2.5).

2.2.3 Sulfation plates

Lead dioxide sulfation plates have been previously used to measure industrial sulfate deposition (Huey, 1968) and have also successfully been applied in volcanic settings including at Masaya (Delmelle *et al.* , 2001). They comprise a petri dish containing a layer of lead dioxide paste, which reacts with deposited substances. This can then be

Figure 2.6: a) Photograph of SO_2 (purple) and acid gas (green) diffusion tubes and a sulfation plate attached to a tree. b) Photograph of a sulfation plate secured in a rock at ground level.

extracted and analysed using Ion Chromatography (IC), and from the amount of sulfate it is possible to estimate the deposition rate of SO_2. Like the diffusion tubes, these are exposed for a known length of time, which is used to calculate a deposition rate. These have also been shown to detect volcanic chloride (Delmelle *et al.* , 2001) and are also thought to detect fluoride (P. Delmelle, pers. comm. 22 January 2015) although there has been no independent verification of the validity of using sulfation plates to detect HF deposition.

Deposition rates of sulfate, and estimated deposition rates of chloride and fluoride from the volcano were directly measured using sulfation plates. These were prepared and analysed in the EGL labs at the Open University following the method of Huey (1968). A lead dioxide paste was prepared and approximately 10 ml of this was placed in 50 mm petri dishes and dried overnight at 60° C. The dried lead dioxide paste in the petri dish forms the sulfation plate. To prevent contamination during storage and transportation, each was covered with a lid and sealed with parafilm.

As with the diffusion tubes, sulfation plates were attached to trees (Figure 2.6) or structures (e.g. a hut) where available, or placed on the ground at upwind, crater and downwind locations (Figure 2.1). Plates were exposed facing the volcano and secured as close to vertical as possible. Deposited sulfur reacts with lead oxide in the plate to form lead sulfate. Similar reactions are also thought to occur with chloride and fluoride, to form lead chloride and lead fluoride. Sulfation plates were exposed for a recorded amount of time, typically between one to two weeks.

On collection, the plates were re-sealed with their lid and parafilm before being transported to the UK for analysis. The lead dioxide 'pad' was removed from the petri dish and placed in a 5% sodium carbonate solution for extraction. The extracts were heated to ensure all lead sulfate, lead chloride and lead fluoride was in solution and then filtered, before being analysed using Ion Chromatography on an IC3000 for sulfate, chloride and fluoride concentrations. For samples that were expected to be beyond the measuring range (over 100 mg/l sulfate) these were further diluted (1 in 4 or 1 in 10) to ensure accurate results and to prevent damage to the IC.

Field blanks (unexposed sulfation plates) and lab blanks (extraction solution with no sulfation plate added) were also run on the IC to identify any possible sources of contamination. Blank deposition rates were calculated from the field blanks. In December 2013 there was a suspected HCl contamination in some but not all of the plates. This was found in the lab blank from the extraction batch of these likely contaminated samples (lab blank: 11.1 mg l^{-1} HCl, whereas other blank values were typically less than 1 mg l^{-1} HCl). Therefore, this probably represents contamination from the water used in the sodium carbonate solution for extractions. The exposed plates affected by this contamination (codes S10/1 to S10/15) were excluded from the chloride data set, but the sulfate and fluoride data were unaffected and, therefore, retained. Another plate, S11/48 (February 2014, Site 23G), was also removed from all data analysis as it had very high levels of sulfate, chloride and fluoride, all of which were several times larger than neighbouring plates.

Season	Sulfate	Chloride	Fluoride
Dec-13	0.00	0.93	0.84
Feb-13	0.00	0.79	1.09
Feb-14	0.67	0.77	1.63
May-Jun 2014	1.50	1.03	1.39

Table 2.2: Blank sulfation plate results in mg l^{-1} for February 2013, December 2013, February 2014 and May-June 2014. 1 mg l^{-1} represents a deposition rate of 4.12 mg m^{-2} day^{-1} over a 7 day period.

The method detection limit, calculated from three standard deviations from the mean of all the blanks was 3.1 mg l^{-1} for sulfate, 2.6 mg l^{-1} for chloride and 2.9 mg l^{-1} for fluoride.

The average of all the blanks for a given sampling period (Table 2.2) was subtracted from the raw data, and any blank subtracted values lower than 0 were removed. The results for sulfate, chloride and fluoride contents of the extracts of the sulfation plates (mg l^{-1}) were then converted to dry deposition rates of SO_2, HCl and HF (mg m^{-2} day^{-1}) based on their length of exposure and the area of the sulfation plate as well as the dilution during their extraction using:

$$D_x = ((m_x - m_b) * d)/a)/t \tag{2.2}$$

where D_x is the estimated deposition rate at location x, m_x is the measured concentration of sulfate, chloride or fluoride on a plate exposed at location x in mg l^{-1}, m_b is the average blank concentration for sulfate, chloride of fluoride for the corresponding sampling period in mg l^{-1}, d is the dilution, a is a constant relating to the surface area of the plate (=0.00173494 m^2) and t is the time exposed in hours. Blank corrected data are displayed in the appendix (Tables A.1, A.2 and A.3).

Using pairs of plates, exposed at the same place for the same length of time, it was possible to calculate the mean relative deviation for sulfate (8%), chloride (15%) and fluoride (7%).

2.2.4 HYSPLIT model

When looking at volcanic gas distribution patterns it is important to understand how meteorological conditions affect plume dispersal. HYSPLIT, Hybrid Single-Particle Lagrangian Integrated Trajectory (Draxler, 2013), is a model that uses gridded meteorological data for the calculation of air parcel trajectories (Cerón *et al.* , 2005; Allen *et al.* , 2010; Watt *et al.* , 2007) and for determining wind speeds (Witt *et al.* , 2008), that has been applied at Masaya for the sampling periods.

The model had been run using the GDAS meteorological data set available from NOAA's ARL. For all runs of the model, hourly trajectories have been calculated from 10 m above the ground level of the same starting point, the actively degassing crater (11.984°N, -86.168°E). The model was programmed to start a new trajectory every hour, and each trajectory lasted 15 minutes. Each run covered the length of the sampling periods during which diffusion tubes and sulfation plates were exposed.

For each sampling period the average point reached by 15 minutes from the start time (endpoint) was calculated to allow comparisons between seasons and with degassing data. This was done by calculating the mean latitude, longitude and height of

all the endpoints at 15 minutes for each sampling period. This shows how far and in what direction gases emitted at the crater are modelled to have travelled during this time. A 15 minute period was used because it was most appropriate for covering the study area. The distance and bearing from the crater to the average 15 minute endpoint was measured for each sampling period, and an estimate of the wind speed was calculated from the distance measurement. Additionally, using trigonometry, an approximate centreline position along the transect (to match with the Gaussian fit to the gas concentration and deposition rate data) was calculated from the bearing.

2.2.5 Data analysis

Pearson's correlation was used to test the relationship between pairs of data for gas concentrations (diffusion tubes) and deposition rates at tree and ground height (sulfation plates) for SO_2, HCl and HF exposed at the same site. A strong positive correlation would suggest a common, volcanic, origin for these gases.

2.2.5.1 Gaussian profile along the transect

Gas concentration and deposition rate data has been collected at sites along the transect. However, to better understand how these might affect the downwind ecosystem, a profile of volcanic gas concentrations and deposition rate is more useful as it can allow for a value to be estimated at any given point.

When a pollutant is continuously emitted from a point source, such as Santiago Crater at Masaya Volcano, it is subjected to advection and lateral dispersion such that the pollutant concentration in the plume varies with distance from the plume axis according to a Gaussian distribution (Vallero, 2007). Along a transect at ground level (of constant downwind distance and height) that creates a cross section through the plume, the expected pollutant concentration ($C_{volc,x}$) at point x m along a transect can be calculated from an expected distribution:

$$C_{volc,x} = C_{volc,0} exp(-\frac{(x - x_0)^2}{2\sigma^2}) \tag{2.3}$$

where the peak concentration at the centre-line of the plume, $C_{volc,0}$, occurs at the centreline x_0 and σ is the standard deviation of the distribution in concentration in m (width). A Gaussian model is useful since it allows for comparisons of plume parameters (peak gas concentration, centreline position and plume width), between different sampling data sets.

Sites along the transect did not form a precise straight line and were not perfectly perpendicular to the plume axis, but they provide a useful approximation. There was a change in altitude of about 100 m along the transect (Figure A.1 in the Appendix), therefore the measurements were not made at a constant height. Additionally, processes such as deposition, chemical reactions in the plume and atmospheric instability (e.g. changes in wind direction through time) might have influenced local gas concentrations and therefore, modified the Gaussian distribution. Nevertheless, it is expected that a Gaussian model could be fitted to gas concentration data along the transect which formed an approximate cross-section through the plume.

2.2.5.1.1 Gas concentrations

Prior to the fitting of the model, the transect data was background corrected using the average of the upwind sites to give the volcanic pollutant concentration:

$$C_m = C_v + C_b \tag{2.4}$$

$$C_v = C_m - C_b \tag{2.5}$$

where C_m is the measured concentration, C_b is the background concentration and C_v is the concentration as a result of volcanic degassing.

Each point along the transect was background corrected (using the average of Regis, Comalito and Meteo sites, locations shown in Figure 2.1), and values lower

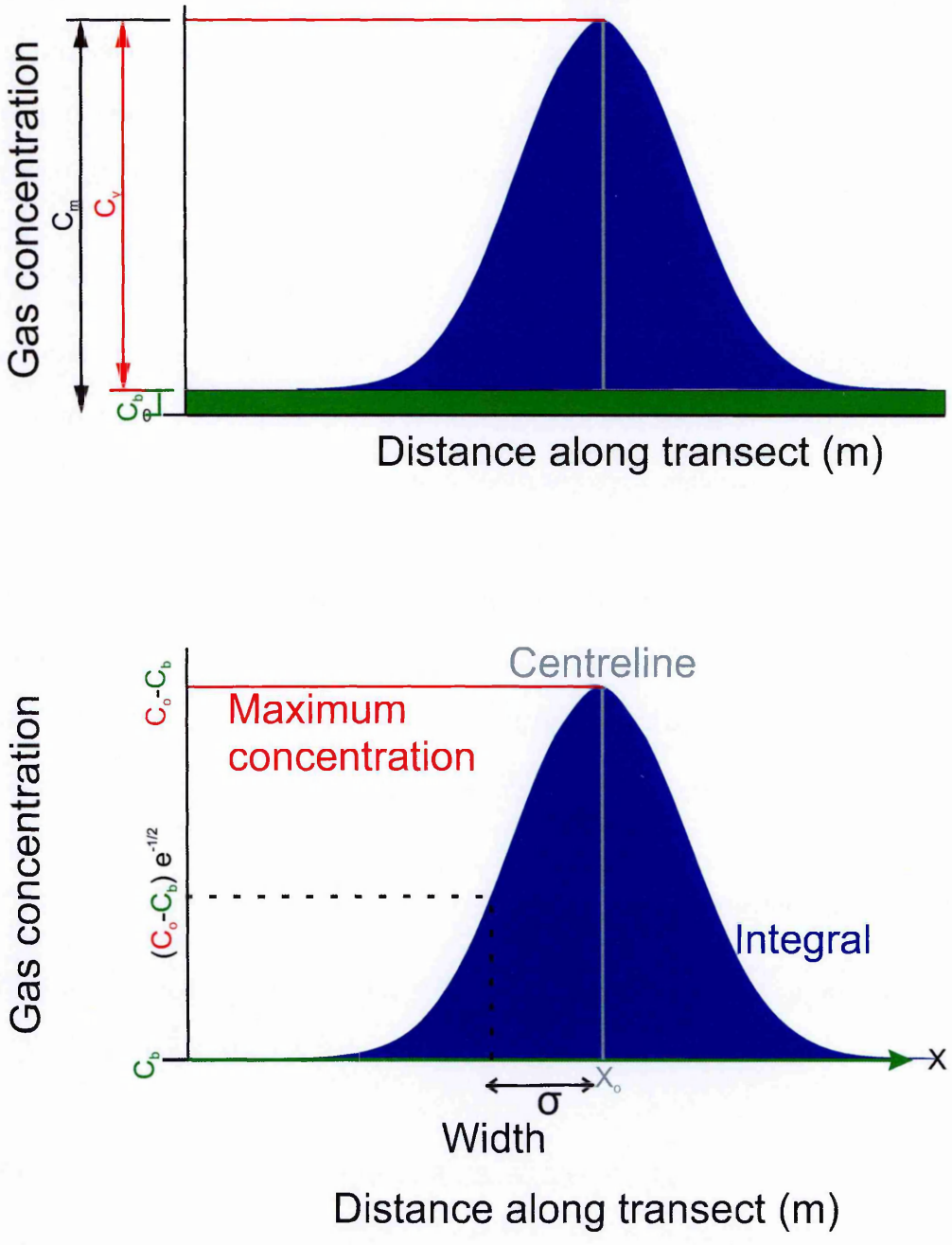

Figure 2.7: Diagram showing a) volcanic and background components of the measured gas concentrations (Equation 2.5) and b) the parameters used to describe the Gaussian profile, described in Equation 2.3

than the background were discarded for the fitting of the Gaussian distribution. The distance along the transect was defined by the direct distance from site 21, thought to be near the centreline of the plume. Negative values represent the start of the transect (S from site 21) with positive values being at the end of the transect in the agricultural area (N from site 21).

The following Gaussian model was used to estimate the concentration of a gas ($C_{est,x}$) at a location at cross-wind distance x using:

$$C_{est,x} = C_0 exp(-\frac{(x - x_{0,C})^2}{2\sigma_C^2}) \tag{2.6}$$

A non-linear least-squares method (nls function in R (2014), version 3.1.1) was used estimate best fit values for the maximum concentration ($C_{0,C}$), centreline position (x_0) and plume width (σ_C) that produced the lowest sum of residuals squared between estimated ($C_{est,x}$) and C_v, the background corrected measured values (C_m-C_b).

The best fit values were used to calculate parameters which describe the distribution of gas concentrations (Figure 2.7) Where possible, this was done for all sampling periods (February 2013, December 2013, February 2014, May 2014 and June 2014) and gases (SO_2, HCl and HF). The maximum concentration (C_0) refers to the maximum gas concentration estimated by the Gaussian fit for diffusion tubes (measured in μg m^{-3}). The centreline ($x_{0,C}$) is the distance in m along the transect from site 21. The width parameter, given in m, is σ_C and this is the equivalent of one standard deviation of the distribution of the gas from the centreline. The integral of the Gaussian fit ($Integral_C$), i.e. the area under the curve, was calculated using Equation 2.7. This provides an estimate of the total mass of gas reaching a cuboid shaped cross section through the plume with dimensions of length $-\infty$ to ∞ from the centreline, and a width of 1m and a height of 1m. For the diffusion tube data this is displayed using a unit of mg.

$$Integral_C = C_0 \sigma \sqrt{2\pi} \tag{2.7}$$

To assess the goodness of the fit of the Gaussian model to the measured data the Normalized Root Mean Square Error (NRMSE) was calculated. The NRMSE is displayed as a percentage variation from the mean measured concentration value, calculated by:

$$RMSE = \frac{\sqrt{\sum (y_o - y_p)^2}}{n} \tag{2.8}$$

$$NRMSE = 100 * \frac{RMSE}{\overline{y_o}} \tag{2.9}$$

where y_o is observed or measured values and y_p is values predicted by the Gaussian model. The Gaussian model was considered acceptable when NRMSE $\leq$ 35%, which excluded those that had a poor fit to the original data. Residual plots were also used to check for any systematic spatial variation from the model, and an example is shown in the Appendix (Figure A.2).

2.2.5.1.2 Deposition rates

If the deposition rate of a gas is proportional to its concentration in the atmosphere, deposition rates would also be expected to follow a Gaussian distribution. Using the same method as for with gas concentration, the following Gaussian model was used to estimate the concentration of a gas ($D_{est,x}$) at a location at cross-wind distance x for tree:

$$Dt_{est,x} = Dt_0 exp(-\frac{(x - x_{0,Dt})^2}{2\sigma_{Dt}^2}) \tag{2.10}$$

and ground heights:

$$Dg_{est,x} = Dg_0 exp(-\frac{(x - x_{0,Dg})^2}{2\sigma_{Dg}^2}) \tag{2.11}$$

A non-linear least-squares method (nls function in R) was used estimate best fit values for tree (Dt_0, $x_{0,Dt}$ and σ_{Dt}), and ground (Dg_0, $x_{0,Dg}$ and σ_{Dg}) parameters, that

produced the lowest sum of residuals squared between estimated ($Dt_{est,x}$ or $Dg_{est,x}$) and background corrected measured deposition rates (D_{vt}=D_{mt}-D_b and D_{vg}=D_{mg}-D_b) as explained in Equation 2.5.

Parameters from the Gaussian best fit to tree and ground deposition rate will be displayed alongside the concentration parameters. The maximum deposition rate at tree ($D_{0,t}$) and ground ($D_{0,g}$) height is measured in mg m^{-2} day^{-1} and the centreline and width are measured in m as above ($x_{0,Dt}$ and σ_{Dt}, and $x_{0,Dg}$ and σ_{Dg}). The integral of the Gaussian fit to tree ($Integral_t$) and ground ($Integral_g$) data was calculated using a similar formula to the diffusion tube concentration data (Equations 2.12, 2.13). For both tree and ground heights, this gives the total volcanic gas deposition in g day^{-1} on a rectangle of length $-\infty$ to ∞ and with 1m. The NRMSE$_t$ and NRMSE$_g$ calculated as above (Equation 2.9) are also displayed.

$$Integral_t = D_{0,t}\sigma\sqrt{2\pi} \tag{2.12}$$

$$Integral_g = D_{0,g}\sigma\sqrt{2\pi} \tag{2.13}$$

A comparison between tree and ground height deposition rate measurements will also be made using a paired t-test.

2.2.5.2 Explaining variation in downwind volcanic gas levels

Correlation between the Gaussian parameters (centreline and width) and HYSPLIT data, including wind direction, wind speed and plume height, was used to test whether the wind data is able to identify the affected area. Additionally, correlation between crater rim measurement and integral of the concentration and deposition rates was also performed.

2.2.5.3 Deposition velocities

Using the integrals from the Gaussian fits for concentration and deposition rate data it was possible to calculate deposition velocities for season and height (h= t or g repre-

senting tree and ground height respectively):

$$V_h = c * (D_h/C_t) \tag{2.14}$$

where V_h is the deposition velocity at tree or ground height, or gas transfer rate for a given season and with a unit of cm/s, D_h is the integral of the deposition of a gas onto a sulfation plate exposed for that season at tree or ground height measured in g day over a 1 m wide rectangle of infinite length $^{-1}$ using sulfation plates and C_t is the gas concentration integral at that location at tree height in mg over a cube of 1 m height, 1m depth and infinite length. The constant (c) has a value 1.157 required to convert g to mg (*1000), m to cm (*100) and days to seconds(/86400). The deposition velocity represents the rate at which a species was transferred from the atmosphere to a surface, in this case sulfation plates, which is thought to be a useful approximation for vegetation, and was calculated for all measured gases (SO_2, HCl and HF) and all seasons at both tree and ground height where a Gaussian model had been successfully fitted. However, since concentration data were only collected at tree height, deposition velocity at ground height provides an estimate.

2.3 Results

2.3.1 Control sites

For each sampling season the upwind control sites were located within the park (Meteo and/or Comalito) and in the nearby town of Masaya at the Regis Hotel (Figure 2.1). Upwind results for sulfation plates and diffusion tubes, after blank correction, suggested that there were negligible or low gas concentrations and deposition rates at these sites (Tables 2.3 and 2.4). SO_2 concentrations at all sites were below the limit of detection, with the exception of Regis in May and June 2014 which was just above the limit of detection. Similarly, SO_2 deposition was below the limit of detection for most sampling seasons and sites, except Comalito in February 2014 and Regis in May and June 2014.

HCl gas concentrations recorded by diffusion tubes were mostly below detection at upwind sites, but were high for the contaminated tubes in December 2013, reaching up to 16 μg m^{-3}. Sulfation plates recorded HCl deposition rates ranging from below the limit of detection (Meteo in February 2013, Comalito and Regis in December 2013) to 1 mg m^{-2} day^{-1} (Comalito in May-June 2014). HF gas concentrations measured by diffusion tubes were not always below the limit of detection, but low concentrations were detected ranging from 0.37 μg m^{-3} (Regis in February 2014) to 4.62 μg m^{-3} (Meteo in February 2013). HF deposition rate detected on sulfation plates ranged from below the limit of detection to 1.2 mg m^{-2} day^{-1} (Regis in February 2014).

Although gases were not always below the limit of detection at upwind sites, their measured concentrations and deposition rates were considerably lower than those found near the crater edge and along the transect.

	Season	Site	Hours	SO_2	HCl	HF
F13/U1	Feb-13	Meteo	244	BD	BD	BD
F13/U2	Feb-13	Regis	201	BD	BD	4.62
D13/U1	Dec-13	Comalito	215	BD	15.68	BD
D13/U2	Dec-13	Regis	244	BD	10.51	BD
F14/U1	Feb-14	Comalito	315	BD	BD	0.87
F14/U2	Feb-14	Regis	351	BD	1.53	0.37
MJ14/U1	May-June 2014	Comalito	333	BD	BD	4.34
MJ14/U2	May-June 2014	Regis	353	1.81	BD	1.71

Table 2.3: Concentrations of gases (μg m^{-3}) measured by diffusion tubes at upwind sites. Row names are the unique sample codes for diffusion tubes, which can be matched to the additional information in the appendix (Table A.1). BD= Below detection.

	Season	Site	Hours	SO_2	HCl	HF
S6/52	Feb-13	Comalito	340	BD	0.91	0.36
B11/01	Feb-13	Regis	201	BD	BD	BD
B11/02	Feb-13	Regis	201	BD	BD	BD
B11/03	Feb-13	Meteo	244	BD	BD	BD
S10/54	Dec-13	Regis	244	BD	BD	1.19
S10/56	Dec-13	Comalito	215	BD	BD	1.01
S11/96	Feb-14	Comalito	315	1.61	0.11	0.35
S11/102	Feb-14	Regis	351	BD	0.1	0.73
S16/99	MJ14	Regis	354	7.11	0.4	BD
S16/97	MJ14	Comalito	333	BD	1.07	BD

Table 2.4: Deposition rates (mg m^{-2} day^{-1}) measured using sulfation plates at upwind sites. Row names are the unique sample codes for sulfation plates, which can be matched to the additional information in the appendix (Table A.3). BD= Below detection.

2.3.2 Crater sites

The highest recorded gas concentrations (Table 2.5) and deposition rates (Table 2.6) were found at H1 when data were available for this site (in December 2013 for SO_2 concentration, February 2014 for HCl and HF concentration for diffusion tubes, and in February 2014 for SO_2 and HCl deposition rate whilst February 2013 had the highest HF deposition rate). The lowest gas concentrations (diffusion tubes) at a crater site were recorded at OCP in June and NCP in February 2013, whereas the lowest deposition rates (sulfation plates) were recorded in December 2013 at NCP. Due to the varying position of the tube at NCP (Figure 2.8) and a lack of data for H1 across all the sampling seasons, these sites provided less useful information about variation in degassing throughout the duration of the studied periods, so OCP was used as a reference point for crater values.

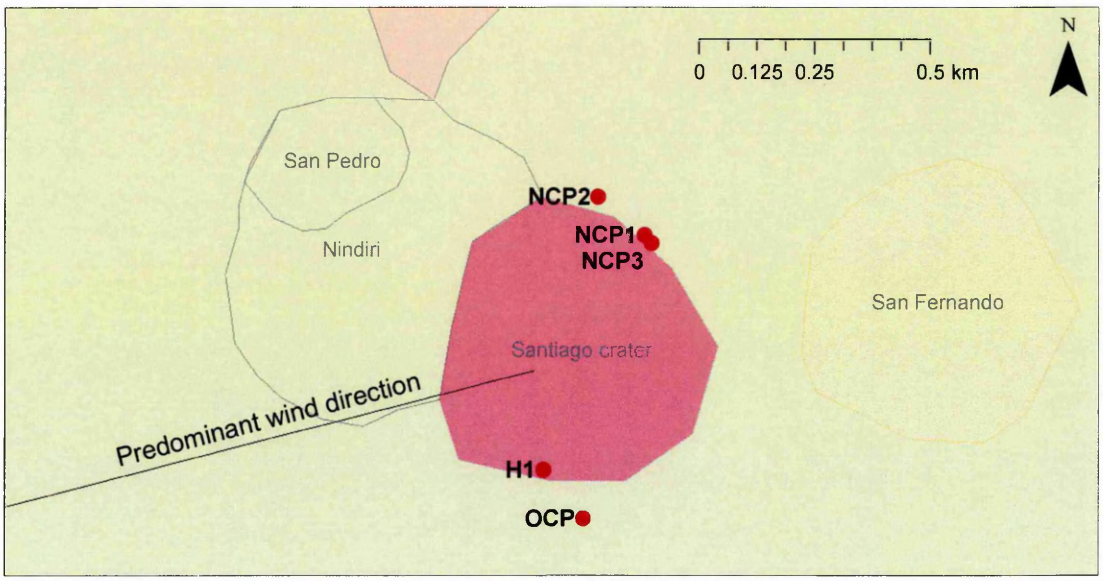

Figure 2.8: Locations of crater sites. The position of NCP was changed between sampling periods as a result of diffusion tubes and sulfation plates being lost.

At OCP, SO_2 concentration decreased through the sampling seasons from February 2013 to June 2014 (Figure 2.9). HCl increased from February 2013 to December 2013 but then decreased in the following sampling periods. HF increased from February 2013 to December 2013 and February 2014 before decreasing in May/June 2014.

Gas deposition rates were higher in February 2013, December 2013 and February

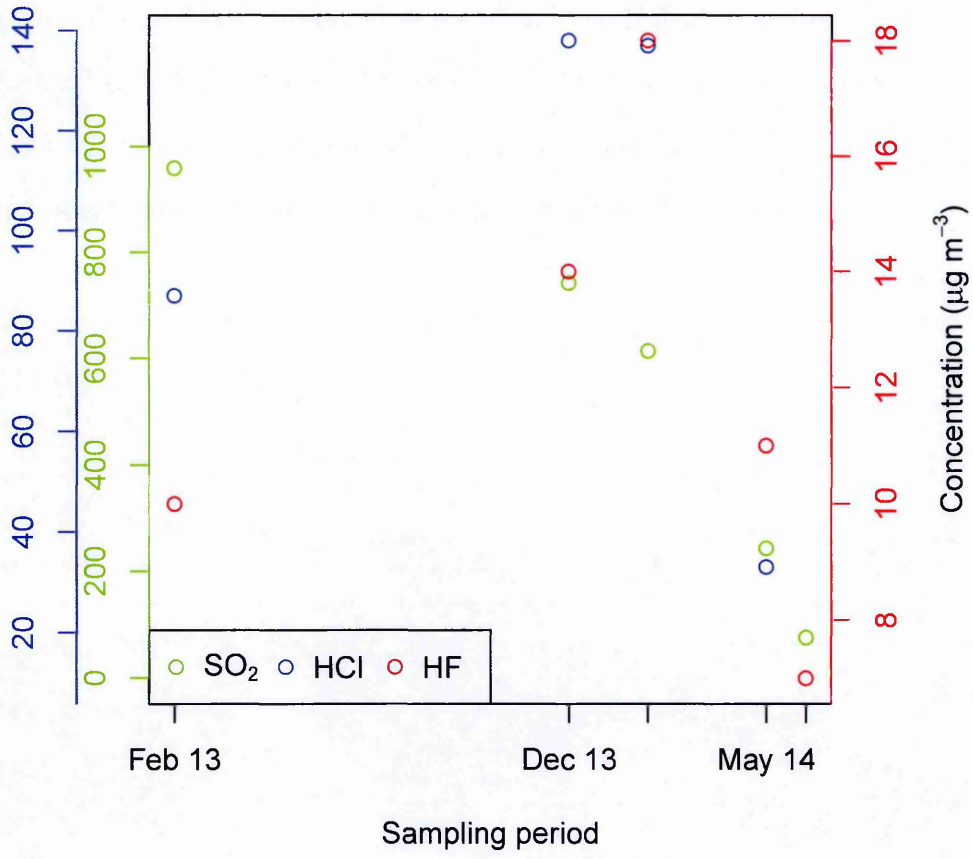

Figure 2.9: Background corrected OCP diffusion tube results for SO_2 (green), HCl (blue) and HF (red) in μg m^{-3} for February 2013, December 2013, February 2014, May 2014 and June 2014. Note the different scales for SO_2, HCl and HF.

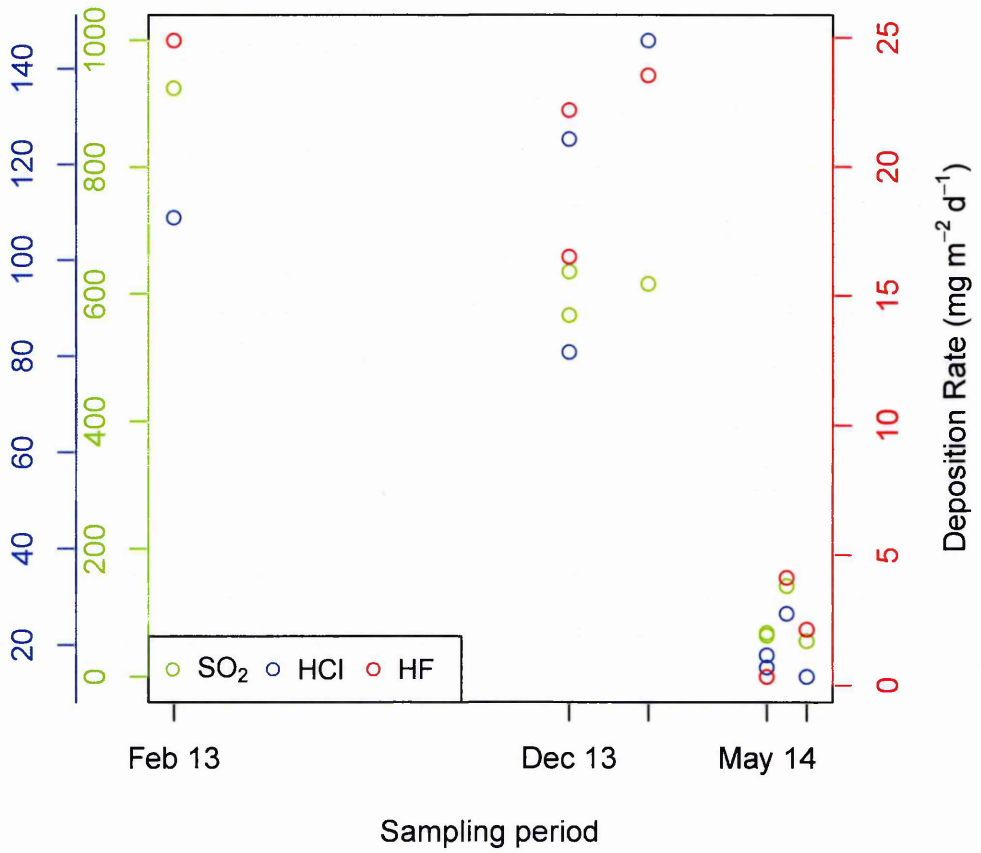

Figure 2.10: Background corrected OCP sulfation plate results for SO_2, HCl and HF in mg m^{-2} day^{-1} for February 2013, December 2013, February 2014, May 2014 and June 2014. Note the different scales for SO_2, HCl and HF.

	Season	Site	Hours	SO_2	HCl	HF
F13/C1	Feb-13	NCP1	218	183	17	4
F13/C2	Feb-13	OCP	166	959	87	8
D13/C2	Dec-13	OCP	256	742	125	14
D13/C3	Dec-13	H1	257	2083	764	79
F14/C1	Feb-14	NCP2	336	377	90	11
F14/C2	Feb-14	OCP	342	614	136	17
F14/C3	Feb-14	H1	341	1766	2055	195
M14/C1	May-14	NCP3	168	483	123	26
M14/C2	May-14	OCP	169	242	33	8
J14/C1	Jun-14	NCP3	165	295	39	16
J14/C2	Jun-14	OCP	161	75	11	4
J14/C3	Jun-14	H1	168	881	263	32
MJ14/C	May-June 2014	OCP**	330	176	29	6

Table 2.5: Background corrected concentrations of gases (μg m^{-3}) measured by diffusion tubes at crater sites. ** These tubes were exposed over both the May 2014 and June 2014 sampling periods, and are, therefore, expected to represent an average of these.

2014 than during the May and June 2014 sampling periods.

	Season	Site	Hours	SO_2	HCl	HF
S6/2	Feb-13	H1	48	6764	1177	181.2
S6/4	Feb-13	H1	22	2234	414	68
S6/15	Feb-13	OCP g	192	925	109	24.9
S6/17	Feb-13	NCP1 t	219	72	11	4.8
S10/57	Dec-13	NCP1 g	263	31	8	0.3
S10/58	Dec-13	OCP t	256	635	125	22.2
S10/59	Dec-13	OCP g	256	567	81	16.5
S10/62	Dec-13	H1	256	6326	466	115.8
S11/97	Feb-14	H1	341	7772	1596	79.5
S11/100	Feb-14	NCP2 g	336	130	33	1.7
S11/101	Feb-14	OCP t	342	616	146	23.5
S16/22	May-14	NCP3 t	168	589	110	15
S16/24	May-14	OCP g	169	69	18	0.3
S16/25	May-14	OCP t	169	64	15	0.3
S16/59	Jun-14	NCP3 g	165	108	22	4.3
S16/60	Jun-14	NCP3 t	165	233	48	8.7
S16/62	Jun-14	OCP t	161	56	13	2.1
S16/63	Jun-14	H1	168	589	140	20.7
S16/64	Jun-14	H1	168	591	137	36.3
S16/61	MJ14	OCP t	330	142	26	4.1

Table 2.6: Background corrected deposition rates (mg m^{-2} day^{-1}) measured using sulfation plates at crater sites. t=tree height, g=ground level.

2.3.3 Transect sites

A summary of the data collected along the transect for each season is displayed in Tables 2.7, 2.8 and 2.9. A full table of gas concentration and deposition rate at tree and ground height for the transect sites can be found in the appendix (Tables A.1, A.2 and A.3). For each measurement SO_2 had the largest concentrations and deposition rates, followed by HCl and HF. There was considerable variation between the seasons for each gas. Gas deposition rates were typically lower at ground than at tree height.

Season	Mean SO_2	Min SO_2	Max SO_2	Mean HCl	Min HCl	Max HCl	Mean HF	Min HF	Max HF
Feb-13	583	77.0	861	96	16.4	186	13	3.1	22
Dec-13	432	5.0	900	65	9.0	115	13	0.2	26
Feb-14	722	4.4	1156	162	0.1	292	18	0.2	34
May-14	138	5.7	361	43	14.1	59	9	2.1	16
Jun-14	280	67.8	538	55	24.0	89	13	0.2	20

Table 2.7: Summary table for gas concentrations over the seasons.

Season	Mean SO_2	Min SO_2	Max SO_2	Mean HCl	Min HCl	Max HCl	Mean HF	Min HF	Max HF
Feb-13	339	38	875	90	50.9	180	10	0.3	26
Dec-13	1282	41	2900	129	6.4	294	31	5.0	66
Feb-14	523	6	1106	100	0.4	214	19	0.0	38
May-14	111	13	237	24	4.0	49	4	0.8	8
Jun-14	136	7	269	35	0.1	63	5	0.3	8

Table 2.8: Summary table for gas deposition rates at tree height over the seasons.

Season	Mean SO_2	Min SO_2	Max SO_2	Mean HCl	Min HCl	Max HCl	Mean HF	Min HF	Max HF
Dec-13	298	34	745	87	24.2	159	9	0.6	23
Feb-13	625	30	1548	63	4.0	180	18	5.0	41
Feb-14	352	0	797	75	0.6	160	13	0.0	31
Jun-14	91	5	182	18	6.5	34	3	0.3	6
May-14	119	9	221	27	2.2	65	4	0.8	8

Table 2.9: Summary table for gas deposition rates at ground height over the seasons.

2.3.3.1 Relationships between gas concentrations and deposition rates

Given that the different measured gases and deposited particles are thought to be of volcanic origin it is expected that they will correlate well together. There is a strong relationship between all volcanic gases and their deposition measured at tree and ground height at each site, and this is significant according to Pearson's Correlation for all gases ($p \leq 0.05$) shown in Table 2.10. The ratios between the gas concentrations and deposition rates are shown in Table 2.11.

	C SO_2	C HCl	C HF	D_t SO_2	D_t HCl	D_t HF	D_g SO_2	D_g HCl	D_g HF
C SO_2	1.00	0.94	0.86	0.90	0.90	0.88	0.83	0.79	0.81
C HCl	0.94	1.00	0.82	0.90	0.89	0.89	0.70	0.68	0.69
C HF	0.86	0.82	1.00	0.85	0.81	0.77	0.59	0.54	0.58
D_t SO_2	0.90	0.90	0.85	1.00	0.90	0.96	0.78	0.73	0.78
D_t HCl	0.90	0.89	0.81	0.90	1.00	0.96	0.78	0.80	0.80
D_t HF	0.88	0.89	0.77	0.96	0.96	1.00	0.73	0.68	0.77
D_g SO_2	0.83	0.70	0.59	0.78	0.78	0.73	1.00	0.88	0.95
D_g HCl	0.79	0.68	0.54	0.73	0.80	0.68	0.88	1.00	0.91
D_g HF	0.81	0.69	0.58	0.78	0.80	0.77	0.95	0.91	1.00

Table 2.10: Correlation between gas concentration and deposition rate data at tree and ground height along the transect. C= Concentration (at tree height only), D_t= Deposition rate at tree height and D_g = Deposition rate at ground height. All possible data pairs from the five sampling periods were used. All were significant at $p \leq 0.05$

	C SO_2	C HCl	C HF	D_t SO_2	D_t HCl	D_t HF	D_g SO_2	D_g HCl	D_g HF
C SO_2	1.00	0.19	0.06	0.56	0.13	0.02	0.44	0.15	0.02
C HCl	6.78	1.00	0.23	3.46	0.82	0.12	3.19	0.82	0.11
C HF	31.39	7.25	1.00	20.97	4.79	0.84	17.61	4.57	0.72
D_t SO_2	2.15	0.36	0.23	1.00	0.27	0.06	0.87	0.58	0.03
D_t HCl	9.39	1.44	0.50	5.50	1.00	0.23	3.91	1.52	0.18
D_t HF	58.34	10.43	2.23	31.12	5.82	1.00	27.14	6.62	0.94
D_g SO_2	3.21	0.44	0.17	1.35	0.35	0.05	1.00	0.40	0.04
D_g HCl	9.50	1.84	0.43	5.44	1.22	0.22	4.52	1.00	0.19
D_g HF	84.77	13.33	3.83	39.09	8.58	1.31	29.97	7.34	1.00

Table 2.11: Ratios between gas concentration and deposition rate data at tree and ground height along the transect. C= Concentration (at tree height only) in μg m^{-3}, D_t= Deposition rate at tree height in mg m^{-2} day^{-1} and D_g = Deposition rate at ground height in mg m^{-2} day^{-1}. All possible data pairs from the five sampling periods were used. Each ratio has been calculated by column/row.

2.3.3.2 SO_2 along the transect

The highest peak SO_2 gas concentration estimated from the Gaussian fit (Table 2.12) was found in February 2014 (1137 μg m^{-3}). June 2014 had the lowest SO_2 gas concentration peak (364 μg m^{-3}). The centreline for June 2014 was also farther north along the transect at around 770 m, but it was relatively consistent during the other seasons where it was between 100 m and 170 m. December 2013 had the widest plume (σ_C = 704 m) and it was between 510 m and 550 m during the other seasons. December 2013 and February 2014 had similar integrals around 1460 mg m^{-2}, suggesting that the high concentrations found in February 2014 were balanced by the large plume width in December 2013. February 2013 had a slightly lower integral at 1224 mg m^{-2}, but much lower values were found in May (649 mg m^{-2}) and June (501 mg m^{-2}). For all seasons, the NRMSE was below 20% for the Gaussian fit to SO_2 concentrations, confirming the model provided a good fit to the measured data.

SO_2 deposition was considerably higher at tree height than at ground level. The highest peak SO_2 deposition estimated from the Gaussian fit was found in February 2013 (2604 mg m^{-2} day^{-1}) for tree and February 2014 (620 mg m^{-2} day^{-1} for ground), though it was not possible to successfully fit a Gaussian curve to the February 2013 ground data. This is likely because the data collected during this sampling period did not straddle the centreline. June 2014 had the lowest SO_2 deposition maximum peak (240 mg m^{-2} day^{-1} for tree and 187 mg m^{-2} day^{-1} for ground). The centreline for June 2014 was also further north along the transect at around 790 m for both tree and ground. Other seasons had values between 40 m and 430 m for both site types for the centreline. For tree and ground sites, December 2013 had the widest plume. For tree height, the maximum plume integral was in February 2013, produced by the very high maximum deposition found during this time period. At ground level, the maximum integral was in February 2014. May and June 2014 had the lowest integrals for tree and ground sites for SO_2 deposition. Overall the NRMSE suggested the fit to the gas concentration data was much better than the deposition data.

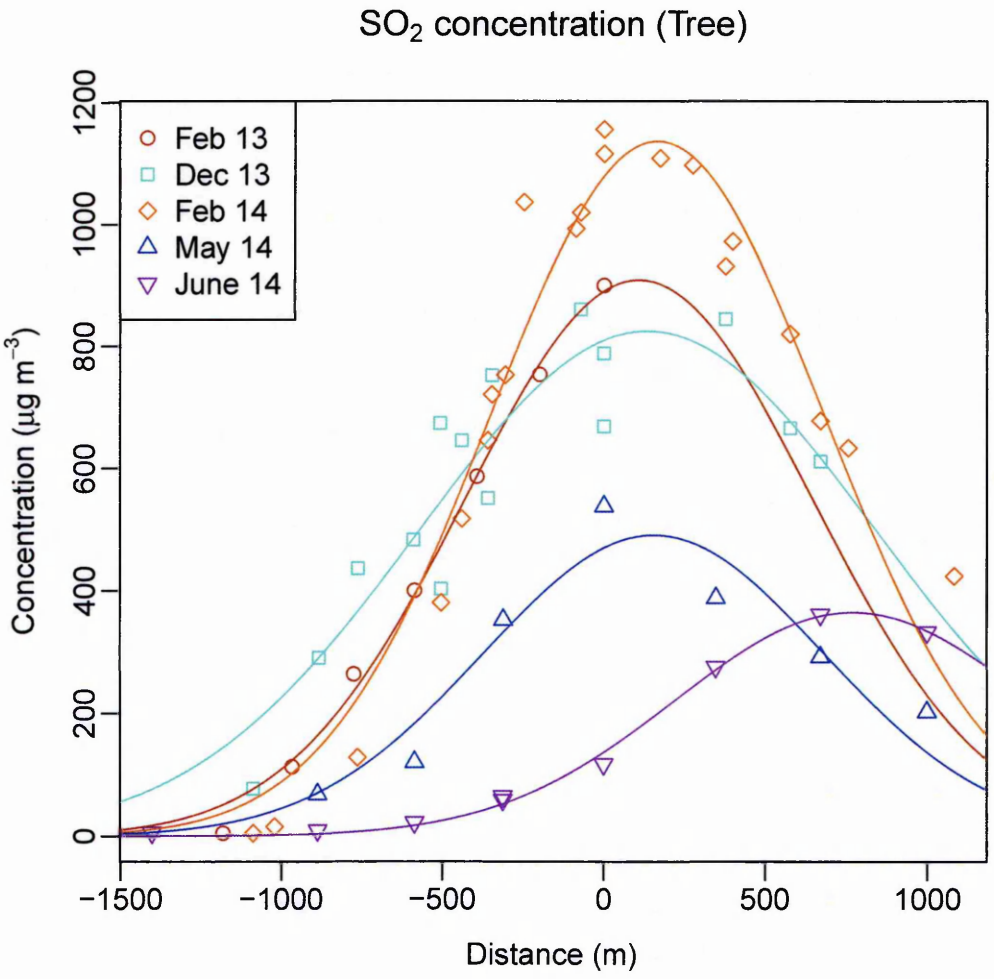

Figure 2.11: Variation in background corrected SO_2 gas concentration at tree height along the transect in the different sampling periods. The lines are best fit Gaussian curves, with parameters given in Table 2.12.

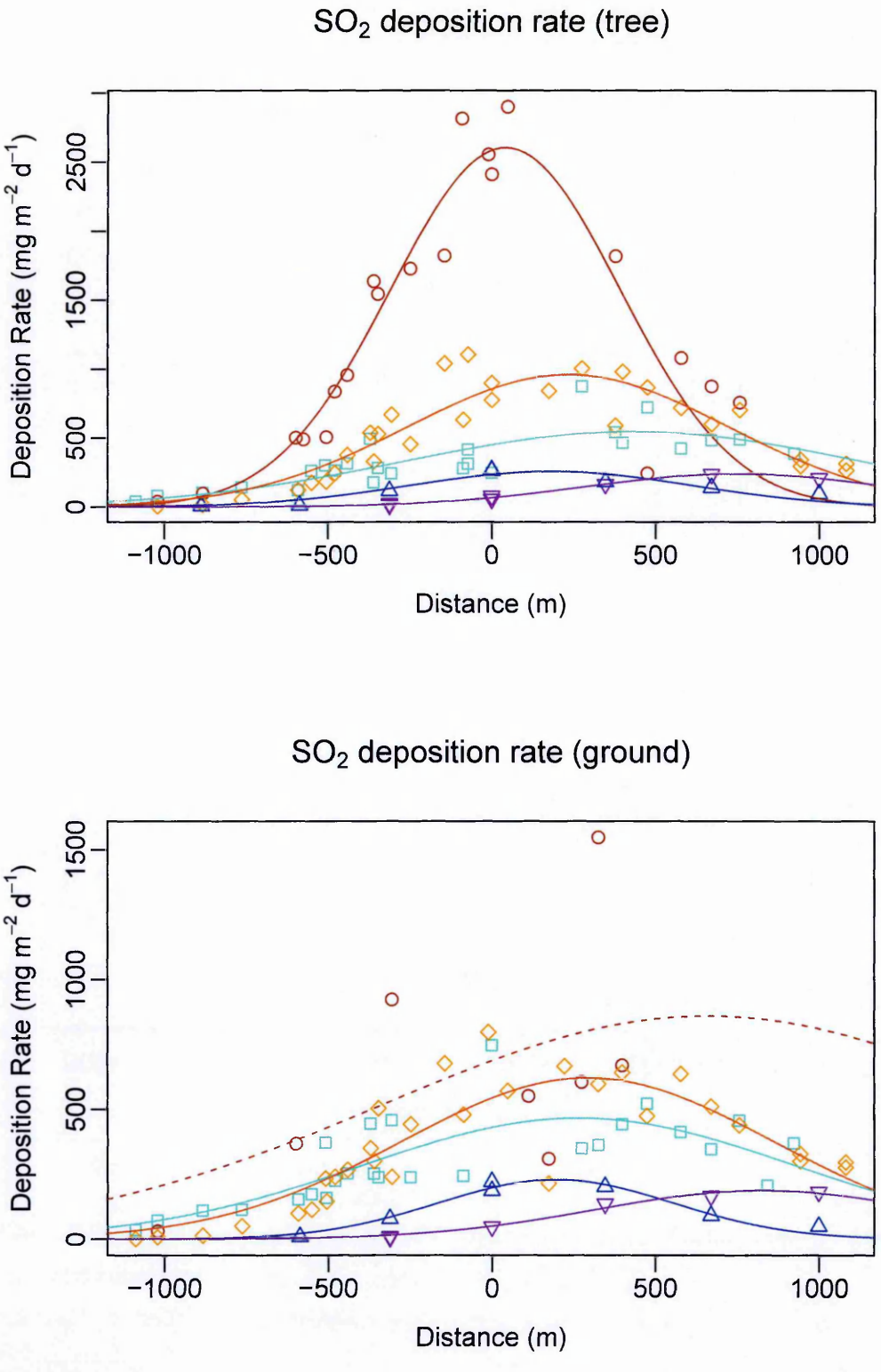

Figure 2.12: Variation in background corrected SO_2 deposition rate at tree and ground height along the transect in the different sampling periods. Colours and symbols as in gas concentration plots and a dashed line is used to show the curves that could not be successfully fitted, i.e. an NRMSE of less than 35%.

	Feb-13 SO_2	Dec-13 SO_2	Feb-14 SO_2	May-14 SO_2	Jun-14 SO_2
C_0 (μg m^{-3})	909	825	1137	490	364
$x_{0,C}$ (m)	108	135	165	155	770
σ_C (m)	537	704	515	528	549
$Integral_C$ (mg)	1224	1456	1468	649	501
$NRMSE_C$ (%)	5	14	11	18	6
Dt_0 (mg m^{-2} day^{-1})	2604	546	960	257	240
$x_{0,Dt}$ (m)	41	433	233	182	751
σ_{Dt} (m)	349	697	489	430	470
$Integral_{Dt}$ (g day^{-1})	2280	954	1177	277	282
$NMSE_{Dt}$ (%)	25	34	25	26	6
Dg_0 (mg m^{-2} day^{-1})		465	620	229	187
$x_{0,Dg}$ (m)		267	293	196	828
σ_{Dg} (m)		664	568	359	508
$Integral_{Dg}$ (g day^{-1})		774	884	206	239
$NMSE_{Dg}$ (%)		35	32	14	11

Table 2.12: Gaussian fit parameters for SO_2 gas concentrations at tree height and deposition rates at tree and ground heights along the transect across the different sampling periods. For the concentration data, C_0 is the maximum concentration, which occurs at distance $x=x_{0,C}$ and σ_C is the width parameter. The integral (calculated by Equation 2.7) and the $NRMSE_C$ (the normalized root mean squared error expressed as a percentage as in Equation 2.9) are both also shown. For the deposition data at tree ($_t$) and ground ($_g$) heights, D_0 is the maximum concentration, which occurs at distance $x=x_{0,D}$ and σ_D is the width parameter. The integral (calculated from Equations 2.12 and 2.13) and the $NRMSE_D$ (Equation 2.9) are both also shown. For both the concentration and deposition data, if the NRMSE were beyond the bounds of acceptability ($\geq$35%), the results in the table are blank.

2.3.3.3 HCl along the transect

Like SO_2, the highest maximum concentration for HCl estimated by the Gaussian fit (Table 2.13) was found during February 2014 (287 μg m^{-3}), and the lowest during the June 2014 sampling period (62 μg m^{-3}). Similarly, the centreline for June 2014 was considerably further along the transect (704 m) than the other sampling periods (less than 170 m). December 2013 had the widest plume (σ = 730 m) compared with other seasons (350 m to 470 m). February 2014 had the highest integral values (309 mg m^{-2}) and the lowest integral was June with 69 mg m^{-2}. According to the NRMSE the Gaussian fit was good for all seasons, though December 2013, had the highest NRMSE (29 %). This batch of acid gas diffusion tubes has suffered a chloride contamination, and this may have reduced the accuracy and precision of the data collected.

HCl deposition at tree height also reached a highest maximum in February 2013 (246 mg m^{-2} day^{-1}), and lowest maximum in June 2014 (50 mg m^{-2} day^{-1}). It was not possible to successfully fit a Gaussian distribution to the February 2013 ground data. The highest maximum deposition at ground level was in February 2014 (128 mg m^{-2} day^{-1}) whilst the lowest was June 2014 (35 mg m^{-2} day^{-1}). Like SO_2, the centreline was consistent between most seasons (February 2013, December 2013, February 2014 and May 2014) but a more northerly centreline was found in June 2014 (718 m for tree and 1058 m for ground). The widest plume was in December 2013 for tree (742 m) and in June 2014 for ground (912 m). February 2013 and February 2014 had high integrals for tree (244 mg km^{-1} day^{-1} and 202 mg km^{-1} day^{-1} respectively) and February 2014 had the highest integral for ground (177 mg km^{-1} day^{-1}). June 2014 had the lowest integrals for both tree and ground. As with SO_2 the NRMSE suggested that the fit to the gas concentration data was better than the deposition data.

2.3.3.4 HF along the transect

The peak HF concentration estimated by the Gaussian fit (Table 2.14) was highest in February 2014 (30 μg m^{-3}) and the lowest was in June 2014 (15 μg m^{-3}). The

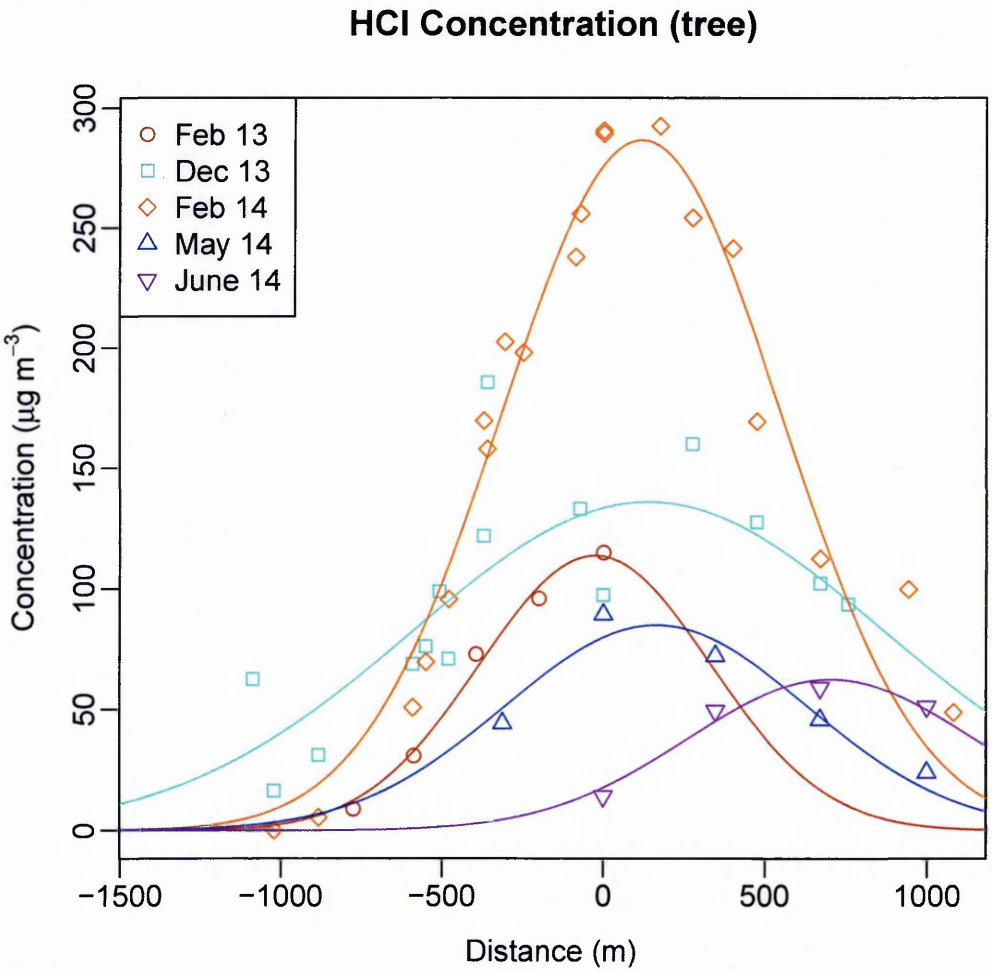

Figure 2.13: Variation in background corrected HCl gas concentrations at tree height along the transect across the different sampling periods. The lines are best fit Gaussian curves, with parameters given in Table 2.13.

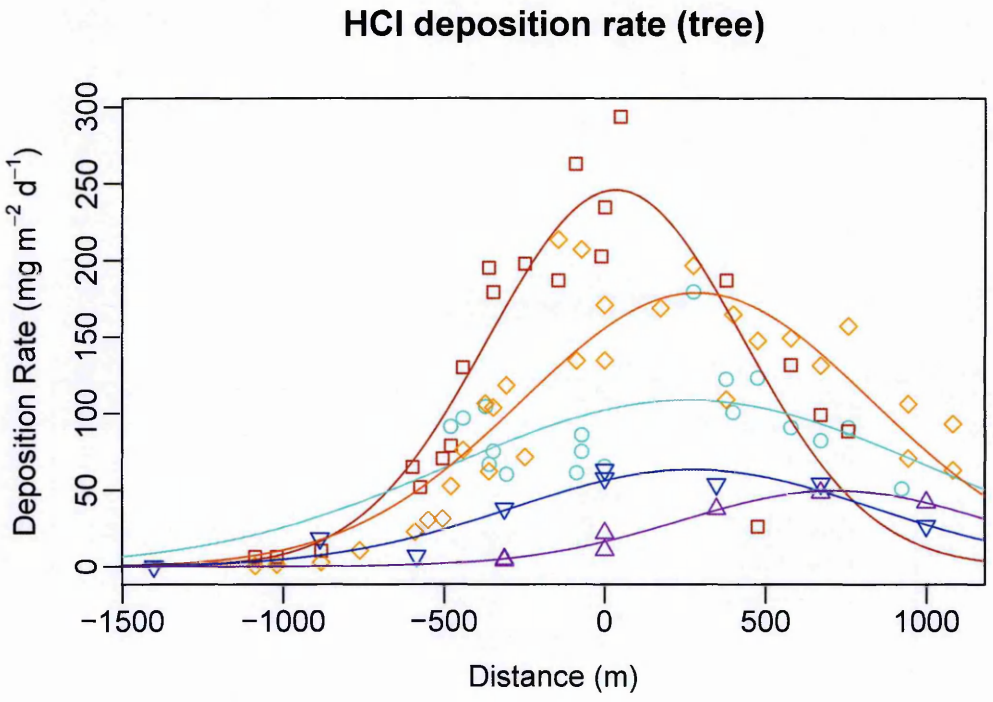

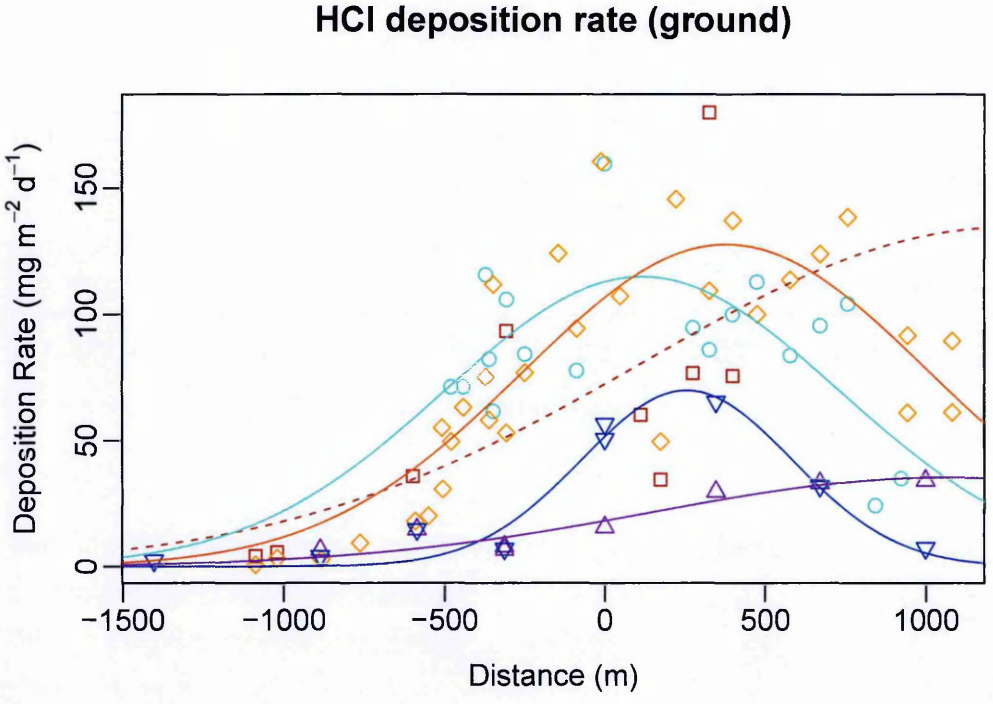

Figure 2.14: Variation in background corrected HCl deposition rates at tree and ground heights along the transect across the different sampling periods. The lines are best fit Gaussian curves, with parameters given in Table 2.13.

	Feb-13 HCl	Dec-13 HCl	Feb-14 HCl	May-14 HCl	Jun-14 HCl
C_0 (μg m^{-3})	114	136	287	85	62
$x_{0,C}$ (m)	-25	139	116	164	704
σ_C (m)	356	730	430	467	443
$Integral_C$ (mg)	102	249	309	99	69
$NRMSE_C$ (%)	6	29	13	12	8
Dt_0 (mg m^{-2} day^{-1})	246	109	179	63	50
$x_{0,Dt}$ (m)	34	261	287	275	718
σ_{Dt} (m)	396	742	544	560	481
$Integral_{Dt}$ (g day^{-1})	244	202	244	89	60
$NMSE_{Dt}$ (%)	28	29	29	20	13
Dg_0 (mg m^{-2} day^{-1})		115	128	70	35
$x_{0,Dg}$ (m)		117	379	256	1058
σ_{Dg} (m)		615	630	328	912
$Integral_{Dg}$ (g day^{-1})		177	202	57	81
$NMSE_{Dg}$ (%)		26	32	21	21

Table 2.13: Gaussian fit parameters for HCl gas concentrations at tree height and deposition rate at tree height and ground height along the transect across the different sampling periods. See Table 2.12 for a description of the parameters.

	Feb-13 HF	Dec-13 HF	Feb-14 HF	May-14 HF	Jun-14 HF
C_0 (μg m^{-3})	26	18	30	20	15
$x_{0,C}$ (m)	-47	163	149	338	1019
σ_C (m)	473	787	504	566	876
$Integral_C$ (mg)	30	36	38	28	33
$NRMSE_C$ (%)	9	25	29	24	30
Dt_0 (mg m^{-2} day^{-1})	57		33	8	8
$x_{0,Dt}$ (m)	32		240	198	862
σ_{Dt} (m)	414		504	486	650
$Integral_{Dt}$ (g day^{-1})	59		42	9	13
$NMSE_{Dt}$ (%)	24		26	11	12
Dg_0 (mg m^{-2} day^{-1})				10	7
$x_{0,Dg}$ (m)				210	827
σ_{Dg} (m)				242	522
$Integral_{Dg}$ (g day^{-1})				6	9
$NMSE_{Dg}$ (%)				8	10

Table 2.14: Gaussian fit parameters for HF gas concentrations at tree height along the transect across the different sampling periods. See Table 2.12 for a description of the parameters.

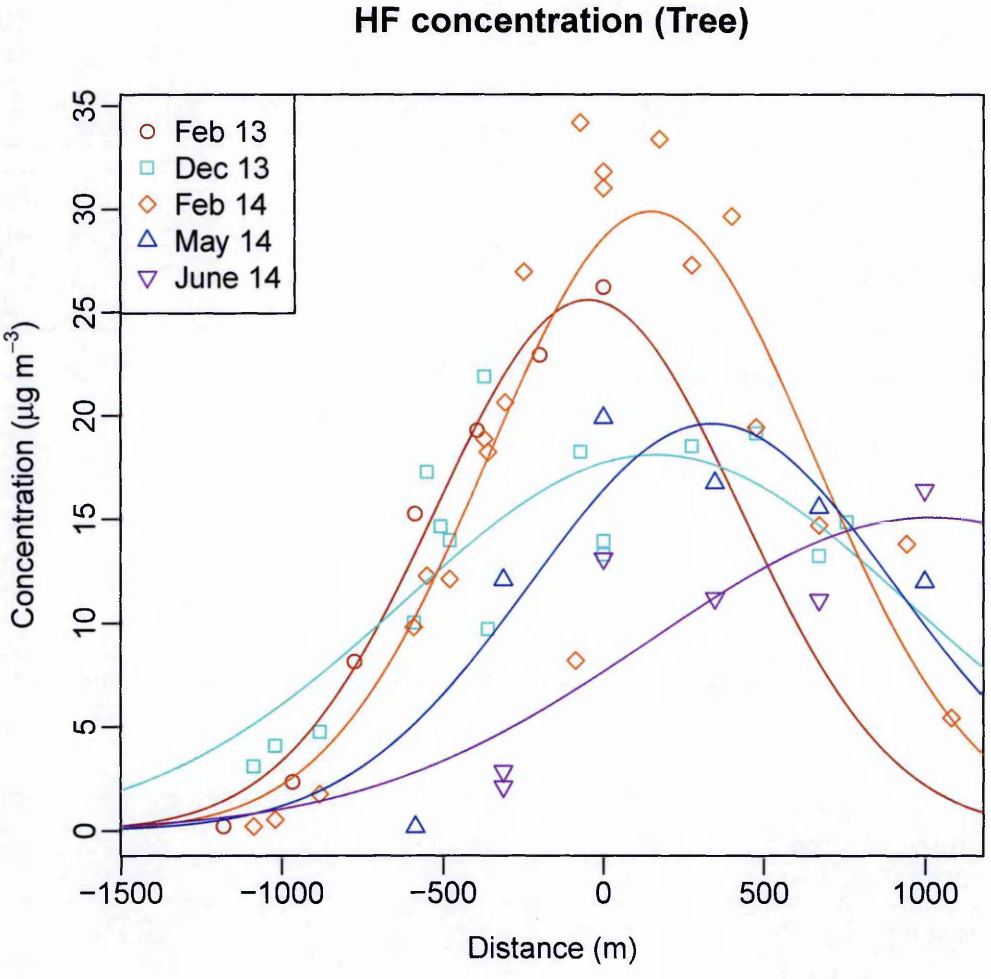

Figure 2.15: Variation in background corrected HF gas concentrations at tree height along the transect across the different sampling periods. The lines are best fit Gaussian curves, with parameters given in Table 2.14.

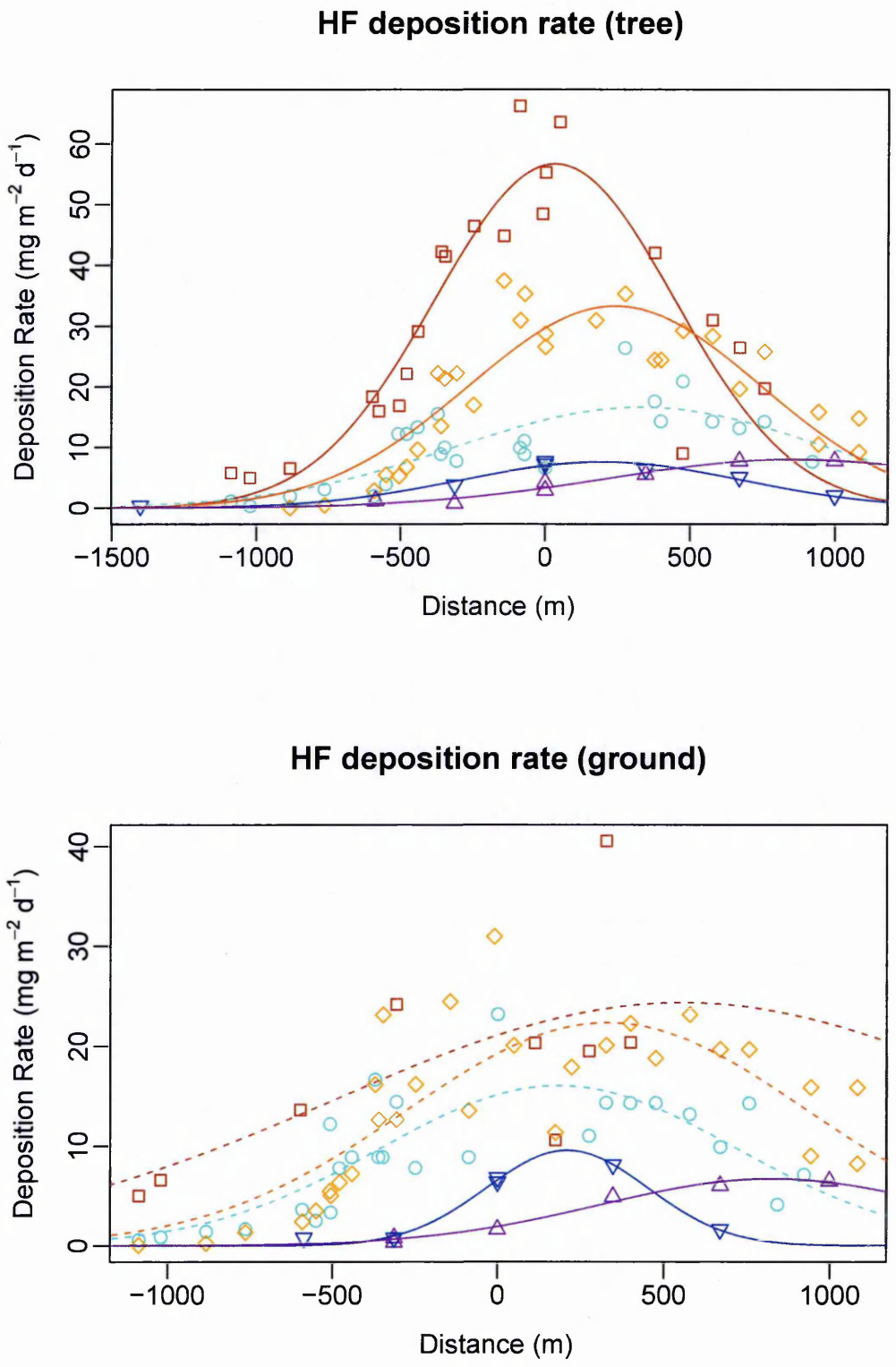

Figure 2.16: Variation in background corrected HF deposition rate at tree and ground height along the transect across the different sampling periods. The lines are best fit Gaussian curves, with parameters given in Table 2.14.

centreline position was more variable for HF, ranging from -47 m in February 2013 and extending as far as 1019 m for June 2014. The plume in the December 2013 sampling season was again wide, though June 2014 also had a large plume footprint for HF (876 m). The integral was between 28 mg m^{-2} and 38 mg m^{-2}. The NRMSE was very good (less than 10%) for the February 2013 Gaussian fit and was high but still within the bounds of acceptability for the other seasons for HF.

It was not always possible to successfully fit a Gaussian model to HF deposition at tree and ground height as the NRMSE value were too high and beyond the bounds of acceptability. The highest measured peak for tree height was in February 2013 (57 mg m^{-2} day^{-1}). The lowest maximums were in May and June 2014 (8 mg m^{-2} day^{-1}) for tree and June 2014 (7 mg m^{-2} day^{-1}) for ground. As with the other gases, the centreline for HF deposition was consistent between most seasons (February 2013, February 2014 and May 2014) but a more northerly centreline was found in June 2014 (862 m for tree and 827 m for ground). The widest plume was in June 2014 for tree (650 m) and ground (522 m). February 2013 had the largest integrals for tree (59 mg km^{-1} day^{-1}), and very low integrals were found in May and June 2014 at tree and ground height.

2.3.4 Deposition rates at tree and ground height

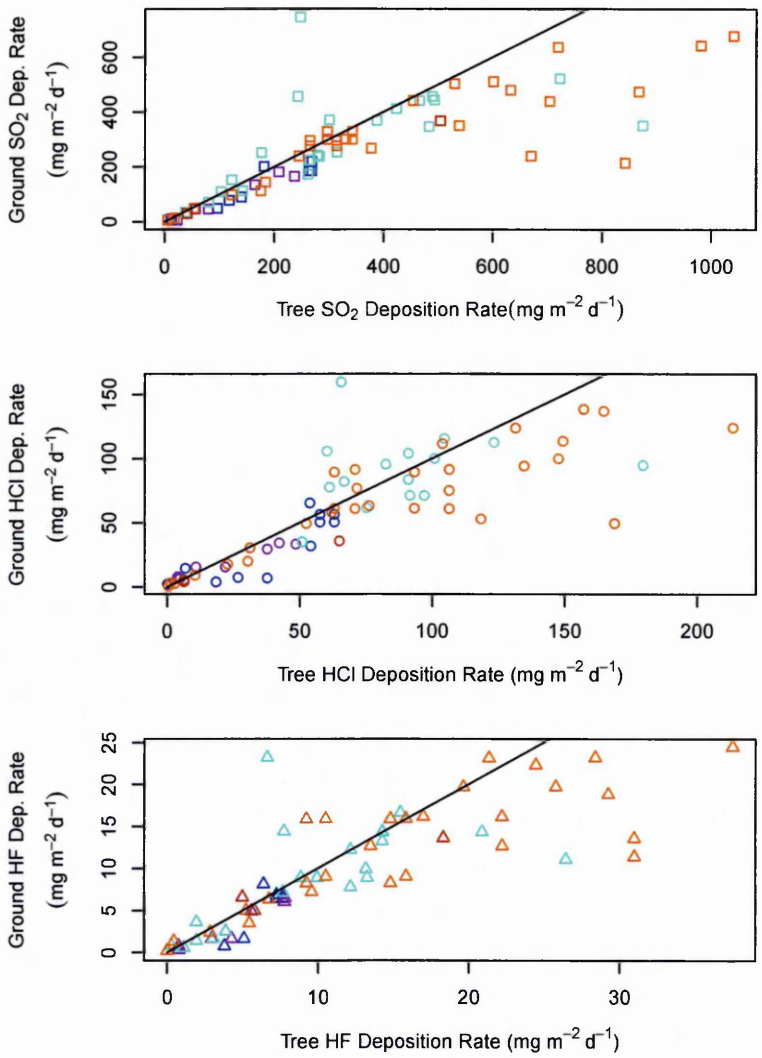

Figure 2.17: Variation in SO_2, HCl and HF deposition rate between tree and ground height along the transect across the different sampling periods. The line on the plots is 1:1. Seasons coloured as in previous plots.

The deposition rate of SO_2, HCl and HF was lower at ground level than it was at tree height (Figure 2.17). Some of the instances where ground deposition exceeded tree deposition might be explained by the variability in the sulphation plate data caused by analytical error. However, SO_2 deposition was 17.9 % lower at ground sites, HCl deposition was 15 % lower at ground sites and HF deposition was 16.8 % lower at ground sites, and this difference was significant at $p \leq 0.05$ for the three gases according to a paired t-test. The difference in deposition rate between tree and ground sites is

most pronounced at higher deposition rates.

2.3.5 Deposition velocities

For all gases, the estimated dry deposition velocities were lower at ground than at tree height, with the exception of HCl in June 2014 (Table 2.15). The difference in dry deposition velocities between tree and ground height might be because the concentration was only measured at tree height, whilst deposition rate was measured at both tree and ground height. It is not possible to determine whether the lower deposition velocity at ground height is as a result of a lower concentration at ground height, or because the environmental conditions closer to the ground produce a lower deposition velocity for a given atmospheric concentration.

	SO_2 T	SO_2 G	HCl T	HCl G	HF T	HF G
Dec 13	0.76	0.62	0.94	0.82		
Feb 14	0.93	0.70	0.91	0.75	1.29	
May 14	0.49	0.37	1.04	0.67	0.38	0.24
Jun 14	0.65	0.55	1.00	1.35	0.46	0.31

Table 2.15: Deposition velocities (cm s^{-1}) calculated from the integral of the Gaussian fit to gas concentration data and deposition data at tree (T) and ground (G) height. Since the exposure periods for the diffusion tubes and sulfation plates did not overlap during February 2013, this data has been omitted from the calculation of deposition velocities. Deposition velocities could not be calculated for HF at tree level in December 2013 and at ground level in December 2013 and February 2014, because it was not possible to successfully fit a Gaussian curve to these data.

At both tree and ground height, SO_2 had the highest deposition velocity in the driest month, February 2014. Deposition velocities were lower in December 2013, May 2014 and June 2014, at the end and beginning of the wet season. For HCl very similar deposition velocities were found across all sampling seasons at tree height. More variable lower velocities were found at ground height, with the exception of June 2014, where a high deposition velocity was estimated. Like SO_2, HF has the highest deposition velocity at tree height in February 2014. The lowest HF deposition velocities were found in May and June 2014 at tree height. It was only possible to estimate ground deposition velocities for May and June 2014 for HF, but these gave very low values.

2.3.6 HYSPLIT model

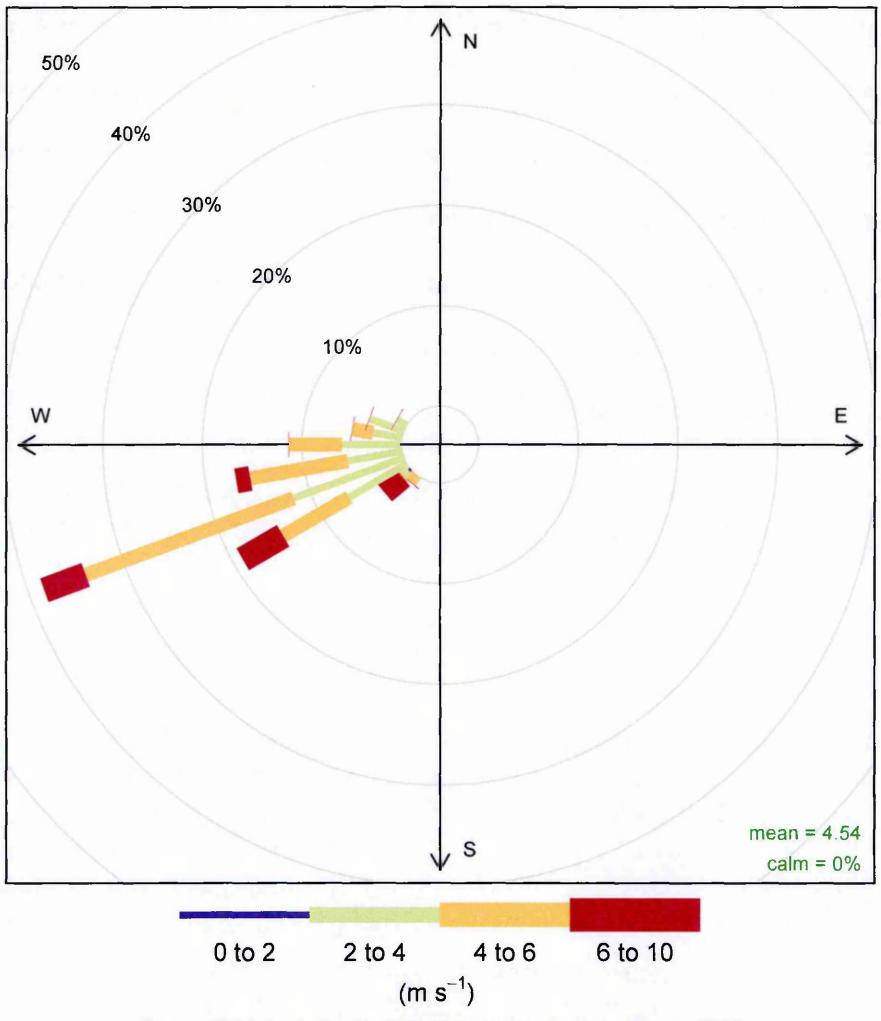

Figure 2.18: Wind rose of HYSPLIT trajectories for February 2013.

According to the HYSPLIT model, February 2013 had consistent winds that would blow the volcano's plume in a WSW direction, with relatively high wind speeds (Figure 2.18). In December 2013 (Figure 2.19), the area most likely affected by Masaya's volcanic gases was to the SW of the volcano, and wind speeds were slower than in February 2013. February 2014 (Figure 2.20) had a very similar wind rose to February 2013, but wind speeds were typically lower. In May and June 2014 (Figures 2.21 and 2.22)the majority of trajectories were towards the WSW of the volcano, but there were also more in the NW sector than in previous periods. Additionally, wind speeds were

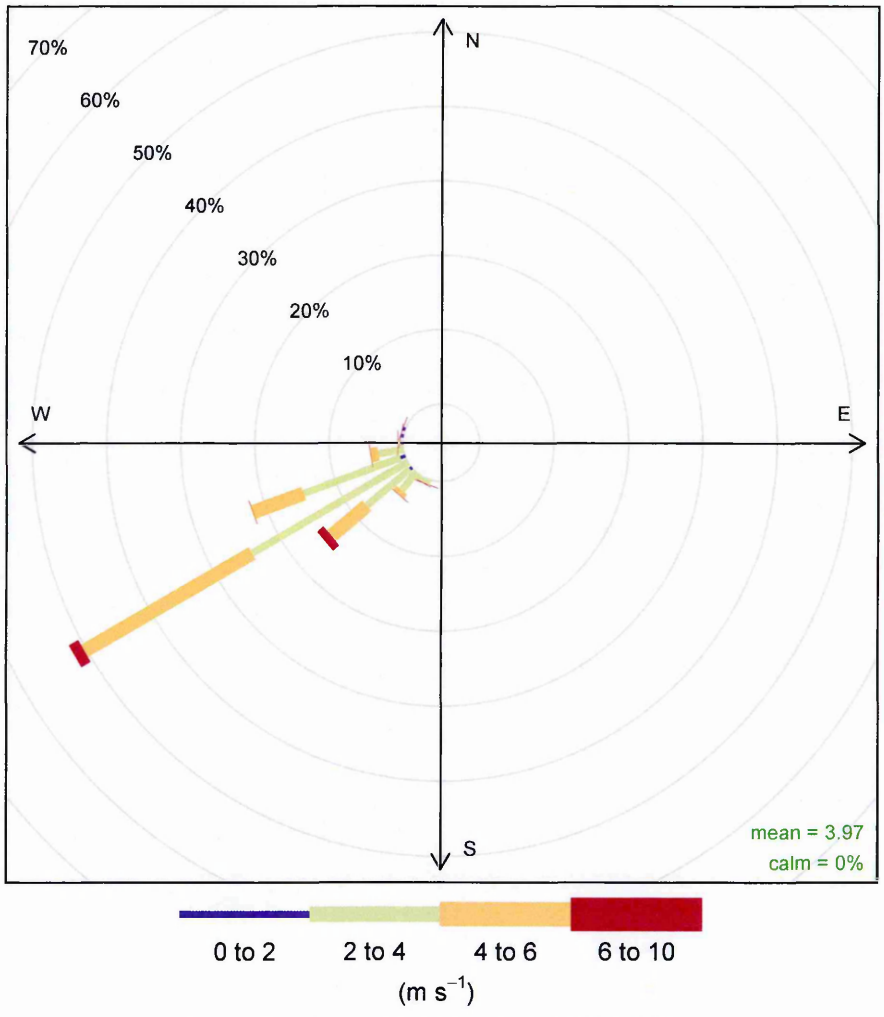

Figure 2.19: Wind rose of HYSPLIT trajectories for December 2013.

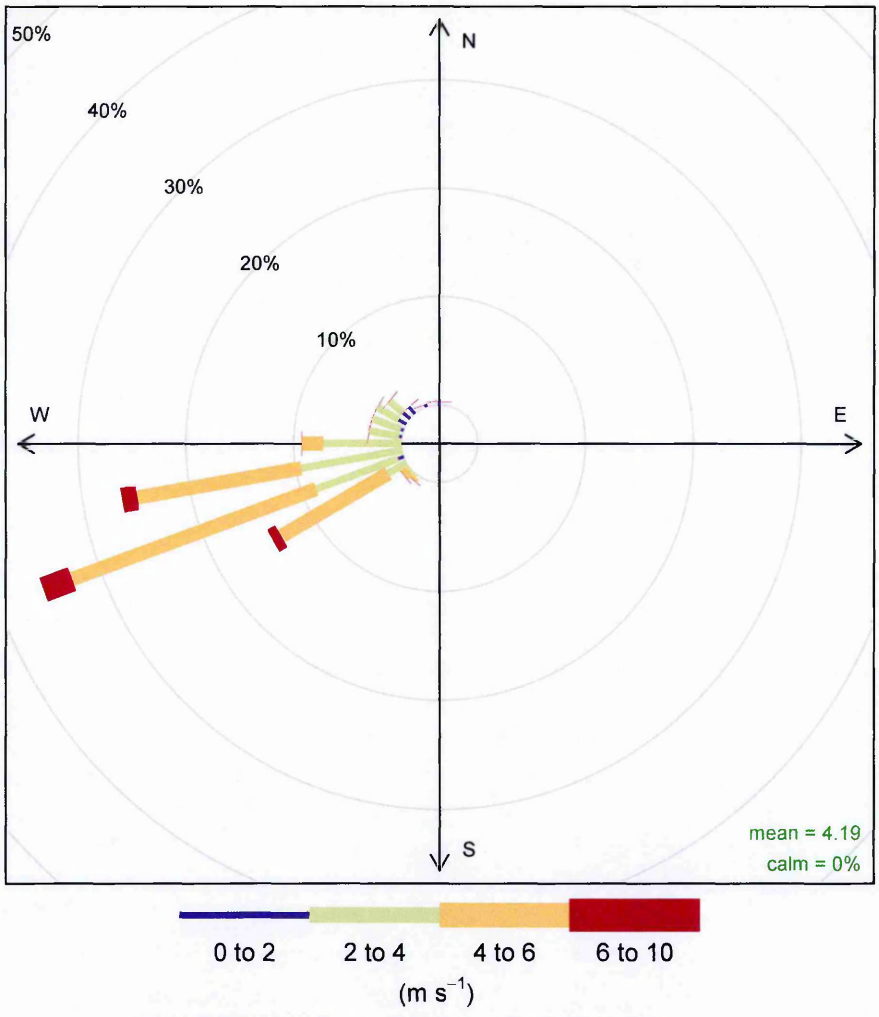

Figure 2.20: Wind rose of HYSPLIT trajectories for February 2014.

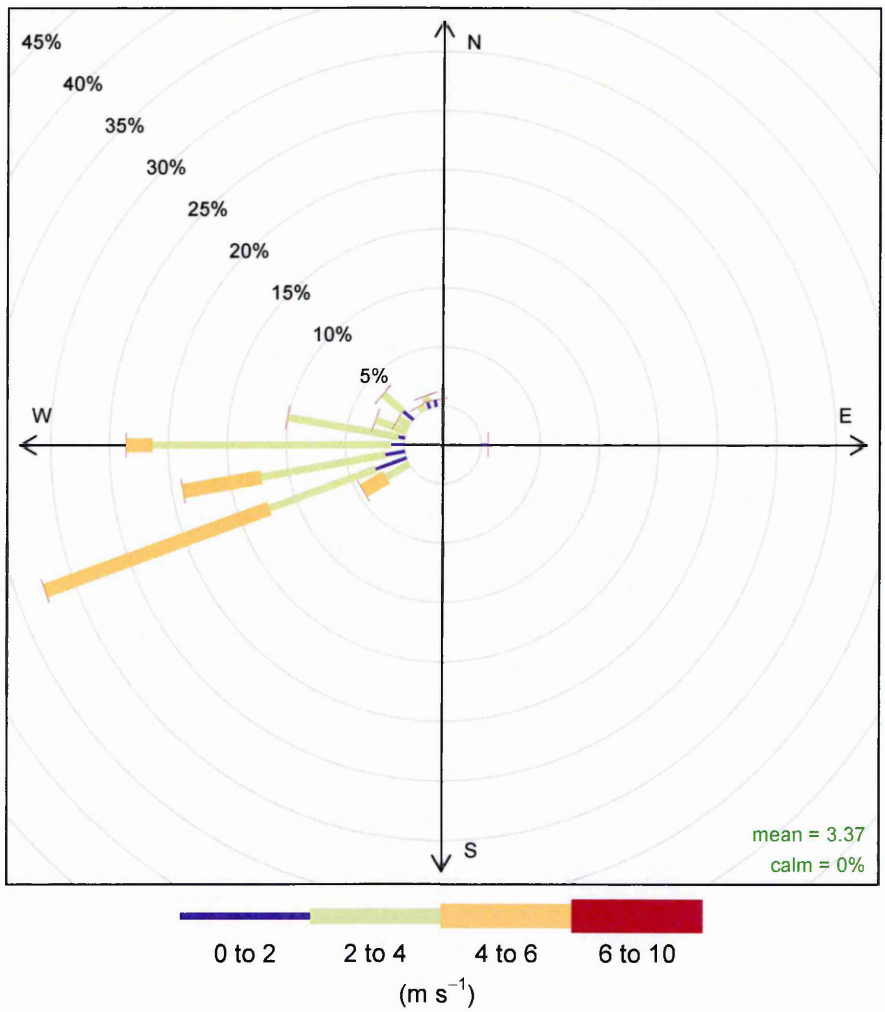

Figure 2.21: Wind rose of HYSPLIT trajectories for May 2014.

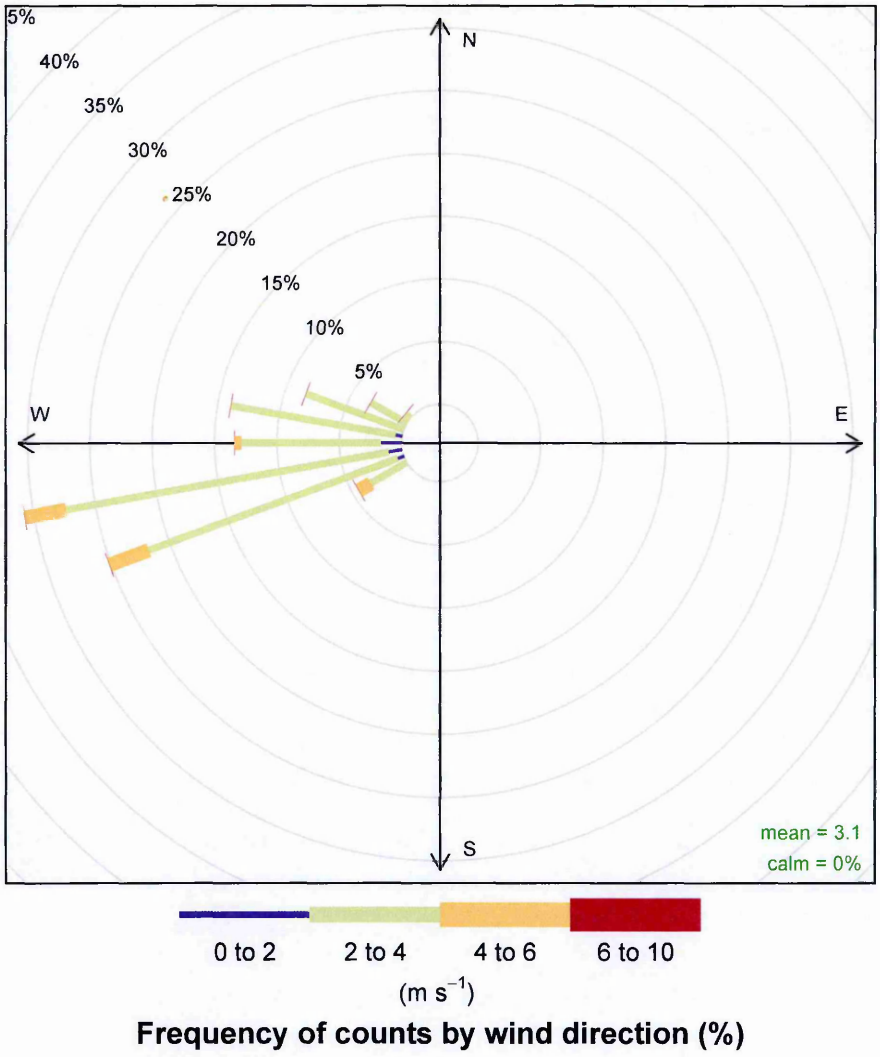

Figure 2.22: Wind rose of HYSPLIT trajectories for June 2014.

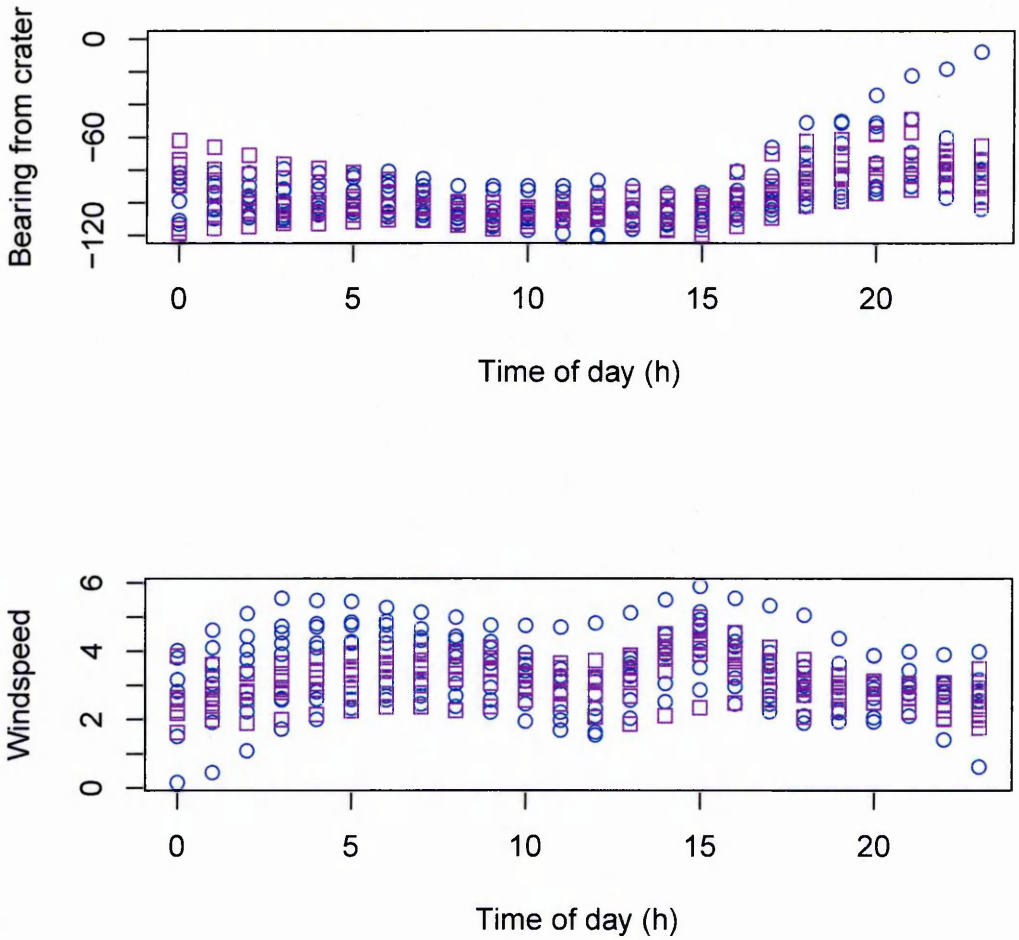

Figure 2.23: Influence of time of day on a) Bearing and b) Windspeed. Data shown is for May and June 2014.

considerably lower than in previous sampling periods.

Particularly in the May and June 2014 data sets, the wind direction and strength had a strong dependency on the time of day (Figure 2.23). In the day (6-18 h), the bearing is typically highly negative (less than 90), suggesting that the area to the SW of the volcano is most likely to be affected by volcanic gases. Additionally wind speeds are high, particularly early morning and mid afternoon. In contrast, during the nights (18-6 h) the bearing is slightly negative (between 0 and -90) indicating that the area to the NW of the volcano is most likely to be affected by volcanic gases. Additionally, there is a significant decrease in wind speed, which suggests that there had been a

weakening of trade winds. This would have strong implications for the impacted area depending on what time of day gases were emitted.

2.4 Interpretation

Data collected at the upwind sites showed very low background SO_2, HCl and HF gas concentrations, often below the limit of detection. Likewise, their deposition rates were low or below the limit of detection at upwind sites. Therefore, it is unlikely that there were any significant sources of the measured gases during the sampling periods, other than the actively degassing Santiago vent of Masaya volcano. A strong positive correlation between measured gas concentrations and deposition rates along the transect supports an argument that these are all of the same, volcanic, origin (Table 2.10). However, there was variability in gas concentration and deposition rates at the crater and along the downwind transect between sampling periods.

2.4.1 Crater

Very high gas concentrations (Table 2.5) and deposition rates (Table 2.6) were recorded at the crater rim sites. May 2014 and June 2014 had significantly lower gas concentrations and deposition rates than the other seasons, with the exception of HF concentration (Figures 2.9 and 2.10). Whilst this may appear to show a decrease in gas emissions from Masaya volcano during this study, this must be interpreted with caution because the data collected represent periods of several weeks and it is not possible to quantify emissions outside of these sampling periods. This data does highlight the long-term variability in gas emissions between the different sampling periods. There is an order of magnitude difference between the maximum and minimum recorded gas concentrations and deposition rates during the five sampling seasons. Additionally, gas concentrations at the crater were twice as high during the May 2014 sampling period than the following week in June 2014. Therefore, there is also considerable short-term variation in gas emission rates from Masaya volcano.

2.4.2 Transect

Variations in Gaussian distribution parameters for gas concentrations and deposition rate were found between the seasons along the downwind transect. These were likely affected by the emission rate of volcanic gases and wind characteristics at the time of emission.

2.4.2.1 Gas concentration and deposition rate integral

The integral, which represents the total gas concentration or deposition along the transect, is calculated as a product of the peak concentration (or deposition rate) and the width. There was no relationship between the peak concentration or deposition rate predicted from the Gaussian best fit model and the width (Figure 2.24). Additionally, there is a larger variation in peak concentration or deposition rate than there is in the width parameter for all Gaussian fits across the seasons. The peak concentration will likely have been controlled by gas emission rates at the crater, as well as wind parameters, and the width is likely to vary according to wind parameters.

Therefore, the gas emission rate at the crater is likely to be a strong control on downwind gas concentrations and deposition rates, and consequently the calculated integral values. With the exception of all HF measurements and SO_2 deposition rate at ground height, there was a significant relationship between measurements at the crater at site OCP and the integral (Figure 2.25). Additionally, wind speed, the height of the plume, the standard deviation (or width) of this height and atmospheric stratification could also have affected the peak concentration and therefore integral of gases along the downwind transect. Although atmospheric stratification was not measured during this study, the plume height and wind speed could be estimated from the HYSPLIT model but these did not explain variation in the transect integral or width.

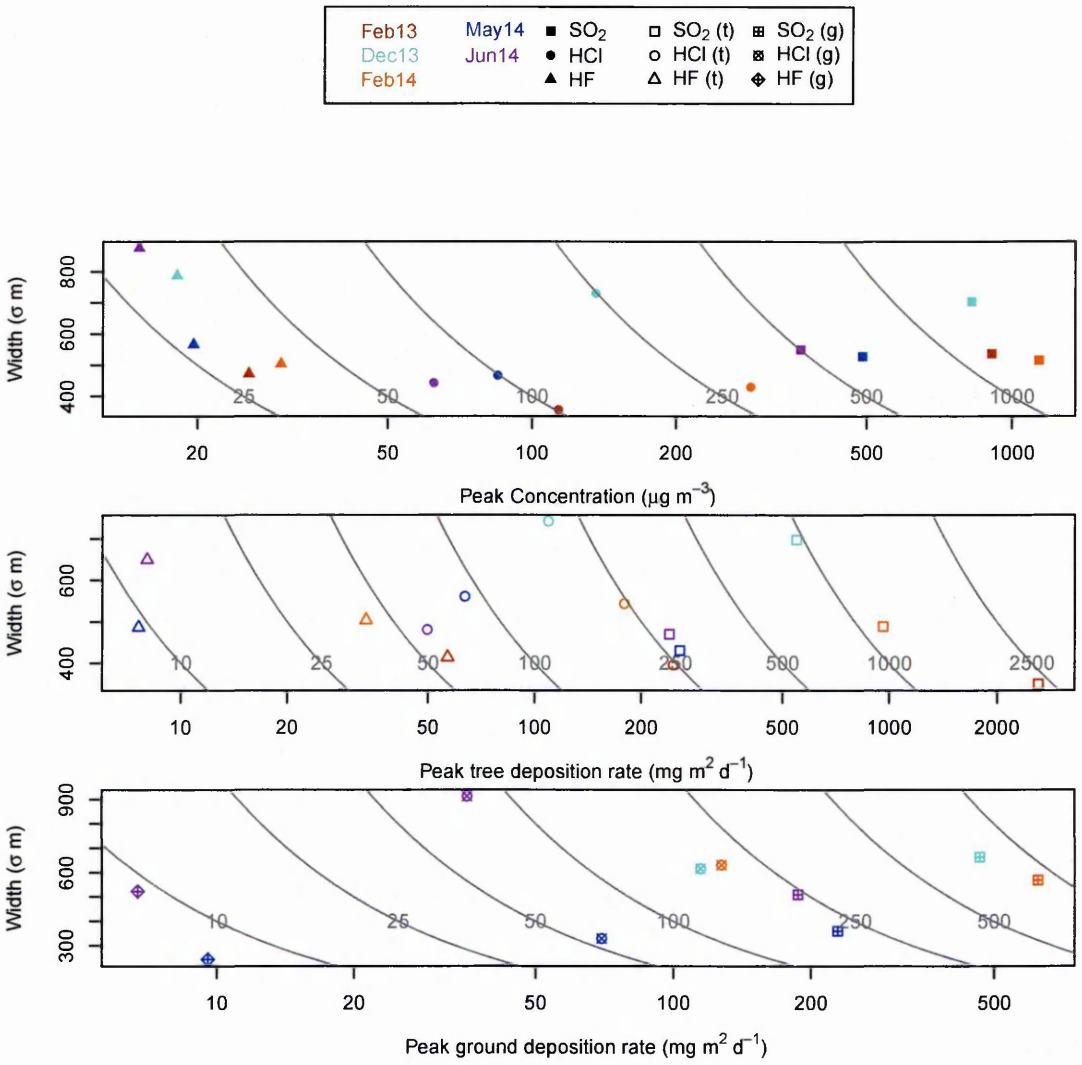

Figure 2.24: Maximum concentration/deposition rate and width for all seasons, using a logarithmic scale for peak concentration or deposition rate. Grey lines show integral values measured in mg for concentration data and g day^{-1} for deposition rate data at tree and ground height.

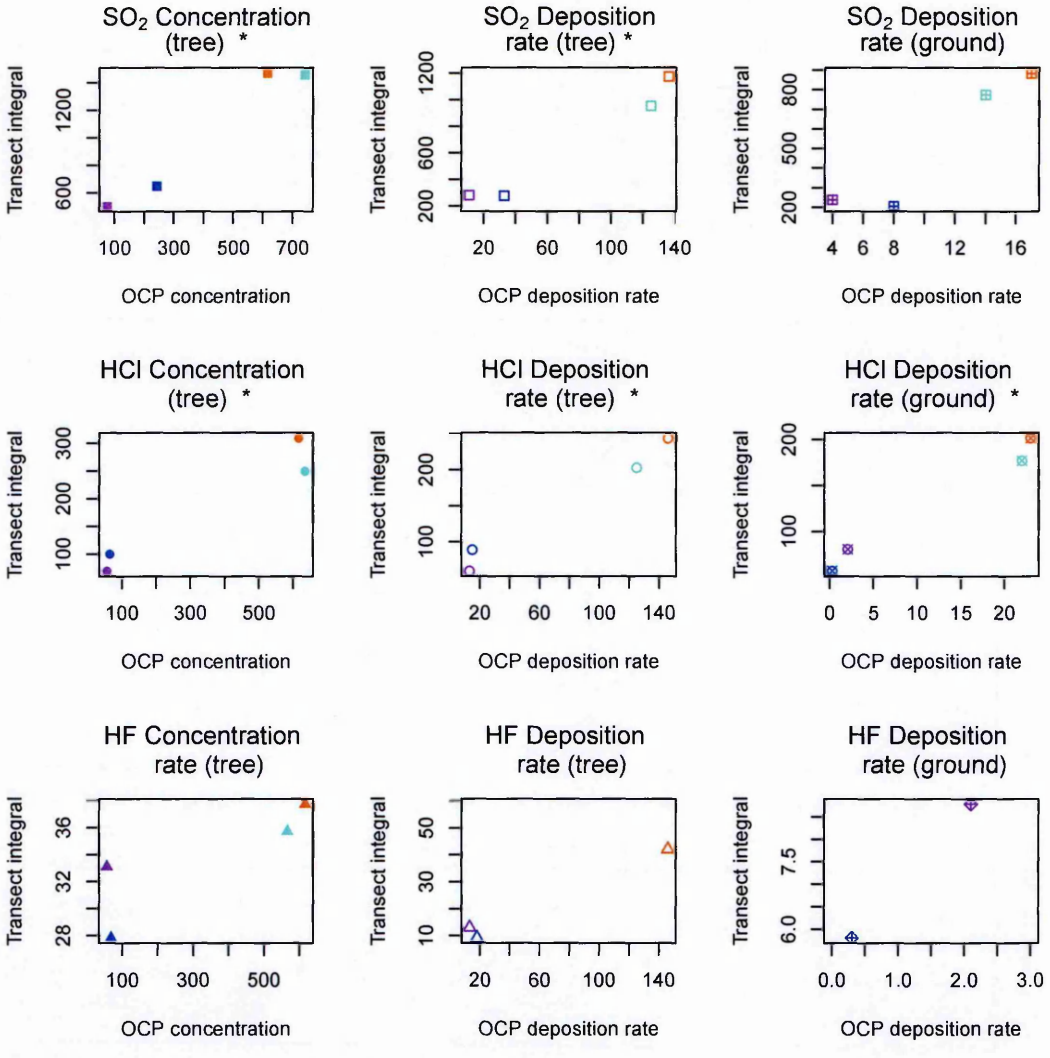

Figure 2.25: Concentration or deposition rate measured at OCP (crater) against the transect integral, for each gas. Season colours are as in previous plots. The concentration at OCP (Old Car Park crater site) is measured in μg m^{-3} and the deposition rate at this site is measured in mg m^{-2} day^{-1}. The integral has a unit of mg for concentration data and g day^{-1} for deposition rate data. A star shows correlations significant at the p$\leq$0.05 level. Where a tree or ground height measurement was not available from the OCP site, the other was used as a substitute. February 2013 has been excluded from this analysis as the data collected along the transect did not coincide with the data collected at OCP.

2.4.2.2 Plume direction and width

Within seasons, the estimated plume centreline and width remained similar between gases and measurement type (Figure 2.26). February 2014 and May 2014 had similar distributions of width and centreline estimates (Figure 2.26). February 2013 had a much lower centreline, whilst June 2014 had a much higher centreline. A wider plume distinguished December 2013. This consistency between the different gases measured in the same seasons supports the validity of the Gaussian best fit models. There was greater variation in estimated values for the position of the centreline than the width.

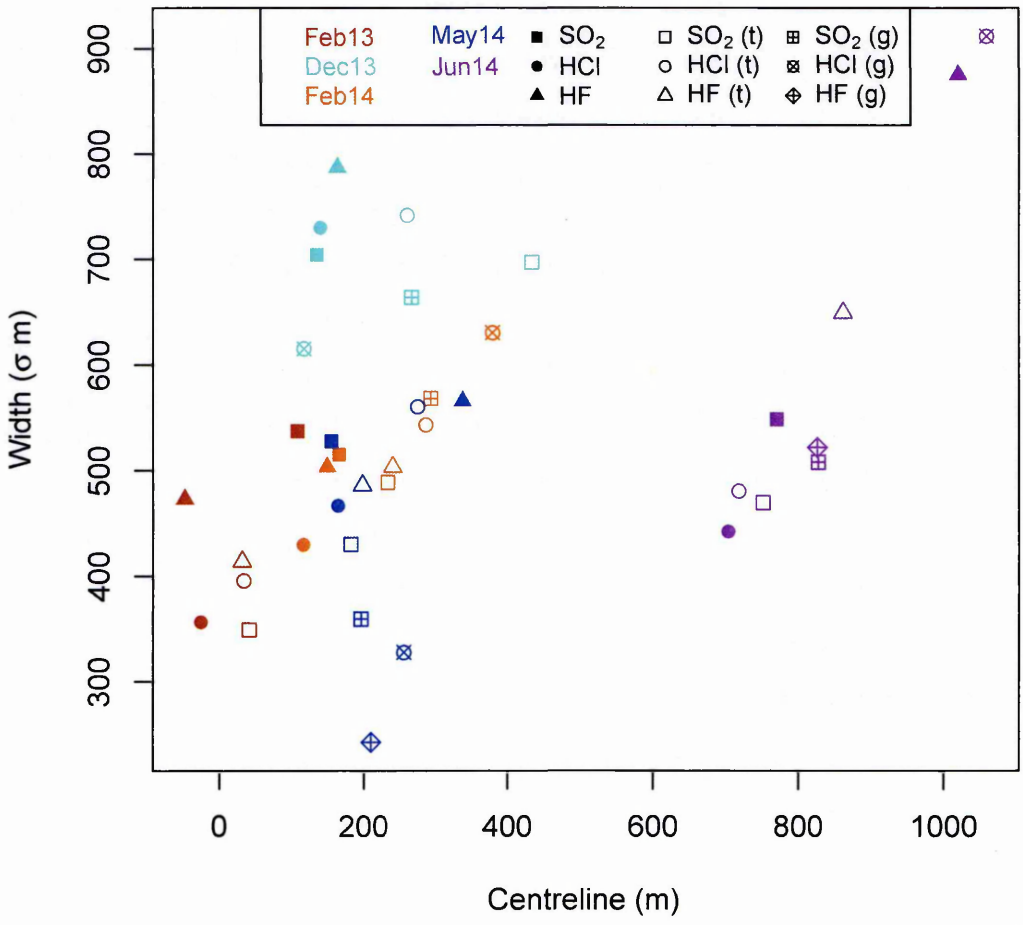

Figure 2.26: Centreline and width parameters for all seasons and gases. Colours and symbols as in previous plots.

It is expected that the mean bearing of the wind direction, i.e. the predominant direction in which the wind was blowing, would have an effect on the position of the centreline. It was possible to convert the wind bearing from the HYSPLIT model to an estimated position along the transect using trigonometry. The centreline position for all measured gas concentrations and deposition rates (SO_2, HCl, HF) was taken from the Gaussian best fit model. Correlation between these two was significant at $p \leq 0.01$ (Figure 2.27).

Differences between the observed Gaussian centreline and the HYSPLIT bearing are likely because both degassing and the wind direction are temporally variable on very short timescales (hours, minutes), so gas emission rates might have been high when the wind direction was atypical. Additionally, it is possible that the height of the plume varied with the time of day, and that an inversion layer could trap the plume near the ground at night causing more intense fumigation. Local topography, such as the caldera wall might also have influenced the wind direction.

The rate of degassing from the crater, as approximated by gas concentration and deposition rates at OCP appears to be a strong control on the total volume of gas reaching the downwind transect. The wind direction determines the area most affected by emitted gases. Therefore, using gas emission and wind direction data might allow for forecasts of how downwind areas might be affected by degassing without the need for extensive measurements. This data is of great use to identifying potential impacts on the downwind environment, including local people. This approach could also be tested at other volcanoes to produce similar profiles of the downwind gas concentration and deposition rate along a transect through the plume. Further work is required to constrain the contribution of other wind parameters (wind speed, plume height and atmospheric stratification) to the seasonal variation in the gas concentration and deposition rate patterns along the transect.

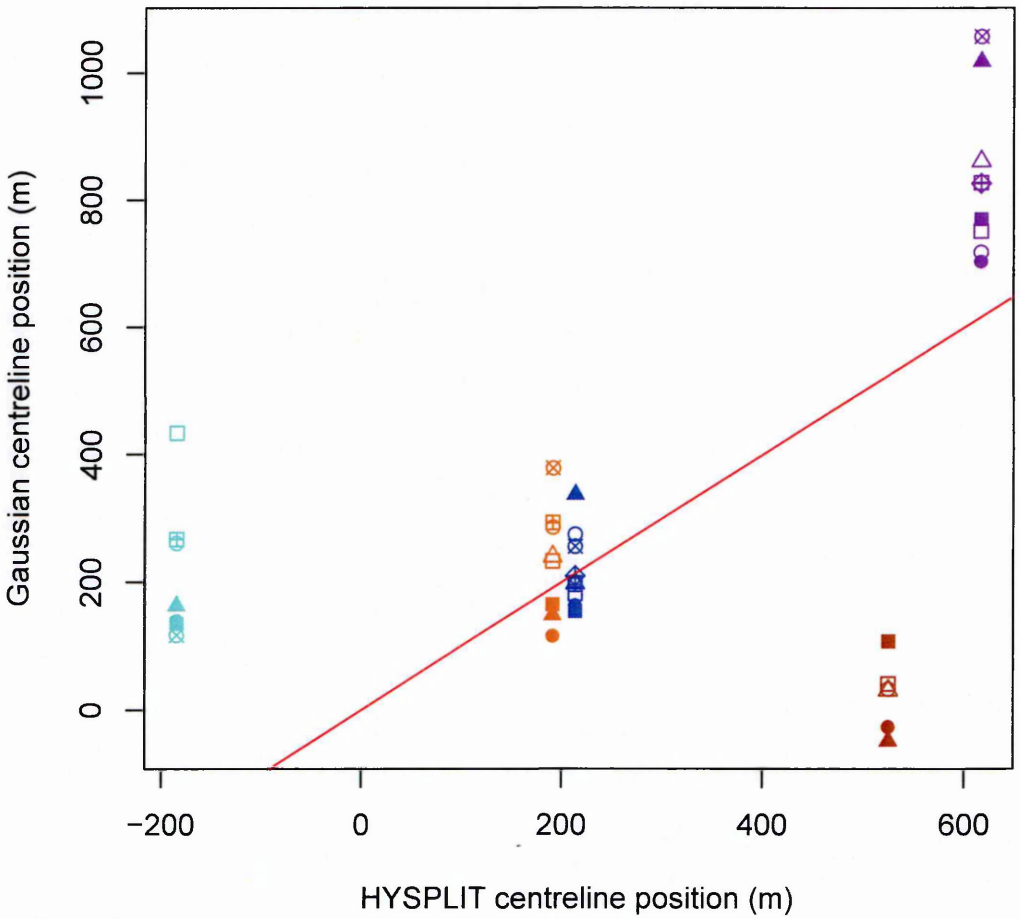

Figure 2.27: Centreline estimated from the bearing from HYSPLIT model against the Gaussian centreline estimated for each season and gas. Colours and symbols as in previous plots. A 1:1 line is shown in red.

2.4.3 Deposition rates at tree and ground height

Along the transect, it was also evident that deposition rates were lower at ground level than at tree height, which is most noticeable for the sites where deposition rates are highest, i.e. those closest to the centreline of the plume. Deposition rates are a function of the atmospheric concentration of a gas and the deposition velocity for that gas onto a particular surface. Since diffusion tubes were only exposed at tree height, and not ground height, it was not possible to determine whether there was a lower atmospheric concentration of the SO_2, HCl and HF at ground level than at tree height. Additionally, it is possible that atmospheric conditions such as wind speed and turbulence were slightly different at the two heights, therefore, producing a difference in deposition rates.

Although this difference cannot be explained, it is likely to have implications for the exposure of plants growing at different heights. A vertical gradient in exposure to volcanic gases might produce shorter growing plants or favour species with low forms e.g. grasses and herbs over trees. This will be explored in later chapters on the ecological impacts of these gases. Further study of how volcanic gas concentrations and deposition rates change with height would be beneficial in determining the extent to which this might influence vegetation.

2.4.4 Deposition velocities

Further downwind of Masaya, SO_2 deposition velocity was estimated at a mean of 1.6 ± 0.8 cm s^{-1} with a range of 0.5 to 3.8 cm s^{-1} (Delmelle *et al.* , 2001). The deposition velocities calculated for SO_2 in this study (Table 2.15) are slightly lower than those obtained by Delmelle *et al.* (2001) but are still within their range. A likely explanation for this difference is the sampling season, since Delmelle *et al.* (2001) collected their data during the driest months of the year (February and March). In this study, deposition velocities were highest during the driest sampling period (February 2014). This is possibly because sulfation plates measure dry deposition only, so do

not account for wet deposition through precipitation, which occurred more frequently during the rainy season (December 2013, May 2014 and June 2014).

No previous estimates of chloride or fluoride deposition velocities were found at Masaya. Since the deposition efficiency of chloride and fluoride onto sulphation plates is unknown, the values estimated in this study may be incorrect. However, given there was a strong relationship between all measured atmospheric concentrations and deposition rates, they provide a useful estimate and identify a significant source of acid loading to the proximal downwind environment.

2.4.5 Comparison with other studies

One previous study has reported volcanic gas concentrations measured with diffusion tubes at the crater edge of Masaya (Allen, 2002), which found a mean of 4756 μg m^{-3} SO_2, 929 μg m^{-3} HCl and 203 μg m^{-3} during sampling in May 2001. Their sampling location appears to be closest to H1 reported in this study and their sampling methods were similar. Compared with the study by Allen et al (2002), results presented here for H1 show considerably lower gas concentrations, with the exception of HCl in February 2014 which had a very high value (Table 2.16). Similarly, atmospheric gas concentrations measured using filter-packs in 2001 and 2003 detected significantly higher gas concentrations of 7736-11073 μg m^{-3} SO_2, 1680-1982 μg m^{-3} HCl and 124-214 μg m^{-3} HF. Therefore, it appears that gas emissions were much lower during the study periods reported here than they were in 2001.

	SO_2		HCl		HF	
	a	b	a	b	a	b
Minimum	916	881	183	263	25	35
Maximum	7950	2083	1300	2056	448	196
Mean	4756	1577	929	1032	203	103
Standard Deviation	3314	622	432	923	171	83

Table 2.16: Comparing crater values from a) Allen et al. (2002) and b) site H1 from this study using diffusion tubes measured in μg m^{-3}.

No previous studies have looked at proximal downwind gas concentrations, though

further downwind (about 6 km) a maximum of 610 μg m^{-3} SO_2 was recorded in 1999 (Delmelle *et al.* , 2002). Another study across a similar area in 2012 (van Manen 2014b) found a maximum recorded SO_2 concentration of 471 μg m^{-3}, that of HCl was 40 μg m^{-3} and HF was 7.6 μg m^{-3}. It would be expected that higher gas concentrations would be found closer to the volcano, which fits with SO_2 measurements for February 2013, December 2013 and February 2014, but not for the May and June 2014 sampling season in this study. All HCl and HF measurements in this study were higher than those recorded previously further downwind.

This supports the hypothesis that gas emissions from the volcano were much lower than previously in May and June 2014, and possibly during other seasons too. This variability in gas emissions is due to the cyclical nature of degassing from Masaya (Rymer *et al.* , 1998). This suggests that maximum gas concentrations and deposition rates would have previously been much higher along the transect, when gas emissions from the crater were higher.

The World Health Organization (WHO) recommends that human exposure to SO_2 concentrations above 500 μg m^{-3} for periods of more than 10 minutes, or to concentrations above 20 μg m^{-3} over a 24 hour period, should be avoided as these are hazardous to human health (WHO, 2011). SO_2 concentrations measured at the crater are clearly highly toxic, though human exposure to these is variable. For tourists, who might come to the crater (nearest site is NCP) it's unlikely that this short term exposure will damage their health, but for local people who work around the volcano, including long periods at the crater edge, and are continuously exposed to low gas concentrations elsewhere, this is likely to produce health problems. For example, some park guards regularly complain of headaches and nausea that they believe is related to long-term exposure to volcanic gases from Masaya.

Despite an apparent decrease in volcanic gas emissions at Masaya, gas concentrations and deposition rates measured at the crater and along the transect were incredibly high. Studies of gas concentrations ($\leq$ 25 μg m^{-3}) and deposition rates ($\leq$ 250 mg m^{-2} day^{-1}) estimated using the same methods downwind of industrial sites found

considerably lower values (Lynch *et al.* , 1978; Bourque & Arp, 1996; Ta *et al.* , 2005; Tasdemir & Gunez, 2006; Staszewski *et al.* , 2011; Godoi *et al.* , 2013). Equally, bulk deposition estimates, which include precipitation, were much lower (10-40 mg m^{-2} day^{-1}) in previous studies at industrial sites (Likens *et al.* , 2001; Gauci *et al.* , 2004). A maximum of 720 μg m^{-3} SO_2 was found at Mt Etna using diffusion tubes (Bellomo *et al.* , 2007), whereas almost three times this amount was measured at the crater rim in this study. Many other studies of volcanic gas emissions use spectroscopy (Horton *et al.* , 2005; Williams-Jones *et al.* , 2005; Palma *et al.* , 2008; Barrancos *et al.* , 2008), providing results in tonnes of SO_2 emitted per day. Whilst it is not possible to compare these data to concentration or deposition rate data collected in this study, both of these methods show temporal variability in measured values on a variety of scales.

This is a highly important consideration for studies aiming to use volcanic (or industrial) gas data collected over a short time periods to define thresholds for the environmental or ecological response. This is because a short measurement period may not be fully representative of the long-term conditions, as both volcanic emissions and their dispersal vary through time. The downwind environment and ecosystems may be responding to current, recent and past gas concentrations and deposition rates.

2.4.6 Applications

In the following chapter on the effects of these gases on the vegetation community as a whole, an average exposure based on the centreline and width from each season from the SO_2 concentration data is used. Concentration data generally had a stronger fit to the Gaussian curve than deposition data, and SO_2 had a stronger fit than other measured gases. Only SO_2 concentration was selected as gas concentration and deposition rates had strong correlations with each other, implying a high degree of collinearity.

Chapter 4, which considers the growth response of individual plants, will use the SO_2 concentration and deposition rate data collected in the corresponding season, since

the subject of this chapter is expected to show a more immediate response to fluctuating gas levels. Additionally, this chapter considers two plant species growing at different heights. This means that having SO_2 deposition data at tree and ground height will be useful.

As well as allowing for estimates of gas concentrations and deposition rates along the transect, fitting a Gaussian model to the volcanic gas emission data reported in this chapter contributes to our understanding of the dispersal of plumes. Further work to quantify the impact of other meteorological variables and variation in gas emission rates would allow for forecasts of volcanic or industrial gas distributions without the need for extensive measurements over a large spatial area.

2.5 Conclusions

Data collected using diffusion tubes and sulfation plates have shown that there are no significant sources of volcanic gases in the atmosphere (SO_2, HCl and HF) or their deposition rate at sites upwind of the volcano. This is supported by strong consistent WSW wind directions predicted using the HYSPLIT model. Extremely high gas concentrations and deposition rates were found at the crater. Although gas concentrations exceeded WHO guidelines (WHO, 2011), considerably higher concentrations have been detected during previous sampling (Allen, 2002).

Measurements collected along a downwind transect for both gas concentrations and deposition rate data fitted a Gaussian distribution with the exception of some of the deposition rate data. This supports the use of a Gaussian model in our understanding of the dispersal of gas plumes. Between the seasons and gases, there was variation in the peak, width and centreline position of the fitted Gaussian model. There were strong differences between deposition rates of plates exposed at different heights (tree and ground), particularly at high deposition rates. This will likely have different implications for different vegetation types depending on their growth height.

Variation in gas emission rates from Masaya, estimated by OCP (crater) concentration and deposition rate values, was able to explain the total amount of most volcanic pollutants measured downwind of Masaya. The centreline from the Gaussian fit was correlated with the wind bearing modelled using HYSPLIT. Additionally, during the wetter sampling periods, dry deposition velocity was lower, probably as a result of increased wet deposition through precipitation. Alongside further work on the role of other meteorological data (wind speed and height) in influencing downwind concentration and deposition rates, these findings could be used to forecast how downwind areas might be affected by volcanic degassing at Masaya and other volcanoes.

The high atmospheric gas concentrations and deposition rates detected at the crater and along the downwind transect suggest that they are likely to have significant environmental and ecological impacts. Volcanic gas emissions such as S, Cl and F are

known to have acidifying impacts (Delmelle *et al.* , 2001), and damage to vegetation has been observed from satellite data (Nadeau, 2004). Additionally, the high levels of SO_2, imply that nearby human populations would be affected by volcanic degassing since these exceeded the WHO's recommendations. These impacts would have likely been greater when gas emissions were much higher in previous years.

A successful Gaussian fit to the data was useful, because it allows for the distribution of gas concentrations and deposition rates to be estimated at any point along the transect from actual measurements. In particular, this will allow for the calculation of gas concentrations or deposition rates in Chapters 3 and 4, where ecological data were collected but there were no measurements of volcanic gas concentrations or deposition rates. Since all measured volcanic gas concentrations and deposition rates were strongly correlated with each other, it is appropriate to select just one of these to represent exposure to volcanic gases. SO_2 data produced the best Gaussian fits, and therefore will be used in the following chapters to represent a gradient of exposure to volcanic gases.

Chapter 3

Plant communities downwind of Masaya

Results from plant community surveys are presented alongside environmental data. Exposure to the volcanic plume produced a significant change in species richness, type and composition. The volcanic plume is likely to have caused a variety of feedbacks with environmental and ecological variables, producing a unique vegetation community downwind of Masaya.

3.1 Introduction

There are many possible disturbances to ecosystems (e.g. hurricane, volcanoes, fire, human activity etc.) which can vary in magnitude on both spatial and temporal scales. A disturbance gradient, such as exposure to volcanic degassing, produces a change in environmental conditions, including abiotic factors such as atmospheric gas concentrations and soil pH and nutrient content. These can have feedbacks with the biota through canopy cover and leaf litter thickness and decomposition, to produce a unique ecosystem.

Plants and plant communities are used to define ecological regions because they are intrinsically important components of ecosystems, responsible for primary production. This makes them useful subjects for the study of ecological response to stress and disturbance. A simple measure of the ecological response to disturbance is how plant species richness, i.e. the total number of plant species in a given area or quadrat, responds to changing conditions. Studies of vegetation composition, including plant type and species, provide a more detailed assessment of how an ecosystem responds to a particular disturbance. Equally, the ecological response to an environmental gradient of disturbance such as volcanic degassing may be considered at the individual species level, which is the subject of Chapter 4.

3.1.1 Volcanic degassing and its impacts

Gas plumes released from persistently degassing volcanoes contain a mixture of gases including H_2O, CO_2, SO_2, HCl, HF and metals (Oppenheimer, 2003). Whilst H_2O and CO_2 are required for plant photosynthesis, other emissions have known environmental impacts, including acidification (Johnson & Parnell, 1986; Delmelle *et al.* , 2002). Since the composition of volcanic emission is comparable to some examples of industrial pollution, a similar response in the vegetation downwind of a degassing volcano might be expected. The effects of air pollution in North America and Europe are

well-known (Winner *et al.* , 1986; Fowler *et al.* , 1999; Bobbink *et al.* , 1998; Conti, 2001; Stoate *et al.* , 2001; Phoenix *et al.* , 2006). However, like many other ecological studies, there has been less of a historical focus on tropical ecosystems (Delmelle *et al.* , 2001), which might respond differently because of different climatic conditions.

3.1.2 Plant community response to disturbance

Both volcanic (Kamijo *et al.* , 2008) and industrial or urban pollution (Angold, 1997; Bernhardt-Römermann *et al.* , 2006; Vávrová *et al.* , 2009) have been associated with tree defoliation, which produces gaps in the canopy. These allow more light to penetrate to the understory, which benefits many herbaceous species and can increase species richness (Burton *et al.* , 2014). This provides some evidence for the intermediate disturbance hypothesis (Fox & Connell, 1979), where high biodiversity might be expected to occur where there has been moderate disturbance because a large variety of species from different seral stages may be able to grow there. Both colonized lava flows (Chevennement, 1990; Munguía, 2013) and landslide sites (Velázquez & Gómez-Sal, 2009) on volcanoes were found to have high species richness in previous studies. This is attributed to a species rich herbaceous layer.

Nevertheless, disturbances that produce canopy gaps can also negatively affect the understory, producing a decrease in species richness with increasing levels of disturbance (Salemaa *et al.* , 2001; Stevens *et al.* , 2004). Along a gradient of exposure to a saline water-mud mix extruded from mud volcanoes in Borneo (Ting & Poulsen, 2009), there is an increase in species richness with distance from the disturbance. This is because changes in the soil chemistry as a result of the mud volcano had a negative impact on the herbaceous layer. In these cases, an intermediate level of disturbance does not allow for competitive release, and biodiversity decreases with the disturbance.

Other disturbances can also have similar community scale responses, which is more evident when the gradient is considered as time from the event. Secondary succession after volcanic eruptions, such as that of Mt St Helens in 1980 (del Moral & Jones,

2002) or Krakatau in 1883 (Whittaker *et al.* , 1989; Thornton, 1996; Tagawa *et al.* , 2013), as well as other disturbances such as landslides (Velázquez & Gómez-Sal, 2008) involves a change in species richness and composition. However, species attributes for colonization and secondary succession (Tsuyuzaki & Del Moral, 1995) might, therefore, be different from those adapted to low magnitude but high frequency disturbances such as pollution.

3.1.3 Aims

Persistent volcanic degassing from Masaya has been ongoing since 1993 Rymer *et al.* (1998); Delmelle *et al.* (1999); Martin *et al.* (2012), with other previously documented episodes. It is known to acidify the downwind environment (Delmelle *et al.* , 2002) and studies of the Normalized Difference Vegetation Index (NDVI) have linked this to significant vegetation damage (Nadeau, 2004). However, an assessment of its impacts on vegetation species richness and composition has not been undertaken.

This study aims to use the gradient of exposure to volcanic SO_2 concentration defined by the Gaussian profile identified to Chapter 2 to identify the response of downwind vegetation communities. Both environmental and ecological variables were measured along the same transect, which represents a cross section through Masaya's gas plume. These data are used to prioritize the most important environmental factors which affect plant species richness and composition. Additionally, feedbacks within the ecosystem that enhance the effects of exposure to the volcanic plume are discussed.

3.2 Methods

3.2.1 Location and sampling strategy

During fieldwork in December 2013, February 2014 and May 2014, data were collected on plant communities, volcanic degassing, and other environmental data (including canopy openness, leaf litter layer and soil properties) along the Los Chocoyos trail (Figure 3.1). This trail provided a 4 km transect where the vegetation grades from tropical dry forest to a grass dominated ecosystem under the gas plume and then to an area set aside for local agriculture (though no sites studied were currently under cultivation). It lies approximately 2 km downwind of the actively degassing Santiago Crater and is restricted to the south west by the parks border which runs along the steep caldera wall. The whole of the area is underlain by lava from the same Late Quaternary but pre-Columbian eruption (Walker *et al.* , 1993).

Along the transect, 33 sampling sites were established by random selection. The same sites were surveyed during each sampling trip. In May 2014, an additional 6 sites at the beginning of the transect (forest) as well as an additional 5 sites at the end (agricultural) were randomly selected to extend the sampling area.

3.2.2 Plant communities

At each site, plant species data were collected using 16 m^2 (4 m by 4 m) quadrats. Species were identified from plant field guides for Costa Rica by Zuchowski (2007) and Gargiullo (2008) as well as the Tropicos plant database (Stevens, 2015). A total of 90 species were recorded, 70 of which were identified to family or species level. Unidentified species were included for the calculations of species richness but were excluded from all other analyses.

In December 2013 and February 2014 presence-absence data was collected, and in May 2014, plant species data were collected under three classifications: presence-absence, Braun-Blanquet cover abundance and a height classification. The presence-

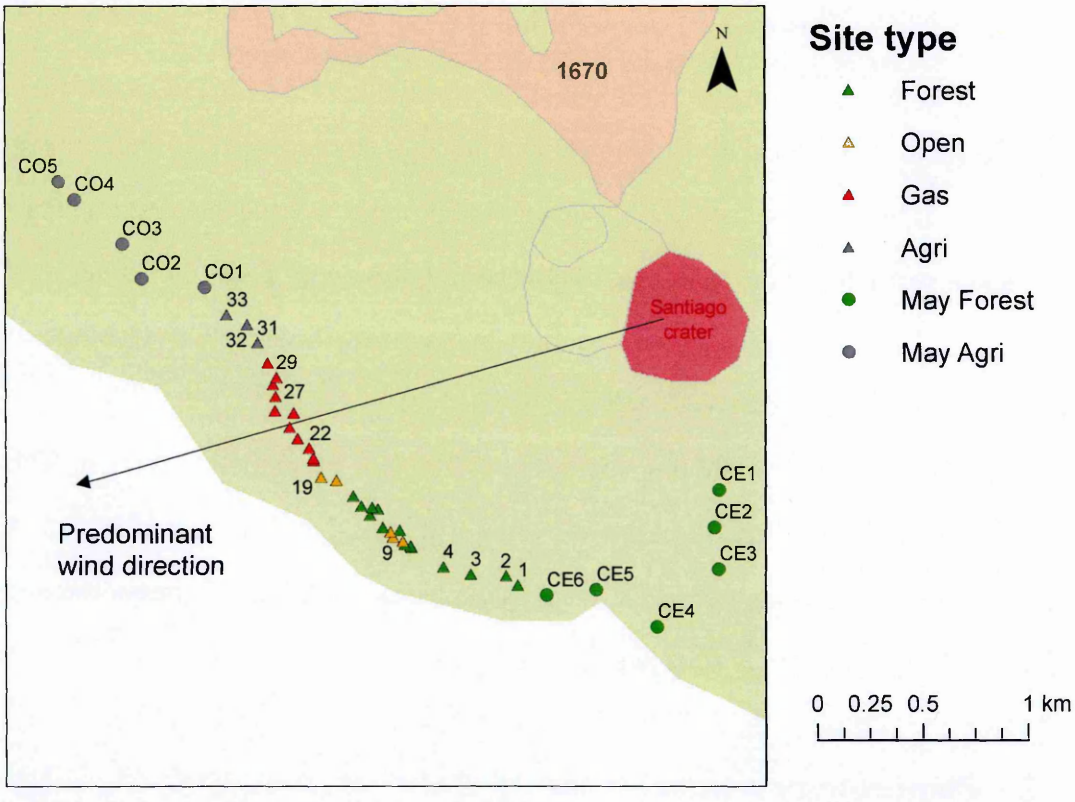

Figure 3.1: Map of all plant community sampling sites. Note the different symbol for those sampled in May-June 2014 only. The active Santiago crater and predominant wind direction are also marked. The change in topography between these sites is shown in the Appendix (Figure B.1).

absence data were binary, where a value of 0 means the species was not present and 1 means the species was present in a given quadrat. Percentage cover for each species was noted based on a visual estimate, and given that vegetation layers can overlap the total cover the total can exceed 100%. This data was converted to a 6 point Braun-Blanquet scale, based on the NVC recommendations (Rodwell, 2006), where 1 is the least cover and 6 is the most cover for present species (Table B.1 in Appendix). Additionally, the maximum height reached by a given species at each site was measured using a tape measure to the nearest centimetre. This was converted to a 6 point height classification where 1 is the lowest maximum height and 6 is the highest maximum height (Table B.2 in Appendix).

3.2.3 Environmental data

As well as volcanic gas concentration data displayed in Chapter 2, data on other environmental variables was also collected at the quadrat sites during sampling. These included canopy openness, leaf litter layer depth and soil properties, all of which are thought to respond to volcanic gases.

3.2.3.1 Volcanic degassing

Results from the Gaussian best fit to February 2013, December 2013, February 2014, May 2014 and June 2014 SO_2 data (Table 2.12), as described in Chapter 2 were added together to estimate the average volcanic influence at each site. To remove the effect of variation in gas emission rate between sampling periods, each were given a maximum concentration value of 1, and the centreline position and plume width values estimated from the Gaussian fit were used. This gave each site an exposure rating ranging from 0 to 5, with higher values representing greater exposure to the volcano's plume. This allowed for an estimate of the average exposure at each site, which was thought to be more appropriate given that the vegetation will be responding to long term patterns of degassing, including seasonal changes.

This rating was used to separate the sites into low (0-2), medium (2-4) and high (4+) depending on their exposure rating. This gives a useful measure of exposure to volcanic gases, without using absolute values of SO_2, whose measurements over short sampling periods may not have been representative of the long term trend so it would not be appropriate to use these to define threshold values. Plume sites were defined as those with an exposure value greater than 4 (high exposure). The exposure rating for each site is shown in the Appendix (Table B.9).

3.2.3.2 Canopy openness

Canopy openness, was measured from hemispherical photographs taken at ground level at each site during the December 2013, February 2014 and May 2014 sampling periods. Following recommendation by Rich (1990), the photographs were taken (where possible) under overcast conditions producing low and even light. Photos were taken in RAW format with a 0.20x fish-eye lens attached to a Sony NEX-3N. The focus ring was set to infinity and exposure bracketing was used to take three photographs one f-stop above and below the original, allowing for the most appropriate to be selected for analysis.

The photos were then analysed in SolarCalc to obtain a percentage canopy openness value for each site (Mailly *et al.* , 2013). Given the variable weather conditions, and a lack of cloud when some photos were taken, some had to be manually adjusted prior to analysis, to get a correct distinction between forest canopy and open sky.

Although this method is not as reliable as other methods such as the Cajanus tube or line intersect sampling (Korhonen *et al.* , 2006), it is a cheap and rapid method. Additionally, since a high variability in canopy openness is expected as along the gradient of volcanic pollution, it is thought that hemispherical photography will provide a sufficiently accurate estimate of canopy openness for the purposes of this study. The average of the December 2013, February 2014 and May 2014 canopy openness was used.

3.2.3.3 Leaf litter layer

During all three sampling seasons, at each site three measurements of leaf litter layer depth to the nearest centimetre were taken using a tape measure and the average of these was calculated. The average leaf litter layer depth of the three sampling periods was used. Notes were also made on the main substrate type, e.g. bare lava, bare soil or leaf litter.

3.2.3.4 Soil properties

Soil samples were collected from three different points within the quadrat at each site during May 2014. The leaf litter layer was removed, and the three topsoil samples collected from different points in the quadrat were placed together in one sealed zip-lock bag for each site. These were returned to the UK where they were oven dried at 40° C before being ground and sieved to 2 mm. By adding distilled water to the powdered soil, in a ratio of 1:5, a soil solution was created. This was shaken horizontally for an hour at 120 rpm to ensure adequate mixing of the soil in the solution.

These were then measured using a Thermo Scientific Orion Versostar advanced electrochemistry meter with probes for pH and EC. The pH probe (Orion 8157BNUMD) was calibrated using pH 7.00 and 4.01; and the EC probe (Orion 013005MD) using 1413 μS/cm and 12.9 μS/cm solutions. The pH and EC meters were tested using a standard in-house reference material of known pH and EC (R1/06). The calibration solutions, reference material and one site were re-measured every 10 samples and this showed that there was no drift in the measurements. The probes were carefully rinsed in clean distilled water between measurements of each sample.

3.2.4 Statistical analyses

Using plant species presence absence data for all seasons (December 2013, February 2014 and May 2014), species richness (total number of different species in each quadrat) was calculated. The relationship between all measured variables (species

richness, SO_2 concentration, canopy openness, leaf litter layer depth, May soil pH and May soil conductivity) was tested using Pearson's correlation.

To further understand the relationship between plant species composition and exposure to the volcanic plume, the plant species percentage cover data collected in May 2014 was used to determine dominant species types. The average percentage cover of each plant type was calculated for low, medium and high exposure to the volcanic plume.

Canonical Correspondence Analysis (CCA) was used to explore the relationship between plant species, sampling sites and their environmental conditions (using R 2014, version 3.1.1, package 'vegan' by Oksanen *et al.* 2013). This is a popular technique for identifying relationships between species and their environment along a gradient (Kent, 2011). Using a model building technique, only significant variables were retained. This was done for the presence absence data for all sampling periods (December 2013, February 2014 and May 2014) together, computed using forward stepwise model building with the R package 'vegan' (Oksanen *et al.* , 2013). The significance of the variables was tested using Monte-Carlo permutations (999). In the appendix (Figures B.2, B.3 and B.4), CCA with all environmental variables fitted was computed for May 2014 using all species data types (presence-absence, Braun-Blanquet and height), to demonstrate that in this instance presence-absence data is sufficient to identify the relationships between species, sites and environmental variables. This supports the use of presence absence data, which was collected for December 2013 and February 2014 as well as May 2014, enabling the use of a larger data set covering different times of the year. Each individual environmental variable was also taken for DCCA analysis in CANOCO. This allowed for a numerical estimate of the significance of each variable in determining the plant species composition, avoiding the arch effect and axis compression found using CCA for single variable analysis.

Using presence absence data, the results of the CCA were compared with cluster analysis for both species and sites. Cluster analysis was performed using hierarchical clustering of Bray Curtis dissimilarities and Ward's method. CCA uses weighted chi-

squared criteria, so cluster analysis provides a useful comparison between two distinct methods for analysing plant community data.

3.3 Results

3.3.1 Data along the transect

The average SO_2 exposure is close to a Gaussian distribution, but the northerly centreline from June 2014 makes it slightly skewed, and there is a large variability in the peak concentration reached between the seasons (Figure 3.2). For other measured environmental variables, this variation between the seasons is less apparent.

Leaf litter layer depth reaches a minimum under the plume (around 0-500 m on the transect), and there is an increase into the agricultural area. These results are consistent between the seasons. Canopy openness reaches a maximum peak in all seasons before 0 m on the transect and, with the exception of February 2014, stays at nearly 100% openness into the agricultural area, although canopy openness does decrease in the five sites sampled in May 2014. This is likely because trees have been cut down in the agricultural area, but also the plume footprint in the undisturbed forest is wider for canopy openness than for other variables. As with leaf litter layer depth, these results are consistent between the seasons, but in the agricultural area values have not returned to those at the beginning of the transect.

In May 2014 soil pH reached a minimum under the plume, and in the agricultural area values did not return to the high pH recorded at the beginning of the transect (Figure 3.3). There was no obvious pattern with electrical conductivity along the transect. Species richness reached a minimum under the plume, approximately where recorded SO_2 and canopy openness were highest, and leaf litter layer and soil pH were lowest. Species richness did not appear to be affected by the sampling season, suggesting this and other environmental variables were more stable between the seasons than SO_2 concentration.

With the exception of soil electrical conductivity in May, there was a significant correlation between the measured environmental data and species richness in all the seasons (Figure 3.4). This strong relationship between the measured variables implies

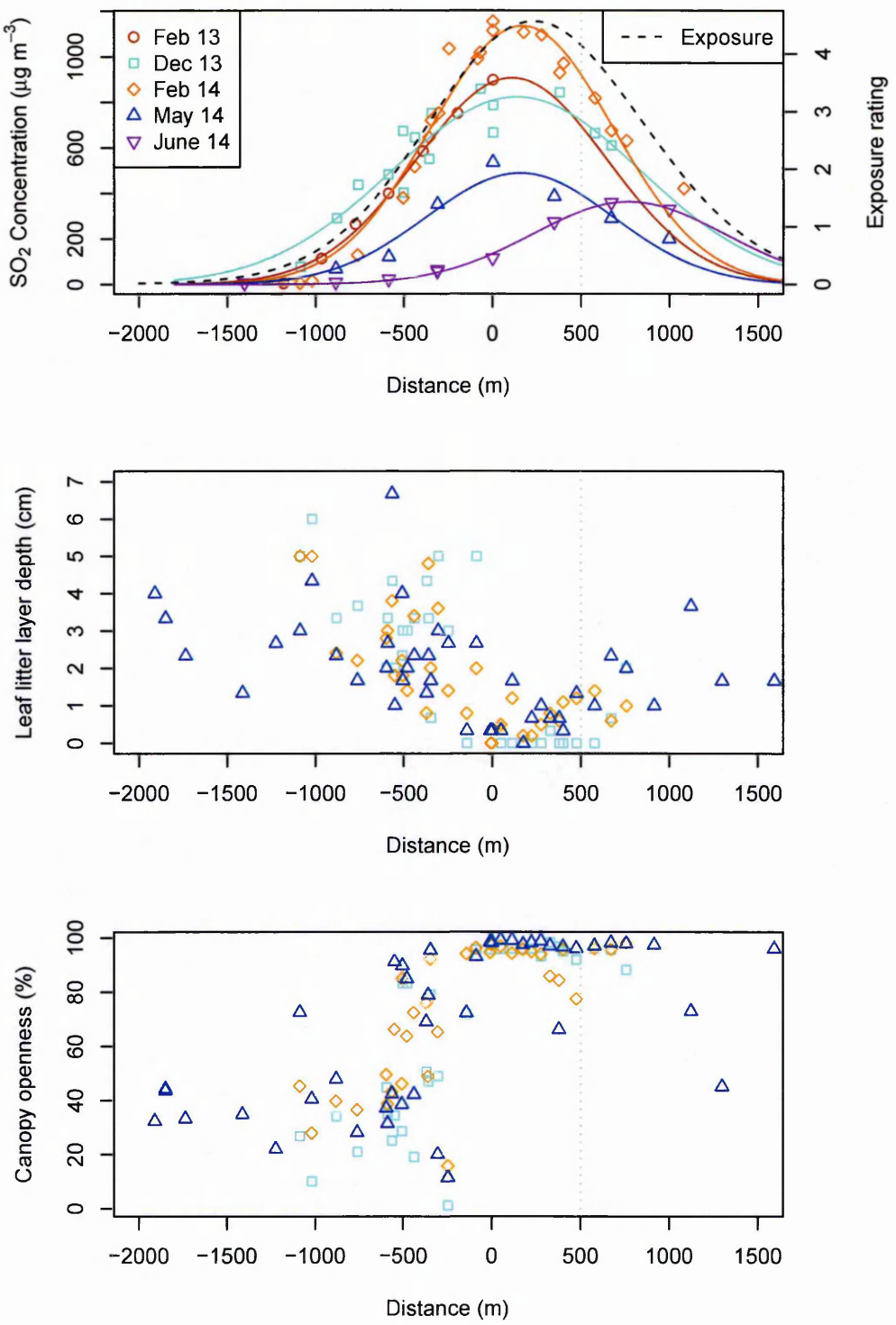

Figure 3.2: SO_2 concentration, leaf litter layer depth and canopy openness along the transect. SO_2 data and their Gaussian best fit lines are shown for each season, alongside the average exposure calculated from the Gaussian best fit parameters for centreline and width. Leaf litter layer depth and canopy openness data were collected in December 2013, February 2014 and May 2014 only. The grey dotted line denotes the boundary to the agricultural area, which covers the right hand portion of the plot.

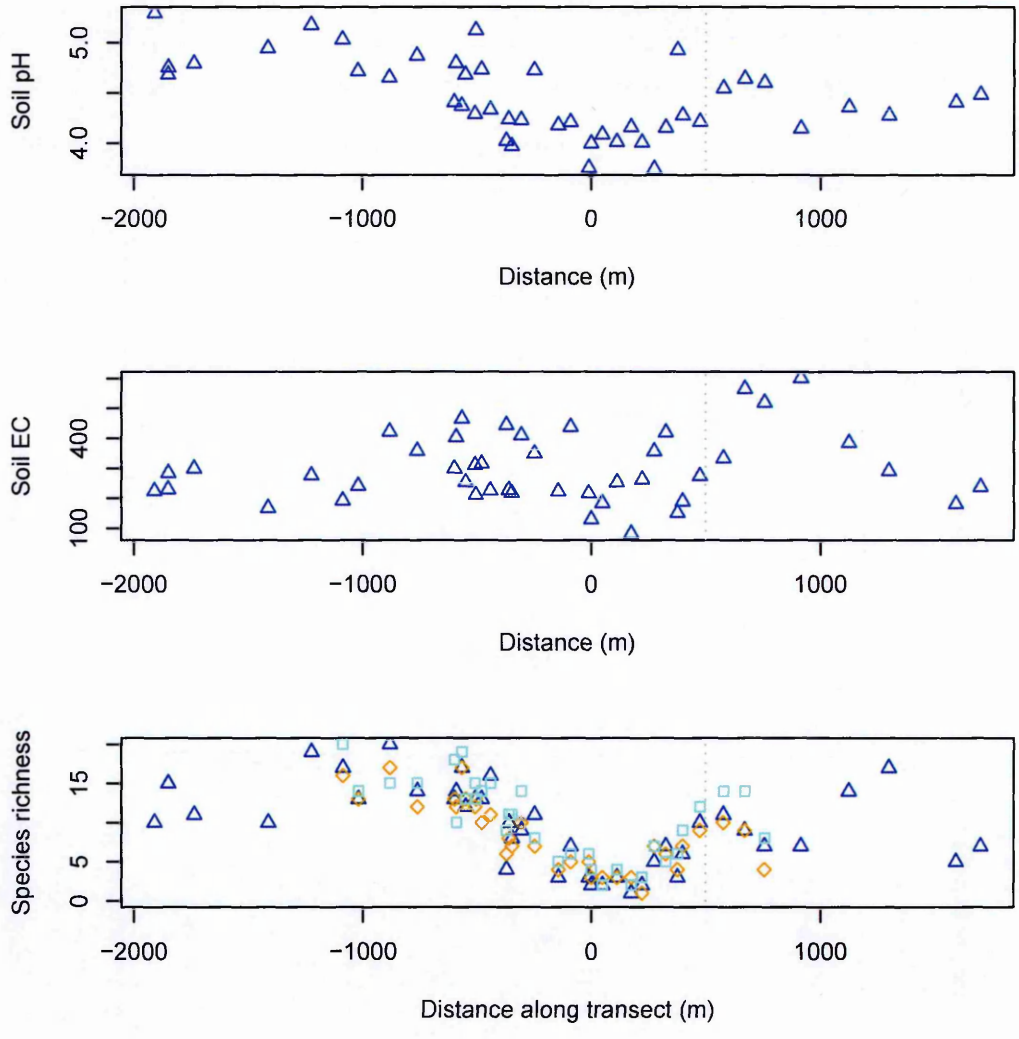

Figure 3.3: Soil pH and soil conductivity (EC measured in μS) in May 2014 only, and species richness from December 2013, February 2014 and May 2014 along the transect. Colours as in previous plot.

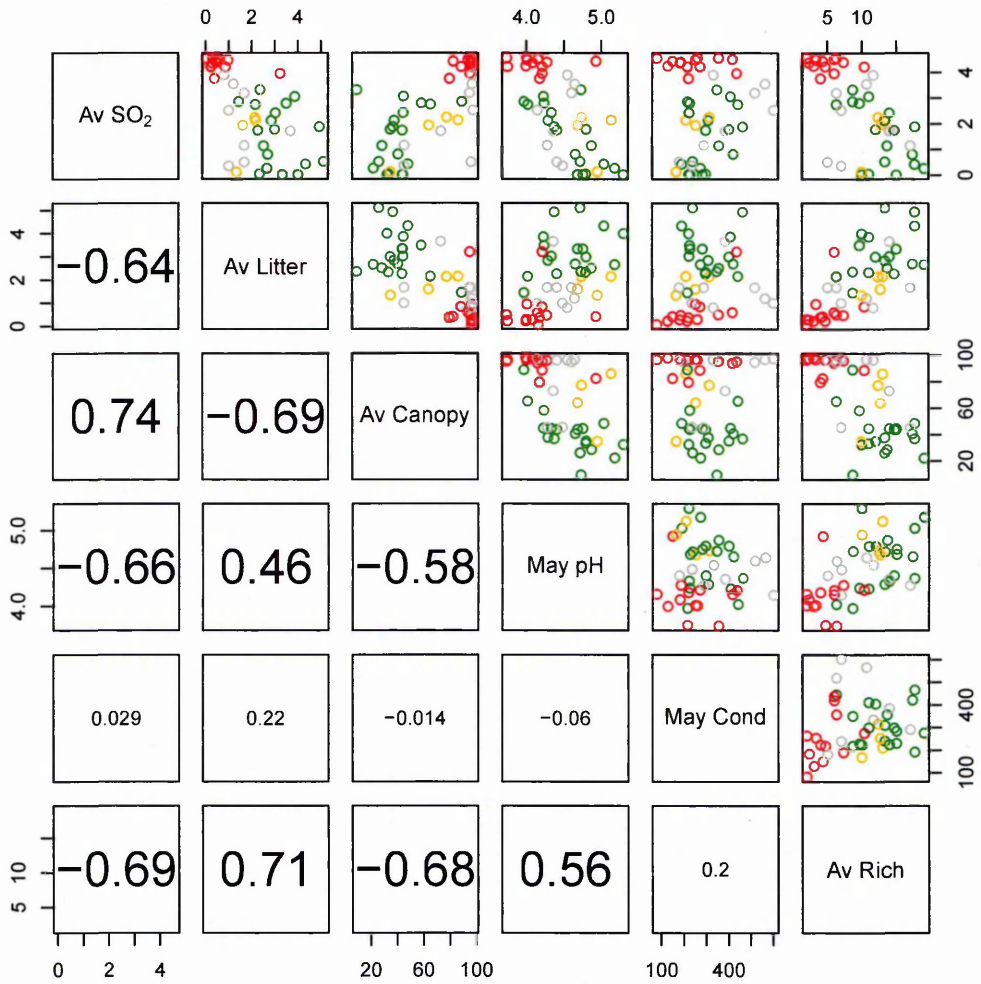

Figure 3.4: Correlation of SO_2 exposure, average litter, average canopy, May pH, May conductivity and average species richness. The colours represent site type as in Figure 3.1; green= forest, orange=open, red=gas and grey= agricultural. The bottom half of the plot shows Pearson's correlation values. Those highlighted are significant at $p \leq 0.05$ (0.294).

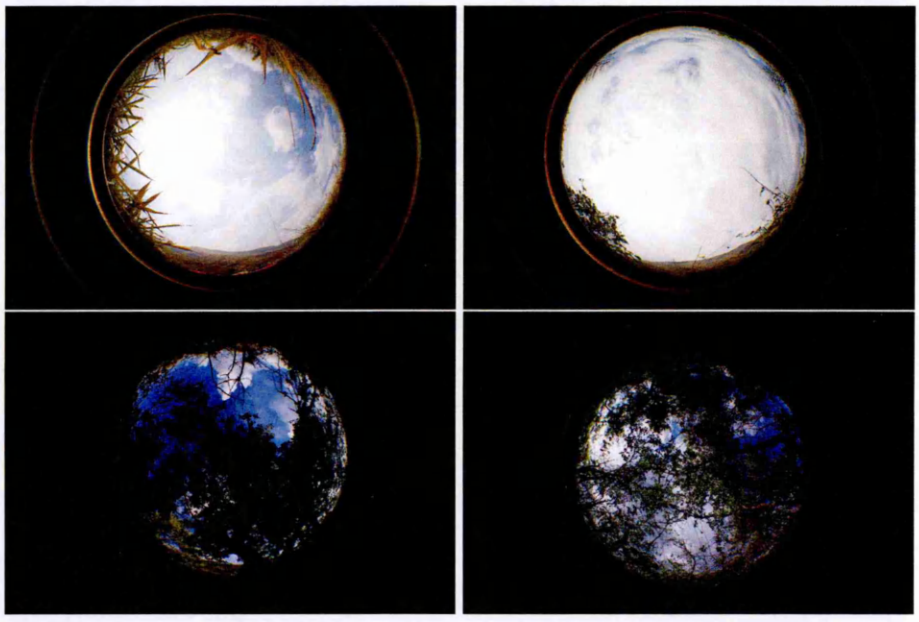

Figure 3.5: Comparison of canopy photos of open areas (top left - Site 30 and top right - Site 32) and forested areas (bottom left - Site 7 and bottom right - Site 3).

that there are likely to be interactions between these.

3.3.2 Plant type cover at different exposures

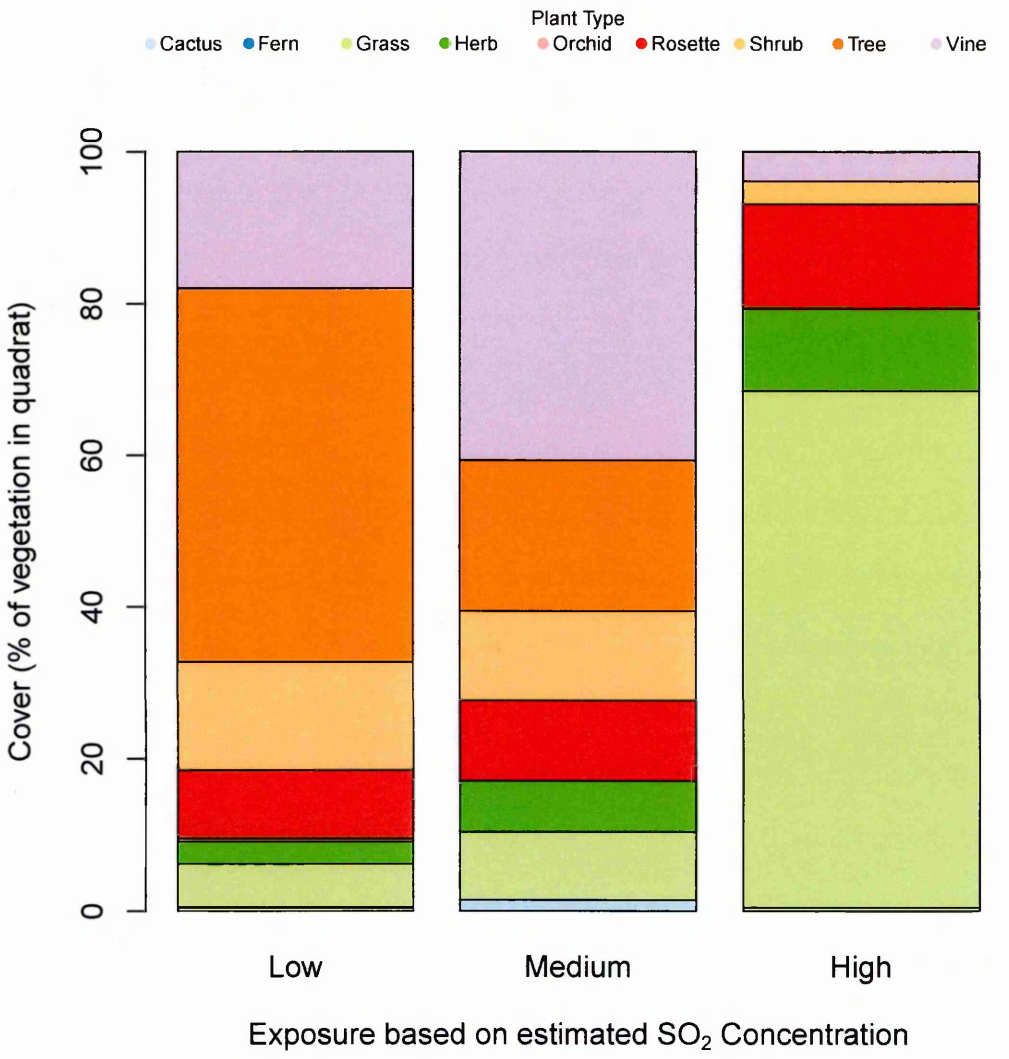

Figure 3.6: Percentage cover of plant species types (May 2014) at different exposures.

Data collected in May 2014 on the percentage cover of different plant types shows that these vary considerably with exposure to the plume. At low exposures trees account for the majority of the vegetation cover in the quadrats, with shrubs and vines also prominent. At medium exposures vines are the most abundant plant form, but trees and shrubs are also common. At high exposures, over 60 % of vegetation cover is a grass. This demonstrates that the ecological impact of volcanic degassing can be noted using a simple classification of plant types, without formal identification.

3.3.3 Ordination

CCA with environmental variables fitted shows the patterns in the plant community composition based on presence-absence data collected in December 2013, February 2014 and May 2014. This explained 21% of the variation in the data of which 44% was explained by CCA1 and 22% was explained by CCA2. Sites and species scores for CCA1 and CCA2 are displayed in the Appendix (Tables B.10, B.11). It is evident that there is no distinct change in plant community composition between the seasons, as using season as a factor was not significant according to the CCA model building. Therefore, the sampling season had little influence on plant community composition. However, SO_2 exposure, canopy openness, leaf litter layer depth, soil pH and conductivity were significant according to stepwise selection.

CCA1, the principal axis, clearly distinguishes plume sites (triangles) from forest sites (squares). The most important variable that explains this variation in plant community composition is the average SO_2 exposure This is correlated with high canopy openness, low leaf litter layer depth and low soil pH. According to DCCA single variable analysis for each of the environmental variables, SO_2 and leaf litter layer depth were the most significant variables explaining the variation in the plant species data.

High positive values for CCA1 are found where exposure to SO_2 is estimated to be very high. Here, the most prominent species is a grass, *Cenchrus*. Species in this genus are known to grow in open disturbed areas, including beaches, in Nicaragua (Stevens, 2015). Another grass was only found in the gas area, *Melinis repens*, during December 2013 and February 2014 but not May 2014. This species is a common pioneer species on more recent lava flows from the volcano. It is probably growing in this area because there is a lot of bare lava, but since it is not very abundant, it does not appear to be as tolerant as *Cenchrus* is towards volcanic gases.

In the area under the plume, the herb, *Diodia*, a ruderal plant known to prefer very dry and sandy areas (Stevens, 2015), was also common. Additionally, during December 2013 and February 2014, *Pityrogramma calomelanos*, a fern that is quick

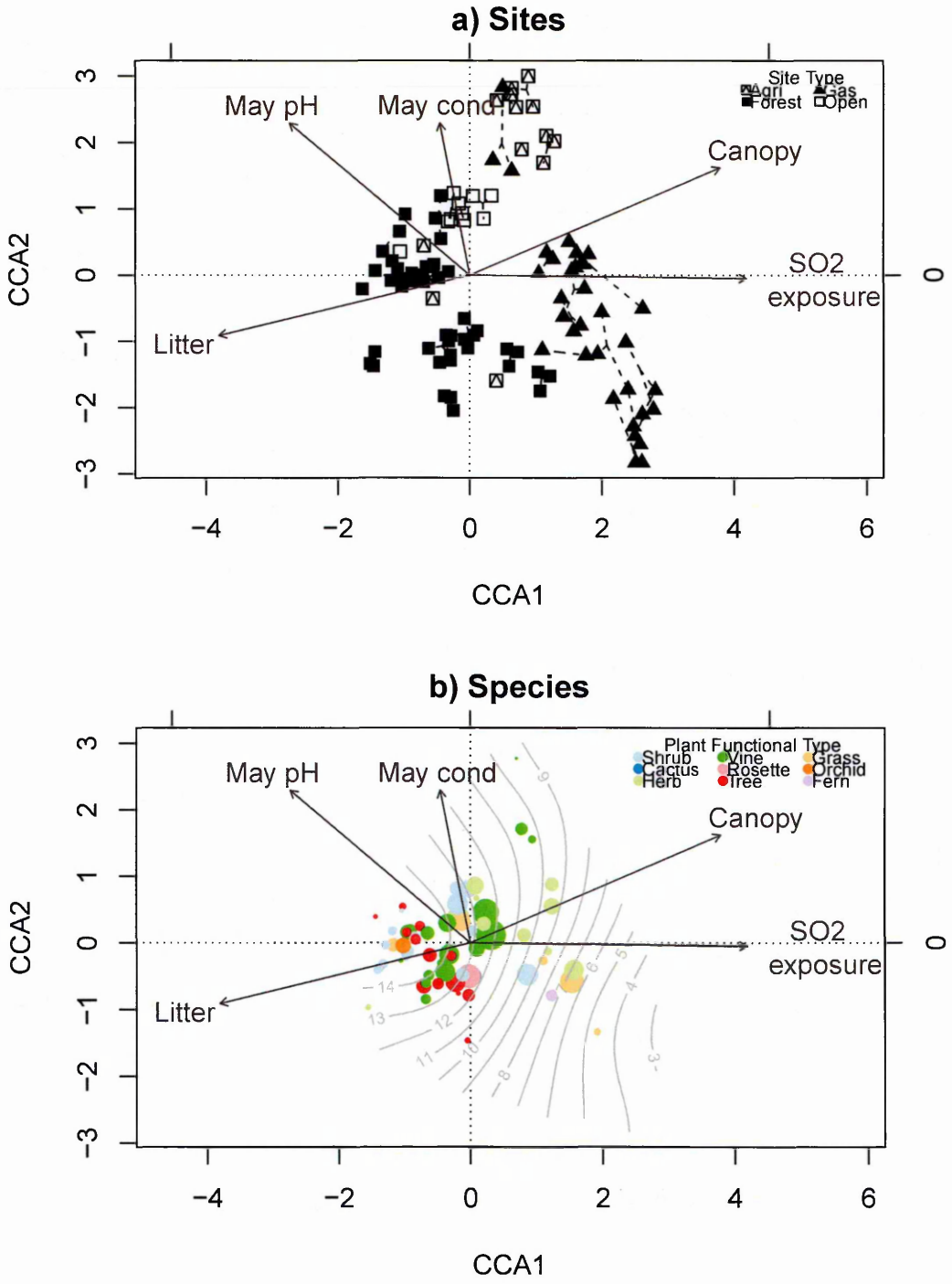

Figure 3.7: CCA (Canonical Correspondence Analysis) of plant species presence-absence data for December 2013, February 2014 and May 2014, with environmental variables (SO_2 concentration, leaf litter layer depth, canopy openness, May 2014 pH and May 2014 conductivity). Sites are classified by their type. The sites, which were sampled in three different seasons, are linked by dashed lines all plot close to each other on the ordination diagram (lone sites represent the extra May 2014 quadrats). Species have been coloured by their type, and their size represents their total abundance across all sampled quadrats. A fitted surface for species richness is shown in grey.

	CCA1	CC2
Acanthocereus tetragonus	0.04	-0.49
Ageratum conyzoides	1.24	0.55
Blepharodon mucronatum	-0.32	-0.18
Bromelia pinguin	-0.03	-0.50
Cenchrus	1.53	-0.57
Cissus microcarpa	0.10	-0.09
Cissus verticillata	0.31	0.12
Cleome viscosa	-0.18	0.39
Dalechampia scandens	0.24	0.46
Diodia	1.57	-0.40
Euphorbia colletiades	-0.22	-0.59
Iresine calea	-0.02	0.81
Justicia carthaginensis	0.08	0.86
Mimosa albida	0.87	-0.48
Oplismenus burmannii	-0.13	0.32
Senna pallida	-0.19	0.59
Serjania grosii	-0.34	0.30
Smilax spinosa	-0.38	-0.44

Table 3.1: Species scores for CCA1 and CCA2 for abundant species using presence-absence data from all seasons. Species scores for all species are found in the appendix (Table B.11).

Variable	Percent explained	Eigenvalue ratio
Exposure (SO_2)	8.80	1.42
Litter	7.80	1.35
Canopy	7.60	0.89
May pH	5.60	0.86
May conductivity	3.70	0.41

Table 3.2: Summary of DCCA using single constraining variables

to colonize volcanic landscapes in the tropics (Chevennement, 1990; Velázquez & Gómez-Sal, 2009; Tagawa *et al.* , 2013), was abundant in the gas area too. A shrub, *Mimosa albida*, was also abundant in the area exposed to the plume. No trees were recorded at the gas sites, and plant heights (both of individuals and species) are generally low.

Highly negative CCA1 values are found for a variety of plant types, including the orchid *Oeceoclades maculata*, shrubs (e.g. *Aphelandra scabra* and *Acalypha*), trees (*Pisonia macranthocarpa*, *Stemmadenia* and *Gliricidia sepium*) and vines (*Pithecocte-*

Figure 3.8: Photograph of typical downwind plants including *Cenchrus* spp., *Diodia* spp. and *Bromelia pinguin* at Site 23.

nium crucigerum and *Blepharodon mucratonum*). These forest and understory species are common to tropical dry forests (Figure 3.9), as well as other forest types, and can also be found in more open second growth forests (Gargiullo, 2008). As noted previously, there is a greater species richness at lower SO_2 concentrations (Figure 3.12).

Species with a large point size (Figure 3.7) that are found around a score of 0 for CCA1 are common across all site types, and these include *Cissus verticillata*, *Dalechampia scandens* and *Bromelia pinguin*.

CCA2 distinguished agricultural and open sites, that had positive CCA2 scores, from forest sites which had negative CCA2 scores (Figure 3.7). These sites were associated with a high canopy openness and high pH, but a thin leaf litter layer. A vine, *Amphilophium paniculatum*, which is known to prefer open disturbed areas, was most common here. Additionally, a Fabaceae vine (thought to be a cultivated bean), alongside *Physalis* in December 2013, were both found at some of these agricultural sites. Both of these species may have escaped from cultivation nearby.

Other herbs and shrubs found here (e.g. *Ruellia blechum*, *Lantana camara*, *Sida rhombifolia*, *Senna pallida*, *Turnera scabra* and *Kallstroemia*), are common to open disturbed areas (Stevens, 2015). Conversely, low CCA2 values were associated with forest trees and understory plants. This distinction along the CCA2 axis was also

Figure 3.9: Photograph of a forested area (Site 2) and understory (Site 1) with a large variety of plant species.

Figure 3.10: Photograph of typical plants in the agricultural area including *Cissus verticilata*, *Amphilophium paniculatum* and *Rauvolfia tetraphylla* at Site 32.

evident with cluster analysis of sites, but not of plant species. Soil conductivity (EC) does not explain a significant amount of variation in the data according to DCCA (Table 3.2). It appears that positive CCA1 scores represented volcanic disturbance whilst negative CCA2 scores represented human disturbance.

Overall, it appears that the forest sampled along the transect was not primary or virgin tropical dry forest. Many large climax tree species were not encountered, e.g. *Ceiba pentandra*, *Enterolobium cyclocarpum* and *Gyrocarpus americanus* (Marenco *et al.* , 2012), though this may have been biased by the quadrat size used for sampling. However, the presence of many species of second growth and moderate disturbance supports a hypothesis that there was some level of disturbance across the forested areas, including those unaffected by the gas plume. This may be as a result of proximity to human settlements, where exploitation of forest resources, such as firewood extraction, have been occurring.

Nevertheless, the forest surveyed represented a clearly different environment to the grass dominated landscape downwind of the volcano, as demonstrated by the variation in environmental variables and species composition. Additionally, species such as *Bursera simarouba*, which were encountered during this sampling, are important to the forest ecosystem as they support a large number of insect and mammal species (Zu-

Figure 3.11: Photograph of typical plants of the open forest areas including *Senna pallida*, *Cissus microcarpa* and *Lantana camara* at Site 8.

chowski, 2007). Therefore, highly negative CCA1 values might represent the type of ecosystem that might be expected downwind of the volcano if there was no degassing, and moderate levels of human disturbance, and so provide a clear control for the study of plant communities along a gradient of exposure to volcanic gases.

3.3.4 Cluster Analysis

Cluster analysis for sites, using the same plant species presence-absence data as in the CCA ordination, identifies four distinct groups. Those with high positive CCA1 scores are mostly plume sites and those with high positive CCA2 scores are made up of mostly agricultural and open sites. A group with negative CCA1 scores is made up of forest and open sites, with some agricultural sites from the May 2015 sampling period and another group comprising mostly forest sites has negative CCA2 scores. With species, there is a clearly defined group comprising plume and some agricultural species with high CCA1 scores. The remaining groups are tropical dry forest tree and

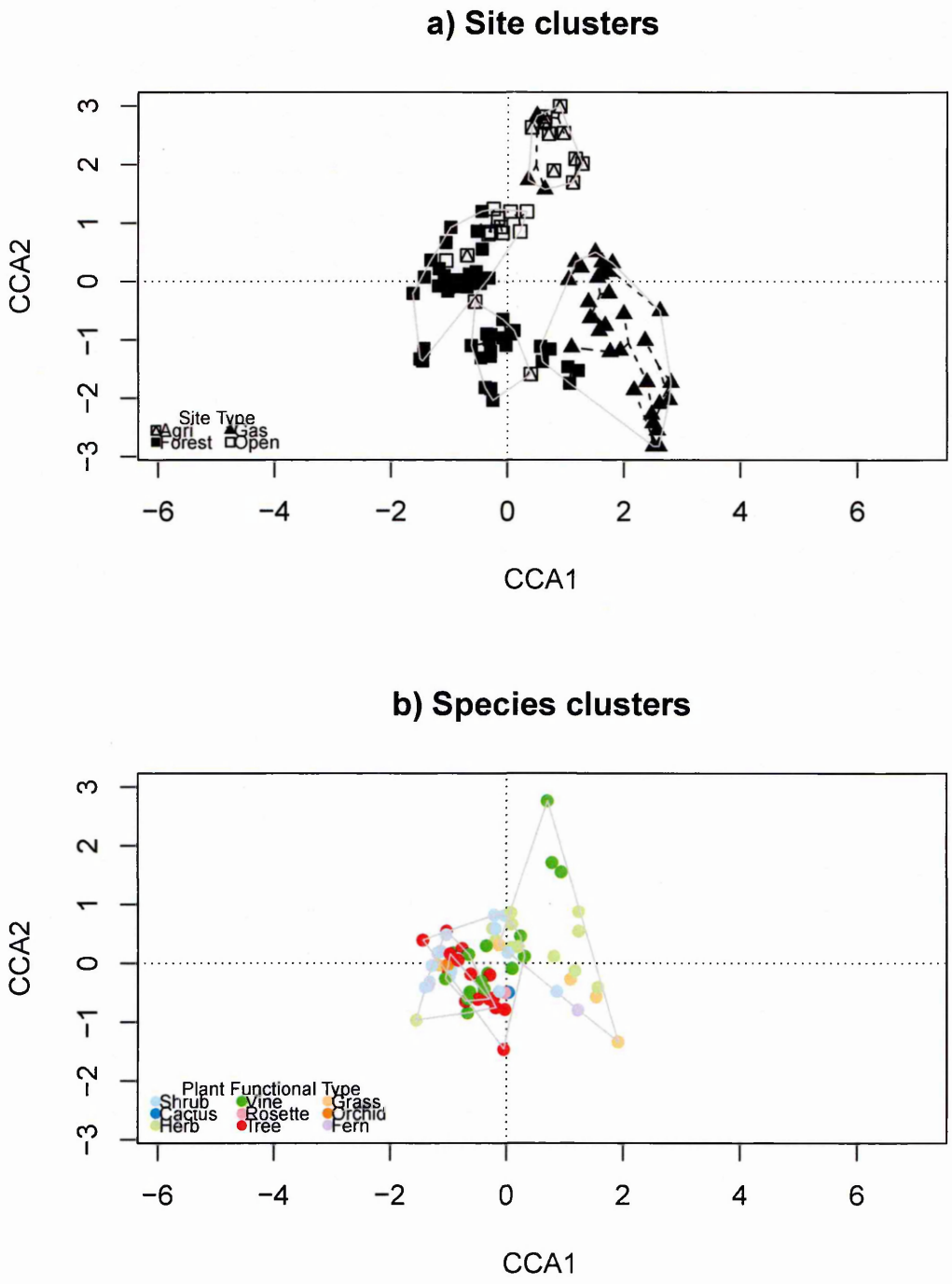

Figure 3.12: CCA of plant species presence-absence data for December 2013, February 2014 and May 2014 with cluster analysis for a) sites and b) species using Ward's method are shown by grey shapes.

understory plant species that have mostly negative CCA1 scores.

3.4 Interpretation

3.4.1 Environmental and ecological variables along the transect

A peak in exposure to volcanic SO_2 was matched with a peak in canopy openness and troughs in leaf litter layer depth, soil pH and species richness (Figures 3.2 and 3.3). No trend for soil conductivity was found along the transect. Correlation between measured environmental (SO_2, canopy, litter, soil pH and soil conductivity) and ecological (species richness) variables was highly significant for all pairs, with the exception of those with soil conductivity. These variables are highly interrelated, and could be linked to exposure to volcanic SO_2.

A marked decrease in species richness observed here is comparable to the effects of high levels of industrial pollution (Salemaa *et al.* , 2001; Stevens *et al.* , 2004) and a study of plant communities at two mud volcanoes in Indonesia (Ting & Poulsen, 2009). Environmental conditions were too extreme for a lack of trees to stimulate significant understory herbaceous growth. This may be as a result of the frequency of the disturbance, since degassing has been ongoing since 1993 at Masaya, and there have been many cycles of high gas concentrations prior to this (Stix, 2007). These results are not in agreement with the intermediate disturbance hypothesis (Fox & Connell, 1979).

As with plant species richness, studies of other taxonomic groups (e.g. fauna) tend to find a decrease in species richness in response to high levels of industrial pollution (Hoffmann *et al.* , 2000; Liška & Herben, 2008; Miller & Watmough, 2009; Babin-Fenske & Anand, 2011). Similar effects of volcanic pollution other biota downwind of Masaya might be expected.

3.4.2 Plant species composition

Overall, the pattern of the relationship between sites, species and environmental variables was similar between the presence absence data for all sampling periods (Decem-

ber 2013, February 2014 and May 2014 in Figure 3.7) and the different classifications for plant species data in May 2014; presence absence (Figure B.2), Braun-Blanquet cover (Figure B.3) and height classification (Figure B.4).

As well as a change in species richness, there was also a change in species composition along the transect. When plant species are categorized by their type, there was an evident shift from forest, where trees represented most of the cover along with vines and shrubs in the undisturbed section of the transect, to a grass dominated environment at high exposure to the volcanic plume (Figure 3.6). This pattern was also reflected in the ordination of the data using CCA (Figure 3.7), which also included other environmental variables. Positive CCA1 values are associated with sites that had high exposure to SO_2 and an open canopy and where grass species were abundant. Most trees, and associated understory plants, as well as leaf litter layer depth had negative CCA values. Plume sites had the highest positive CCA1 scores, and this was supported by cluster analysis of sites, which identified these as a distinct group of sites (Figure 3.12). A cluster of species with positive CCA1 values included plume species, as well as some agricultural species.

There is evidence that some biota benefit from high pollution levels, as this disturbance can make light and nutrients more available to ruderal species tolerant of these conditions (Angold, 1997; Bernhardt-Römermann *et al.* , 2006), which may competitively exclude other plants (Bobbink *et al.* , 1998), leading to a slower recovery time with some species missing (Šebesta *et al.* , 2011). Areas that have an open canopy as a result of pollution, e.g. volcanic degassing from Turrialba, Costa Rica (Duarte & Fernandez, 2011; Burson, 2012) or industrial pollution in the Krkonose (Giant) Mountains, Czech Republic (Vávrová *et al.* , 2009) allow herbs to thrive, since trees would have prevented enough light from penetrating to the understory. Species associated with plume sites in this study were either not encountered in the nearby forest, or some were only found in the most open patches. This suggests that in the downwind zone these few grass, shrub, herb and fern species were benefiting from competitive release. However, species richness decreased with exposure to the plume, suggesting that the

benefits of an open canopy were outweighed by high volcanic gas levels for the majority of tropical dry forest plants.

Grass species are common as a results of disturbance. A grass species was observed to dominate following a landslide at Casita Volcano (Velázquez & Gómez-Sal, 2009) in the most affected area where pre-disturbance soils did not remain. Equally, on Miyake-Jima Island (Kamijo *et al.* , 2008) after an ash eruption followed by several years of volcanic degassing, the ecosystem became dominated by two tussock grass species from early and late succession. One of these is a pioneer species already known for its preference of acidic soils, which typically would out-compete the other, a climax species. At Masaya, the dominant grass was *Cenchrus* which is known to inhabit disturbed areas, and this dominated over the pioneer grass, *Melinis repens*. Other ruderal plants including herbs and a fern were present in the area most affected by the volcano. These plant groups are also commonly found in disturbed areas in other studies (Angold, 1997; Kamijo *et al.* , 2008). Only some of these species were observed to be growing on the two most recent lava flow (1670 and 1772) upwind of the volcano.

Therefore, as a result of degassing there was a secondary succession that allowed for colonization by stress tolerant and ruderal species that grow in open areas, but that could also tolerate high SO_2 and acidic conditions. The plant community in the grassland in the area most affected by the volcanic gases differs from a lava flow that is in the early stages of succession.

In some cases, such as ozone pollution (Payne *et al.* , 2011), studies have found a compositional change, but not a reduction in species richness (Dirnbock *et al.* , 2014). The results of this study are most comparable with cases of extremely high industrial pollution, where there is a marked reduction in species richness, but with some ruderal plant species increasing in abundance with exposure to volcanic gases. This may be because multiple interacting pollutants have a much greater effect on the ecosystems than just a single one (Payne *et al.* , 2011). At Masaya, SO_2, HCl and HF are likely to affect the downwind ecosystem directly and through acidification, and other volcanic emissions including H_2O, CO_2 and heavy metals might also be having

ecological consequences. Separating the effects of these can be incredibly difficult, particularly when they are correlated with each other (Payne *et al.* , 2014).

3.4.3 Environmental and ecological feedbacks

The lack of trees, leaf litter layer and an open canopy as a result of degassing in the area downwind of Masaya is significant. Geological mapping of Masaya volcano suggests that the whole of the study area shares the same substrate, a Late Quaternary, but pre-Columbian lava flow (Walker *et al.* , 1993). Therefore, if age and type of lava flow were the primary environmental controls on vegetation communities in this area, a similar species composition along the transect might be expected. However the unaffected dry tropical forest contains well established trees. Whilst a few individuals were observed growing in the area most affected by the volcanic plume, none were encountered during this sampling.

Early successional trees are vital for colonization because they contribute to soil formation through leaf litter, and their canopy provides shade for understory vegetation. Additionally some colonizer trees can be nitrogen fixing, and without any nitrogen fixers the rate of plant cover accumulation is slowed during succession (Chang & del Moral, 2015). Also, trees provide perches for birds which disperse other plant species (Campbell *et al.* , 1990). Therefore, if trees could survive the SO_2 pollution, it is possible that some understory plants that could tolerate high concentrations of SO_2, but not an open canopy and thin leaf litter layer, might have been able to survive in the gas region.

Species richness is highest where there is a greater leaf litter layer depth. This means that there is a feedback between the presence, or absence, of species that produce large quantities of litter (particularly trees) and the micro-environment created as a results of this. Additionally, where pollution levels are highest in tropical dry forest in India (Singh *et al.* , 2004), there is reduced litter production, attributed to lower biomass production. Litter decomposition was also found to be slowed by air

pollution, as a result of decreased microbial activity. Both of these factors contributed to a low turnover of nutrients. It is likely that similar mechanisms would slow leaf litter production and decomposition downwind of Masaya where there is even higher concentration of SO_2 pollution and a more acidic soil than the area in India studied by Singh *et al.* (2004).

Changes to the substrate through leaf litter decomposition are required to facilitate the arrival of late successional species (Read & Lawrence, 2003). Without a developed soil, seedlings may germinate, but not develop into trees in the downwind zone. The lack of soil formation in the area downwind of the volcano would likely reduce the availability of a seed bank, which is an important contributor to secondary succession by providing dispersal opportunities through time, and not just space (Niño *et al.* , 2014). Germination could potentially happen during periods of low gas levels if there was an established seed bank. Therefore, a high seed rain would be required to contribute new colonizers to the area downwind of the volcano. Volcanic degassing at Turrialba (Duarte & Fernandez, 2011; Burson, 2012) and anthropogenic pollution in the Czech Republic (Vávrová *et al.* , 2009) may have killed all or most of the trees, but there is well developed soil that could support the return of trees with declining gas emissions, which is not the case at Masaya. This means that the time for this area to return to established forest if emissions were to stop instantly could be closer to the time-scales for primary succession, which could be several hundred years.

It is known that Masaya has been degassing for several periods lasting years to decades since the mid 19th century (McBirney, 1956; Stix, 2007), and it has quite possibly had other degassing periods prior to this. Although volcanic degassing will not result in primary succession, it is a more intense and frequent disturbance that other examples of secondary succession, therefore the recovery would likely be even slower, closer to that of primary succession. Therefore, it is unlikely that there would have been a sufficiently large break in volcanic degassing during the last few hundred years to allow for succession to progress significantly, particularly given the poor establishment of trees and the lack of soil development. This might be indicating that volcanic

degassing has been modifying the typical path of succession on this section of the lava flow, for longer than is currently known from historical records.

Chapter 2 identified variation in gas emission rates and the dispersal of the volcanic plume between sampling periods and it is known that Masaya's degassing episodes are variable in intensity on a variety of timescales. Whilst these variations might have implications for the plant communities, it was noted in this chapter that there were not considerable differences between vegetation composition between the three sampling periods that could not be explained by seasonal variation. This suggests that the plant communities are responding to the pattern of dispersal of the plume, more than changes in gas emission rates. This means that absolute SO_2 values measured in Chapter 2 cannot be reliably used to define response thresholds in the plant community.

The consistency of the results between seasons, and the strong relationship between plant community composition and exposure to volcanic SO_2 supports an argument that the dispersal of Masaya's plume has followed a similar pattern in previous years and decades. This suggests the vegetation community might provide a useful indicator of volcanic gas dispersal, which when applied alongside pollen records might be used to reconstruct fossil volcanic plumes.

Feedbacks with soil pH, leaf litter layer depth and canopy openness were likely buffering potential changes from fluctuating gas levels during the measurement periods in this study. Additionally, plant communities are expected to respond on longer timescales. Whilst plants may die rapidly under a sudden change to extreme conditions, there is a lag time in vegetation recovery as successful seed germination (and possibly even dispersal) are required which may take several seasons. However, a repeat of this study over a period of years rather than months might reveal such changes in plant communities in response to variation in gas levels. The timing of a disturbance within the plant's cycle can affect the magnitude of its impacts (Peguero & Espelta, 2011). A short term response to volcanic gases might be expected to be more pertinent at the individual plant level, which is the subject of the following Chapter 4.

3.5 Conclusions

Degassing from Masaya volcano produces a gradient of exposure to atmospheric SO_2 pollution and this has strong environmental and ecological impacts. In the downwind zone there is an open canopy, a thin leaf litter layer and a low soil pH and there are few species. The vegetation community is made up of small plants, comprising grasses, herbs, and a fern and shrub species, many of which are not found on newly colonized lava flows. This contrasts to the established forest, that is probably moderately disturbed by human activity, found on the unexposed section of the same lava flow. Here there is a denser canopy, a thick leaf litter layer and many tropical dry forest trees and understory plants can be found, which contributes to much higher species richness. These results were similar to those of previously documented episodes of volcanic degassing and some industrial pollution studies. There was no significant variation between the three sampling seasons (December 2013, February 2014 and May 2014), or in the analysis using plant cover abundance and plant height data collected in May 2014.

The unusual plant community downwind of the volcano confirms that degassing has played a major role in shaping the ecosystem here. Additionally, local feedbacks from SO_2 pollution relating to presence of trees and their canopy, the development of the leaf litter layer and soil formation have also contributed to this unique seral stage on the section of the old lava flow that is affected by volcanic gases. This might also suggest that the volcano has been degassing for longer than is known from historical records.

Chapter 4

Dalechampia scandens response to volcanic gases

Volcanic gas concentration and deposition rates measured in Chapter 2 are used as a environmental gradient of exposure to Masaya's plume to explore the plant morphological response. Leaf and flower traits of a vine, *Dalechampia scandens*, were measured along a the transect and results are compared with another abundant plant, *Byrsonima crassifolia*. Possible mechanisms to explain the enhanced growth of *D. scandens* leaves under the volcanic plume are discussed.

4.1 Introduction

4.1.1 Individual species response to an environmental gradient

A simple way of assessing the response of an individual plant to an environmental gradient or stress is to consider its growth, through measurements such as leaf size (length or area), leaf number, plant height and biomass. No studies have looked at this with respect to volcanic degassing, but several have considered the impacts of industrial pollution on individual species. Most report a negative effect of the exposure to pollution on plant growth (Pandey & Agrawal, 1994; Verma & Agrawal, 1996; Dodd & Doley, 1998; Tricker *et al.* , 2004; Yang *et al.* , 2006; Pourkhabbaz *et al.* , 2010; Tiwari *et al.* , 2010; Nikula *et al.* , 2011; Maisto *et al.* , 2013; Leghari, 2013). However both inhibition and stimulation of growth were found in a controlled experiment looking at urban pollution effects on several species (Honour *et al.* , 2009). Other stresses, such as low water availability are also linked to a smaller leaf size (Nobel, 2009; Chalcoff *et al.* , 2008). The gradient of exposure to volcanic SO_2 provides a unique field setting for a study of the effects of volcanic gases on plant growth.

4.1.2 Impact of volcanic gases on plants

Volcanic gases are known to affect plants both directly and indirectly. Volcanic SO_2, amongst other acid emissions such as HCl and HF causing damage to leaves such as chlorosis (Nelson & Sewake, 2008). However there is evidence that the negative effects of these gases can be balanced by high CO_2 (Jenkins, 2012). Some plants have mechanisms to deal with exposure to volcanic pollution, such as base cation transfer to neutralize acid rain (Johnson & Parnell, 1986). However, volcanic emissions are associated with increasing soil acidity, and they produce environmental conditions that few plants can tolerate, as demonstrated in Chapter 3. This is evident when looking at satellite imagery, including Normalized Difference Vegetation Index (NDVI), where areas downwind of degassing volcanoes such as Masaya have high levels of vegetation

damage (Nadeau, 2004). Overall, there may be competing effects of volcanic gases on individual plant species and different functional parts of the same plant may have varying responses (Abe *et al.* , 2014). Using a gradient of exposure characterized by volcanic SO_2 levels, the response of plant traits can be explored. Vegetative and floral trait variability can also be compared along this gradient.

4.1.3 *Dalechampia scandens*

Dalechampia scandens is a neotropical vine with serially homologous vegetative and pollination traits, and it is widespread across Central and South America. It is of particular interest because it has a specialized pollination system composed of two involucral bracts, that are thought to have evolved from leaves given their morphological similarity. These bracts surround a resin gland, which produces resin as a reward for the bees that pollinate it.

4.1.3.1 Berg Hypothesis

The Berg Hypothesis (Berg, 1960) states that in plants with specialized pollination systems (i.e. those relying on a small number of pollinator species), variation in the size of floral structures (e.g. blossoms) will be decoupled from vegetative parts (e.g. leaves). Vegetative traits, such as leaf size are likely to be more phenotypically variable depending on environmental conditions. The floral structures of plants with specialized pollination systems are expected to have strong selection for precision (Hansen *et al.* , 2007), thus producing consistently sized inflorescences. This is because they are reliant upon a consistent match in size with their pollinator(s), to ensure pollen is transferred when the reward is collected. This means that floral traits need to be buffered against environmental variation to ensure that pollination continues to occur (Frazee & Marquis, 1994)), as this is vital for the production of a seed set and its subsequent germination. The bracts may also be subjected to stabilizing selection. Large bracts which act as floral advertisements may be more likely to attract more polli-

nators, but they may also increase the probability of seed predation (Pérez-Barrales *et al.* , 2013). This will act to maintain a consistent size of floral structures within a population.

The decoupling of floral and vegetative structures occurs because different factors drive selection for the size of these traits. The size of floral structures is genetically linked to pollinator fauna whilst the vegetative structure respond phenotypically to abiotic and biotic environmental conditions. This also means that it is expected that there might be greater variability in vegetative traits than in floral trait as a result of these different selection processes. Understanding these differences contributes to out knowledge of the evolution of plants and the contribution of genetic and environmental factors to plant phenotypic characteristics. The Berg Hypothesis has been demonstrated in a variety of different plants (Frazee & Marquis, 1994; Pérez-Barrales *et al.* , 2007; Herrera, 2005; Chalcoff *et al.* , 2008), including *Dalechampia scandens* grown in greenhouses (Hansen *et al.* , 2003, 2007; Pélabon *et al.* , 2005, 2011, 2012).

4.1.3.2 *D. scandens* response to environmental conditions

D. scandens has been the subject of many greenhouse studies (Hansen *et al.* , 2007; Pélabon *et al.* , 2005, 2011, 2012). Its response to different environmental conditions has been previously tested through manipulation of light and nutrient availability. There was a strong response in leaf size to different growing conditions, whilst bract size remained unaffected (Pélabon *et al.* , 2011), and this supports the Berg Hypothesis (Berg, 1960). Under favourable environmental conditions, such as higher nutrient availability, *D. scandens* leaf blade length increased. If a plant can put more resources into growing larger leaves, it is then likely to benefit from a greater photosynthetic surface area. Therefore, there is an advantage of vegetative traits being phenotypically variable, which does not apply to floral traits that are involved in pollination.

To date, published studies have only focused on greenhouse populations of this species and not wild *D. scandens* plants. The varying environmental conditions around Masaya Volcano National Park, produced by volcanic degassing provide a natural lab-

oratory in which to observe the response of *D. scandens*' vegetative and floral traits. *D. scandens* is commonly found in other disturbed areas across the park, including forest openings and grassland areas on recent lava flows. The species is common across the Pacific side of Nicaragua in seasonally dry to moist forests and second growth (Gargiullo, 2008). It is a climbing herbaceous vine characterized by stinging hairs (Stevens, 2015) . It has been the subject of many plant trait studies in the context of the Berg Hypothesis, but these have been conducted in a laboratory setting, rather than with wild-growing plants.

4.1.4 *Byrsonima crassifolia*

Byrsonima crassifolia is a tree found growing in similar environments to *D. scandens*. It is of great value to local people who use its wood and eat the fruit, which is also known to have pharmacological uses (Maldini *et al.* , 2009; Guilhon-Simplicio & de Meneses Pereira, 2011; Herrera-Ruiz *et al.* , 2011). It is also known to bio-accumulate pollutants, such as fluoride (Olivares & Pena, 2004).

No previous studies of the response of this tree to environmental conditions were found. Although some studies found tree species to have a negative response to exposure to pollution (Pourkhabbaz *et al.* , 2010; Nikula *et al.* , 2011; Leghari, 2013), others find no effect (Khavaninzadeh *et al.* , 2014; Jochner *et al.* , 2015). This might be because trees are less phenotypically plastic than other plant types. Additionally, no examples of the Berg Hypothesis have been previously found in tree species (Armbruster *et al.* , 1999). Therefore, *B. crassifolia* provides an interesting comparison to *D. scandens* as it is a valuable plant to the local community and a different response to volcanic gases might be expected because of its contrasting life history.

4.1.5 Aims

Using Masaya Volcano National Park as a 'natural laboratory' this study aims to explore the response of *D. scandens* and *B. crassifolia* traits to the environmental gradient

of volcanic degassing as defined using data collected in Chapter 2. This provides an opportunity for the first test of the Berg Hypothesis in a field setting for *D. scandens*, and for *B. crassifolia* is the second example of a study on the Berg Hypothesis in a tree species .

Secondly, this study aims to identify the environmental conditions under which *D. scandens* and *B. crassifolia* produce the longest leaf blades. Leaves would be expected to grow larger under more favourable environmental conditions, i.e. away from the volcanic plume. As noted in the previous Chapter, volcanic gases may also be affecting plants through feedbacks with environmental conditions such as soil pH and canopy openness.

4.2 Methods

4.2.1 Sampling strategy

During fieldwork in February and March 2014, *D. scandens* individuals were sampled from four areas within Masaya Volcano National Park, covering upwind of the volcano, an area partly affected by degassing, downwind of the volcano where gas levels were highest and near the crater (Figure 4.1. Precise locations and site names are given in Table C.1 in the Appendix). The areas were defined by exposure to the plume.

Plants were sampled between 20th of February and the 6th March 2014 and individuals that had blossoms in a recent state of opening, i.e. were presenting pollen and had an intact resin gland, were collected for measuring. As many sampling units (leaves and floral parts) as available were collected with a total of five from the Upwind zone, 19 from the Gas zone and 12 from the partly affected zone and four from the Crater zone.

As a comparison, in May and June 2014, *B. crassifolia* was sampled using a similar methodology (Figure 4.1 and Table C.2 in the Appendix). The sampling area was larger and extended into an agricultural area which is partly affected by the gases and also human activity, and these were classified with the Part samples as they had a low or irregular exposure to the gas plume. Plants were sampled between the 24th May and the 8th June 2014 and units that had blossoming flowers were selected for sampling. An average of three units were measured per site, with a total of 21 sites (five in Gas, seven in Part, and nine in Upwind).

4.2.2 *Dalechampia scandens* morphology

Each sampling unit comprised the upper (distal) and lower (proximal) bracts and the enclosed resin gland and styles, and the corresponding distal and proximal leaves found on the same stem (Figure 4.2). This is the typical growth form for *D. scandens*, and only samples with all of these components intact were selected. Measurements were

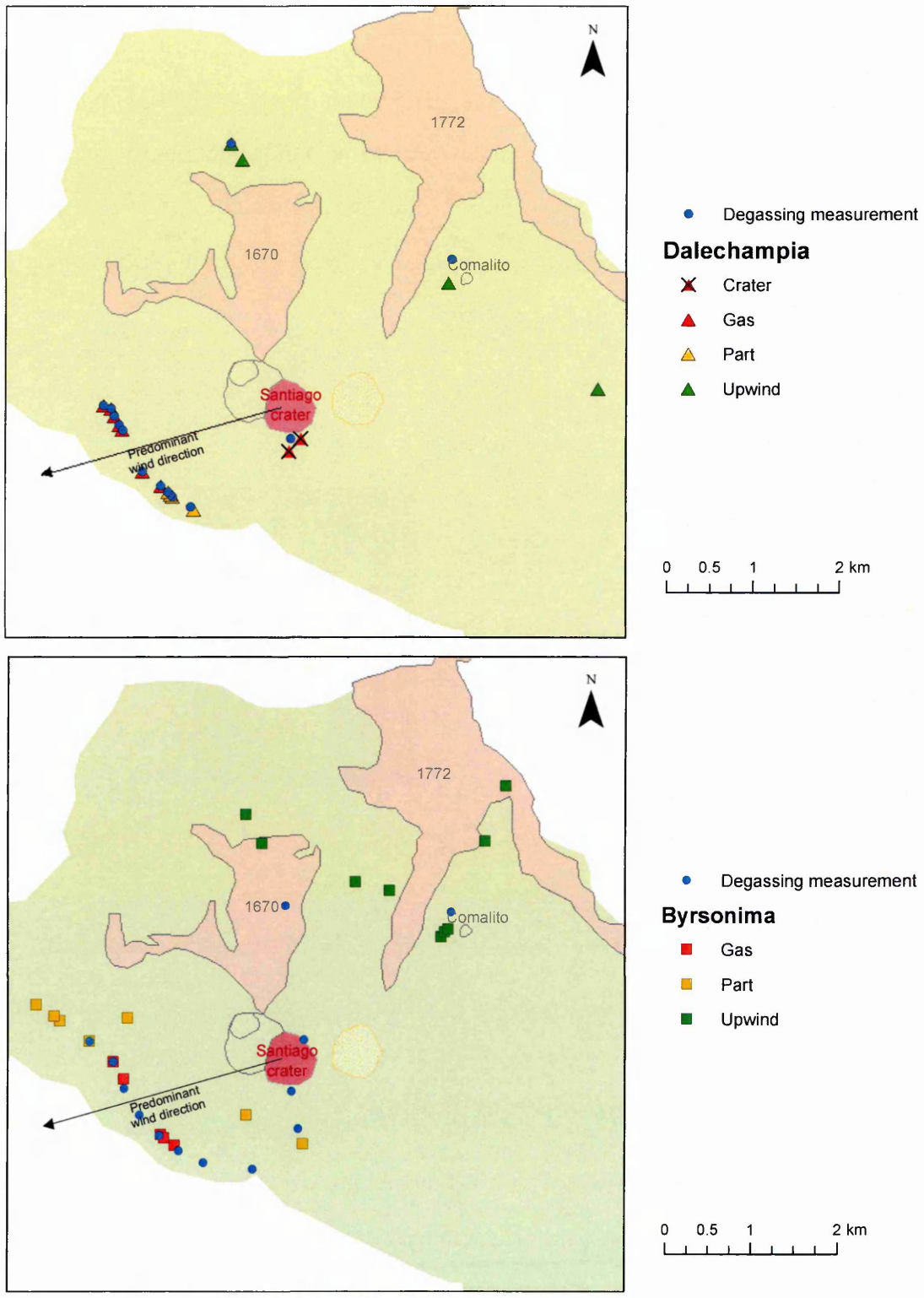

Figure 4.1: Map of Masaya Volcano National Park showing *D. scandens* and *B. crassifolia* sampling sites separated into four categories, and location of degassing measurements.

made of the leaf blade lengths (LD and LP) and the bract lengths (BD and BP), gland (G) and style (S). Leaf and bract lengths were taken with the adaxial surface of the organ facing upwards. Gland area (Ga) was calculated by multiplying the average of the left and right gland heights (Gh) by the gland width (Gw). G, the square root of the gland area, was used in order to keep the measurement units the same as the other traits (mm). The style length (S) was taken as the average length of the three styles present. All measurement were made using digital callipers (0.01 mm precision) and, where needed, a hand lens (x 10) was also used.

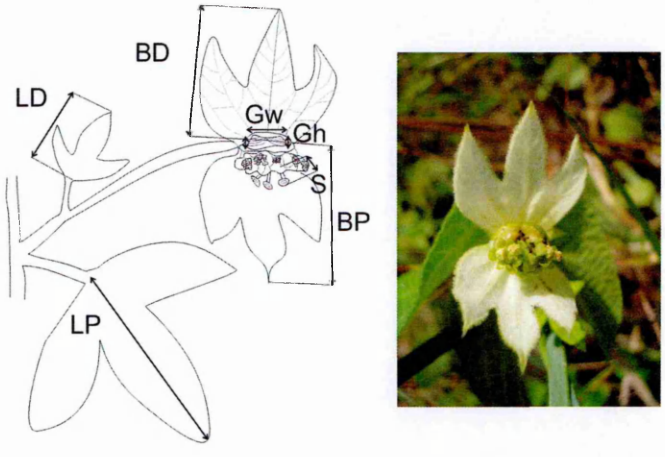

Figure 4.2: Drawing and photo of *D. scandens* to show leaf and blossom traits measured.

4.2.3 *Byrsonima crassifolia* morphology

For each individual tree, between two and four sampling units were measured. Each sampling unit (leaves and blossom) was removed from the tree where it branched off from the main stem, and measurements were made on the leaves, stem and blossom (Figure 4.3). The length (LL) and maximum width (LW) of the upper (closest to the blossom) pair of leaves were measured. The total stem length (SFL) was measured from the point at which it was cut off from the main branch to the tip of the blossom.

The blossom stem length (FL) was defined as the distance from the tip of the blossom to the point where the first florescence was found, and the leaf stem length (SL) was the distance from here to the point at which the unit was cut off from the main branch. All measurements were made using digital callipers (0.01 mm precision). The total number of pairs of leaves (Tot) was also noted.

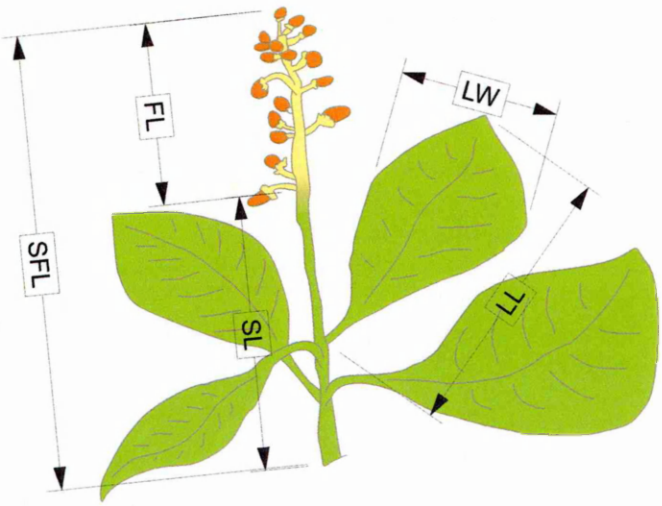

Figure 4.3: Drawing of *B. crassifolia* showing leaf and blossom traits measured.

4.2.4 Volcanic emissions

Volcanic gas (SO_2) concentrations and deposition rate were measured using diffusion tubes and sulfation plates respectively as described in Chapter 2. Since a measurement was not made at all sampling sites, SO_2 concentrations and deposition rate was taken from the Gaussian fit for sites along the transect (Gas and Part), or the nearest measurement (Upwind and Crater). Data from the closest sampling period were used, i.e. results from February 2014 were used with the *D. scandens* data, whilst results from May and June 2014 were used with the *B. crassifolia* data. The results from both May and June 2014 were included with the *B. crassifolia* data because they had very different profiles of volcanic gas concentrations. May 2014 had a very similar profile to February 2014, albeit with lower concentrations, whilst June 2014 had a much more

northerly centreline. Additionally, both May 2014 and February 2014 followed similar patterns to the average exposure to SO_2 (Chapter 3), suggesting that these provide good representations of long-term exposure too. The deposition rate data were also split into tree and ground heights, and both of these were used for *D. scandens*, but just the tree height data were used for *B. crassifolia*, to account for the growth height of the two different plants.

4.2.5 Soil pH and EC

Soil samples were collected at all *D. scandens* sites in February 2014, but due to time constraints this was not possible with *B. crassifolia* samples. At each sampling location, the organic layer was removed and three topsoil samples were collected and placed together in a sealed zip-lock bag. These were returned to the UK and analysed as described in Chapter 3 for soil pH and soil conductivity.

4.2.6 Statistical analyses

To test the Berg Hypothesis using the *D. scandens* data, the mean, standard deviation, range and coefficient of variation (CV) for each of the measured parameters for leaves and bracts were compared. Pearson's Correlation was used to identify any relationships between the measured morphological traits.

For *D. scandens* and *B. crassifolia*, Pearson's Correlation was used to identify the relationships between the measured morphological variables and environmental variables.

4.3 Results

Results tables are displayed in the appendix (Tables C.1 and C.2).

4.3.1 Variability and relationships amongst traits

Leaf parameters had a much higher standard deviation than bract parameters (Table 4.1), and their range was also much larger with distinctions between habitats. Leaf parameters also had higher coefficients of variation than bract parameters (Table 4.1).

	Mean	Standard Deviation	Minimum	Maximum	CV
Leaf (Distal)	21.52	9.84	7.96	45.37	0.46
Leaf (Proximal)	42.65	13.99	11.00	70.33	0.33
Bract (Distal)	12.45	3.17	6.76	20.37	0.25
Bract (Proximal)	13.97	4.21	5.66	22.69	0.30
Gland	3.45	0.45	2.63	4.23	0.13
Style	4.33	0.83	2.68	6.02	0.19

Table 4.1: Summary statistics on leaf and bract morphological measurements of *D. scandens*. All measurements in mm. n=40

4.3.1.1 Correlation

There was a positive correlation between proximal and distal leaf length, as well as between proximal bract length, distal bract length, gland size and style length (Table 4.2). There was no correlation between any leaf and bract parameters.

	LD	LP	BD	BP	G	SL	pH	EC	Conc. SO_2	Tree SO_2	Ground SO_2
LD	1.00	0.57					-0.55	0.40	0.62	0.58	0.47
LP	0.57	1.00					-0.41	0.35	0.44	0.47	0.44
BD			1.00	0.90	0.38	0.79				0.34	0.35
BP			0.90	1.00	0.35	0.76					
G			0.38	0.35	1.00	0.43					
SL			0.79	0.76	0.43	1.00					
pH	-0.55	-0.41					1.00	-0.53	-0.89	-0.92	-0.88
EC	0.40	0.35					-0.53	1.00	0.51	0.41	0.31
Conc. SO_2	0.62	0.44					-0.89	0.51	1.00	0.96	0.88
Tree SO_2	0.58	0.47	0.34				-0.92	0.41	0.96	1.00	0.96
Ground SO_2	0.47	0.44	0.35				-0.88	0.31	0.88	0.96	1.00

Table 4.2: Correlation between morphological and environmental variables for *D.scandens*. Only significant relationships at $p \leq 0.05$ level (0.304) are shown. Df= 38 (or 34 for pairs including EC) LD= distal leaf length, LP= proximal leaf length, BD= distal bract length, BP= proximal bract length, G= gland dimensions, SL= mean style length. Soil pH and EC, as well as SO_2 concentration and deposition rate (at tree and ground height) are included.

	LL	LW	SFL	FL	SL	Total	May SO_2	June SO_2	May (t) SO_2	June (t) SO_2
LL	1.00	0.77								
LW	0.77	1.00								
SFL			1.00	0.92	0.70					
FL			0.92	1.00						
SL			0.70		1.00					
Total						1.00				
May SO_2							1.00	0.53	0.98	0.54
June SO_2							0.53	1.00	0.53	0.99
May (t) SO_2							0.98	0.53	1.00	0.54
June (t) SO_2							0.54	0.99	0.54	1.00

Table 4.3: Correlation between morphological and environmental variables for *B. crassifolia*. Only significant relationships at $p \leq 0.05$ level (0.413) are shown. Df= 19. LL=leaf length, LW= leaf width, SFL= total stem length, FL= blossom stem length, SL= leaf stem length and Tot= total number of leaves. SO_2 concentration and deposition rate at tree height (t) has been included for May and June 2014.

4.3.2 Responses to different environments

SO_2 concentration, and deposition rate at both tree and ground level as well as soil pH and EC had a significant positive relationship (Table 4.2) with *D. scandens* distal and proximal leaf lengths (LD and LP). The distal bract length (BD) was correlated with SO_2 deposition rate at both tree and ground level, but there were no other significant correlations between bract characteristics and environmental variables.

B. crassifolia had a very strong relationship between leaf length and width (Table 4.3). Additionally, all stem characteristics were well correlated with each other, with the exception of blossom stem length (FL) and leaf stem length (SL). The environmental variables were correlated with each other, but not with any of the morphological data.

4.4 Interpretation

4.4.1 *Dalechampia scandens*

4.4.1.1 Variability and relationships among traits

There was considerable variation in leaf blade length. This was not as strong in bract length, or other characteristics of the blossom (Table 4.1). Given the relative proximity of all the samples in this study, it is likely that they were part of the same population, so would all have been potentially able to interbreed. This means that they would have been pollinated by the same species of bee and, therefore, expected to have very similar sized bracts. Some of the variation in bract size might be related to the developmental stage of the floral structure, as it was not possible to ascertain whether each one was sampled on the first day of opening (flowering may last for over one week, Armbruster *et al.* (2009)).

The dimensions of the four floral traits (BP, BD, G and S) were positively correlated amongst themselves (Table 4.2). There was a strong relationship between upper and lower bract lengths (Table 4.2). This is likely because the bracts are under strong selection for precision, meaning that they must be of a consistent corresponding size to serve their role in protecting the floral bud (Hansen *et al.* , 2007). The leaf structures (proximal and distal leaf) were correlated with each other but not with the floral structures. This supports the Berg hypothesis, because it implies that different selection pressures are operating on the vegetative and reproductive traits.

4.4.1.2 Responses to different environments

Pearson's correlation analysis found that factors relating to high exposure to volcanic degassing (high SO_2 concentration and deposition rate at tree and ground level alongside a low soil pH) had a strong positive correlation with leaf lengths, but not with bract variables. This contrasts with a decrease in leaf size typically associated with increased

exposure to pollutants (Pandey & Agrawal, 1994; Dodd & Doley, 1998; Honour *et al.* , 2009; Pourkhabbaz *et al.* , 2010; Leghari, 2013).

Greenhouse studies (Pélabon *et al.* , 2011) found an increase in *D. scandens* leaf blade length under higher nutrient and light environments. Therefore, this suggests that growing conditions for *D. scandens* were more favourable in the area that is most affected by volcanic degassing. Whilst this may seem counter-intuitive, since volcanoes release many pollutants into the downwind environment, it is possible that the volcanic plume provided some advantages to *D. scandens* growing in this area.

Sulfur dioxide is a key volcanic constituent and it is also known from industrial pollution to have highly damaging effects on plants (Winner *et al.* , 1986; Nelson & Sewake, 2008; Chung *et al.* , 2011). Plants growing under high gas conditions might have required a larger leaf size in order to obtain sufficient CO_2 from the atmosphere. However, it appeared that plants were growing vigorously in the downwind zone and there was no evidence of necrosis or chlorosis on the leaves of these plants, which suggests that the SO_2 concentrations were not too high. Previous work near Masaya identified two plant species that were able to neutralize volcanogenic acid rain (Johnson & Parnell, 1986) by adding base cations (e.g. K^+) to the water. If *D. scandens* had a similar mechanism for dealing with volcanic pollution it might have been able to directly or indirectly benefit from these volcanic emissions.

Volcanic SO_2 might have been linked to increased photosynthesis (Gu *et al.* , 2003). When volcanic sulfur dioxide is oxidized to sulfate aerosols in the atmosphere, this produces a ground level increase in the amount of diffuse sunlight and cooling through a reduction in surface radiation (Lamb, 1970; Robock *et al.* , 2007). Although this process is associated with stratospheric volcanic sulfur emissions from large explosive eruptions, persistent degassing from volcanoes like Masaya is likely to have similar effects on incoming radiation (Schmidt *et al.* , 2012), because the source of the sulfate aerosols is being continually replenished. This could reduce the impacts of the midday depression, where photosynthesis in tropical forests decreases as the temperature becomes too high (Pons & Welschen, 2003).This supports a greenhouse study where a

simulated longer day length was linked to larger leaf growth in D. scandens (Pélabon *et al.* , 2011).

Degassing volcanoes principally emit water vapour H_2O and CO_2 (Oppenheimer, 2003). Where there were high volcanic SO_2 concentrations and deposition rates it can be inferred that there would also have been elevated CO_2 and H_2O concentrations. Both of these are used in photosynthesis by plants during the day and have been previously associated with enhanced plant growth (Nobel, 2009; Kläring *et al.* , 2007; Chalcoff *et al.* , 2008). Elevated atmospheric concentrations of CO_2 and H_2O might have been benefiting those plants that can tolerate the high concentrations of other toxic gases, such as SO_2. Using the previously estimated mass ratios (Burton *et al.* , 2000) of SO_2 and H_2O (18-20), and SO_2 and CO_2 (1.5-1.7) from Fourier transform spectrometery at Masaya, it was possible to estimate the volcanic contribution to the atmospheric concentrations of these gases. For both H_2O and CO_2, it appears that volcanic degassing would have increased the atmospheric concentration by less than 1%. Therefore, it seems unlikely that either of these were responsible for increasing the leaf size of *D. scandens* plants growing downwind of Masaya.

However, a study at Turrialba Volcano in Costa Rica found that the rate of photosynthesis *Gunnera insignis* appeared unaffected along a gradient of exposure to volcanic degassing, where high SO_2 and CO_2 concentrations were found (Jenkins, 2012). It is possible that volcanic CO_2 may have accumulated near the ground as it is denser than air (e.g. Lake Nyos disaster in 1986). CO_2 is known to reduce the damaging effects of SO_2 pollution on plants (Baker *et al.* , 1997; Mulpuri & Luit, 1994; Agrawal & Singh Deepak, 2003). This is because the physiological response of a leaf to elevated atmospheric CO_2 concentrations reduces the amount of SO_2 that can enter the leaf, and elevated CO_2 can allow for more carbon to detoxify SO_2. Therefore, it is possible that volcanogenic CO_2 was accumulating near the ground downwind of Masaya, and enhancing *D. scandens*' growth.

Volcanoes also directly emit small amounts of many trace elements and metals such as iron, and if any of these are key nutrients for *D. scandens* this might have been en-

hancing its growth in the downwind zone. Equally, a decrease in soil pH caused by the deposition of acidifying compounds, such as sulfate, chloride and fluoride (Delmelle *et al.* , 2003), will affect the bioavailability of nutrients. An increase in available nutrients for *D. scandens* might have also occurred as a result of ash fertilization (Frogner *et al.* , 2001; Lansing *et al.* , 2001; Shoji & Takahashi, 2002), as dispersal from a small eruption is likely to follow that of the gas plume. There was a slight increase in the EC (electrical conductivity of the soil, a possible indicator of nutrient level) in the downwind zone, but it did not have a strong relationship with leaf length characteristics. Therefore, it seems unlikely that total nutrient availability explains the more vigorous growth of *D. scandens* in the downwind zone, though it is possible that there are one or two specific nutrients that are more bioavailable here. Further study is required to determine any possible nutrients emitted by Masaya that would otherwise be lacking in the downwind zone and be required by *D. scandens*.

Individual plants form a part of the ecosystem, which as identified in Chapter 3 will also be responding to longer term patterns in volcanic gas emission and dispersal. Since the downwind zone is partially vegetated, this might have reduced competition for resources, particularly light where there were fewer trees. However, this is not thought to be an important factor, since individuals from the upwind group were growing in similarly open areas too (e.g. Pencas). Those in the partly affected group had the most canopy cover and greatest density of surrounding vegetation, but these did not have the largest leaves.

In summary, it is challenging to attribute enhanced leaf growth in *D. scandens* directly or indirectly to one volcanic gas. It appears than under current levels, SO_2 is not damaging to this plant. If downwind atmospheric CO_2 or H_2O ratios are different downwind from previous measurement at the crater, perhaps as a result of topography, this seems like the most likely explanation for enhanced leaf growth. Measurements of light levels, atmospheric CO_2 and H_2O and soil micro nutrients would be beneficial in determining the cause of larger leaf growth in *D. scandens* downwind of Masaya.

4.4.2 *Byrsonima crassifolia*

4.4.2.1 Variability and relationships among traits

B. crassifolia leaf measurement were strongly associated with each other, but not with measurements of floral characteristics. This suggests that this species supports the Berg Hypothesis as its vegetative traits are decoupled from floral traits. Whilst *B. crassifolia* is known to be pollinated by 25 different species of oil collecting bee (Alvarez & Landeiro, 2008), these results suggest that this tree may have evolved a specialized pollination system, whose morphology is decoupled from vegetative traits and environmental variation. Although it may have a range of pollinator species, if these are of similar size and behaviour, they may perform the same function for *B. crassifolia.*

4.4.2.2 Responses to different environments

No *B. crassifolia* morphological variables showed any significant relationship with gas concentrations. This suggests that this plant is tolerant of the environmental conditions produced by current and past degassing from Masaya Volcano, despite no evidence of any benefits to this species. This species is highly valuable in the local community as it provides wood and fruit, and it is also known to have pharmacological uses (Maldini *et al.* , 2009; Guilhon-Simplicio & de Meneses Pereira, 2011; Herrera-Ruiz *et al.* , 2011). It may be a useful pollutant tolerant species to grow in the area downwind of the volcano.

4.4.3 Comparison

It is possible that these differences between the two species can be explained by their growth form; *D. scandens* is a vine whereas *B. crassifolia* is a tree. This might be a results of a higher exposure to volcanic gas emissions for *B. crassifolia* than *D. scandens*, because of typically higher deposition rates at tree than ground height as recognised in Chapter 2.

These two plant species, whilst able to grow in a similar location, will have different limiting conditions with respect to other environmental variables, such as water availability and nutrients. Difference in life-histories might mean that trees such as *B. crassifolia* less phenotypically plastic, and therefore less likely to show a response.

This suggests that the relationship seen in *D. scandens* is not found in all plant species that grow under the highly polluted conditions produced by Masaya Volcano, and may be unique to this plant. Therefore, further work is required to fully understand why *D. scandens* produced larger leaves where volcanic pollution was highest.

4.4.4 Implications and further work

A better understanding of the individual plant response to volcanic gases would benefit our forecasts of the potential impacts of increased air pollution in the tropics, which is expected to be a key component of future global change (Pozzer *et al.* , 2012). This might be applied to develop pollution resistant crops and better agricultural practices in a polluted environment.

Explaining *D. scandens* leaf variability is challenging, particularly given that many volcanic environmental variables co-vary, and therefore it is difficult to separate them. Since there was not a similar pattern found in another plant species, *B. crassifolia*, it is perhaps unlikely that volcanic gas emissions were enhancing photosynthesis. Further work isolating the direct and indirect effects of individual volcanic gas constituents (e.g. CO_2 and H_2O) might be able to identify which is responsible for enhanced leaf growth in *D. scandens*.

It would also be beneficial to consider other aspects of *D. scandens* and *B. crassifolia* vitality in a future study. Previous work has shown that volcanic pollution can also affect reproductive success, both positively and negatively (Abe *et al.* , 2014). It would be necessary to consider how volcanic gases affect pollination and seed dispersal to ascertain whether they are producing any long-term impacts to these plant species.

Previous studies of the impacts of industrial pollution on plant growth have found notable seasonal variation in both pollutant composition and plant response (Tiwari *et al.* , 2010; Leghari, 2013). Impacts on plants might also depend on the stage in the life cycle, as younger plants are thought to be more sensitive (Honour *et al.* , 2009). Pollution can also effect plant phenology (Honour *et al.* , 2009; Jochner *et al.* , 2015) including timing of senescence and flowering. Chapter 2 identified variation in both gas emission rate and the dispersal of the volcanic plume through time. The timing of high volcanic gas concentrations and deposition rates might have a strong influence on the individual plant response. A repeat of this study at different times of the year and under different gas levels would be beneficial in supporting the results presented here.

4.5 Conclusions

This study has confirmed the Berg Hypothesis using wild *Dalechampia scandens* growing in a field setting. Variability in vegetative traits is greater than those of the blossom, and these two are decoupled. Interestingly, the largest leaves, which have previously been associated with higher nutrient availability and therefore favourable growing conditions, are found in the mostly devegetated zone downwind of the volcano where exposure to volcanic gases is high. It is unclear exactly which volcanic gas constituents are producing this unexpected relationship, which was not found in another plant, *B. crassifolia*, that also tolerates growing in the area immediately downwind of the volcano. *D. scandens* is, therefore, an interesting candidate species for future research in the context of tolerance of extreme environmental conditions. By understanding how *D. scandens* can tolerate and thrive under highly polluted conditions, it may be possible to apply this to the development of pollution resistant crop species. Further research could inform our understanding of how different plant species respond to complex mixes of volcanic emissions.

Chapter 5

Conclusions

5.1 Summary

5.1.1 Volcanic gas concentrations and deposition rates downwind of Masaya

Chapter 2 aimed to quantify volcanic gas concentrations and deposition rates (of SO_2, HCl and HF) along a transect several kilometres downwind from Masaya. Across five sampling seasons (February 2013, December 2013, February 2014, May 2014 and June 2014), data were collected upwind, at the crater and along a transect downwind of the volcano. There was no significant upwind contribution to the measured volcanic gas concentrations or their deposition rate. There were considerable differences in the rate of degassing between the sampling periods, as estimated by measurements at the crater rim. Additionally, most of the data collected followed a Gaussian distribution and the maximum concentrations and integrals estimated by this along the transect were also highly variable between sampling periods.

A significant relationship between the transect integral and measurements at the crater (OCP) was found for SO_2 concentration and deposition rate at tree height and all HCl measurements. Overall, the gas emissions measured appeared to be much lower than in previous studies, implying that higher volcanic gas levels might have been

previously found along the transect. Nevertheless, very high concentrations of SO_2 were found at most sampling sites, considerably exceeding World Heath Organization recommendations for human exposure.

From both the centreline estimated by the Gaussian fit to concentration and deposition rate data, and wind data calculated from the HYSPLIT model, it appeared that the plume direction was relatively consistent, with the exception of a more northerly bearing in June 2014. There was a significant link between these Gaussian models and the HYSPLIT data. Calculated dry deposition velocities for SO_2 and HF were lower during wet season measurements, which is likely as a result of preferential wet precipitation. No measurements were made during the height of the rainy season, when greater changes in wind direction and deposition regimes might have been expected. Additionally, further work is required to understand the role of wind speed, plume height and atmospheric stratification on the resulting gas distribution (e.g. width parameter). Overall, this chapter identified high gas emissions from Masaya, with a strong potential for environmental and ecological impacts.

5.1.2 Plant communities downwind of Masaya

A plant community scale study was used with the aim of quantifying the impacts of volcanic degassing on the vegetation as a whole along the transect. The gradient produced by volcanic SO_2 from Masaya had a strong influence on a range of ecological and environmental factors. Downwind of the volcano, there was a species poor community, comprising small plants (grasses, herbs, fern and a shrub). This was likely as a result of the high pollution and low soil pH, as well as feedbacks with the leaf litter layer and canopy cover. This contrasted with a species rich and diverse tropical dry forest community on an unexposed section of the same lava flow, as well as newly colonized lava flows. The presence of trees produced a denser canopy, more leaf litter and encouraged the presence of understory species. This study provided limited evidence for the Intermediate Disturbance Hypothesis.

The environmental and ecological data suggest that exposure to volcanic SO_2 has played an important role in shaping the ecosystem downwind of the volcano, and this had been supported by feedbacks between tree establishment, leaf litter and soil formation, all of which influence the direction of succession. The lack of evidence for succession in the area downwind of the volcano suggests that volcanic degassing might have continued further back in time than is known from historical records. If this is correct, further work could allow for plant community studies to infer past gas outputs at other volcanoes.

5.1.3 *Dalechampia scandens* response to volcanic gases

There were two aims of Chapter 3: to test the Berg Hypothesis using *Dalechampia scandens* and *Byrsonima crassifolia* in a field setting and to test the response of these species to high concentrations of volcanic SO_2. Measurements of leaf and bract characteristics found strong evidence for the decoupling of units, which supports the Berg Hypothesis for both species.

D. scandens leaf length responded positively to an increase in SO_2 concentration, indicating that the gas plume is providing a more favourable environment for the growth of this species. This relationship was also tested in another species that was found abundantly around the volcano, *B. crassifolia*, and no relationship was found between the leaf or bract characteristics of this species and exposure to volcanic gases.

D. scandens might be benefiting directly from volcanic emissions (e.g. CO_2, H_2O, trace metals), or indirectly through the effects of SO_2 on incoming radiation or changes to the soil (increased acidity affecting nutrient availability or ash fertilization). Although it was not possible to determine the precise mechanism by which *D. scandens* leaves grow bigger, this chapter has shown that it is a pollution tolerant plant, making it an interesting candidate species for future research.

5.2 Concluding remarks and future work

The volcanic gas concentrations measured in this study were considerably lower than in previous research. This variability of volcanic degassing over different timescales makes it challenging to determine a threshold at which an ecological response can be predicted. However, the low variability in the wind direction at Masaya produces a gradient of exposure, which appear to be relatively consistent. With this in mind, it is possible that the plant community chapter represents a long-term response to volcanic degassing, whilst *D. scandens* is responding to more contemporary gas levels. This is because vegetation succession happens over very long timescales as it requires inputs of seeds and the growth of plants to maturity. Individuals of *D. scandens* however, that were able to tolerate previously high gas concentrations, might have been able to grow rapidly in a nutrient rich and competition free environment as pollution decreased. This highlights the importance of scale, when measuring the ecological response to an environmental disturbance.

The volcanic gas concentrations and deposition rates measured in this study clearly pose a threat to human health, particularly to local people living and working in proximity to the volcano. Additionally, there is an indirect impact from the gases on vegetation and, therefore, crops and livestock grazing in the area affected by the volcano. However, the identification of pollution tolerant species that are local to the area might be able to provide possible solutions for local farmers.

A continuous long-term data set of gas emissions would be helpful in determining the extent to which volcanic emissions are typical, high or low on both short and long times-scales. Additionally, a more continuous data set, with more measurements from the wet season would also be useful, alongside quantification of wet deposition.

This, alongside regular data on the plant communities would also allow for a better understanding of the response of different plant species to variations in gas emission rates, particularly if there were large increases or decreases in the amount of gas emitted from the volcano. It would allow for the determination of time-scales of disturbance

and recovery specific to the tropical dry forest ecosystem at Masaya. Future studies would also benefit from including fauna in an ecological assessment, as volcanic gas emissions are likely to have both a direct impact, as well as an indirect effect through vegetation. Additionally, similar studies at other degassing volcanoes would be useful for comparison between different ecosystems.

More work is also required to better understand the relationship between exposure to the volcanic plume and *D. scandens* growth. This could involve measurements of photosynthesis at the leaf level, chemical analyses of soil and plant material or greenhouse or field experiments with plants. As with the plant communities data, another sampling season, with different gas fluxes would also be beneficial, which might allow for thresholds to be defined.

Additionally, this work could be used to inform future studies on the ecological impacts of volcanic or industrial pollution in the tropics.

Bibliography

Abe, H., Takahashi, T., & Hasegawa, M. 2014. Effects of volcanic disturbance on the reproductive success of Eurya japonica and its reproductive mutualisms. *Plant Ecology*, **215**(11), 1361–1372.

Abrams, M. D. 2011. Adaptations of forest ecosystems to air pollution and climate change. *Tree Physiology*, **31**(3), 258–261.

Agrawal, M., & Singh Deepak, S. 2003. Physiological and biochemical response of two cultivars of wheat to elevated levels of CO_2 and SO_2, singly and in combination. *Environmental Pollution*, **121**, 189–197.

Aiuppa, A., Baker, D. R., & Webster, J. D. 2009. Halogens in volcanic systems. *Chemical Geology*, **263**(1-4), 1–18.

Allen, A. G., Cardoso, A. A., Wiatr, A. G., Machado, C. M. D., Paterlini, W. C., & Baker, J. 2010. Influence of Intensive Agriculture on Dry Deposition of Aerosol Nutrients. *Journal of Brazilian Chemical Society*, **21**(1), 87–97.

Allen, G. 2002. Primary sulfate aerosol and associated emissions from Masaya Volcano, Nicaragua. *Journal of Geophysical Research*, **107**(D23), 4682.

Alvarez, C.B., & Landeiro, M. 2008. *Pollinators Management in Brazil*. Tech. rept. Ministry of the Environment.

Andres, R. J., & Kasgnoc, A. D. 1998. A time-averaged inventory of subaerial volcanic sulfur emissions. *Journal of Geophysical Research*, **103**(D19), 25251.

Angold, P.G. 1997. The impact of a road upon adjacent heathland vegetation: effects on plant species composition. *Journal of Applied Ecology*, **34**, 409–417.

Armbruster, W. S., Hansen, T. F., Pélabon, C., Pérez-Barrales, R., & Maad, J. 2009. The adaptive accuracy of flowers: measurement and microevolutionary patterns. *Annals of botany*, **103**(9), 1529–1545.

Armbruster, W. Scott, Di Stilio, Veronica S., Tuxill, John D., Flores, T. Christopher, & Velasquez Runk, Julie L. 1999. Covariance and decoupling of floral and vegetative traits in nine Neotropical plants: a re-evaluation of Berg's correlation-pleiades concept. *Am. J. Botany*, **86**(1), 39–55.

Babin-Fenske, J., & Anand, M. 2011. Patterns of insect communities along a stress gradient following decommissioning of a Cu-Ni smelter. *Environmental Pollution*, **159**(10), 3036–3043.

Baker, J. T., Allen Jr., L. H., Boote, K. J., & Pickering, N. B. 1997. Rice responses to drought under carbon dioxide enrichment. 1. Growth and yield. *Global Change Biology*, **3**, 119–128.

Barrancos, J., Roselló, J. I, Calvo, D., Padrón, E., Melián, G., Hernández, P.A., Pérez, N.M., Millán, M.M., & Galle, B. 2008. SO_2 Emission from Active Volcanoes Measured Simultaneously by COSPEC and mini-DOAS. *Pure and Applied Geophysics*, **165**(1), 115–133.

Bashan, Y., Li, C. Y., Lebsky, V. K., Moreno, M., & De-Bashan, L. E. 2002. Primary Colonization of Volcanic Rocks by Plants in Arid Baja California, Mexico. *Plant Biology*, **4**(3), 392–402.

Bellomo, S., Aiuppa, A., D'Alessandro, W., & Parello, F. 2007. Environmental impact of magmatic fluorine emission in the Mt. Etna area. *Journal of Volcanology and Geothermal Research*, **165**(1-2), 87–101.

Berg, R. L. 1960. The Ecological Significance of Correlation Pleiades. *Evolution*, **14**(2), 171–180.

Bernhardt-Römermann, M., Kirchner, M., Kudernatsch, T., Jakobi, G., & Fischer, a. 2006. Changed vegetation composition in coniferous forests near to motorways in Southern Germany: The effects of traffic-born pollution. *Environmental Pollution*, **143**, 572–581.

Bobbink, R., Hornung, M., & Roelofs, J. G. M. 1998. The effects of air-borne nitrogen pollutants on species diversity in natural and semi-natural European vegetation. *Journal of Ecology*, **86**, 717–738.

Bourque, C.P.A., & Arp, P.A. 1996. Simulating sulfur dioxide plume dispersion and subsequent deposition downwind from a stationary point source: a model. *Environmental Pollution*, **91**(3), 363–380.

Briffa, K. R., Jones, P. D., Schweingruber, F. H., & Osborn, T. J. 1998. Influence of volcanic eruptions on Northern Hemisphere summer temperature over the past 600 years. *Nature*, **393**, 450–455.

Burson, B. R. 2012. *Deposition from Volcán Turrialba's plume on surrounding vegetation*. Undergraduate Dissertation, University of Cambridge.

Burton, J. I., Mladenoff, D. J., Forrester, J. A., & Clayton, M. K. 2014. Experimentally linking disturbance, resources and productivity to diversity in forest ground-layer plant communities. *Journal of Ecology*, **102**, 1634–1648.

Burton, M. R., Oppenheimer, C., Horrocks, L. A., & Francis, P. W. 2000. Remote sensing of CO_2 and H_2O emission rates from Masaya volcano, Nicaragua. *Geology*, **28**(10), 915.

Campbell, B. M., Lynam, T., & Hatton, J. C. 1990. Small-Scale Patterning in the Recruitment of Forest Species during Succession in Tropical Dry Forest, Mozambique. *Vegetatio*, **87**(1), 51–57.

Carr, M. J. 1984. Symmetrical and segmented variation of physical and geochemical characteristics of the central american volcanic front. *Journal of Volcanology and Geothermal Research*, **20**(3-4), 231–252.

Cerón, R. M., Cerón, J. G., Córdova, A. V., Zavala, J., & Muriel, M. 2005. Chemical Composition of Precipitation at Coastal and Marine Sampling sites in Mexico. *Global NEST Journal*, **7**(2), 212–221.

Chalcoff, V. R., Ezcurra, C., & Aizen, M. A. 2008. Uncoupled geographical variation between leaves and flowers in a South-Andean Proteaceae. *Annals of Botany*, **102**(1), 79–91.

Chang, C. C., & del Moral, R. 2015. Multiple assessments of succession rates on Mount St . Helens. *Plant Ecology*, **216**, 165–176.

Chevennement, R. 1990. La colonisation vegetale d'un champ de lave de la Reunion. *Compte Rendu des Seances de la Societe de Biogeographie*, **66**(2), 47–63.

Chung, C. Y., Chung, P. L., & Liao, S. W. 2011. Carbon fixation efficiency of plants influenced by sulfur dioxide. *Environmental Monitoring and Assessment*, **173**(1-4), 701–707.

Conti, M. 2001. Biological monitoring: lichens as bioindicators of air pollution assessment a review. *Environmental Pollution*, **114**(3), 471–492.

Cutler, N. 2009. Long-term primary succession: a comparison of non-spatial and spatially explicit inferential techniques. *Plant Ecology*, **208**(1), 123–136.

D'Alessandro, W., Bellomo, S., & Parello, F. 2008. Fluorine speciation in topsoils of three active volcanoes of Sicily (Italy). *Environmental Geology*, **56**(2), 413–423.

del Moral, R., & Jones, C. 2002. Vegetation development on pumice at Mount St Helens, USA. *Plant Ecology*, **162**(9-22).

Delfosse, T., Delmelle, P., Iserentant, A., & Delvaux, B. 2005. Contribution of SO_3 to the acid neutralizing capacity of Andosols exposed to strong volcanogenic acid and SO_2 deposition. *European Journal of Soil Science*, **56**(1), 113–125.

Delmelle, P., Baxter, P., Beaulieu, A., Burton, M., Francis, P., Garcia-Alvarez, J., Horrocks, L., Navarro, M., Oppenheimer, C., Rothery, D., Rymer, H., St. Amand, K., Stix, J., Strauch, W., & Williams-Jones, G. 1999. Origin, effects of masaya volcano's continued unrest probed in Nicaragua. *Eos*, **80**(48), 575–581.

Delmelle, P., Stix, J., Bourque, C. P. A., Baxter, P. J., Garcia-Alvarez, J., & Barquero, J. 2001. Dry Deposition and Heavy Acid Loading in the Vicinity of Masaya Volcano, a Major Sulfur and Chlorine Source in Nicaragua. *Environ Sci Technol*, **35**(7), 1289–1293.

Delmelle, P., Barquero, J., Stix, J., Baxter, P., & Garcia-Alvarez, J. 2002. Atmospheric dispersion, environmental effects and potential health hazard associated with the low-altitude gas plume of Masaya volcano, Nicaragua. *Bulletin of Volcanology*, **64**(6), 423–434.

Delmelle, P., Delfosse, T., & Delvaux, B. 2003. Sulfate, chloride and fluoride retention in Andosols exposed to volcanic acid emissions. *Environmental Pollution*, **126**(3), 445–457.

Dirnbock, T., Grandin, U., Bernhardt-Romermann, M., Beudert, B., Canullo, R., Forsius, M., Grabner, M. T., Holmberg, M., Kleemola, S., Lundin, L., Mirtl, M., Neumann, M., Pompei, E., Salemaa, M., Starlinger, F., Stszewski, T., & Uzieblo, A. K. 2014. Forest floor vegetation response to nitrogen deposition in Europe. *Global Change Biology*, **20**, 429–440.

Dodd, I C, & Doley, D. 1998. Growth responses of cucumber seedlings to sulphur dioxide fumigation in a tropical environment. *Environmental and Experimental Botany*, **39**, 41–47.

Draxler, R. R. 2013. *HYSPLIT4 user's guide.*

Duarte, E., & Fernandez, E. 2011. *Ampliacion y Profundizacion de Efectos por Lluvia Acida en el Volcan Turrialba (Basado en vistas al campo entre febrero y marzo de 2011).* Tech. rept. OVSICORI-UNA.

Evans, C. D., Monteith, D. T., Fowler, D., Cape, J. N., & Brayshaw, S. 2011. Hydrochloric acid: an overlooked driver of environmental change. *Environment, Science and Technology*, **45**(5), 1887–1894.

Floor, G. H., Calabrese, S., Roman-Ross, G., D'Alessandro, W., & Aiuppa, A. 2011. Selenium mobilization in soils due to volcanic derived acid rain: An example from Mt Etna volcano, Sicily. *Chemical Geology*, **289**(3-4), 235–244.

Fowler, D., Cape, J. N., Coyle, M., Flechard, C., Kuylenstierna, J., Hicks, K., Derwent, D., Johnson, C., & Stevenson, D. 1999. The global exposure of forests to air pollutants. *Water, Air, and Soil Pollution*, **116**(1-2), 5–32.

Fox, J. F., & Connell, J. H. 1979. Intermediate-Disturbance Hypothesis. *Science*, **204**(4399), 1344–1345.

Frazee, J. E., & Marquis, R. J. 1994. Environmental Contribution to Floral Trait Variation in Chamaecrista fasciculata (Fabaceae : Caesalpinoideae). *American Journal of Botany*, **81**(2), 206–215.

Frogner, P., Gíslason, S. R., & Óskarsson, N. 2001. Fertilizing potential of volcanic ash in ocean surface water. *Geology*, **29**(6), 487–490.

Fuhrer, J., Skarby, L., & Ashmore, M.R. 1997. Critical levels for ozone effects on vegetation in Europe. *Environmental Pollution*, **97**(1), 91–106.

Gargiullo, M. B. 2008. *A Field Guide to Plants of Costa Rica.* Oxford: Oxford University Press.

Gauci, V, Matthews, E, Dise, N, Walter, B, Koch, D, Granberg, G, & Vile, M. 2004. Sulfur pollution suppression of the wetland methane source in the 20th and 21st centuries. *Proc Natl Acad Sci U S A*, **101**(34), 12583–12587.

Gillespie, T. W., & Walter, H. 2001. Distribution of bird species richness at a regional scale in tropical dry forest of Central America. *Journal of Biogeography*, **28**, 651–662.

Godoi, R. H. M., Godoi, A. F. L., Gonçalves Junior, S. J., Paralovo, S. L., Borillo, G. C., Gonçalves, G. B C, Arantes, M.G., Charello, R.C., Rosário Filho, N. A., Grassi, M.T., Yamamoto, C.I., Potgieter-Vermaak, S., Rotondo, G.G., De Wael, K., & van Grieken, R. 2013. Healthy environment–indoor air quality of Brazilian elementary schools nearby petrochemical industry. *The Science of the Total Environment*, **463-464**(Oct.), 639–46.

Gradko Environmental. 2012. *Technical Data Sheet : TDS 5, DIF 900 RTU Sulphur Dioxide*.

Gradko Environmental. 2014a. *How do Palmes diffusion tubes work?*

Gradko Environmental. 2014b. *Technical Data Sheet : TDS 3A, DIF 900 RTU - Acid Gases*.

Grasso, M. F., Clocchiatti, R., Carrot, F., Deschamps, C., & Vurro, F. 1999. Lichens as bioindicator in volcanic areas: Mt. Etna and Vulcano Island (Italy). *Environmental Geology*, **37**(3), 207–217.

Gu, L., Baldocchi, D. D., Wofsy, S. C., Munger, J. W., Michalsky, J. J., Urbanski, S. P., & Boden, T. A. 2003. Response of a deciduous forest to the Mount Pinatubo eruption: enhanced photosynthesis. *Science*, **299**, 2035–2038.

Guilhon-Simplicio, F., & de Meneses Pereira, M. 2011. Aspectos Quimicos e farmacologicos de Byrsonima (Malpighiaceae). *Quim. Nova*, **34**(6), 1032–1041.

Hansen, T. F., Armbruster, W. S., Carlson, M. L., & Pélabon, C. 2003. Evolvability and Genetic Constraint in Dalechampia Blossoms : Genetic Correlations and Conditional Evolvability. *Journal of Experimental Zoology (Mol Dev Evol)*, **296B**, 23–39.

Hansen, T. F., Pélabon, C., & Armbruster, W. S. 2007. Comparing Variational Properties of Homologous Floral and Vegetative Characters in Dalechampia scandens: Testing the Berg Hypothesis. *Evolutionary Biology*, **34**(1-2), 86–98.

Harrison, R.M., & McCartney, H.A. 1980. A comparison of the predictions of simple Gaussian plume dispersion model with measurements of pollutant concentration at ground level and aloft. *Atmospheric Environment*, **14**, 589–593.

Hartter, J., Lucas, C., Gaughan, A. E., & Lizama Aranda, L. 2008. Detecting tropical dry forest succession in a shifting cultivation mosaic of the Yucatán Peninsula, Mexico. *Applied Geography*, **28**(2), 134–149.

Herrera, J. 2005. Flower size variation in Rosmarinus officinalis: individuals, populations and habitats. *Annals of Botany*, **95**(3), 431–7.

Herrera-Ruiz, M., Zamilpa, A., González-Cortazar, M., Reyes-Chilpa, R., & León, E. 2011. Phytomedicine Antidepressant effect and pharmacological evaluation of standardized extract of flavonoids from Byrsonima crassifolia. *European Journal of Integrative Medicine*, **18**(14), 1255–1261.

Hoffmann, B.D., Griffiths, A.D., & Andersen, A.N. 2000. Responses to ant communities to dry sulfur deposition from mining emissions in semi-arid tropical Australia, with implications for the use of functional groups. *Austral Ecology*, **25**, 653–663.

Honour, S L, Bell, J N, Ashenden, T W, Cape, J N, & Power, S A. 2009. Responses of herbaceous plants to urban air pollution: effects on growth, phenology and leaf surface characteristics. *Environ Pollut*, **157**(4), 1279–1286.

Horrocks, L. A. 2001. *Infrared spectroscopy of volcanic gases at Masaya, Nicaragua.* PhD, Open University.

Horton, K. A., Williams-Jones, G., Garbeil, H., Elias, T., Sutton, A. J., Mouginis-Mark, P., Porter, J. N., & Clegg, S. 2005. Real-time measurement of volcanic SO_2 emissions: validation of a new UV correlation spectrometer (FLYSPEC). *Bulletin of Volcanology*, **68**(4), 323–327.

Huey, N. A. 1968. The Lead Dioxide Estimation Of Sulfur Dioxide Pollution. *Journal of the Air Pollution Control Association*, **18**(9), 610–611.

Jenkins, M. W. 2012. Exploring the edge of a natural disaster. *Open Journal of Ecology*, **02**(4), 222–232.

Jochner, S., Markevych, I., Beck, I., Traidl-Hoffmann, C., Heinrich, J., & Menzel, A. 2015. The effects of short- and long-term air pollutants on plant phenology and leaf characteristics. *Environmental Pollution*, **206**(x), A3–A5.

Johnson, N., & Parnell, R. A. 1986. Composition, distribution and neutralization of "acid rain" derived from Masaya volcano, Nicaragua. *Tellus*, **38**(B), 106–117.

Johnson, N. C., & Wedin, D. A. 1997. Soil Carbon, Nutrients, and Mycorrhizae During Conversion of Dry Tropical Forest To Grassland. *Ecological Applications*, **7**(1), 171–182.

Kamijo, T., Kawagoe, M., Kato, T., Kiyohara, Y., Matsuda, M., Hashiba, K., & Shimada, K. 2008. Destruction and Recovery of Vegetation Caused by the 2000-Year Eruption on Miyake-Jima Island , Japan. *Journal of Disaster Research*, **3**(3), 226–227.

Kamijo, T. K., & Hashiba, K. H. 2003. Island Ecosystem and Vegetation Dynamics before and after the 2000-Year Eruption on Miyake-jima Island , Japan, with Implications for Conservation of the Islands Ecosystem. *Island ecosystem and vegetation dynamics*, 69–78.

Kent, M. 2011. *Vegetation Description and Data Analysis: A Practical Approach.* Wiley.

Khavaninzadeh, A.R., Veroustraete, F., Buytaert, J.A.N., & Samson, R. 2014. Leaf injury symptoms of Tilia sp. as an indicator of urban habitat quality. *Ecological Indicators*, **41**(June), 58–64.

Kläring, H. P., Hauschild, C., Heißner, a., & Bar-Yosef, B. 2007. Model-based control of CO2 concentration in greenhouses at ambient levels increases cucumber yield. *Agricultural and Forest Meteorology*, **143**(3-4), 208–216.

Korhonen, L., Korhonen, K. T., Rautiainen, M., & Stenberg, P. 2006. Estimation of forest canopy cover: a comparison of field measurement techniques. *Silvia Fennica*, **40**(4), 577–588.

Lamb, H. H. 1970. Volcanic dust in the atmosphere; with a chronology and assessment of its meteorological significance. *Philos. Trans. R. Soc. London, Ser. A,*, 425–533.

Langmann, B., Hort, M., & Hansteen, T. 2009. Meteorological influence on the seasonal and diurnal variability of the dispersion of volcanic emissions in Nicaragua: A numerical model study. *Journal of Volcanology and Geothermal Research*, **182**(1-2), 34–44.

Lansing, J. S., Kremer, J. N., Gerhart, V., Kremer, P., Arthawiguna, A., Surata, S. K. P., Suprato, Suryawan, I. B., Arsana, I. G., Scarborough, V. L., Schoenfelder, J., & Mikita, K. 2001. Volcanic fertilization of Balinese rice paddies. *Ecological Economics*, **38**(3), 383–390.

Larkin, C., Kwit, C., Wunderle, J. M. Jr., Helmer, E. H., Stevens, M. H. H., Roberts, M. T. K., & Ewert, D. N. 2012. Disturbance Type and Plant Successional Communities in Bahamian Dry Forests. *Biotropica*, **44**(1), 10–18.

Leghari, S.K.and Zaidi, M.A. 2013. Effect of air pollution on the leaf morphology

of common plant species of Quetta city. *Pakistan Journal of Botany*, **45**(SPL.ISS), 447–454.

Likens, G.E., Butler, T.J., & Buso, D.C. 2001. Long- and short-term changes in sulfate deposition : Effects of the 1990 Clean Air Act Amendments. *Biogeochemistry*, **52**, 1–11.

Liška, J., & Herben, T. 2008. Long-term changes of epiphytic lichen species composition over landscape gradients: an 18 year time series. *The Lichenologist*, **40**(5), 437–448.

Lynch, A J, McQuaker, N R, & Gurney, M. 1978. Calibration factors and Estimation of Atmospheric SO_2 and Fluoride by Use of Solid Absorbents. *Environment, Science and Technology*, **12**, 169–173.

Mailly, D., Turbis, S., & Chazdon, R. L. 2013. solarcalc 7.0: An enhanced version of a program for the analysis of hemispherical canopy photographs. *Computers and Electronics in Agriculture*, **97**(Sept.), 15–20.

Maisto, G., Santorufo, L., & Arena, C. 2013. Heavy metal accumulation in leaves affects physiological performance and litter quality of Quercus ilex L. *Journal of Plant Nutrition and Soil Science*, **176**(5), 776–784.

Maldini, M., Sosa, S., Montoro, P., Giangaspero, A., Balick, M. J., Pizza, C., & Loggia, R. D. 2009. Screening of the topical anti-inflammatory activity of the bark of Acacia cornigera Willdenow, Byrsonima crassifolia Kunth, Sweetia panamensis Yakovlev and the leaves of Sphagneticola trilobata Hitchcock. *Journal of Ethnopharmacology*, **122**, 430–433.

Marenco, E., Diaz, L., & Guevera, G. 2012. *Plan de Manejo del Parque Nacional Volcan Masaya*. Tech. rept. MARENA, Masaya.

Marler, T.E., & Moral, R. 2013. Primary succession in Mount Pinatubo Habitat avail-

ability and ordination analysis. *Communicative and Intergrative Biology*, **6**(December), 1–7.

Martin, R. S., Mather, T. A., Pyle, D. M., Power, M., Tsanev, V. I., Oppenheimer, C., Allen, A. G., Horwell, C. J., & Ward, E. P. W. 2009a. Size distributions of fine silicate and other particles in Masaya's volcanic plume. *Journal of Geophysical Research*, **114**(D9).

Martin, R. S., Mather, T. A., Pyle, D. M., Watt, S. F. L., Day, J. A., Collins, S. J., Wright, T. E., Aiuppa, A., & Calabrese, S. 2009b. Sweet chestnut (Castanea sativa) leaves as a bio-indicator of volcanic gas, aerosol and ash deposition onto the flanks of Mt Etna in 20052007. *Journal of Volcanology and Geothermal Research*, **179**(1-2), 107–119.

Martin, R. S., Mather, T. A., Pyle, D. M., Day, J. A., Witt, M. L. I., Collins, S. J., & Hilton, R. G. 2010. Major and trace element distributions around active volcanic vents determined by analyses of grasses: implications for element cycling and biomonitoring. *Bulletin of Volcanology*, **72**(8), 1009–1020.

Martin, R. S., Sawyer, G. M., Day, J. A., LeBlond, J. S., Ilyinskaya, E., & Oppenheimer, C. 2012. High-resolution size distributions and emission fluxes of trace elements from Masaya volcano, Nicaragua. *Journal of Geophysical Research*, **117**(B8).

Mather, T. A., Allen, A. G., Davison, B. M., Pyle, D. M., Oppenheimer, C., & McGonigle, A. J. S. 2004. Nitric acid from volcanoes. *Earth and Planetary Science Letters*, **218**(1-2), 17–30.

Mather, T. A., Pyle, D. M., Tsanev, V. I., McGonigle, A. J. S., Oppenheimer, C., & Allen, A. G. 2006. A reassessment of current volcanic emissions from the Central American arc with specific examples from Nicaragua. *Journal of Volcanology and Geothermal Research*, **149**(3-4), 297–311.

Mather, T.A., Pyle, D.M., & Oppenheimer, C. 2003. Tropospheric volcanic aerosol. *Volcanism and the Earth's Atmosphere*, **American G**(139), 189–212.

McBirney, A. R. 1956. The Nicaraguan Volcano Masaya and Its Caldera. *Transcations American Geophysical Union*, **37**(1), 83–96.

McElrone, A. J., Choat, B., Gambetta, G. A., & Brodersen, C. R. 2013. Water uptake and transport in vascular plants. *Nature Education Knowledge*, **4**(6).

Mehdizadeh, F., & Rifai, H.S. 2004. Modeling point source plumes at high altitudes using a modified Gaussian model. *Atmospheric Environment*, **38**(6), 821–831.

Miller, D.E., & Watmough, S.A. 2009. Air pollution, climate, soil acidity, and indicators of forest health in Ontarios sugar maple forests. *Canadian Journal of Forest Research*, **39**, 2065–2079.

Mulpuri, V., & Luit, J. 1994. Interactive Effects of High CO_2 and SO_2 on Growth and Antioxidant Levels in Wheat. *Phyton*, **34**(2), 279–290.

Munguía, S. B. 2013. *Heterogenidad floristica y estructural de los encinared del Parque Nacional el Tepozteco, Mexico*. Ph.D. thesis, Universidad Nacional Autonoma de Mexico.

Myers, N., Mittermeier, R. A., Mittermeier, C. G., Da Fonseca, G. A., & Kent, J. 2000. Biodiversity hotspots for conservation priorities. *Nature*, **403**(6772), 853–858.

Nadeau, P. A. 2004. *A multi-parameter investigation of volcanic plume behaviour and resultant environmental impact at a persistently degassing volcano, Masaya, Nicaragua*. Master of Science, Simon Fraser University.

Nash, D G, & Leith, D. 2010. Use of passive diffusion tubes to monitor air pollutants. *Journal of Air Waste Management Association*, **60**(2), 204–209.

Nelson, S., & Sewake, K. 2008. Volcanic Emissions Injury to Plant Foliage. *Plant Disease*, **47**, 1–11.

Niño, M., McLaren, K. P., Meilby, H., Lévesque, M., Wilson, B., & McDonald, M. 2014. Long-term changes in above ground biomass after disturbance in a neotropical dry forest, Hellshire Hills, Jamaica. *Plant Ecology*, **215**(10), 1081–1097.

Nikula, S., Manninen, S., Vapaavuori, E., & Pulkkinen, P. 2011. Growth, leaf traits and litter decomposition of roadside hybrid aspen (Populus tremula L. P. tremuloides Michx.) clones. *Environmental Pollution (Barking, Essex : 1987)*, **159**(7), 1823–30.

Nobel, P.S. 2009. *Physicochemical and Environmental Plant Physiology*. Academic Press.

Oksanen, J., Blanchet, F. G., Kindt, R., Legendre, P., Minchin, P. R., O'Hara, R. B., Simpson, G. L., Solymos, P., Stevens, M. H. H., & Wagner, H. 2013. *Package vegan*.

Olivares, E., & Pena, E. 2004. Fluoride and metals in Byrsonima crassifolia, a medicinal tree from the neotropical savannahs. *Interciencia*, **29**(3), 145–153.

Oppenheimer, C. 2003. Volcanic Degassing. *Pages 123–166 of:* Holland, H D, & Turekian, KK (eds), *Treatise on Geochemistry (Vol. 3)*, vol. 213. Oxford: Elsevier-Pergamon.

Palma, J.L., Calder, E.S., Basualto, D., Blake, S., & Rothery, D.A. 2008. Correlations between SO_2 flux, seismicity, and outgassing activity at the open vent of Villarrica volcano, Chile. *Journal of Geophysical Research*, **113**(B10).

Pandey, J, & Agrawal, M. 1994. Evaluation of air pollution phytotoxicity in a seasonally dry tropical urban environment using three woody perenials. *New Phytologist*, **126**(1), 53–61.

Payne, R. J., Stevens, C. J., Dise, N. B., Gowing, D. J., Pilkington, M. G., Phoenix, G. K., Emmett, B. A., & Ashmore, M. R. 2011. Impacts of atmospheric pollution on the plant communities of British acid grasslands. *Environ Pollut*, **159**(10), 2602–2608.

Payne, R. J., Caporn, S. J. M., Stevens, C. J., Carroll, J. A., Edmondson, J. L., Gowing, D. J., & Dise, N. B. 2013. Inferring nitrogen deposition from plant community composition. *Ecological Indicators*, **26**(Mar.), 1–4.

Payne, R.J., Caporn, S.J.M., Field, C.D., Carroll, J.A., Edmondson, J.L., Britton, A., & Dise, N.B. 2014. Heather Moorland Vegetation and Air Pollution: A Comparison and Synthesis of Three National Gradient Studies. *Water, Air, & Soil Pollution*, **225**(7), 1998.

Peguero, G., & Espelta, J. M. 2011. Disturbance intensity and seasonality affect the resprouting ability of the neotropical dry-forest tree Acacia pennatula: do resources stored below-ground matter? *Journal of Tropical Ecology*, **27**(05), 539–546.

Pélabon, C., Carlson, M. L., Hansen, T. F., & Armbruster, W. S. 2005. Effects of crossing distance on offspring fitness and developmental stability in Dalechampia scandes (Euphorbiaceae). *American Journal of Botany*, **92**(5), 842–851.

Pélabon, C., Armbruster, W. S., & Hansen, T. F. 2011. Experimental evidence for the Berg hypothesis: vegetative traits are more sensitive than pollination traits to environmental variation. *Functional Ecology*, **25**(1), 247–257.

Pélabon, C., Thöne, P., Hansen, T. F., & Armbruster, W. S. 2012. Signal honesty and cost of pollinator rewards in Dalechampia scandens (Euphorbiaceae). *Annals of Botany*, **109**(7), 1331–40.

Pérez-Barrales, R., Arroyo, J., & Armbruster, W. S. 2007. Differences in pollinator faunas may generate geographic differences in floral morphology and integration in Narcissus papyraceus (Amaryllidaceae). *Oikos*, **116**(11), 1904–1918.

Pérez-Barrales, R., Bolstad, G. H., Pélabon, C., Hansen, T. F., & Armbruster, W. S. 2013. Pollinators and seed predators generate conflicting selection on Dalechampia blossoms. *Oikos*, **122**(March), 1411–1428.

Phoenix, G. K., Hicks, W. K., Cinderby, S., Kuylenstierna, J. C. I., Stock, W. D., Dentener, F. J., Giller, K. E., Austin, A. T., Lefroy, R. D. B., Gimeno, B. S., Ashmore, M. R., & Ineson, P. 2006. Atmospheric nitrogen deposition in world biodiversity hotspots: The need for a greater global perspective in assessing N deposition impacts. *Global Change Biology*, **12**(3), 470–476.

Pons, T. L., & Welschen, R. A. M. 2003. Midday depression of net photosynthesis in the tropical rainforest tree Eperua grandiflora: contributions of stomatal and internal conductances, respiration and Rubisco functioning. *Tree physiology*, **23**, 937–947.

Post, J. D. 1977. *The last great subsistence crisis in the Western World.* Baltimore MD: The Johns Hopkins University Press.

Pourkhabbaz, A., Rastin, N., Olbrich, A., Langenfeld-Heyser, R., & Polle, A. 2010. Influence of environmental pollution on Leaf properties of urban plane trees, Platanus orientalis L. *Bulletin of Environmental Contamination and Toxicology*, **85**(3), 251–255.

Pozzer, A., Zimmermann, P., Doering, U. M., Van Aardenne, J., Tost, H., Dentener, F., Janssens-Maenhout, G., & Lelieveld, J. 2012. Effects of business-as-usual anthropogenic emissions on air quality. *Atmospheric Chemistry and Physics*, **12**(15), 6915–6937.

R, Development Core Team. 2014. *R: a language and environment for statistical computing.*

Read, L., & Lawrence, D. 2003. Litter Nutrient Dynamics During Succession in Dry Tropical Forests of the Yucatan: Regional and Seasonal Effects. *Ecosystems*, **6**(8), 747–761.

Rich, P. M. 1990. Characterizing plant canopies with hemispherical photographs. *Remote Sensing Reviews*, **5**(1), 13–29.

Robock, A. 2000. Volcanic eruptions and climate. *Reviews of Geophysics*, **28**(2), 191–219.

Robock, A., Adams, T., Moore, M., Oman, L., & Stenchikov, G. 2007. Southern Hemisphere atmospheric circulation effects of the 1991 Mount Pinatubo eruption. *Geophysical Research Letters*, **34**(23).

Rodwell, J. S. 2006. *National Vegetation Classification: Users' handbook.* Tech. rept. Peterborough.

Rymer, H., van Wyk de Vries, B., Stix, J., & Williams-Jones, G. 1998. Pit crater structure and processes governing persistent activity at Masaya Volcano , Nicaragua. *Bulletin of Volcanology*, 345–355.

Salemaa, M., Vanha-Majamaa, I., & Derome, J. 2001. Understorey vegetation along a heavy-metal pollution gradient in SW Finland. *Environmental pollution (Barking, Essex : 1987)*, **112**(3), 339–50.

Schmidt, A., Carslaw, K. S., Mann, G. W., Rap, A., Pringle, K. J., Spracklen, D. V., Wilson, M., & Forster, P. M. 2012. Importance of tropospheric volcanic aerosol for indirect radiative forcing of climate. *Atmospheric Chemistry and Physics*, **12**(1998), 7321–7339.

Shiels, A. B., & Walker, L. R. 2003. Bird Perches Increase Forest Seeds on Puerto Rican Landslides. *Restoration Ecology*, **11**(4), 457–465.

Shoji, S., & Takahashi, T. 2002. Environmental and Agricultural Significance of Volcanic Ash Soils. *Global Environmental Research*, 113–135.

Singh, A., & Agrawal, M. 2008. Acid rain and its ecological consequences. *Journal of Environmental Biology*, **29**(1), 15–24.

Singh, R. K., Dutta, R. K, & Agrawal, M. 2004. Litter decomposition and nutrient release in relation to atmospheric deposition of S and N in a dry tropical region. *Pedobiologia*, **48**(4), 305–311.

Staszewski, T., Kubiesa, P., & ukasik, W. 2011. Response of spruce stands in national parks of southern Poland to air pollution in 19982005. *European Journal of Forest Research*, **131**(4), 1163–1173.

Stevens, C. J., Dise, N. B., Mountford, J. O., & Gowing, D. J. 2004. Impact of nitrogen deposition on the species richness of grasslands. *Science (New York, N.Y.)*, **303**(5665), 1876–1879.

Stevens, W. D. 2015. *Flora de Nicaragua.*

Stix, J. 2007. Stability and instability of quiescently active volcanoes: The case of Masaya, Nicaragua. *Geology*, **35**(6), 535–538.

Stoate, C., Boatman, N. D., Borralho, R. J., Carvalho, C. R., de Snoo, G. R., & Eden, P. 2001. Ecological impacts of arable intensification in Europe. *Journal of Environmental Management*, **63**(4), 337–365.

Stoiber, R. E., Williams, S. N., & Huebert, B. J. 1986. Sulfur and halogen gases at Masaya cladera complex, Nicaragua: Total flux and variations in time. *Journal of Geophysical Research*, **91**(B12), 215–231.

Ta, W., Wei, C., & Chen, F. 2005. Long-term measurements of SO2 dry deposition over Gansu Province, China. *Atmospheric Environment*, **39**(37), 7095–7105.

Tagawa, H., Suzuki, E., Partomihardjo, T., & Suriadarma, A. 2013. Vegetation and Succession on the Krakatau Islands , Indonesia. *Vegetatio*, **60**(3), 131–145.

Tasdemir, Y., & Gunez, H. 2006. Dry deposition of sulfur containing species to the water surface sampler at two sites. *Water, Air, and Soil Pollution*, **175**(1-4), 223–240.

Thornton, I. 1996. *Krakatau.* Harvard University Press.

Ting, T. M., & Poulsen, A. D. 2009. Understorey Vegetation at Two Mud Volcanoes in North-East Borneo. *Journal of Tropical Forest Science*, **21**(3), 198–209.

Tiwari, S, Agrawal, M, & Marshall, F A. 2010. Seasonal variations in adaptational strategies of Beta vulgaris L. plants in response to ambient air pollution: Biomass allocation, yield and nutritional quality. *Tropical Ecology*, **51**(2S), 353–363.

Tricker, P.J., Calfapietra, C., Kuzminsky, E., Puleggi, R., Ferris, R., Nathoo, M., Pleasants, L.J., Alston, V., de Angelis, P., & Taylor, G. 2004. Long-term acclimation of leaf production, development, longevity and quality following 3 yr exposure to free-air CO_2 enrichment during canopy closure in Populus. *New Phytologist*, **162**(2), 413–426.

Tsuyuzaki, S., & Del Moral, R. 1995. Species attributes in early primary succession of volcanoes. *Journal of Vegetation Science*, **6**(4), 517–522.

Vallero, D. 2007. *Fundamentals of Air Pollution.* Academic Press.

van Manen, S. M. 2014a. Hazard and risk perception at Turrialba volcano (Costa Rica); implications for disaster risk management. *Applied Geography*, **50**(June), 63–73.

van Manen, S. M. 2014b. Perception of a chronic volcanic hazard: persistent degassing at Masaya volcano, Nicaragua. *Journal of Applied Volcanology*, **3**(1), 9.

Vávrová, E., Cudlín, O., Vavíček, D., & Cudlín, P. 2009. Ground vegetation dynamics in mountain spruce (Picea abies (L.) Karsten) forests recovering after air pollution stress impact. *Plant Ecology*, **205**(2), 305–321.

Velázquez, E., & Gómez-Sal, A. 2008. Landslide early succession in a neotropical dry forest. *Plant Ecology*, **199**(2), 295–308.

Velázquez, E., & Gómez-Sal, A. 2009. Changes in the Herbaceous Communities on the Landslide of the Casita Volcano, Nicaragua, during Early Succession. *Folia Geobotanica*, **44**(1), 1–18.

Verma, M, & Agrawal, M. 1996. Alleviation of injurious effects of sulphur dioxide on soybean by modifying NPK nutrients. *Agriculture, Ecosystem and Environment*, **57**, 49–55.

Šebesta, J., Šamonil, P., Lacina, J., Oulehle, F, Houška, J, & Buc, A. 2011. Acidification of primeval forests in the Ukraine Carpathians : Vegetation and soil changes over six decades. *Forest Ecology and Management*, **262**, 1265–1279.

Wahid, A. 2006. Influence of atmospheric pollutants on agriculture in developing countries: a case study with three new wheat varieties in Pakistan. *Sci Total Environ*, **371**(1-3), 304–313.

Walker, J. A., Williams, S. N., Kalamarides, R. I., & Feigenson, M. D. 1993. Shallow open system evolution of basaltic magma beneath a subduction zone volcano: the Masaya Caldera Complex, Nicaragua. *Journal of Volcanology and Geothermal Research*, **56**, 379–400.

Watt, S. F., Pyle, D. M., Mather, T. A., Day, J. A., & Aiuppa, A. 2007. The use of tree-rings and foliage as an archive of volcanogenic cation deposition. *Environ Pollut*, **148**(1), 48–61.

Weil, J.C., & Jepsen, A.F. 1977. Evaluation of the Gaussian plume model at the Dickerson power plant. *Atmospheric Environment*, **11**, 901–910.

Wermundsen, T. 1999. Seasonal and diurnal variation in Pacific Parakeet Aratinga strenua flock sizes in Nicaragua. *Ardeola*, **46**(1), 39–43.

Whittaker, R. J., Bush, M. B., & Richards, K. 1989. Plant recolonization and vegetation succession on the Krakatau Islands, Indonesia. *Ecological Monographs*, 59–123.

WHO. 2011. *Air quality and health.*

Williams, S.N. 1983. *Geology and eruptive mechanisms of Masaya Caldera Complex, Nicaragua.* Ph.D. thesis, Dartmouth Coll., Hanover, NH.

Williams-Jones, G., Rymer, H., & Rothery, D. A. 2003. Gravity changes and passive SO_2 degassing at the Masaya caldera complex, Nicaragua. *Journal of Volcanology and Geothermal Research*, **123**(1-2), 137–160.

Williams-Jones, G., Horton, K. A., Elias, T., Garbeil, H., Mouginis-Mark, P. J., Sutton, A. J., & Harris, A. J. L. 2005. Accurately measuring volcanic plume velocity with multiple UV spectrometers. *Bulletin of Volcanology*, **68**(4), 328–332.

Williams-Linera, G., Alvarez-Aquino, C., Hernández-Ascención, E., & Toledo, M. 2010. Early successional sites and the recovery of vegetation structure and tree species of the tropical dry forest in Veracruz, Mexico. *New Forests*, **42**(2), 131–148.

Willig, M. R., Presley, S. J., & Bloch, C. P. 2011. Long-term dynamics of tropical walking sticks in response to multiple large-scale and intense disturbances. *Oecologia*, **165**(2), 357–68.

Winner, W. E., Mooney, H. A., & Goldstein, R. A. 1986. *Sulfur Dioxide and Vegetation: Physiology, Ecology and Policy Issues*. Stanford: Stanford Univeristy Press.

Witt, M. L. I., Mather, T. A., Pyle, D. M., Aiuppa, A., Bagnato, E., & Tsanev, V. I. 2008. Mercury and halogen emissions from Masaya and Telica volcanoes, Nicaragua. *Journal of Geophysical Research*, **113**(B6).

Yang, L., Stulen, I., & De Kok, L.J. 2006. Sulfur dioxide: Relevance of toxic and nutritional effects for Chinese cabbage. *Environmental and Experimental Botany*, **57**(3), 236–245.

Zuchowski, W. 2007. *Tropical Plants of Costa Rica*. Ithaca: Cornell University Press.

Appendix A

Degassing

A.1 Degassing data

A.1.1 Topography along the transect

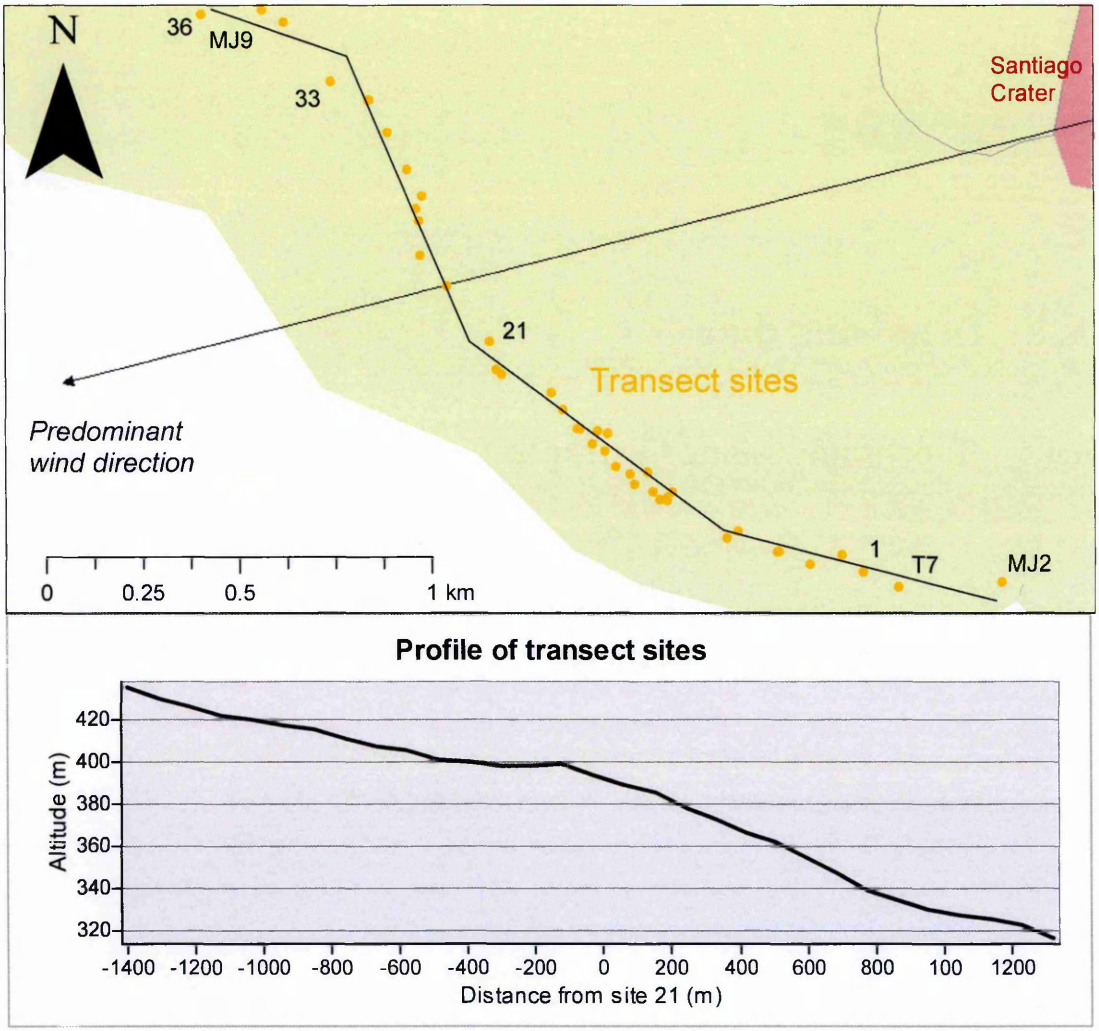

Figure A.1: Topography along the transect. Sites at the beginning and end of the transect for each sampling period have been shown.

A.1.2 Diffusion tube data

Table A.1: All diffusion tube data in $\mu g\ m^{-3}$. Distance refers to distance along the transect from site 21, with negative values to the south and positive values to the north. No distance is displayed for crater and upwind sites. Data below the limit of detection are shown as BD, a blank cell is where data was not collected. All results for SO_2, HCl and HF are blank corrected, but not background corrected.

Code	Site	Latitude	Longitude	Hours	Installed	Collected	Distance	SO_2	HCl	HF
F13/U1	Meteo	12.0034	-86.1485	244	05/02/13 09:40	15/02/13 14:05		BD	BD	BD
F13/U2	Regis	11.9780	-86.0959	201	07/02/13 08:10	15/02/13 17:00		BD	BD	5
D13/U1	Comalito	11.9992	-86.1508	215	06/12/13 09:50	15/12/13 09:15		BD	16	BD
D13/U2	Regis	11.9780	-86.0959	244	06/12/13 17:45	16/12/13 21:45		BD	11	BD
F14/U1	Comalito	11.9992	-86.1508	315	20/02/14 13:20	05/03/14 16:23		BD	BD	1
F14/U2	Regis	11.9780	-86.0959	351	19/02/14 18:00	06/03/14 09:00		BD	2	BD
MJ14/U1	Comalito	11.9992	-86.1508	333	25/05/14 16:04	08/06/14 13:15		BD	BD	4
MJ14/U2	Regis	11.9780	-86.0959	353	27/05/14 17:48	11/06/14 11:30		2	BD	2
F13/C1	NCP1	11.9864	-86.1664	218	14/02/13 09:00	22/02/13 09:15		183	17	6
F13/C2	OCP	11.9811	-86.1676	166	14/02/13 09:10	23/02/13 12:30		959	87	10
D13/C2	OCP	11.9811	-86.1676	256	05/12/13 17:15	16/12/13 09:30		742	138	14
D13/C3	H1	11.9820	-86.1684	257	05/12/13 17:00	16/12/13 09:30		2083	777	79
F14/C1	NCP2	11.9872	-86.1673	336	19/02/14 16:07	05/03/14 16:10		377	91	12
F14/C2	OCP	11.9811	-86.1676	342	19/02/14 10:10	05/03/14 15:41		614	137	18
F14/C3	H1	11.9820	-86.1684	341	19/02/14 10:25	05/03/14 15:52		1766	2056	196
M14/C1	NCP3	11.9863	-86.1663	168	25/05/14 15:43	01/06/14 16:06		484	123	29
M14/C2	OCP	11.9811	-86.1676	169	25/05/14 15:28	01/06/14 16:01		243	33	11
J14/C1	NCP3	11.9863	-86.1663	165	01/06/14 16:06	08/06/14 13:03		296	39	19
J14/C2	OCP	11.9811	-86.1676	161	01/06/14 16:01	08/06/14 09:20		76	11	7
J14/C3	H1	11.9820	-86.1684	168	01/06/14 09:22	08/06/14 09:30		882	263	35
MJ14/C	OCP**	11.9811	-86.1676	330	25/05/14 15:28	08/06/14 09:20		177	29	9

Continued on next page

Table A.1: All diffusion tube data in $\mu g\ m^{-3}$. Distance refers to distance along the transect from site 21, with negative values to the south and positive values to the north. No distance is displayed for crater and upwind sites. Data below the limit of detection are shown as BD, a blank cell is where data was not collected. All results for SO_2, HCl and HF are blank corrected, but not background corrected.

Code	Site	Latitude	Longitude	Hours	Installed	Collected	Distance	SO_2	HCl	HF
F13/D1	Choc1	11.9730	-86.1740	240	05/02/13 12:50	15/02/13 13:00	-1182	5		3
F13/D2	Choc2	11.9735	-86.1761	167	08/02/13 13:30	15/02/13 12:45	-967	113		5
F13/D3	Choc3	11.9742	-86.1778	166	08/02/13 14:40	15/02/13 12:35	-775	264	9	10
F13/D4	Choc4	11.9751	-86.1793	237	05/02/13 15:00	15/02/13 12:30	-587	401	31	18
F13/D5	Choc5	11.9761	-86.1809	237	05/02/13 14:50	15/02/13 12:20	-394	587	73	22
F13/D6	Choc6	11.9774	-86.1821	237	05/02/13 14:20	15/02/13 11:30	-199	754	96	25
F13/D7	Choc7	11.9786	-86.1836	237	05/02/13 13:50	16/02/13 11:50	0	900	115	29
D13/D1	1	11.9733	-86.1749	264	05/12/13 15:50	16/12/13 15:35	-1088	77	76	3
D13/D2	2	11.9737	-86.1754	263	05/12/13 16:00	16/12/13 15:25	-1021		29	4
D13/D3	3	11.9738	-86.1769	263	05/12/13 15:45	16/12/13 14:55	-883	290	44	5
D13/D4	4	11.9741	-86.1780	263	05/12/13 15:35	16/12/13 14:50	-763	436		
D13/D5	6	11.9749	-86.1794	263	05/12/13 15:25	16/12/13 14:40	-591	483	82	10
D13/D6	8	11.9751	-86.1798	263	05/12/13 15:20	16/12/13 14:35	-550		89	17
D13/D7	9	11.9753	-86.1802	263	05/12/13 15:10	16/12/13 14:30	-505	402		
D13/D8	10	11.9756	-86.1799	263	05/12/13 15:05	16/12/13 14:20	-508	674	112	15
D13/D9	11	11.9755	-86.1803	263	05/12/13 15:00	16/12/13 14:13	-479		84	14
D13/D10	12	11.9757	-86.1806	263	05/12/13 14:50	16/12/13 14:05	-441	645		
D13/D11	13	11.9762	-86.1812	263	05/12/13 14:25	16/12/13 13:25	-360	551	199	10
D13/D12	14	11.9765	-86.1808	263	05/12/13 14:20	16/12/13 13:35	-371		135	22
D13/D13	15	11.9765	-86.1810	263	05/12/13 14:05	16/12/13 13:30	-347	752		
D13/D14	19r	11.9779	-86.1834	264	05/12/13 13:25	16/12/13 12:55	-72	861	146	18
D13/D15	21	11.9786	-86.1836	264	05/12/13 12:50	16/12/13 12:40	0	788	110	14

Continued on next page

Table A.1: All diffusion tube data in μg m^{-3}. Distance refers to distance along the transect from site 21, with negative values to the south and positive values to the north. No distance is displayed for crater and upwind sites. Data below the limit of detection are shown as BD, a blank cell is where data was not collected. All results for SO_2, HCl and HF are blank corrected, but not background corrected.

Code	Site	Latitude	Longitude	Hours	Installed	Collected	Distance	SO_2	HCl	HF
D13/D16	21	11.9786	-86.1836	264	05/12/13 12:50	16/12/13 12:40	0	668	110	13
D13/D17	26	11.9805	-86.1852	264	05/12/13 12:00	16/12/13 12:15	275		173	19
D13/D18	28	11.9816	-86.1853	264	05/12/13 11:40	16/12/13 12:05	377	845		
D13/D19	30	11.9825	-86.1855	265	05/12/13 11:10	16/12/13 11:50	475		141	19
D13/D20	31	11.9833	-86.1859	265	05/12/13 10:55	16/12/13 11:45	578	666		
D13/D21	32	11.9841	-86.1864	265	05/12/13 10:45	16/12/13 11:35	671	611	115	13
D13/D22	33	11.9845	-86.1872	265	05/12/13 10:25	16/12/13 11:30	757		107	15
F14/D1	1	11.9733	-86.1749	335	19/02/14 11:45	05/03/14 11:00	-1088	4		1
F14/D2	2	11.9737	-86.1754	335	19/02/14 11:53	05/03/14 11:06	-1021	15	1	1
F14/D3	3	11.9738	-86.1769	335	19/02/14 12:00	05/03/14 11:17	-883		6	2
F14/D4	4	11.9741	-86.1780	335	19/02/14 12:08	05/03/14 11:22	-763	128		
F14/D5	6	11.9750	-86.1796	335	19/02/14 12:17	05/03/14 11:26	-591		52	10
F14/D6	8	11.9751	-86.1798	335	19/02/14 12:24	05/03/14 11:30	-550		70	13
F14/D7	9	11.9753	-86.1802	335	19/02/14 12:29	05/03/14 11:32	-505	380		
F14/D8	11	11.9755	-86.1803	335	19/02/14 13:04	05/03/14 11:36	-479		96	13
F14/D9	12	11.9757	-86.1806	334	19/02/14 13:12	05/03/14 11:39	-441	518		
F14/D10	13	11.9762	-86.1812	334	19/02/14 13:20	05/03/14 11:42	-360	646	159	19
F14/D11	14	11.9765	-86.1808	334	19/02/14 13:26	05/03/14 11:43	-371		171	19
F14/D12	15	11.9765	-86.1810	334	19/02/14 13:33	05/03/14 11:45	-347	721		
F14/D13	16	11.9766	-86.1815	334	19/02/14 13:41	05/03/14 11:47	-306	753	203	21
F14/D14	17	11.9770	-86.1819	334	19/02/14 13:50	05/03/14 11:51	-248	1037	199	28
F14/D15	19	11.9778	-86.1833	334	19/02/14 13:57	05/03/14 11:57	-87	993	239	9

Continued on next page

Table A.1: All diffusion tube data in $\mu g\ m^{-3}$. Distance refers to distance along the transect from site 21, with negative values to the south and positive values to the north. No distance is displayed for crater and upwind sites. Data below the limit of detection are shown as BD, a blank cell is where data was not collected. All results for SO_2, HCl and HF are blank corrected, but not background corrected.

Code	Site	Latitude	Longitude	Hours	Installed	Collected	Distance	SO_2	HCl	HF
F14/D16	19r	11.9779	-86.1834	334	19/02/14 14:08	05/03/14 12:01	-72	1020	257	35
F14/D17	21	11.9786	-86.1836	334	19/02/14 14:20	05/03/14 12:10	0	1116	290	32
F14/D18	21	11.9786	-86.1836	334	19/02/14 14:20	05/03/14 12:10	0	1156	291	32
F14/D19	24	11.9798	-86.1846	334	19/02/14 14:31	05/03/14 12:20	174	1109	293	34
F14/D20	26	11.9805	-86.1852	334	19/02/14 14:41	05/03/14 12:24	275	1098	255	28
F14/D21	28	11.9816	-86.1853	334	19/02/14 14:55	05/03/14 12:31	377	932		
F14/D22	29	11.9819	-86.1851	334	19/02/14 15:00	05/03/14 12:35	399	973	242	30
F14/D23	30	11.9825	-86.1855	334	19/02/14 15:05	05/03/14 12:39	475		170	20
F14/D24	31	11.9833	-86.1859	334	19/02/14 15:11	05/03/14 12:42	578	820		
F14/D25	32	11.9841	-86.1864	333	19/02/14 15:17	05/03/14 12:45	671	678	113	15
F14/D26	33	11.9845	-86.1872	333	19/02/14 15:24	05/03/14 12:50	757	633		
F14/D27	34	11.9859	-86.1883	286	21/02/14 14:36	05/03/14 12:54	943		101	14
F14/D28	36	11.9860	-86.1903	287	21/02/14 14:22	05/03/14 13:01	1082	424	50	6
M14/D1	2	11.9731	-86.1716	167	25/05/14 10:36	01/06/14 09:52	-1403		BD	1
M14/D2	3	11.9738	-86.1768	168	25/05/14 11:03	01/06/14 10:55	-887	69	BD	3
M14/D3	4	11.9750	-86.1794	168	25/05/14 11:21	01/06/14 11:30	-586	121	BD	3
M14/D4	5	11.9766	-86.1815	168	25/05/14 11:44	01/06/14 11:58	-312	353	44	15
M14/D5	6	11.9786	-86.1836	168	25/05/14 11:55	01/06/14 12:13	0	539	89	23
M14/D6	7	11.9813	-86.1852	168	25/05/14 12:17	01/06/14 12:38	347	389	72	20
M14/D7	8	11.9841	-86.1864	168	25/05/14 12:39	01/06/14 13:02	671	293	46	19
M14/D8	9	11.9861	-86.1889	169	25/05/14 13:19	01/06/14 13:51	999	203	24	15
J14/D1	2	11.9731	-86.1716	168	01/06/14 09:52	08/06/14 10:11	-1403	7	BD	3

Continued on next page

Table A.1: All diffusion tube data in μg m^{-3}. Distance refers to distance along the transect from site 21, with negative values to the south and positive values to the north. No distance is displayed for crater and upwind sites. Data below the limit of detection are shown as BD, a blank cell is where data was not collected. All results for SO_2, HCl and HF are blank corrected, but not background corrected.

Code	Site	Latitude	Longitude	Hours	Installed	Collected	Distance	SO_2	HCl	HF
J14/D2	3	11.9738	-86.1768	167	01/06/14 10:55	08/06/14 10:24	-887	10	BD	2
J14/D3	4	11.9750	-86.1794	167	01/06/14 11:30	08/06/14 10:35	-586	23	BD	2
J14/D4	5	11.9766	-86.1815	167	01/06/14 11:58	08/06/14 10:44	-312	65	BD	5
J14/D5	5	11.9766	-86.1815	167	01/06/14 12:13	08/06/14 10:53	-312	59	BD	6
J14/D6	6	11.9786	-86.1836	167	01/06/14 12:13	08/06/14 10:53	0	118	14	16
J14/D7	7	11.9813	-86.1852	166	01/06/14 12:38	08/06/14 11:06	347	277	49	14
J14/D8	8	11.9841	-86.1864	166	01/06/14 13:02	08/06/14 11:12	671	362	59	14
J14/D9	9	11.9861	-86.1889	165	01/06/14 13:51	08/06/14 11:20	999	333	51	19

A.1.3 Sulfation plate data

Table A.2: Sulfation plate exposure information.

Season	Labcode	Site	Latitude	Longitude	Installed	Collected	Hours
Feb-13	S6/2	H1	11.9823	-86.1687			48
Feb-13	S6/4	H1	11.9823	-86.1687			22
Feb-13	S6/15	OCP g	11.9811	-86.1676	14/02/13 09:00	22/02/13 09:15	192
Feb-13	S6/17	NCP1 t	11.9864	-86.1664	14/02/13 09:10	23/02/13 12:30	219
Feb-13	S6/18	1	11.9733	-86.1749	18/02/13 14:40	22/02/13 09:45	91
Feb-13	S6/19	1	11.9733	-86.1749	18/02/13 14:40	22/02/13 09:45	91
Feb-13	S6/20	2	11.9737	-86.1754	18/02/13 14:50	22/02/13 09:55	91
Feb-13	S6/21	2	11.9737	-86.1754	18/02/13 14:50	22/02/13 09:55	91
Feb-13	S6/22	3	11.9738	-86.1769	18/02/13 14:30	22/02/13 10:10	92
Feb-13	S6/23	5	11.9749	-86.1794	18/02/13 14:15	22/02/13 10:25	92
Feb-13	S6/24	5	11.9749	-86.1794	18/02/13 14:15	22/02/13 10:25	92
Feb-13	S6/25	6	11.9750	-86.1796	18/02/13 14:10	22/02/13 10:30	92
Feb-13	S6/26	9	11.9753	-86.1802	18/02/13 13:55	22/02/13 13:50	96
Feb-13	S6/27	10	11.9755	-86.1803	18/02/13 13:45	22/02/13 10:40	93
Feb-13	S6/28	11	11.9757	-86.1806	18/02/13 13:40	22/02/13 10:45	93
Feb-13	S6/29	12	11.9762	-86.1812	18/02/13 13:25	22/02/13 10:50	93
Feb-13	S6/30	13	11.9765	-86.1810	18/02/13 13:30	22/02/13 10:55	93
Feb-13	S6/31	14	11.9766	-86.1815	18/02/13 12:55	22/02/13 11:00	94
Feb-13	S6/32	15	11.9770	-86.1819	18/02/13 12:50	22/02/13 11:10	94
Feb-13	S6/33	16	11.9776	-86.1826	18/02/13 12:45	22/02/13 11:15	94
Feb-13	S6/34	17	11.9778	-86.1832	18/02/13 12:35	22/02/13 11:20	95
Feb-13	S6/35	18	11.9785	-86.1835	18/02/13 12:30	22/02/13 11:25	95
Feb-13	S6/36	19	11.9786	-86.1836	18/02/13 12:30	22/02/13 11:30	95

Continued on next page

Table A.2: Sulfation plate exposure information.

Season	Labcode	Site	Latitude	Longitude	Installed	Collected	Hours
Feb-13	S6/37	20	11.9790	-86.1837	18/02/13 12:25	22/02/13 11:40	95
Feb-13	S6/38	21	11.9794	-86.1842	18/02/13 10:15	22/02/13 11:40	97
Feb-13	S6/39	22	11.9798	-86.1846	18/02/13 10:20	22/02/13 11:45	97
Feb-13	S6/40	24	11.9805	-86.1852	18/02/13 10:30	23/02/13 10:15	120
Feb-13	S6/41	25	11.9811	-86.1852	18/02/13 10:35	22/02/13 11:55	97
Feb-13	S6/42	26	11.9816	-86.1853	18/02/13 10:50	22/02/13 12:00	97
Feb-13	S6/43	27	11.9819	-86.1851	18/02/13 10:55	22/02/13 12:05	97
Feb-13	S6/44	28	11.9825	-86.1855	18/02/13 11:00	22/02/13 13:10	98
Feb-13	S6/45	29	11.9833	-86.1859	18/02/13 11:25	22/02/13 12:10	97
Feb-13	S6/46	30	11.9841	-86.1864	18/02/13 11:30	22/02/13 12:20	97
Feb-13	S6/47	31	11.9845	-86.1872	18/02/13 11:50	22/02/13 12:25	97
Feb-13	S6/52	Comalito	11.9992	-86.1508	04/02/13 11:45	18/02/13 15:30	340
Feb-13	B11/01	Regis	11.9780	-86.0959			201
Feb-13	B11/02	Regis	11.9780	-86.0959			201
Feb-13	B11/03	Meteo	12.0034	-86.1485			244
Dec-13	S10/1	1g	11.9733	-86.1749	05/12/13 15:50	16/12/13 15:35	264
Dec-13	S10/2	1t	11.9733	-86.1749	05/12/13 15:50	16/12/13 15:35	264
Dec-13	S10/3	2g	11.9737	-86.1754	05/12/13 16:00	16/12/13 15:25	263
Dec-13	S10/4	2t	11.9737	-86.1754	05/12/13 16:00	16/12/13 15:25	263
Dec-13	S10/5	3g	11.9738	-86.1769	05/12/13 15:45	16/12/13 14:55	263
Dec-13	S10/6	3t	11.9738	-86.1769	05/12/13 15:45	16/12/13 14:55	263
Dec-13	S10/7	4g	11.9741	-86.1780	05/12/13 15:35	16/12/13 14:50	263
Dec-13	S10/8	4t	11.9741	-86.1780	05/12/13 15:35	16/12/13 14:50	263
Dec-13	S10/9	6g	11.9749	-86.1794	05/12/13 15:25	16/12/13 14:40	263

Continued on next page

Table A.2: Sulfation plate exposure information.

Season	Labcode	Site	Latitude	Longitude	Installed	Collected	Hours
Dec-13	S10/10	6t	11.9749	-86.1794	05/12/13 15:25	16/12/13 14:40	263
Dec-13	S10/11	8g	11.9751	-86.1798	05/12/13 15:20	16/12/13 14:35	263
Dec-13	S10/12	8t	11.9751	-86.1798	05/12/13 15:20	16/12/13 14:35	263
Dec-13	S10/13	9g	11.9753	-86.1802	05/12/13 15:10	16/12/13 14:30	263
Dec-13	S10/14	10g	11.9756	-86.1799	05/12/13 15:05	16/12/13 14:20	263
Dec-13	S10/15	10t	11.9756	-86.1799	05/12/13 15:05	16/12/13 14:20	263
Dec-13	S10/16	11g	11.9755	-86.1803	05/12/13 15:00	16/12/13 14:13	263
Dec-13	S10/17	11t	11.9755	-86.1803	05/12/13 15:00	16/12/13 14:13	263
Dec-13	S10/18	12g	11.9757	-86.1806	05/12/13 14:50	16/12/13 14:05	263
Dec-13	S10/19	12t	11.9757	-86.1806	05/12/13 14:50	16/12/13 14:05	263
Dec-13	S10/20	13g	11.9762	-86.1812	05/12/13 14:25	16/12/13 13:25	263
Dec-13	S10/21	13t	11.9762	-86.1812	05/12/13 14:25	16/12/13 13:25	263
Dec-13	S10/22	14g	11.9765	-86.1808	05/12/13 14:20	16/12/13 13:35	263
Dec-13	S10/23	14t	11.9765	-86.1808	05/12/13 14:20	16/12/13 13:35	263
Dec-13	S10/24	15g	11.9765	-86.1810	05/12/13 14:05	16/12/13 13:30	263
Dec-13	S10/25	15t	11.9765	-86.1810	05/12/13 14:05	16/12/13 13:30	263
Dec-13	S10/26	16g	11.9766	-86.1815	05/12/13 13:55	16/12/13 13:15	263
Dec-13	S10/27	17g	11.9770	-86.1819	05/12/13 13:50	16/12/13 13:05	263
Dec-13	S10/28	16t	11.9766	-86.1815	05/12/13 13:55	16/12/13 13:15	263
Dec-13	S10/29	19g	11.9778	-86.1833	05/12/13 13:30	16/12/13 13:00	264
Dec-13	S10/30	19t	11.9778	-86.1833	05/12/13 13:30	16/12/13 13:00	264
Dec-13	S10/31	19.5t	11.9779	-86.1834	05/12/13 13:30	16/12/13 13:00	264
Dec-13	S10/32	19.5t	11.9779	-86.1834	05/12/13 13:30	16/12/13 13:00	264
Dec-13	S10/33	21g	11.9786	-86.1836	05/12/13 12:50	16/12/13 12:40	264

Continued on next page

Table A.2: Sulfation plate exposure information.

Season	Labcode	Site	Latitude	Longitude	Installed	Collected	Hours
Dec-13	S10/34	21t	11.9786	-86.1836	05/12/13 12:50	16/12/13 12:40	264
Dec-13	S10/35	26g	11.9805	-86.1852	05/12/13 12:00	16/12/13 12:15	264
Dec-13	S10/36	26t	11.9805	-86.1852	05/12/13 12:00	16/12/13 12:15	264
Dec-13	S10/37	27g	11.9811	-86.1852	05/12/13 11:50	16/12/13 12:10	264
Dec-13	S10/38	28t	11.9816	-86.1853	05/12/13 11:40	16/12/13 12:05	264
Dec-13	S10/39	29g	11.9819	-86.1851	05/12/13 11:25	16/12/13 12:00	265
Dec-13	S10/40	29t	11.9819	-86.1851	05/12/13 11:25	16/12/13 12:00	265
Dec-13	S10/41	30g	11.9825	-86.1855	05/12/13 11:10	16/12/13 11:50	265
Dec-13	S10/42	30t	11.9825	-86.1855	05/12/13 11:10	16/12/13 11:50	265
Dec-13	S10/43	31g	11.9833	-86.1859	05/12/13 10:55	16/12/13 11:45	265
Dec-13	S10/44	31t	11.9833	-86.1859	05/12/13 10:55	16/12/13 11:45	265
Dec-13	S10/45	32g	11.9841	-86.1864	05/12/13 10:45	16/12/13 11:35	265
Dec-13	S10/46	32t	11.9841	-86.1864	05/12/13 10:45	16/12/13 11:35	265
Dec-13	S10/47	33g	11.9845	-86.1872	05/12/13 10:25	16/12/13 11:30	265
Dec-13	S10/48	33t	11.9845	-86.1872	05/12/13 10:25	16/12/13 11:30	265
Dec-13	S10/49	34g	11.9851	-86.1877	05/12/13 10:10	16/12/13 11:20	265
Dec-13	S10/50	35g	11.9853	-86.1888	05/12/13 09:40	16/12/13 11:10	266
Dec-13	S10/51	35t	11.9853	-86.1888			266
Dec-13	S10/54	Regis	11.9780	-86.0959	06/12/13 17:45	16/12/13 21:45	244
Dec-13	S10/56	Comalito	11.9992	-86.1508	06/12/13 09:50	15/12/13 09:15	215
Dec-13	S10/57	NCP1 g	11.9864	-86.1664	05/12/13 17:25	16/12/13 16:30	263
Dec-13	S10/58	OCP t	11.9811	-86.1676	05/12/13 17:15	16/12/13 09:30	256
Dec-13	S10/59	OCP g	11.9811	-86.1676	05/12/13 17:15	16/12/13 09:30	256
Dec-13	S10/62	H1	11.9823	-86.1687	05/12/13 17:00	16/12/13 09:30	256

Continued on next page

Table A.2: Sulfation plate exposure information.

Season	Labcode	Site	Latitude	Longitude	Installed	Collected	Hours
Feb-14	S11/2	1T	11.9733	-86.1749	19/02/14 11:45	05/03/14 11:00	335
Feb-14	S11/3	1G	11.9733	-86.1749	19/02/14 11:45	05/03/14 11:00	335
Feb-14	S11/4	2T	11.9737	-86.1754	19/02/14 11:53	05/03/14 11:06	335
Feb-14	S11/5	2G	11.9737	-86.1754	19/02/14 11:53	05/03/14 11:06	335
Feb-14	S11/6	3T	11.9738	-86.1769	19/02/14 12:00	05/03/14 11:17	335
Feb-14	S11/7	3G	11.9738	-86.1769	19/02/14 12:00	05/03/14 11:17	335
Feb-14	S11/8	4T	11.9741	-86.1780	19/02/14 12:08	05/03/14 11:22	335
Feb-14	S11/9	4G	11.9741	-86.1780	19/02/14 12:08	05/03/14 11:22	335
Feb-14	S11/11	6T	11.9749	-86.1794	19/02/14 12:17	05/03/14 11:26	335
Feb-14	S11/12	6G	11.9749	-86.1794	19/02/14 12:17	05/03/14 11:26	335
Feb-14	S11/13	8T	11.9751	-86.1798	19/02/14 12:24	05/03/14 11:30	335
Feb-14	S11/14	8G	11.9751	-86.1798	19/02/14 12:24	05/03/14 11:30	335
Feb-14	S11/15	9T	11.9753	-86.1802	19/02/14 12:29	05/03/14 11:32	335
Feb-14	S11/16	9G	11.9753	-86.1802	19/02/14 12:29	05/03/14 11:32	335
Feb-14	S11/17	10G	11.9756	-86.1799	19/02/14 13:00	05/03/14 11:34	335
Feb-14	S11/19	11T	11.9755	-86.1803	19/02/14 13:04	05/03/14 11:36	335
Feb-14	S11/20	11G	11.9755	-86.1803	19/02/14 13:04	05/03/14 11:36	335
Feb-14	S11/21	12T	11.9757	-86.1806	19/02/14 13:12	05/03/14 11:39	334
Feb-14	S11/22	12G	11.9757	-86.1806	19/02/14 13:12	05/03/14 11:39	334
Feb-14	S11/24	13T	11.9762	-86.1812	19/02/14 13:20	05/03/14 11:42	334
Feb-14	S11/25	13G	11.9762	-86.1812	19/02/14 13:20	05/03/14 11:42	334
Feb-14	S11/26	14T	11.9765	-86.1808	19/02/14 13:26	05/03/14 11:43	334
Feb-14	S11/27	14G	11.9765	-86.1808	19/02/14 13:26	05/03/14 11:43	334
Feb-14	S11/28	15T	11.9765	-86.1810	19/02/14 13:33	05/03/14 11:45	334

Continued on next page

Table A.2: Sulfation plate exposure information.

Season	Labcode	Site	Latitude	Longitude	Installed	Collected	Hours
Feb-14	S11/29	15G	11.9765	-86.1810	19/02/14 13:33	05/03/14 11:45	334
Feb-14	S11/31	16T	11.9766	-86.1815	19/02/14 13:41	05/03/14 11:47	334
Feb-14	S11/32	16G	11.9766	-86.1815	19/02/14 13:41	05/03/14 11:47	334
Feb-14	S11/33	17T	11.9770	-86.1819	19/02/14 13:50	05/03/14 11:51	334
Feb-14	S11/34	17G	11.9770	-86.1819	19/02/14 13:50	05/03/14 11:51	334
Feb-14	S11/35	18T	11.9776	-86.1826	19/02/14 13:57	05/03/14 11:57	334
Feb-14	S11/36	18G	11.9776	-86.1826	19/02/14 13:57	05/03/14 11:57	334
Feb-14	S11/38	19rockT	11.9779	-86.1834	19/02/14 14:08	05/03/14 12:01	334
Feb-14	S11/40	19T	11.9778	-86.1833	19/02/14 14:08	05/03/14 12:01	334
Feb-14	S11/41	19G	11.9778	-86.1833	19/02/14 14:08	05/03/14 12:01	334
Feb-14	S11/42	20G	11.9785	-86.1835	19/02/14 14:13	05/03/14 12:06	334
Feb-14	S11/45	21T	11.9786	-86.1836	19/02/14 14:20	05/03/14 12:10	334
Feb-14	S11/46	21T2	11.9786	-86.1836	19/02/14 14:20	05/03/14 12:10	334
Feb-14	S11/47	22G	11.9790	-86.1837	19/02/14 14:23	05/03/14 12:16	334
Feb-14	S11/49	24T	11.9798	-86.1846	19/02/14 14:31	05/03/14 12:20	334
Feb-14	S11/50	24G	11.9798	-86.1846	19/02/14 14:31	05/03/14 12:20	334
Feb-14	S11/51	25G	11.9804	-86.1844	19/02/14 14:36	05/03/14 12:22	334
Feb-14	S11/52	26T	11.9805	-86.1852	19/02/14 14:41	05/03/14 12:24	334
Feb-14	S11/54	27G	11.9811	-86.1852	19/02/14 14:51	05/03/14 12:29	334
Feb-14	S11/55	28T	11.9816	-86.1853	19/02/14 14:55	05/03/14 12:31	334
Feb-14	S11/57	29T	11.9819	-86.1851	19/02/14 15:00	05/03/14 12:35	334
Feb-14	S11/58	29G	11.9819	-86.1851	19/02/14 15:00	05/03/14 12:35	334
Feb-14	S11/59	30T	11.9825	-86.1855	19/02/14 15:05	05/03/14 12:39	334
Feb-14	S11/60	30G	11.9825	-86.1855	19/02/14 15:05	05/03/14 12:39	334

Continued on next page

Table A.2: Sulfation plate exposure information.

Season	Labcode	Site	Latitude	Longitude	Installed	Collected	Hours
Feb-14	S11/61	31T	11.9833	-86.1859	19/02/14 15:11	05/03/14 12:42	334
Feb-14	S11/62	31G	11.9833	-86.1859	19/02/14 15:11	05/03/14 12:42	334
Feb-14	S11/64	32T	11.9841	-86.1864	19/02/14 15:17	05/03/14 12:45	333
Feb-14	S11/65	32G	11.9841	-86.1864	19/02/14 15:17	05/03/14 12:45	333
Feb-14	S11/67	33T	11.9845	-86.1872	19/02/14 15:24	05/03/14 12:50	333
Feb-14	S11/68	33G	11.9845	-86.1872	19/02/14 15:24	05/03/14 12:50	333
Feb-14	S11/69	34T	11.9859	-86.1883	21/02/14 14:36	05/03/14 12:54	286
Feb-14	S11/70	34G	11.9859	-86.1883	21/02/14 14:36	05/03/14 12:54	286
Feb-14	S11/72	36T	11.9860	-86.1903	21/02/14 14:22	05/03/14 13:01	287
Feb-14	S11/73	36G	11.9860	-86.1903	21/02/14 14:22	05/03/14 13:01	287
Feb-14	S11/69.2	34T	11.9859	-86.1883	21/02/14 14:36	05/03/14 12:54	286
Feb-14	S11/70.2	34G	11.9859	-86.1883	21/02/14 14:36	05/03/14 12:54	286
Feb-14	S11/72.2	36T	11.9860	-86.1903	21/02/14 14:22	05/03/14 13:01	287
Feb-14	S11/73.2	36G	11.9860	-86.1903	21/02/14 14:22	05/03/14 13:01	287
Feb-14	S11/96	Comalito	11.9992	-86.1508	20/02/14 13:20	05/03/14 16:23	315
Feb-14	S11/97	H1	11.9820	-86.1684	19/02/14 10:25	05/03/14 15:52	341
Feb-14	S11/100	NCP2 g	11.9872	-86.1673	19/02/14 16:07	05/03/14 16:10	336
Feb-14	S11/101	OCP t	11.9811	-86.1676	19/02/14 10:10	05/03/14 15:41	342
Feb-14	S11/102	Regis	11.9780	-86.0959	19/02/14 18:00	06/03/14 09:00	351
Feb-14	S11/103	Pencas	12.0111	-86.1739	22/02/14	03/03/14	213
May-14	S16/1	M2g	11.9731	-86.1716	25/05/14 10:36	01/06/14 09:52	167
May-14	S16/2	M2t	11.9731	-86.1716	25/05/14 10:36	01/06/14 09:52	167
May-14	S16/3	M3g	11.9738	-86.1768	25/05/14 11:03	01/06/14 10:55	168
May-14	S16/4	M3t	11.9738	-86.1768	25/05/14 11:03	01/06/14 10:55	168

Continued on next page

Table A.2: Sulfation plate exposure information.

Season	Labcode	Site	Latitude	Longitude	Installed	Collected	Hours
May-14	S16/5	M4g	11.9750	-86.1794	25/05/14 11:21	01/06/14 11:30	168
May-14	S16/6	M4t	11.9750	-86.1794	25/05/14 11:21	01/06/14 11:30	168
May-14	S16/7	M5g	11.9766	-86.1815	25/05/14 11:44	01/06/14 11:58	168
May-14	S16/8	M5t	11.9766	-86.1815	25/05/14 11:44	01/06/14 11:58	168
May-14	S16/9	M6g	11.9786	-86.1835	25/05/14 11:55	01/06/14 12:13	168
May-14	S16/10	M6g	11.9786	-86.1835	25/05/14 11:55	01/06/14 12:13	168
May-14	S16/11	M6t	11.9786	-86.1835	25/05/14 11:55	01/06/14 12:13	168
May-14	S16/12	M6t	11.9786	-86.1835	25/05/14 11:55	01/06/14 12:13	168
May-14	S16/13	M7g	11.9813	-86.1852	25/05/14 12:17	01/06/14 12:38	168
May-14	S16/14	M7t	11.9813	-86.1852	25/05/14 12:17	01/06/14 12:38	168
May-14	S16/15	M8g	11.9841	-86.1864	25/05/14 12:39	01/06/14 13:02	168
May-14	S16/16	M8t	11.9841	-86.1864	25/05/14 12:39	01/06/14 13:02	168
May-14	S16/17	M9g	11.9861	-86.1889	25/05/14 13:19	01/06/14 13:51	169
May-14	S16/18	M9t	11.9861	-86.1889	25/05/14 13:19	01/06/14 13:51	169
May-14	S16/20	Pencast	11.9999	-86.1682	25/05/14 15:49	01/06/14 16:19	168
May-14	S16/22	NCP3 t	11.9863	-86.1663	25/05/14 15:43	01/06/14 16:06	168
May-14	S16/24	OCP g	11.9811	-86.1676	25/05/14 15:28	01/06/14 16:01	169
May-14	S16/25	OCP t	11.9811	-86.1676	25/05/14 15:28	01/06/14 16:01	169
Jun-14	S16/40	M3t	11.9738	-86.1768	01/06/14 10:55	08/06/14 10:24	167
Jun-14	S16/38	M2t	11.9731	-86.1716	01/06/14 09:52	08/06/14 10:11	168
Jun-14	S16/39	M3g	11.9738	-86.1768	01/06/14 10:55	08/06/14 10:24	167
Jun-14	S16/44	M5g	11.9766	-86.1815	01/06/14 11:58	08/06/14 10:44	167
Jun-14	S16/41	M4g	11.9750	-86.1794	01/06/14 11:30	08/06/14 10:35	167
Jun-14	S16/42	M4t	11.9750	-86.1794	01/06/14 11:30	08/06/14 10:35	167

Continued on next page

Table A.2: Sulfation plate exposure information.

Season	Labcode	Site	Latitude	Longitude	Installed	Collected	Hours
Jun-14	S16/43	M5g	11.9766	-86.1815	01/06/14 11:58	08/06/14 10:44	167
Jun-14	S16/48	M6g	11.9786	-86.1835	01/06/14 12:13	08/06/14 10:53	167
Jun-14	S16/49	M6t	11.9786	-86.1835	01/06/14 12:13	08/06/14 10:53	167
Jun-14	S16/37	M2g	11.9731	-86.1716	01/06/14 09:52	08/06/14 10:11	168
Jun-14	S16/51	M7g	11.9813	-86.1852	01/06/14 12:38	08/06/14 11:06	166
Jun-14	S16/52	M7t	11.9813	-86.1852	01/06/14 12:38	08/06/14 11:06	166
Jun-14	S16/53	M8g	11.9841	-86.1864	01/06/14 13:02	08/06/14 11:12	166
Jun-14	S16/54	M8t	11.9841	-86.1864	01/06/14 13:02	08/06/14 11:12	166
Jun-14	S16/55	M9g	11.9861	-86.1889	01/06/14 13:51	08/06/14 11:20	165
Jun-14	S16/56	M9t	11.9861	-86.1889	01/06/14 13:51	08/06/14 11:20	165
Jun-14	S16/45	M5t	11.9766	-86.1815	01/06/14 11:58	08/06/14 10:44	167
Jun-14	S16/46	M5t	11.9766	-86.1815	01/06/14 11:58	08/06/14 10:44	167
Jun-14	S16/47	M6g	11.9786	-86.1835	01/06/14 12:13	08/06/14 10:53	167
Jun-14	S16/50	M6t	11.9786	-86.1835	01/06/14 12:13	08/06/14 10:53	167
Jun-14	S16/58	Pencast	11.9999	-86.1682	01/06/14 16:19	08/06/14 12:50	165
Jun-14	S16/59	NCP3 g	11.9863	-86.1663	01/06/14 16:06	08/06/14 13:03	165
Jun-14	S16/60	NCP3 t	11.9863	-86.1663	01/06/14 16:06	08/06/14 13:03	165
Jun-14	S16/62	OCP t	11.9811	-86.1676	01/06/14 16:01	08/06/14 09:20	161
Jun-14	S16/63	H1	11.9820	-86.1684	01/06/14 09:22	08/06/14 09:30	168
Jun-14	S16/64	H1	11.9820	-86.1684	01/06/14 09:22	08/06/14 09:30	168
MJ14	S16/99	Regis	11.9780	-86.0959	27/05/14 17:48	11/06/14 11:30	354
MJ14	S16/61	OCP t	11.9811	-86.1676	25/05/14 15:28	08/06/14 09:20	330
MJ14	S16/97	Comalito	11.9992	-86.1508	25/05/14 16:04	08/06/14 13:15	333

Table A.3: All sulfation plate data in mg m^{-2} day^{-1}. Data below the limit of detection are shown as BD. All data for SO_2, HCl and HF is blank corrected but not background corrected.

Labcode	Season	Site	Hours	Distance	SO_2	HCl	HF
S6/2	Feb-13	H1	48		6764	1178	182
S6/4	Feb-13	H1	22		2234	415	68
S6/15	Feb-13	OCP g	192		925	110	25
S6/17	Feb-13	NCP1 t	219		72	11	5
S6/18	Feb-13	1	91	-1088	BD	7	6
S6/19	Feb-13	1	91	-1088	BD	5	5
S6/20	Feb-13	2	91	-1021	41	7	5
S6/21	Feb-13	2	91	-1021	30	7	7
S6/22	Feb-13	3	92	-883	98	11	7
S6/23	Feb-13	5	92	-598	504	66	19
S6/24	Feb-13	5	92	-598	367	37	14
S6/25	Feb-13	6	92	-575	492	53	16
S6/26	Feb-13	9	96	-505	508	71	17
S6/27	Feb-13	10	93	-479	840	80	22
S6/28	Feb-13	11	93	-441	958	131	29
S6/29	Feb-13	12	93	-360	1639	196	43
S6/30	Feb-13	13	93	-347	1545	180	42
S6/31	Feb-13	14	94	-306	922	94	25
S6/32	Feb-13	15	94	-248	1728	199	47
S6/33	Feb-13	16	94	-144	1822	188	45
S6/34	Feb-13	17	95	-91	2816	264	67
S6/35	Feb-13	18	95	-11	2555	203	49
S6/36	Feb-13	19	95	0	2411	236	56
S6/37	Feb-13	20	95	48	2900	295	64
S6/38	Feb-13	21	97	112	551	61	21
S6/39	Feb-13	22	97	174	310	35	11
S6/40	Feb-13	24	120	275	605	77	20
S6/41	Feb-13	25	97	326	1548	181	41
S6/42	Feb-13	26	97	377	1818	188	42
S6/43	Feb-13	27	97	399	669	76	21
S6/44	Feb-13	28	98	475	243	27	9
S6/45	Feb-13	29	97	578	1082	133	31
S6/46	Feb-13	30	97	671	876	100	27
S6/47	Feb-13	31	97	757	760	89	20
S6/52	Feb-13	Comalito	340		BD	1	BD
B11/01	Feb-13	Regis	201		BD	BD	BD
B11/02	Feb-13	Regis	201		BD	BD	BD
B11/03	Feb-13	Meteo	244		BD	BD	BD
S10/1	Dec-13	1g	264	-1088	34	BD	2
S10/2	Dec-13	1t	264	-1088	38	BD	2
S10/3	Dec-13	2g	263	-1021	71	BD	2

Continued on next page

Table A.3: All sulfation plate data in mg m^{-2} day^{-1}. Data below the limit of detection are shown as BD. All data for SO_2, HCl and HF is blank corrected but not background corrected.

Labcode	Season	Site	Hours	Distance	SO_2	HCl	HF
S10/4	Dec-13	2t	263	-1021	80	BD	1
S10/5	Dec-13	3g	263	-883	109	BD	2
S10/6	Dec-13	3t	263	-883	103	BD	3
S10/7	Dec-13	4g	263	-763	113	BD	3
S10/8	Dec-13	4t	263	-763	142	BD	4
S10/9	Dec-13	6g	263	-591	153	BD	5
S10/10	Dec-13	6t	263	-591	122	BD	3
S10/11	Dec-13	8g	263	-550	172	BD	4
S10/12	Dec-13	8t	263	-550	262	BD	5
S10/13	Dec-13	9g	263	-505	158	BD	4
S10/14	Dec-13	10g	263	-508	371	BD	13
S10/15	Dec-13	10t	263	-508	301	BD	13
S10/16	Dec-13	11g	263	-479	224	71	9
S10/17	Dec-13	11t	263	-479	264	92	13
S10/18	Dec-13	12g	263	-441	253	71	10
S10/19	Dec-13	12t	263	-441	315	97	14
S10/20	Dec-13	13g	263	-360	252	82	10
S10/21	Dec-13	13t	263	-360	177	67	10
S10/22	Dec-13	14g	263	-371	444	115	18
S10/23	Dec-13	14t	263	-371	493	105	17
S10/24	Dec-13	15g	263	-347	237	61	10
S10/25	Dec-13	15t	263	-347	283	75	11
S10/26	Dec-13	16g	263	-306	457	106	15
S10/27	Dec-13	17g	263	-248	237	84	9
S10/28	Dec-13	16t	263	-306	243	60	9
S10/29	Dec-13	19g	264	-87	243	78	10
S10/30	Dec-13	19t	264	-87	279	61	11
S10/31	Dec-13	19.5t	264	-72	416	86	12
S10/32	Dec-13	19.5t	264	-72	312	75	10
S10/33	Dec-13	21g	264	0	745	159	24
S10/34	Dec-13	21t	264	0	247	66	8
S10/35	Dec-13	26g	264	275	350	95	12
S10/36	Dec-13	26t	264	275	875	180	28
S10/37	Dec-13	27g	264	326	362	86	15
S10/38	Dec-13	28t	264	377	542	122	19
S10/39	Dec-13	29g	265	399	441	100	15
S10/40	Dec-13	29t	265	399	466	101	15
S10/41	Dec-13	30g	265	475	521	113	15
S10/42	Dec-13	30t	265	475	723	123	22
S10/43	Dec-13	31g	265	578	412	84	14
S10/44	Dec-13	31t	265	578	423	91	15
S10/45	Dec-13	32g	265	671	346	95	11

Continued on next page

Table A.3: All sulfation plate data in mg m^{-2} day^{-1}. Data below the limit of detection are shown as BD. All data for SO_2, HCl and HF is blank corrected but not background corrected.

Labcode	Season	Site	Hours	Distance	SO_2	HCl	HF
S10/46	Dec-13	32t	265	671	483	83	14
S10/47	Dec-13	33g	265	757	456	104	15
S10/48	Dec-13	33t	265	757	489	91	15
S10/49	Dec-13	34g	265	843	206	24	5
S10/50	Dec-13	35g	266	923	369	35	8
S10/51	Dec-13	35t	266	923	387	51	9
S10/54	Dec-13	Regis	244	-9330	BD	BD	1
S10/56	Dec-13	Comalito	215		BD	BD	1
S10/57	Dec-13	NCP1 g	263		31	8	1
S10/58	Dec-13	OCP t	256		635	125	23
S10/59	Dec-13	OCP g	256		567	81	18
S10/62	Dec-13	H1	256		6326	466	117
S11/2	Feb-14	1T	335	-1088	BD	1	BD
S11/3	Feb-14	1G	335	-1088	2	1	1
S11/4	Feb-14	2T	335	-1021	7	1	BD
S11/5	Feb-14	2G	335	-1021	9	3	BD
S11/6	Feb-14	3T	335	-883	19	3	1
S11/7	Feb-14	3G	335	-883	15	3	1
S11/8	Feb-14	4T	335	-763	55	11	1
S11/9	Feb-14	4G	335	-763	51	9	2
S11/11	Feb-14	6T	335	-591	124	23	3
S11/12	Feb-14	6G	335	-591	100	18	3
S11/13	Feb-14	8T	335	-550	177	30	6
S11/14	Feb-14	8G	335	-550	115	20	4
S11/15	Feb-14	9T	335	-505	186	31	6
S11/16	Feb-14	9G	335	-505	146	31	6
S11/17	Feb-14	10G	335	-508	235	55	6
S11/19	Feb-14	11T	335	-479	247	53	7
S11/20	Feb-14	11G	335	-479	241	49	7
S11/21	Feb-14	12T	334	-441	379	76	10
S11/22	Feb-14	12G	334	-441	268	63	8
S11/24	Feb-14	13T	334	-360	332	62	14
S11/25	Feb-14	13G	334	-360	302	58	13
S11/26	Feb-14	14T	334	-371	540	107	23
S11/27	Feb-14	14G	334	-371	351	75	17
S11/28	Feb-14	15T	334	-347	531	104	22
S11/29	Feb-14	15G	334	-347	505	112	24
S11/31	Feb-14	16T	334	-306	672	119	23
S11/32	Feb-14	16G	334	-306	241	53	13
S11/33	Feb-14	17T	334	-248	456	72	18
S11/34	Feb-14	17G	334	-248	443	77	17
S11/35	Feb-14	18T	334	-144	1042	214	38

Continued on next page

Table A.3: All sulfation plate data in mg m^{-2} day^{-1}. Data below the limit of detection are shown as BD. All data for SO_2, HCl and HF is blank corrected but not background corrected.

Labcode	Season	Site	Hours	Distance	SO_2	HCl	HF
S11/36	Feb-14	18G	334	-144	678	124	25
S11/38	Feb-14	19rockT	334	-72	1108	207	36
S11/40	Feb-14	19T	334	-87	634	135	32
S11/41	Feb-14	19G	334	-87	481	94	14
S11/42	Feb-14	20G	334	-11	798	160	32
S11/45	Feb-14	21T	334	0	778	135	27
S11/46	Feb-14	21T2	334	0	901	171	29
S11/47	Feb-14	22G	334	48	572	107	21
S11/49	Feb-14	24T	334	174	844	169	32
S11/50	Feb-14	24G	334	174	215	50	12
S11/51	Feb-14	25G	334	222	667	146	18
S11/52	Feb-14	26T	334	275	1007	197	36
S11/54	Feb-14	27G	334	326	598	109	21
S11/55	Feb-14	28T	334	377	592	109	25
S11/57	Feb-14	29T	334	399	983	165	25
S11/58	Feb-14	29G	334	399	643	137	23
S11/59	Feb-14	30T	334	475	869	148	30
S11/60	Feb-14	30G	334	475	475	100	19
S11/61	Feb-14	31T	334	578	721	149	29
S11/62	Feb-14	31G	334	578	637	114	24
S11/64	Feb-14	32T	333	671	603	132	20
S11/65	Feb-14	32G	333	671	512	124	20
S11/67	Feb-14	33T	333	757	706	157	26
S11/68	Feb-14	33G	333	757	440	138	20
S11/69	Feb-14	34T	286	943	299	107	16
S11/70	Feb-14	34G	286	943	302	92	16
S11/72	Feb-14	36T	287	1082	267	93	15
S11/73	Feb-14	36G	287	1082	278	90	16
S11/69.2	Feb-14	34T	286	943	344	71	11
S11/70.2	Feb-14	34G	286	943	330	61	10
S11/72.2	Feb-14	36T	287	1082	316	63	10
S11/73.2	Feb-14	36G	287	1082	297	61	9
S11/96	Feb-14	Comalito	315		2	BD	BD
S11/97	Feb-14	H1	341		7773	1596	80
S11/100	Feb-14	NCP2 g	336		132	33	2
S11/101	Feb-14	OCP t	342		618	146	24
S11/102	Feb-14	Regis	351		BD	BD	1
S11/103	Feb-14	Pencas	213		BD	1	1
S16/1	May-14	M2g	167	-1403	BD	3	BD
S16/2	May-14	M2t	167	-1403	BD	1	BD
S16/3	May-14	M3g	168	-887	4	5	BD
S16/4	May-14	M3t	168	-887	14	19	BD

Continued on next page

Table A.3: All sulfation plate data in mg m^{-2} day^{-1}. Data below the limit of detection are shown as BD. All data for SO_2, HCl and HF is blank corrected but not background corrected.

Labcode	Season	Site	Hours	Distance	SO_2	HCl	HF
S16/5	May-14	M4g	168	-586	16	15	1
S16/6	May-14	M4t	168	-586	18	8	BD
S16/7	May-14	M5g	168	-312	85	8	1
S16/8	May-14	M5t	168	-312	125	39	4
S16/9	May-14	M6g	168	0	228	57	7
S16/10	May-14	M6g	168	0	193	51	6
S16/11	May-14	M6t	168	0	271	58	8
S16/12	May-14	M6t	168	0	276	64	7
S16/13	May-14	M7g	168	347	209	66	8
S16/14	May-14	M7t	168	347	189	55	6
S16/15	May-14	M8g	168	671	97	33	2
S16/16	May-14	M8t	168	671	147	55	5
S16/17	May-14	M9g	169	999	56	8	BD
S16/18	May-14	M9t	169	999	103	27	2
S16/20	May-14	Pencast	168		BD	2	BD
S16/22	May-14	NCP3 t	168		597	111	15
S16/24	May-14	OCP g	169		76	19	BD
S16/25	May-14	OCP t	169		72	16	BD
S16/40	Jun-14	M3t	167	-887	BD	BD	BD
S16/38	Jun-14	M2t	168	-1403	BD	BD	BD
S16/39	Jun-14	M3g	167	-887	2	7	BD
S16/44	Jun-14	M5g	167	-312	17	9	1
S16/41	Jun-14	M4g	167	-586	2	15	BD
S16/42	Jun-14	M4t	167	-586	4	BD	1
S16/43	Jun-14	M5g	167	-312	13	7	BD
S16/48	Jun-14	M6g	167	0	BD	BD	BD
S16/49	Jun-14	M6t	167	0	86	23	4
S16/37	Jun-14	M2g	168	-1403	BD	BD	BD
S16/51	Jun-14	M7g	166	347	142	30	5
S16/52	Jun-14	M7t	166	347	171	38	6
S16/53	Jun-14	M8g	166	671	173	34	6
S16/54	Jun-14	M8t	166	671	244	49	8
S16/55	Jun-14	M9g	165	999	189	35	6
S16/56	Jun-14	M9t	165	999	216	43	8
S16/45	Jun-14	M5t	167	-312	20	5	BD
S16/46	Jun-14	M5t	167	-312	30	6	1
S16/47	Jun-14	M6g	167	0	54	16	2
S16/50	Jun-14	M6t	167	0	63	12	3
S16/58	Jun-14	Pencast	165		BD	3	1
S16/59	Jun-14	NCP3 g	165		116	23	4
S16/60	Jun-14	NCP3 t	165		240	49	9
S16/62	Jun-14	OCP t	161		63	14	2

Continued on next page

Table A.3: All sulfation plate data in mg m^{-2} day^{-1}. Data below the limit of detection are shown as BD. All data for SO_2, HCl and HF is blank corrected but not background corrected.

Labcode	Season	Site	Hours	Distance	SO_2	HCl	HF
S16/63	Jun-14	H1	168		596	141	21
S16/64	Jun-14	H1	168		598	138	36
S16/99	MJ14	Regis	354		7	BD	BD
S16/61	MJ14	OCP t	330		149	27	4
S16/97	MJ14	Comalito	333		BD	1	BD

	Dec 13	Feb 14	May 14	Jun 14
C_0 (μg m^{-3})	551	1954	409	327
$x_{0,C}$ (m)	121	88	171	1072
σ_C (m)	689	416	499	639
$Integral_C$ (mg)	951	2037	511	525
$NRMSE_C$ (%)	23	10	24	12

Table A.4: Gaussian fit parameters for H_2SO_4 gas concentrations across the different sampling periods. C_0 is the maximum concentration, which occurs at distance x=$x_{0,C}$ from the centreline and σ_C is the width parameter. The integral is calculated by $C_0\sigma_C\sqrt{2\pi}$ and the NRMSE is the normalized root mean squared error expressed as a percentage.

A.2 Gaussian fits

A.2.1 H_2SO_4

The Gaussian fit to the H_2SO_4 gas concentration data was very similar to that of SO_2. Overall, SO_2 has better NRMSE values and therefore chose over H_2SO_4 to represent sulfuric gases.

A.2.2 Residuals

There was no correlation between residuals and distance along the transect and predicted values from the Gaussian model (Figure A.2).

Figure A.2: Example of residuals against a) distance and b) predicted values from the Gaussian model from December 2013 SO_2.

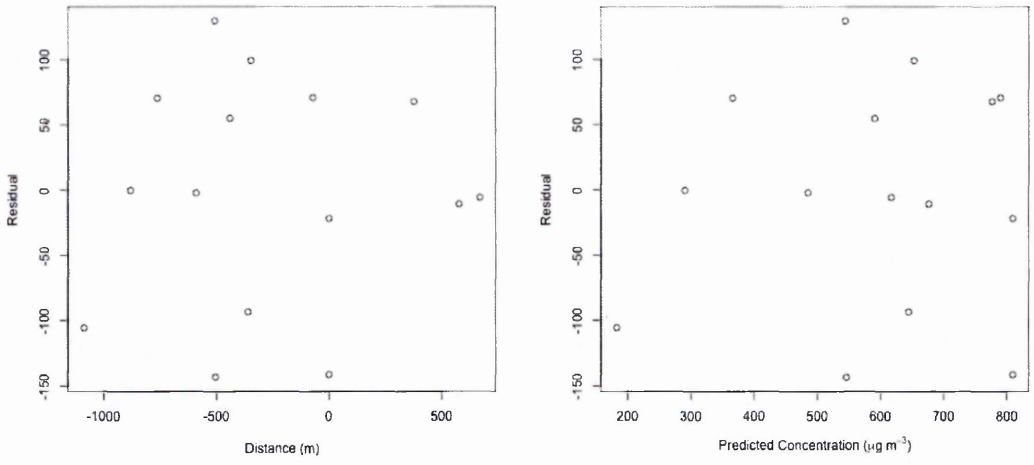

A.3 HYSPLIT model

A.3.1 Testing the model

First, to test the reliability of the model, it has been run at 10 m above ground level every daylight hour (from 6:00 depending on time of year to 18:00) for the five days for which a Google Earth satellite image, with a visible plume was available (22/1/2014, 9/4/2013, 30/1/2011, 31/3/2010 and 18/12/2004).

Figure A.3: HYSPLIT trajectories and Google Earth imagery showing comparison between observed gas plume (visible in Google Earth image) and calculated HYSPLIT trajectory.

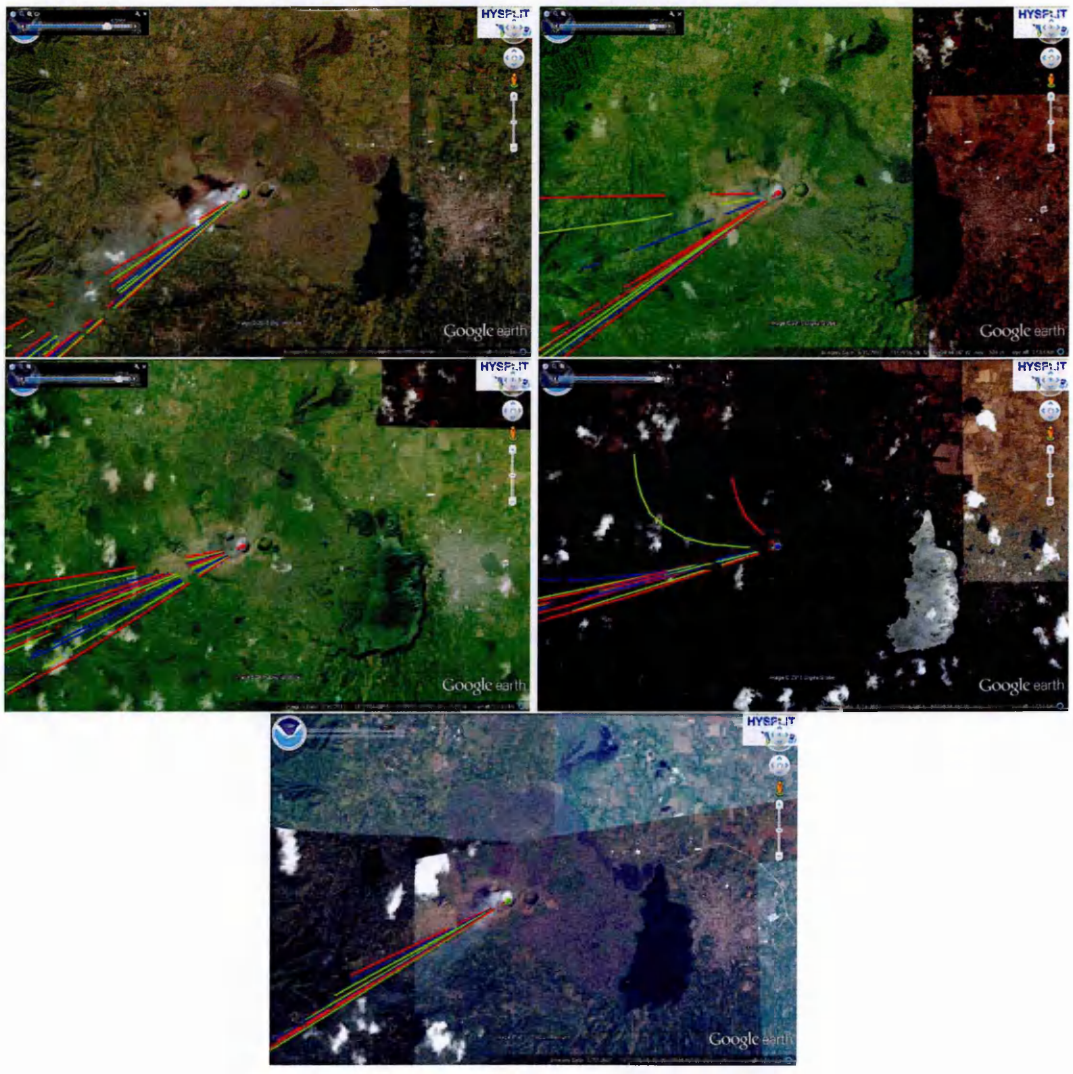

There was a good relationship between the visible plume direction and the direction of the HYSPLIT trajectories for the 5 days shown (Figure A.3). The height at which

the model was run did not appear to be significant in determining the direction of the trajectory. However, the time of day did seem to be significant and for all days there was a slight change in direction, generally more northerly, during the last few hours of daylight, which was particularly evident in April 2013 (Figure A.4).

Figure A.4: HYSPLIT trajectories and Google Earth imagery by time for 9/4/2013. Red is morning, blue is day-time and green is afternoon.

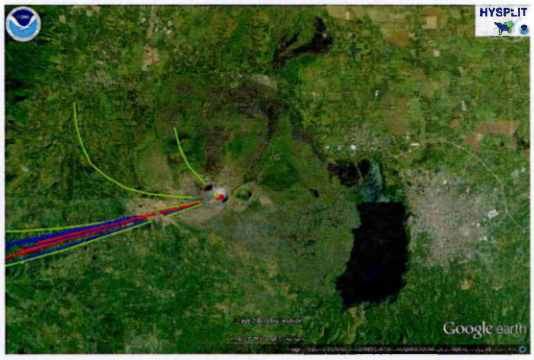

Appendix B

Plant communities

B.1 Plant communities

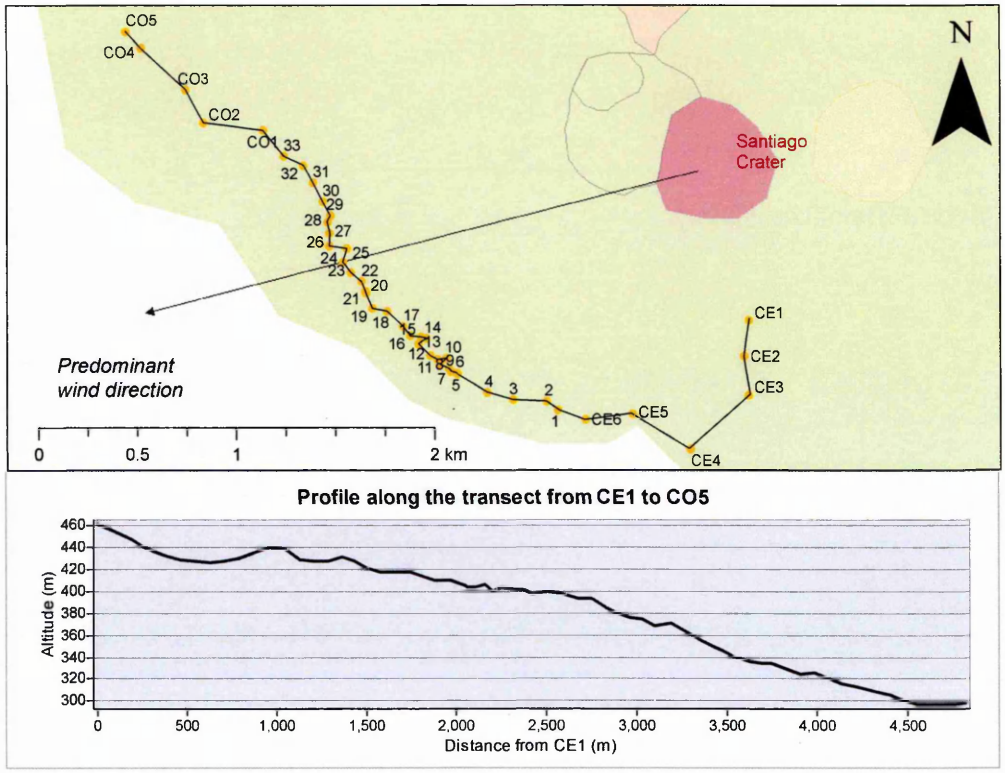

Figure B.1: Topography between sites surveyed for plant communities on the transect.

B.1.1 Classification tables

Cover (%)	Braun-Blanquet scale
Not present	0
<1	1
1-5	2
6-25	3
26-50	4
51-75	5
76-100	6

Table B.1: Braun-Blanquet cover abundance scale

Maximum Height (cm)	Height scale
Not present	0
<10	1
11-25	2
26-50	3
51-100	4
100-200	5
>200	6

Table B.2: Maximum height scale

B.1.2 Plant species results

Table B.3: All identified species and their growth form.

Short	Species	Family	Form
Acalypha	Acalypha	Euphorbiaceae	Shrub
Acantetr	Acanthocereus tetragonus	Cactaceae	Cactus
Agercony	Ageratum conyzoides	Asteraceae	Herb
Amphpani	Amphilophium paniculatum	Bignoniaceae	Vine
Pthcctnm	Pithecoctenium	Bignoniaceae	Vine
Aphescab	Aphelandra scabra	Acanthaceae	Shrub
Bidepilo	Bidens pilosa	Asteraceae	Vine
Blepmucr	Blepharodon mucronatum	Apocynaceae	Vine
Bromping	Bromelia pinguin	Bromeliaceae	Rosette
Burssima	Bursera simaruba	Burseraceae	Tree
Byrscras	Byrsonima crassifolia	Malpighiaceae	Tree
Byttacul	Byttneria aculeata	Malvaceae	Vine
Casecory	Casearia corymbosa	Salicaceae	Tree
Cenchrus	Cenchrus	Poaceae	Grass
Cissmicr	Cissus microcarpa	Vitaceae	Vine
Cissvert	Cissus verticillata	Vitaceae	Vine
Cleovisc	Cleome viscosa	Cleomaceae	Herb
Cochviti	Cochlospermum vitifolium	Bixaceae	Tree
Dalescan	Dalechampia scandens	Euphorbiaceae	Vine
Diodia	Diodia	Rubiaceae	Herb
Eleuindi	Eleusine indica	Poaceae	Grass
Euphcoll	Euphorbia colletiades	Euphorbiaceae	Tree
Euphherb	Euphorbia herb	Euphorbiaceae	Herb
Fabaflow	Fabaceae vine flower	Fabaceae	Vine
Fabapod	Fabaceae vine pod	Fabaceae	Vine
Ficus	Ficus	Moraceae	Tree
Glirsepi	Gliricidia sepium	Fabaceae	Tree
Ipomoea	Ipomoea	Convolvulaceae	Vine
Irescale	Iresine calea	Amaranthaceae	Shrub
Jatrcurc	Jatropha curcas	Euphorbiaceae	Shrub
Justcart	Justicia carthaginensis	Acanthaceae	Herb
Kallstrm	Kallstroemia	Zygophyllaceae	Herb
Lanturti	Lantana urticifolia	Verbenaceae	Shrub
Lasirusc	Lasiacis ruscifolia	Poaceae	Grass
Loncmini	Lonchocarpus minimiflorus	Fabaceae	Tree
Malvconn	Malvaviscus connicus	Malvaceae	Shrub
Maraarun	Maranta arundinacea	Marantaceae	Shrub
Melirepe	Melinis repens	Poaceae	Grass
Micoarge	Miconia argentea	Melastomataceae	Tree

Continued on next page

Table B.3: All identified species and their growth form.

Short	Species	Family	Form
Mimoalbi	Mimosa albida	Fabaceae	Shrub
Oecemacu	Oeceoclades maculata	Orchidaceae	Orchid
Opliburm	Oplismenus burmannii	Poaceae	Grass
Petialli	Petiveria alliacea	Phytolaccaceae	Shrub
Philjacq	Philodendron jacquinii	Araceae	Vine
Physalis	Physalis	Solanaceae	Vine
Pisomacr	Pisonia macranthocarpa	Nyctaginaceae	Tree
Pitycalo	Pityrogramma calomelanos	Pteridaceae	Fern
Plumrubr	Plumeria rubra	Apocynaceae	Tree
Rauvtetr	Rauvolfia tetraphylla	Apocynaceae	Shrub
Ruelblec	Ruellia blechum	Acanthaceae	Herb
Ruelinun	Ruellia inundata	Acanthaceae	Shrub
Russsarm	Russelia sarmentosa	Plantaginaceae	Shrub
Selagnll	Selaginella	Selaginellaceae	Fern
Sennpall	Senna pallida	Fabaceae	Shrub
Serjgros	Serjania grosii	Sapindaceae	Vine
Sidarhom	Sida rhombifolia	Malvaceae	Herb
Sidaspin	Sida spinosa	Malvaceae	Herb
Smilspin	Smilax spinosa	Smilacaceae	Vine
Spermacc	Spermacoce	Rubiaceae	Herb
Stemmadn	Stemmadenia	Apocynaceae	Tree
Tecostan	Tecoma stans	Bignoniaceae	Tree
Thevetia	Thevetia	Apocynaceae	Tree
Trichava	Trichillia havanensis	Meliaceae	Tree
Trigrugo	Trigonia rugosa	Trigoniaceae	Shrub
Tropmori	Tropaeolum moritzianum	Tropaeolaceae	Vine
Turnscab	Turneara scabra	Passifloraceae	Herb
Urerbacc	Urera baccifera	Urticaceae	Tree
Verbovat	Verbesina ovatifolia	Asteraceae	Shrub
Waltindi	Waltheria indica	Malvaceae	Herb
Xantwend	Xanthosoma wendlandii	Araceae	Vine

Table B.4: December 2013 presence absence species data.

	D1	D2	D3	D4	D5	D6	D7	D8	D9	D10	D11	D12	D13	D14	D15	D16	D17	D18	D19	D20	D21	D22	D23	D24	D25	D26	D27	D28	D29	D30	D31	D32	D33
Acalypha	1	0	0	0	0	0	0	0	0	0	0	0	0	0	0	0	0	0	0	0	0	0	0	0	0	0	0	0	0	0	0	0	0
Acantetr	1	0	0	0	0	0	0	0	0	0	0	1	0	0	1	1	1	0	0	0	0	0	0	0	0	0	1	0	0	0	0	0	0
Agercony	0	0	0	0	0	0	0	1	0	0	0	0	0	0	0	0	0	1	0	0	0	0	0	0	0	1	1	1	0	1	1	1	0
Amphpani	0	0	0	0	0	0	0	0	0	0	0	0	0	0	0	0	0	0	1	0	0	0	0	0	0	0	0	0	0	0	1	1	1
Pthcctnm	1	0	1	0	1	0	0	0	0	0	0	0	0	0	0	0	0	0	0	0	0	0	0	0	0	0	0	0	0	0	0	0	0
Aphescab	1	1	1	0	0	0	0	0	0	0	0	0	0	0	0	0	0	0	0	0	0	0	0	0	0	0	0	0	0	0	0	0	0
Bidepilo	1	1	0	1	0	0	0	0	0	0	0	1	0	0	0	0	0	0	0	0	0	0	0	0	0	0	0	0	0	0	0	0	0
Blepmucr	1	0	1	1	1	1	0	1	1	1	1	0	1	0	1	0	0	0	0	0	0	0	0	0	0	0	0	0	0	0	0	0	0
Bromping	1	1	0	1	0	0	0	0	0	1	0	1	1	0	1	1	1	0	0	0	0	0	1	0	0	1	0	0	0	1	0	0	0
Byrscras	0	0	0	0	0	0	0	0	0	1	0	0	1	1	0	1	0	0	0	0	0	0	0	0	0	0	0	0	0	0	0	0	0
Byttacul	1	0	1	0	0	1	1	0	0	0	0	0	0	0	0	0	0	0	0	0	0	0	0	0	0	0	0	0	0	0	0	0	0
Casecory	0	0	1	0	0	0	0	0	0	0	0	0	0	0	0	0	0	0	0	0	0	0	0	0	0	0	0	0	0	0	0	0	0
Cenchrus	0	0	0	0	0	0	0	0	0	0	0	0	0	1	1	0	0	1	0	1	1	1	1	1	1	1	1	1	1	1	0	0	0
Cissmicr	0	0	0	1	1	0	1	1	1	0	1	1	1	0	1	0	0	0	1	0	0	0	0	0	0	0	0	0	1	0	0	0	0
Cissvert	0	0	0	1	1	0	1	1	1	1	1	1	1	1	0	1	1	1	1	0	0	0	0	0	0	1	1	1	0	1	1	1	0
Cleovisc	1	1	0	1	1	0	1	1	1	0	1	0	0	0	0	0	1	0	0	0	0	0	0	0	0	0	0	0	0	0	1	1	0
Cochviti	0	0	0	0	0	0	0	0	0	1	0	0	0	0	1	0	0	0	0	0	0	0	0	0	0	0	0	0	0	0	0	0	0
Dalescan	1	0	0	1	1	1	1	1	1	0	1	1	0	0	1	0	0	0	1	0	0	0	0	0	0	0	0	1	1	1	1	1	1
Diodia	0	0	0	0	0	0	0	0	0	0	0	0	0	0	1	0	0	1	0	1	0	1	1	0	1	0	0	1	1	1	1	0	0
Eleuindi	0	0	0	0	0	0	0	1	0	0	0	0	0	1	1	0	0	0	0	1	0	0	0	0	0	0	0	0	1	1	1	0	0
Euphcoll	0	0	0	1	1	1	0	0	0	0	0	1	1	0	1	1	1	0	0	0	0	0	0	0	0	0	0	0	0	0	0	0	0
Fabaflow	0	0	0	0	0	0	0	0	0	0	0	0	0	0	0	0	0	0	0	0	0	0	0	0	0	0	0	0	0	0	1	0	1
Fabapod	0	0	0	0	0	0	0	0	0	1	0	0	0	0	0	0	0	0	0	0	0	0	0	0	0	0	0	0	0	0	0	0	0
Ficus	0	0	0	0	0	0	0	0	0	0	0	0	0	0	0	1	0	0	0	0	0	0	0	0	0	0	0	0	0	0	0	0	0
Ipomoea	0	0	0	0	0	0	1	1	1	0	1	0	1	0	0	0	0	0	0	0	0	0	0	0	0	0	0	0	0	0	0	0	0
Irescale	0	0	0	1	0	0	1	0	1	0	1	1	0	0	0	0	0	0	0	0	0	0	0	0	0	0	0	0	0	0	0	1	1
Justcart	1	0	0	0	1	1	0	0	0	0	0	0	0	0	0	0	0	0	0	0	0	0	0	0	0	0	0	0	0	0	1	1	1
Lanturti	0	0	0	0	0	0	0	1	1	0	0	0	0	0	0	0	0	0	0	0	0	0	0	0	0	0	0	0	0	0	0	0	0

Continued on next page

Table B.4: December 2013 presence absence species data.

	D1	D2	D3	D4	D5	D6	D7	D8	D9	D10	D11	D12	D13	D14	D15	D16	D17	D18	D19	D20	D21	D22	D23	D24	D25	D26	D27	D28	D29	D30	D31	D32	D33
Lasirusc	1	1	0	0	0	1	0	0	0	0	0	0	0	0	0	0	0	0	0	0	0	0	0	0	0	0	0	0	0	0	0	0	0
Loncmini	0	0	0	0	0	0	0	0	0	0	0	1	0	0	0	0	0	0	0	0	0	0	0	0	0	0	0	0	0	0	0	0	0
Malvconn	1	1	1	0	0	0	1	0	0	0	1	0	0	0	0	0	0	0	0	0	0	0	0	0	0	0	0	0	0	0	0	0	0
Maraarun	0	0	0	0	0	0	0	0	0	0	0	1	0	0	0	0	0	0	0	0	0	0	0	0	0	0	0	0	0	0	0	0	0
Melirepe	0	0	0	0	0	0	0	0	0	0	0	0	0	0	0	0	0	0	0	1	1	0	0	0	0	0	0	0	0	0	0	0	0
Micoarge	0	0	0	0	1	0	1	0	0	0	0	1	0	1	1	1	0	0	0	0	0	0	0	0	0	0	0	0	0	0	0	0	0
Mimoalbi	0	0	0	1	0	0	0	0	0	1	0	1	1	1	0	0	0	1	0	1	1	0	0	0	0	1	0	0	0	1	1	0	0
Oecemacu	1	1	1	1	1	0	1	0	0	0	0	0	0	0	0	0	0	0	0	0	0	0	0	0	0	0	0	0	0	0	0	0	0
Opliburm	1	0	1	1	1	1	1	1	1	1	1	1	1	0	0	1	1	0	1	0	0	0	0	0	0	0	0	0	0	0	1	1	1
Petialli	0	0	0	0	0	0	1	0	0	0	0	0	0	0	0	0	0	0	0	0	0	0	0	0	0	0	0	0	0	0	0	0	0
Philjacq	0	1	0	0	0	0	0	0	0	0	0	0	0	0	0	1	1	0	0	0	0	0	0	0	0	0	0	0	0	0	0	0	0
Physalis	0	0	0	0	0	0	0	0	0	0	0	0	0	0	0	0	0	0	0	0	0	0	0	0	0	0	0	0	0	0	0	1	0
Pisomacr	0	0	1	0	0	0	0	0	0	0	0	0	0	0	0	0	0	0	0	0	0	0	0	0	0	0	0	0	0	0	0	0	0
Pitycalo	0	0	0	0	0	0	0	0	0	0	0	0	0	1	0	1	0	0	0	1	1	0	0	1	0	0	1	0	0	0	0	0	0
Plumrubr	0	0	0	0	1	0	0	0	0	1	0	0	0	0	0	0	0	0	0	0	0	0	0	0	0	0	0	0	0	0	0	0	0
Rauvtetr	0	0	0	0	0	0	0	0	0	0	0	0	0	0	0	0	0	0	0	0	0	0	0	0	0	0	0	0	0	0	1	1	0
Ruelblec	0	0	0	0	0	0	0	1	1	0	1	0	0	0	0	0	0	0	0	0	0	0	0	0	0	0	0	0	0	0	0	0	0
Ruelinun	1	0	0	0	0	0	0	0	0	0	0	0	0	0	0	0	0	0	0	0	0	0	0	0	0	0	0	0	0	0	0	0	0
Russsarm	0	0	1	1	0	0	0	0	0	1	0	0	0	0	0	0	0	0	0	0	0	0	0	0	0	0	0	0	0	0	0	0	0
Selagnll	0	1	0	0	0	0	0	0	0	0	0	0	0	0	0	0	0	0	0	0	0	0	0	0	0	0	0	0	0	0	0	0	0
Sennpall	0	0	1	1	1	1	1	1	1	0	1	0	0	0	0	0	0	0	0	0	0	0	0	0	0	0	0	0	0	1	0	1	0
Serjgros	1	0	1	0	0	0	0	0	1	0	1	0	0	0	0	0	0	0	0	0	0	0	0	0	0	0	0	0	0	1	0	0	0
Sidarhom	1	1	0	0	0	0	0	1	1	0	1	0	0	0	0	0	0	0	0	0	0	0	0	0	0	0	0	0	1	0	0	1	0
Sidaspin	0	1	0	0	0	0	0	0	0	0	0	0	0	0	0	0	0	0	0	0	0	0	0	0	0	0	0	0	0	0	0	0	0
Smilspin	0	1	1	0	1	0	1	0	0	1	1	1	1	1	0	1	1	0	0	0	0	0	0	0	0	0	0	0	0	0	0	0	0
Spermacc	0	0	0	0	1	1	0	0	0	1	0	1	0	1	0	0	0	0	1	0	0	0	1	0	1	1	0	1	1	1	1	1	1
Stemmadn	0	1	0	0	1	0	1	0	0	1	0	0	0	0	0	1	0	0	0	0	0	0	0	0	0	0	0	0	0	0	0	0	0
Tecostan	1	0	1	0	1	0	0	0	0	0	0	0	0	0	0	0	0	0	0	0	0	0	0	0	0	0	0	0	0	0	0	0	0
Thevetia	0	0	0	1	1	1	0	0	0	1	0	0	0	0	0	0	0	0	0	0	0	0	0	0	0	0	0	0	0	0	0	0	0

Continued on next page

Table B.4: December 2013 presence absence species data.

	D1	D2	D3	D4	D5	D6	D7	D8	D9	D10	D11	D12	D13	D14	D15	D16	D17	D18	D19	D20	D21	D22	D23	D24	D25	D26	D27	D28	D29	D30	D31	D32	D33
Trichava	0	0	0	0	0	0	1	0	0	1	0	0	0	0	0	1	0	0	0	0	0	0	0	0	0	0	0	0	0	0	0	0	0
Tropmori	0	0	0	0	0	0	1	0	0	0	0	0	0	0	0	0	0	0	0	0	0	0	0	0	0	0	0	0	0	0	0	0	0
Turnscab	0	0	0	0	0	0	0	0	0	0	0	0	0	0	0	0	0	0	0	0	0	0	0	0	0	1	0	0	1	1	1	1	1
Urerbacc	0	0	1	0	0	0	1	0	0	0	0	0	0	0	0	0	0	0	0	0	0	0	0	0	0	0	0	0	0	0	0	0	0
Verbovat	1	1	0	0	0	0	0	0	0	0	0	0	0	0	0	0	0	0	0	0	0	0	0	0	0	0	0	0	1	0	0	0	0
Waltindi	0	0	0	0	0	0	0	0	0	0	0	0	1	0	0	0	0	0	0	0	0	0	0	0	0	0	0	0	0	0	0	0	0
Xantwend	0	0	0	0	0	0	1	0	0	0	0	0	0	0	0	1	0	0	0	0	0	0	0	0	0	0	0	0	0	0	0	0	0

Table B.5: February 2014 presence absence species data.

	F1	F2	F3	F4	F5	F6	F7	F8	F9	F10	F11	F12	F13	F14	F15	F16	F17	F18	F19	F20	F21	F22	F23	F24	F25	F26	F27	F28	F29	F30	F31	F32	F33
Acalypha	1	0	0	0	0	0	0	0	0	0	0	0	0	0	0	0	0	0	0	0	0	0	0	0	0	0	0	0	0	0	0	0	0
Acantetr	1	0	0	0	1	0	0	0	0	0	0	1	0	0	1	1	1	0	0	0	0	0	0	0	0	0	1	0	0	0	0	0	0
Agercony	0	0	0	0	0	0	0	1	0	0	0	0	0	0	0	0	0	0	0	0	0	0	0	0	0	1	1	1	0	1	1	1	0
Amphpani	0	0	0	0	0	0	0	0	0	0	0	0	0	0	0	0	0	0	1	0	0	0	0	0	0	0	0	0	0	0	1	1	1
Pthcctnm	1	0	1	0	1	1	0	0	0	0	0	0	0	0	0	0	0	0	0	0	0	0	0	0	0	0	0	0	0	0	0	0	0
Aphescab	1	1	0	0	0	0	1	0	0	0	0	0	0	0	0	0	0	0	0	0	0	0	0	0	0	0	0	0	0	0	0	0	0
Bidepilo	0	0	0	0	0	0	0	0	0	0	0	1	0	0	0	0	0	0	0	0	0	0	0	0	0	0	0	0	0	0	0	0	0
Blepmucr	0	0	0	1	1	0	0	0	0	1	1	0	1	0	1	0	0	0	0	0	0	0	0	0	0	0	0	0	0	0	0	0	0
Bromping	1	1	0	1	0	0	0	0	1	1	0	1	1	0	1	1	1	0	0	0	0	0	1	0	0	1	0	0	0	1	0	0	0
Byrscras	0	0	0	0	0	0	0	0	0	1	0	0	1	1	0	0	0	0	0	0	0	0	0	0	0	0	0	0	0	0	0	0	0
Byttacul	1	0	1	0	0	1	1	0	0	0	0	0	0	0	0	0	0	0	0	0	0	0	0	0	0	0	0	0	0	0	0	0	0
Casecory	0	0	1	0	0	0	0	0	0	0	0	0	0	0	0	0	0	0	0	0	0	0	0	0	0	0	0	0	0	0	0	0	0
Cenchrus	0	0	0	0	0	0	0	0	0	0	0	0	0	1	1	0	0	1	0	1	1	1	1	1	1	1	1	1	1	1	0	0	0
Cissmicr	0	0	0	0	0	0	0	1	0	0	0	0	1	0	0	0	0	0	0	0	0	0	0	0	0	0	0	0	0	0	0	0	0
Cissvert	0	1	1	1	1	1	1	1	1	1	1	1	1	1	0	1	1	1	1	0	0	0	1	0	0	1	1	1	1	1	1	1	1
Cleovisc	1	0	0	1	1	1	1	1	1	0	1	0	0	0	0	0	1	0	0	0	0	0	0	0	0	0	0	0	0	0	1	1	0
Cochviti	0	0	0	0	0	0	0	0	1	0	0	0	0	0	0	0	0	0	0	0	0	0	0	0	0	0	0	0	0	0	0	0	0
Dalescan	1	0	1	1	0	0	1	1	1	0	1	1	0	0	1	0	0	0	1	0	0	0	0	0	0	0	0	1	1	1	1	1	1
Diodia	0	0	0	0	0	0	0	0	0	0	0	0	0	0	1	0	0	1	0	1	0	1	0	1	0	1	1	0	1	1	1	0	0
Euphcoll	0	0	0	1	1	1	0	0	0	0	0	1	1	0	1	1	1	0	0	0	0	0	0	0	0	0	0	0	0	0	0	0	0
Euphherb	0	0	0	0	0	0	0	1	0	0	0	0	0	0	0	0	0	0	0	0	0	0	0	0	0	0	0	0	0	0	0	0	0
Fabaflow	0	0	0	0	0	0	0	0	0	0	0	0	0	0	0	0	0	0	0	0	0	0	0	0	0	0	0	0	0	0	1	0	0
Fabapod	0	0	0	0	1	0	0	0	1	1	0	0	0	0	0	0	0	0	0	0	0	0	0	0	0	0	0	0	0	0	0	0	0
Ficus	0	0	0	0	0	0	0	0	0	0	0	0	0	0	0	1	0	0	0	0	0	0	0	0	0	0	0	0	0	0	0	0	0
Ipomoea	0	0	0	0	0	0	1	0	0	0	0	0	0	0	0	0	0	0	0	0	0	0	0	0	0	0	0	0	0	0	0	0	0
Irescale	0	0	0	0	0	1	0	0	1	0	1	0	0	0	0	0	0	0	1	0	0	0	0	0	0	0	0	0	0	0	0	1	0
Justcart	0	0	0	0	1	1	1	0	0	0	0	0	0	0	0	0	0	0	1	0	0	0	0	0	0	0	0	0	0	0	1	1	1
Kallstrm	0	0	0	0	0	0	0	1	1	0	0	0	0	0	0	0	0	0	0	0	0	0	0	0	0	0	0	0	0	0	0	0	0

Continued on next page

Table B.5: February 2014 presence absence species data.

	F1	F2	F3	F4	F5	F6	F7	F8	F9	F10	F11	F12	F13	F14	F15	F16	F17	F18	F19	F20	F21	F22	F23	F24	F25	F26	F27	F28	F29	F30	F31	F32	F33
Lanturti	0	0	0	0	0	0	0	1	1	0	0	1	0	0	0	0	0	0	0	0	0	0	0	0	0	0	0	0	0	0	0	0	0
Lasirusc	1	1	1	1	0	0	0	0	0	0	0	0	0	0	0	0	0	0	0	0	0	0	0	0	0	0	0	0	0	0	0	0	0
Loncmini	0	0	0	0	0	0	0	0	0	0	0	1	0	0	0	0	0	0	0	0	0	0	0	0	0	0	0	0	0	0	0	0	0
Malvconn	1	1	0	0	1	0	1	0	0	0	0	0	0	0	0	0	0	0	0	0	0	0	0	0	0	0	0	0	0	0	0	0	0
Melirepe	0	0	0	0	0	0	0	0	0	0	0	0	0	0	0	0	0	0	0	1	1	0	0	0	0	0	0	0	0	0	0	0	0
Micoarge	0	0	0	0	0	0	1	0	0	0	0	0	0	0	0	0	0	0	0	0	0	0	0	0	0	0	0	0	0	0	0	0	0
Mimoalbi	0	0	0	0	0	0	0	1	0	1	0	1	0	1	0	0	0	1	0	1	1	0	0	0	0	1	1	0	0	1	1	0	0
Oecemacu	1	1	1	1	0	0	0	0	0	0	0	0	0	0	0	0	0	0	0	0	0	0	0	0	0	0	0	0	0	0	0	0	0
Petialli	0	0	0	0	0	0	1	0	0	0	0	0	0	0	0	0	0	0	0	0	0	0	0	0	0	0	0	0	0	0	0	0	0
Philjacq	0	1	0	0	0	0	0	0	0	0	0	0	0	0	0	1	1	0	0	0	0	0	0	0	0	0	0	0	0	0	0	0	0
Pisomacr	0	0	1	0	0	0	0	0	0	0	0	0	0	0	0	0	0	0	0	0	0	0	0	0	0	0	0	0	0	0	0	0	0
Pitycalo	0	0	0	0	0	0	0	0	0	0	0	0	0	1	0	1	0	0	0	1	0	1	0	1	0	0	0	0	0	0	0	0	0
Plumrubr	0	0	0	0	0	0	0	0	0	1	0	0	0	0	0	0	0	0	0	0	0	0	0	0	0	0	0	0	0	0	0	0	0
Rauvtetr	0	0	1	0	0	1	1	1	0	0	1	0	0	0	0	0	0	0	0	0	0	0	0	0	0	0	0	0	0	0	0	0	0
Ruelblec	1	0	1	0	1	1	0	1	1	0	1	0	0	0	0	0	0	0	0	0	0	0	0	0	0	0	0	0	0	0	0	0	0
Ruelinun	0	1	0	0	0	0	0	0	0	0	0	0	0	0	0	0	0	0	0	0	0	0	0	0	0	0	0	0	0	0	0	0	0
Russsarm	0	0	1	1	0	0	0	0	0	1	0	0	0	0	0	0	0	0	0	0	0	0	0	0	0	0	0	0	0	0	0	0	0
Sennpall	1	0	1	1	0	1	1	1	1	0	1	0	0	0	0	0	0	0	0	0	0	0	0	0	0	0	0	0	0	1	0	1	0
Serjgros	1	0	1	1	0	0	0	0	1	0	1	1	0	0	0	0	0	0	0	0	0	0	0	0	0	0	0	0	0	1	0	0	0
Sidarhom	0	0	0	0	0	1	0	1	1	0	0	0	1	0	0	0	0	0	0	0	0	0	0	0	0	0	0	0	1	0	0	0	0
Sidaspin	0	1	0	0	0	0	0	0	0	0	0	0	0	0	0	0	0	0	0	0	0	0	0	0	0	0	0	0	0	0	0	0	0
Smilspin	0	1	1	0	0	0	1	0	0	1	1	1	1	1	0	0	1	0	0	0	0	0	0	0	0	0	0	0	0	0	0	0	0
Stemmadn	0	1	1	0	1	0	1	0	0	1	0	0	0	0	0	1	0	0	0	0	0	0	0	0	0	0	0	0	0	0	0	0	0
Tecostan	1	0	1	0	1	0	0	0	0	0	0	0	0	0	0	0	0	0	0	0	0	0	0	0	0	0	0	0	0	0	0	0	0
Thevetia	0	0	0	1	1	1	0	0	0	1	0	0	0	0	0	0	0	0	0	0	0	0	0	0	0	0	0	0	0	0	0	0	0
Trichava	0	0	0	0	0	0	1	0	0	1	0	0	0	0	0	1	0	0	0	0	0	0	0	0	0	0	0	0	0	0	0	0	0
Turnscab	0	0	0	0	0	0	0	0	0	0	0	0	0	0	0	0	0	0	0	0	0	0	0	0	0	1	0	0	1	0	1	1	0
Urerbacc	0	0	1	0	0	0	1	0	0	0	0	0	0	0	0	0	0	0	0	0	0	0	0	0	0	0	0	0	0	0	0	0	0
Verbovat	1	1	0	0	0	0	0	0	0	0	0	0	0	0	0	0	0	0	0	0	0	0	0	0	0	0	0	0	0	0	0	0	0

Continued on next page

Table B.5: February 2014 presence absence species data.

	F1	F2	F3	F4	F5	F6	F7	F8	F9	F10	F11	F12	F13	F14	F15	F16	F17	F18	F19	F20	F21	F22	F23	F24	F25	F26	F27	F28	F29	F30	F31	F32	F33
Waltindi	0	0	0	0	0	0	0	0	0	0	0	0	0	0	0	1	0	0	0	0	0	0	0	0	0	0	0	0	1	0	0	0	0
Xantwend	0	1	0	0	0	0	1	0	0	0	0	0	0	0	0	0	0	0	0	0	0	0	0	0	0	0	0	0	0	0	0	0	0

Table B.6: May 2014 presence absence species data.

	M1	M2	M3	M4	M5	M6	M7	M8	M9	M10	M11	M12	M13	M14	M15	M16	M17	M18	M19	M20	M21	M22	M23	M24	M25	M26	M27	M28	M29	M30	M31	M32	M33	CE1	CE2	CE3	CE4	CE5	CE6	CO1	CO2	CO3	CO4	CO5
Acalypha	1	0	0	0	0	0	0	0	0	0	0	0	0	0	0	0	0	0	0	0	0	0	0	0	0	0	0	0	0	0	0	0	0	0	0	0	1	1	1	0	0	0	0	0
Acantetr	1	0	0	0	0	0	0	0	0	0	0	1	0	0	1	1	1	0	0	0	0	0	0	0	0	0	1	0	0	0	0	0	0	0	0	0	0	1	0	0	1	1	0	0
Agercony	0	0	0	0	0	0	0	0	0	0	0	0	0	0	0	0	0	0	0	0	0	0	0	0	0	1	1	1	0	1	1	0	1	0	0	0	0	0	0	0	0	0	0	0
Amphpani	0	0	0	0	0	0	0	0	0	0	0	0	0	0	0	0	0	0	1	0	0	0	0	0	0	0	0	0	0	0	1	1	1	0	0	0	0	0	0	0	0	0	0	0
Pthcctnm	1	0	1	0	1	1	1	0	0	0	0	0	0	0	0	0	0	0	0	0	0	0	0	0	0	0	0	0	0	0	0	0	0	1	1	1	1	1	0	0	0	0	0	0
Aphescab	0	1	0	0	0	0	0	0	0	0	0	0	0	0	0	0	0	0	0	0	0	0	0	0	0	0	0	0	0	0	0	0	0	0	0	0	0	0	0	0	0	0	0	0
Bidepilo	0	0	0	0	0	0	0	0	0	0	0	1	0	0	0	0	0	0	0	0	0	0	0	0	0	0	0	0	0	0	0	0	0	0	0	0	0	1	0	0	0	1	1
Blepmucr	0	0	0	1	1	1	0	1	0	1	1	1	1	0	0	0	0	0	0	0	0	0	0	0	0	0	0	0	0	0	0	0	0	1	1	0	0	0	1	0	1	1	0	1
Bromping	1	1	0	1	0	0	0	0	1	1	0	1	1	0	1	1	1	0	0	0	0	0	1	0	0	1	0	0	0	1	0	0	0	1	1	1	1	0	1	0	0	0	0	0
Burssima	0	0	0	0	0	0	0	0	0	0	0	0	0	0	0	0	0	0	0	0	0	0	0	0	0	0	0	0	0	0	0	0	0	1	1	0	0	0	0	0	0	0	0	0
Byrscras	0	0	0	0	0	0	0	0	0	1	0	0	1	1	0	1	0	0	0	0	0	0	0	0	0	0	0	0	0	0	0	0	0	0	0	0	0	0	0	1	0	0	0	0
Byttacul	1	0	1	0	0	1	0	0	0	0	0	0	0	0	0	0	1	0	0	0	0	0	0	0	0	0	0	0	0	0	0	0	0	0	0	0	0	0	1	0	0	1	0	0
Casecory	0	0	1	0	0	0	0	0	0	0	1	0	0	0	0	0	0	0	0	0	0	0	0	0	0	0	0	0	0	0	0	0	0	1	0	0	1	1	0	0	0	1	0	0
Cenchrus	0	0	0	0	0	0	0	0	0	0	0	0	0	1	1	0	0	1	0	1	1	1	1	1	1	1	1	1	1	1	0	0	0	0	0	0	0	0	0	0	0	0	1	0
Cissmicr	0	0	0	1	0	0	0	1	1	0	1	1	1	0	0	0	0	0	1	0	0	0	0	0	0	0	0	0	0	0	0	0	0	0	0	0	0	0	0	0	0	0	0	0
Cissvert	0	1	1	1	1	0	1	0	1	1	1	1	0	1	0	1	1	0	1	0	0	0	1	0	0	1	1	0	0	1	1	1	1	0	0	0	0	0	1	1	0	0	0	0
Cleovisc	1	0	0	1	1	1	0	0	1	0	0	1	1	0	0	0	1	0	0	0	0	0	0	0	0	0	0	0	0	0	1	1	1	0	0	0	0	0	0	0	0	1	0	1
Cochviti	0	0	0	0	0	0	0	0	0	1	0	0	0	0	0	0	0	0	0	0	0	0	0	0	0	0	0	0	0	0	0	0	0	1	0	1	0	0	0	0	0	1	1	1
Dalescan	0	0	1	0	0	1	1	1	1	0	1	1	0	0	1	0	0	0	1	0	0	0	0	0	0	0	0	0	1	1	1	1	1	0	0	0	0	0	1	1	1	1	0	1
Diodia	0	0	0	0	0	0	0	0	0	0	0	0	0	0	1	0	0	1	0	1	0	1	0	0	1	0	1	1	1	1	1	0	0	0	0	0	0	0	0	0	0	0	0	0
Euphcoll	0	0	0	1	1	1	0	0	0	0	0	1	1	0	1	1	1	0	0	0	0	0	0	0	0	0	0	0	0	0	0	0	0	1	0	0	0	0	1	0	0	1	0	0
Fabaflow	0	0	0	0	0	0	0	0	0	0	0	0	0	0	0	0	0	0	0	0	0	0	0	0	0	0	0	0	0	0	1	0	0	0	0	0	0	0	0	1	0	0	0	0
Fabapod	0	0	0	0	0	0	0	0	0	1	0	0	0	0	0	0	0	0	0	0	0	0	0	0	0	0	0	0	0	0	0	0	0	0	0	0	0	1	1	0	0	0	0	0
Glirsepi	0	0	0	0	0	0	0	0	0	0	0	0	1	0	0	0	0	0	0	0	0	0	0	0	0	0	0	0	0	0	0	0	0	1	0	1	0	0	1	0	0	0	0	0
Ipomoea	1	0	1	1	0	0	1	0	0	0	0	0	0	0	0	0	0	0	0	0	0	0	0	0	0	0	0	0	0	0	0	0	0	0	0	0	1	0	1	0	1	1	0	0
Irescale	0	0	1	0	0	1	0	0	1	0	1	1	0	0	0	0	0	0	1	0	0	0	0	0	0	0	0	0	0	0	1	1	0	1	0	0	0	0	0	0	1	1	0	0
Jatrcurc	0	0	0	0	0	0	0	0	0	0	0	0	0	0	0	0	0	0	0	0	0	0	0	0	0	0	0	0	0	0	0	0	0	0	0	0	1	0	0	0	0	0	0	0
Justcart	0	0	0	0	1	1	1	1	0	0	0	0	0	0	0	0	0	0	1	0	0	0	0	0	0	0	0	0	0	0	1	1	1	0	0	0	0	1	0	1	0	1	0	0

Continued on next page

Table B.6: May 2014 presence absence species data.

	M1	M2	M3	M4	M5	M6	M7	M8	M9	M10	M11	M12	M13	M14	M15	M16	M17	M18	M19	M20	M21	M22	M23	M24	M25	M26	M27	M28	M29	M30	M31	M32	M33	CE1	CE2	CE3	CE4	CE5	CE6	CO1	CO2	CO3	CO4	CO5
Kallstrm	0	0	0	0	0	0	0	1	0	0	0	0	0	0	0	0	0	0	0	0	0	0	0	0	0	0	0	0	0	0	0	0	0	0	0	0	0	0	0	0	0	0	0	0
Lanturti	0	0	0	0	1	0	0	1	1	0	0	1	0	0	0	0	0	0	0	0	0	0	0	0	0	0	0	0	0	0	0	0	0	0	0	0	0	0	0	0	0	0	0	0
Lasirusc	1	1	0	1	0	0	0	0	0	0	0	0	0	0	0	0	0	0	0	0	0	0	0	0	0	0	0	0	0	0	0	0	0	1	0	1	0	0	1	0	0	1	0	0
Loncmini	0	0	0	0	0	0	0	0	0	0	0	1	0	0	0	0	0	0	0	0	0	0	0	0	0	0	0	0	0	0	0	0	0	0	0	0	0	0	0	0	0	0	0	0
Malvconn	1	1	1	0	0	0	1	0	0	0	0	0	0	0	0	0	1	0	0	0	0	0	0	0	0	0	0	0	0	0	0	0	0	0	0	0	0	0	0	1	0	0	0	0
Maraarun	0	0	0	0	1	1	0	0	0	1	1	1	1	0	1	1	1	0	1	0	0	0	0	0	0	0	0	0	0	0	0	0	0	1	0	0	0	0	0	1	1	0	0	0
Micoarge	0	0	0	0	0	0	1	0	0	0	0	0	0	0	0	0	0	0	0	0	0	0	0	0	0	0	0	0	0	0	0	0	0	0	0	0	0	0	0	0	0	0	0	0
Mimoalbi	0	0	0	0	0	0	0	1	0	1	0	1	0	1	0	0	0	1	0	1	1	0	0	0	0	1	1	0	0	1	1	0	0	1	0	0	0	0	0	0	0	1	0	
Oecemacu	1	1	1	1	0	0	1	0	0	0	0	0	0	0	0	0	0	0	0	0	0	0	0	0	0	0	0	0	0	0	0	0	0	1	0	0	0	0	0	1	1	0	0	
Opliburm	0	0	0	0	1	0	0	0	1	1	1	0	0	0	0	0	0	0	0	0	0	0	0	0	0	0	0	0	0	0	0	0	0	0	0	0	1	0	1	1	0	0	0	
Petialli	0	0	0	0	0	0	1	0	0	0	0	0	0	0	0	0	0	0	0	0	0	0	0	0	0	0	0	0	0	0	0	0	0	0	0	0	1	0	0	0	0	0	0	
Philjacq	0	1	0	0	0	0	0	0	0	0	0	0	0	0	0	0	1	0	0	0	0	0	0	0	0	0	0	0	0	0	0	0	0	0	0	0	0	0	0	0	0	0	0	
Pisomacr	0	0	1	0	0	0	0	0	0	0	0	0	0	0	0	0	0	0	0	0	0	0	0	0	0	0	0	0	0	0	0	0	0	1	0	0	0	0	0	0	0	0	0	
Plumrubr	1	0	0	0	0	0	0	0	0	1	0	0	0	0	1	0	0	0	0	0	0	0	0	0	0	0	0	0	0	0	0	0	0	0	1	0	0	0	0	0	0	1	1	
Rauvtetr	0	0	1	0	0	1	1	1	0	0	1	0	0	0	0	0	0	0	0	0	0	0	0	0	0	0	0	0	0	0	0	1	0	0	0	0	0	0	0	1	0	0	0	
Ruelblec	0	0	1	0	1	0	0	1	1	0	1	0	0	0	0	0	0	0	0	0	0	0	0	0	0	0	0	0	0	0	0	0	0	0	0	0	0	0	0	0	0	0	0	
Ruelinun	0	0	0	0	0	0	0	0	0	0	0	0	0	0	0	0	0	0	0	0	0	0	0	0	0	0	0	0	0	0	0	0	0	1	1	0	1	0	1	0	0	0	0	
Russsarm	0	0	1	1	0	0	0	0	0	0	0	0	0	0	0	0	0	0	0	0	0	0	0	0	0	0	0	0	0	0	0	0	0	1	1	0	0	0	0	0	0	0	0	
Selagnll	0	0	0	0	0	0	0	0	0	0	0	0	0	0	0	0	0	0	0	0	0	0	0	0	0	0	0	0	0	0	0	0	0	0	0	0	1	0	0	0	0	0	0	
Sennpall	0	0	1	1	0	1	1	1	1	0	1	0	0	0	0	0	0	0	0	0	0	0	0	0	0	0	1	0	0	1	0	1	0	1	0	0	0	0	1	0	0	1	0	
Serjgros	1	0	1	1	0	1	0	1	1	0	1	1	0	0	0	0	0	0	0	0	0	0	0	0	0	0	0	0	0	1	0	0	0	1	1	1	0	0	0	0	0	1	0	
Sidarhom	0	0	0	0	0	0	0	1	1	0	0	0	1	0	0	0	0	0	0	0	0	0	0	0	0	0	0	0	1	0	0	0	0	0	0	0	0	0	0	0	0	0	0	
Sidaspin	0	1	0	0	0	0	0	0	0	0	0	0	0	0	0	0	0	0	0	0	0	0	0	0	0	0	0	0	0	0	0	0	0	0	0	0	0	0	0	0	0	0	0	
Smilspin	0	1	1	0	0	0	1	0	1	1	1	1	1	0	0	0	1	0	0	0	0	0	0	0	0	0	0	0	0	0	0	0	0	0	0	0	0	0	0	1	0	0	0	
Stemmadn	0	1	0	0	1	0	1	0	0	1	0	0	0	0	0	1	0	0	0	0	0	0	0	0	0	0	0	0	0	0	0	0	0	1	0	0	0	0	0	0	0	0	0	
Tecostan	1	0	1	0	1	0	0	0	0	0	0	0	0	0	0	0	0	0	0	0	0	0	0	0	0	0	0	0	0	0	0	0	0	0	0	0	0	0	0	0	0	0	0	
Thevetia	0	0	0	1	1	1	0	0	0	0	0	0	0	0	0	0	0	0	0	0	0	0	0	0	0	0	0	0	0	0	0	0	0	1	1	0	0	0	0	0	1	0	1	
Trichava	0	0	0	0	0	0	1	0	0	1	0	0	0	0	0	1	0	0	0	0	0	0	0	0	0	0	0	0	0	0	0	0	0	0	0	0	0	0	0	1	0	0	0	

Continued on next page

Table B.6: May 2014 presence absence species data.

	M1	M2	M3	M4	M5	M6	M7	M8	M9	M10	M11	M12	M13	M14	M15	M16	M17	M18	M19	M20	M21	M22	M23	M24	M25	M26	M27	M28	M29	M30	M31	M32	M33	CE1	CE2	CE3	CE4	CE5	CE6	CO1	CO2	CO3	CO4	CO5
Trigrugo	0	0	0	0	0	0	0	0	0	0	0	0	0	0	0	0	0	0	0	0	0	0	0	0	0	0	0	0	0	0	0	0	0	0	0	1	0	0	0	0	0	0	0	0
Tropmori	0	0	0	0	0	0	1	0	0	0	0	0	0	0	0	0	0	0	0	0	0	0	0	0	0	0	0	0	0	0	0	0	0	0	0	0	0	0	0	0	0	0	0	0
Turnscab	0	0	0	0	0	0	1	0	0	0	0	0	0	0	0	0	0	0	0	0	0	0	0	0	0	0	0	0	0	0	0	0	0	0	0	0	0	0	0	0	0	0	0	0
Urerbacc	0	0	1	0	0	0	1	0	0	0	0	0	0	0	0	0	0	0	0	0	0	0	0	0	0	0	0	0	0	0	0	0	0	0	0	0	0	0	0	0	0	0	0	0
Verbovat	0	1	0	0	0	0	0	0	0	0	0	0	0	0	0	0	0	0	0	0	0	0	0	0	0	0	0	0	0	0	0	0	0	0	0	0	1	0	0	0	0	0	0	0
Waltindi	0	0	0	0	0	0	0	0	0	0	0	0	0	0	0	0	0	0	0	0	0	0	0	0	0	0	0	0	1	0	0	0	0	0	0	0	0	0	0	1	0	0	0	0
Xantwend	0	0	0	0	0	0	1	0	0	0	0	0	0	0	0	1	1	0	0	0	0	0	0	0	0	0	0	0	0	0	0	0	0	0	0	0	0	0	0	0	0	0	0	0

Table B.7: May 2014 Braun-Blanquet cover species data.

	M1	M2	M3	M4	M5	M6	M7	M8	M9	M10	M11	M12	M13	M14	M15	M16	M17	M18	M19	M20	M21	M22	M23	M24	M25	M26	M27	M28	M29	M30	M31	M32	M33	CE1	CE2	CE3	CE4	CE5	CE6	CO1	CO2	CO3	CO4	CO5
Acalypha	2	0	0	0	0	0	0	0	0	0	0	0	0	0	0	0	0	0	0	0	0	0	0	0	0	0	0	0	0	0	0	0	0	0	0	0	2	2	2	0	0	0	0	0
Acantetr	2	0	0	0	0	0	0	0	0	0	0	3	0	0	2	2	2	0	0	0	0	0	0	0	0	0	0	0	0	0	0	0	0	0	0	0	0	2	0	0	1	2	0	0
Agercony	0	0	0	0	0	0	0	0	0	0	0	0	0	0	0	0	0	0	0	0	0	0	0	0	0	2	1	2	0	2	2	0	2	0	0	0	0	0	0	0	0	0	0	0
Amphpani	0	0	0	0	0	0	0	0	0	0	0	0	0	0	0	0	0	0	5	0	0	0	0	0	0	0	0	0	0	0	5	3	6	0	0	0	0	0	0	0	0	0	0	0
Pthcctnm	2	0	2	0	2	3	2	0	0	0	0	0	0	0	0	0	0	0	0	0	0	0	0	0	0	0	0	0	0	0	0	0	0	0	2	2	2	2	2	0	0	0	0	0
Aphescab	0	2	0	0	0	0	0	0	0	0	0	0	0	0	0	0	0	0	0	0	0	0	0	0	0	0	0	0	0	0	0	0	0	0	0	0	0	0	0	0	0	0	0	0
Bidepilo	0	0	0	0	0	0	0	0	0	0	0	2	0	0	0	0	0	0	0	0	0	0	0	0	0	0	0	0	0	0	0	0	0	2	2	0	0	0	2	0	0	0	2	3
Blepmucr	0	0	0	1	2	1	0	2	0	2	2	2	2	0	0	0	0	0	0	0	0	0	0	0	0	0	0	0	0	0	0	0	0	2	0	0	0	2	0	1	2	0	1	1
Bromping	4	2	0	3	0	0	0	0	2	3	0	4	2	0	2	3	2	0	0	0	0	0	4	0	0	3	0	0	0	6	0	0	0	4	4	4	3	0	3	0	0	0	0	0
Burssima	0	0	0	0	0	0	0	0	0	0	0	0	0	0	0	0	0	0	0	0	0	0	0	0	0	0	0	0	0	0	0	0	0	0	3	2	0	0	0	0	0	0	0	0
Byrscras	0	0	0	0	0	0	0	0	0	0	0	0	0	3	0	1	0	0	0	0	0	0	0	0	0	0	0	0	0	0	0	0	0	0	0	0	0	0	1	0	0	0	0	0
Byttacul	2	0	2	0	0	2	0	0	0	0	0	0	0	0	0	0	1	0	0	0	0	0	0	0	0	0	0	0	0	0	0	0	0	0	0	0	0	0	0	2	0	0	0	0
Casecory	0	0	2	0	0	0	0	0	0	0	2	0	0	0	0	0	0	0	0	0	0	0	0	0	0	0	0	0	0	0	0	0	0	2	0	0	2	3	0	0	0	2	0	0
Cenchrus	0	0	0	0	0	0	0	0	0	0	0	0	0	0	3	2	0	0	4	0	3	3	3	2	6	5	4	5	2	3	0	0	0	0	0	0	0	0	0	0	0	0	5	0
Cissmicr	0	0	0	3	0	0	0	2	2	0	2	2	2	0	0	0	0	0	3	0	0	0	0	0	0	0	0	0	0	0	0	0	0	0	0	0	0	0	0	0	0	0	0	0
Cissvert	0	2	2	3	2	0	2	0	2	2	3	2	0	2	0	1	5	0	3	0	0	0	1	0	0	2	3	0	0	3	2	3	3	0	0	0	0	0	2	2	0	0	0	0
Cleovisc	1	0	0	1	2	1	0	0	2	0	0	2	1	0	0	0	1	0	0	0	0	0	0	0	0	0	0	0	2	2	2	2	2	0	0	0	0	0	0	0	0	1	0	1
Cochviti	0	0	0	0	0	0	0	0	0	1	0	0	0	0	0	0	0	0	0	0	0	0	0	0	0	0	0	0	0	0	0	0	0	0	3	0	2	0	0	0	0	0	2	2
Dalescan	0	0	2	0	0	1	2	2	2	0	3	2	0	0	2	0	0	0	0	0	0	0	0	0	0	0	0	0	2	2	2	2	2	0	0	0	0	0	2	2	2	2	0	1
Diodia	0	0	0	0	0	0	0	0	0	0	0	0	0	0	2	0	0	1	0	2	0	0	2	0	0	2	2	3	2	2	0	0	0	0	0	0	0	0	0	0	0	0	0	0
Euphcoll	0	0	0	4	2	3	0	0	0	0	0	0	2	3	0	3	1	4	0	0	0	0	0	0	0	0	0	0	0	0	0	0	0	2	0	0	0	0	3	0	0	3	0	0
Fabaflow	0	0	0	0	0	0	0	0	0	0	0	0	0	0	0	0	0	0	0	0	0	0	0	0	0	0	0	0	0	2	0	0	0	0	0	0	0	0	0	2	0	0	0	0
Fabapod	0	0	0	0	0	0	0	0	0	2	0	0	0	0	0	0	0	0	0	0	0	0	0	0	0	0	0	0	0	0	0	0	0	0	0	0	2	2	0	0	0	0	0	0
Glirsepi	0	0	0	0	0	0	0	0	0	0	0	0	0	1	0	0	0	0	0	0	0	0	0	0	0	0	0	0	0	0	0	0	0	3	0	3	0	0	4	0	0	0	0	0
Ipomoea	1	0	2	2	0	0	2	0	0	0	0	0	0	0	0	0	0	0	0	0	0	0	0	0	0	0	0	0	0	0	0	0	0	0	0	0	2	0	2	0	1	1	0	0
Irescale	0	0	1	0	0	1	0	0	2	0	0	2	0	0	0	0	0	0	2	0	0	0	0	0	0	0	0	0	2	3	0	2	0	2	0	0	0	0	0	0	2	3	0	0
Jatrcurc	0	0	0	0	0	0	0	0	0	0	0	0	0	0	0	0	0	0	0	0	0	0	0	0	0	0	0	0	0	0	0	0	0	0	0	0	2	0	0	0	0	0	0	0
Justcart	0	0	0	0	2	2	2	2	0	0	0	0	0	0	0	0	0	0	1	0	0	0	0	0	0	0	0	0	2	2	2	2	0	0	0	0	0	2	0	2	0	2	0	0

Continued on next page

Table B.7: May 2014 Braun-Blanquet cover species data.

	M1	M2	M3	M4	M5	M6	M7	M8	M9	M10	M11	M12	M13	M14	M15	M16	M17	M18	M19	M20	M21	M22	M23	M24	M25	M26	M27	M28	M29	M30	M31	M32	M33	CE1	CE2	CE3	CE4	CE5	CE6	CO1	CO2	CO3	CO4	CO5
Kallstrm	0	0	0	0	0	0	0	2	0	0	0	0	0	0	0	0	0	0	0	0	0	0	0	0	0	0	0	0	0	0	0	0	0	0	0	0	0	0	0	0	0	0	0	0
Lanturti	0	0	0	0	2	0	0	2	2	0	0	2	0	0	0	0	0	0	0	0	0	0	0	0	0	0	0	0	0	0	0	0	0	0	0	0	0	0	0	0	0	0	0	0
Lasirusc	2	2	0	2	0	0	0	0	0	0	0	0	0	0	0	0	0	0	0	0	0	0	0	0	0	0	0	0	0	0	0	0	0	2	0	2	0	0	2	0	0	2	0	0
Loncmini	0	0	0	0	0	0	0	0	0	0	0	3	0	0	0	0	0	0	0	0	0	0	0	0	0	0	0	0	0	0	0	0	0	0	0	0	0	0	0	0	0	0	0	0
Malvconn	2	2	2	0	0	0	2	0	0	0	0	0	0	0	0	0	2	0	0	0	0	0	0	0	0	0	0	0	0	0	0	0	0	0	0	0	0	0	0	0	1	0	0	0
Maraarun	0	0	0	0	2	1	0	0	0	2	2	2	2	0	1	2	2	0	1	0	0	0	0	0	0	0	0	0	0	0	0	0	0	0	2	0	0	0	0	0	2	2	0	0
Micoarge	0	0	0	0	0	0	2	0	0	0	0	0	0	0	0	0	0	0	0	0	0	0	0	0	0	0	0	0	0	0	0	0	0	0	0	0	0	0	0	0	0	0	0	0
Mimoalbi	0	0	0	0	0	0	0	2	0	2	0	1	0	3	0	0	0	2	0	2	2	0	0	0	0	1	2	0	0	2	2	0	0	0	3	0	0	0	0	0	0	0	3	0
Oecemacu	1	2	1	1	0	0	2	0	0	0	0	0	0	0	0	0	0	0	0	0	0	0	0	0	0	0	0	0	0	0	0	0	0	0	2	0	0	0	0	0	1	1	0	0
Opliburm	0	0	0	0	2	0	0	0	2	2	2	0	0	0	0	0	0	0	0	0	0	0	0	0	0	0	0	0	0	0	0	0	0	0	0	0	2	0	1	1	0	0	0	0
Petialli	0	0	0	0	0	0	2	0	0	0	0	0	0	0	0	0	0	0	0	0	0	0	0	0	0	0	0	0	0	0	0	0	0	0	0	0	2	0	0	0	0	0	0	0
Philjacq	0	2	0	0	0	0	0	0	0	0	0	0	0	0	0	0	2	0	0	0	0	0	0	0	0	0	0	0	0	0	0	0	0	0	0	0	0	0	0	0	0	0	0	0
Pisomacr	0	0	3	0	0	0	0	0	0	0	0	0	0	0	0	0	0	0	0	0	0	0	0	0	0	0	0	0	0	0	0	0	0	4	0	0	0	0	0	0	0	0	0	0
Plumrubr	1	0	0	0	0	0	0	0	0	2	0	0	0	0	1	0	0	0	0	0	0	0	0	0	0	0	0	0	0	0	0	0	0	0	3	0	0	0	0	0	0	2	2
Rauvtetr	0	0	2	0	0	2	2	2	0	0	3	0	0	0	0	0	0	0	0	0	0	0	0	0	0	0	0	0	0	0	0	3	0	0	0	0	0	0	0	0	2	0	0	0
Ruelblec	0	0	1	0	2	0	0	2	2	0	2	0	0	0	0	0	0	0	0	0	0	0	0	0	0	0	0	0	0	0	0	0	0	0	0	0	0	0	0	0	0	0	0	0
Ruelinun	0	0	0	0	0	0	0	0	0	0	0	0	0	0	0	0	0	0	0	0	0	0	0	0	0	0	0	0	0	0	0	0	0	2	2	0	2	0	2	0	0	0	0	0
Russsarm	0	0	2	1	0	0	0	0	0	0	0	0	0	0	0	0	0	0	0	0	0	0	0	0	0	0	0	0	0	0	0	0	0	2	2	0	0	0	0	0	0	0	0	0
Selagnll	0	0	0	0	0	0	0	0	0	0	0	0	0	0	0	0	0	0	0	0	0	0	0	0	0	0	0	0	0	0	0	0	0	0	0	0	1	0	0	0	0	0	0	0
Sennpall	0	0	2	1	0	3	2	3	2	0	3	0	0	0	0	0	0	0	0	0	0	0	0	0	0	0	2	0	0	2	0	2	0	2	0	0	0	0	2	0	0	2	0	0
Serjgros	1	0	2	2	0	2	0	2	2	0	2	2	0	0	0	0	0	0	0	0	0	0	0	0	0	0	0	0	0	3	0	0	0	2	2	5	0	0	0	0	0	2	0	0
Sidarhom	0	0	0	0	0	0	0	2	2	0	0	0	1	0	0	0	0	0	0	0	0	0	0	0	0	0	0	0	2	0	0	0	0	0	0	0	0	0	0	0	0	0	0	0
Sidaspin	0	2	0	0	0	0	0	0	0	0	0	0	0	0	0	0	0	0	0	0	0	0	0	0	0	0	0	0	0	0	0	0	0	0	0	0	0	0	0	0	0	0	0	0
Smilspin	0	2	1	0	0	0	2	0	2	2	3	2	2	0	0	0	2	0	0	0	0	0	0	0	0	0	0	0	0	0	0	0	0	0	0	0	0	0	0	0	1	0	0	0
Stemmadn	0	3	0	0	2	0	3	0	0	3	0	0	0	0	0	3	0	0	0	0	0	0	0	0	0	0	0	0	0	0	0	0	0	2	0	0	0	0	0	0	0	0	0	0
Tecostan	6	0	3	0	4	0	0	0	0	0	0	0	0	0	0	0	0	0	0	0	0	0	0	0	0	0	0	0	0	0	0	0	0	0	0	0	0	0	0	0	0	0	0	0
Thevetia	0	0	0	4	2	3	0	0	0	0	0	0	0	0	0	0	0	0	0	0	0	0	0	0	0	0	0	0	0	0	0	0	0	1	2	0	0	0	0	0	0	2	0	1
Trichava	0	0	0	0	0	0	6	0	0	3	0	0	0	0	0	2	0	0	0	0	0	0	0	0	0	0	0	0	0	0	0	0	0	0	0	0	0	0	0	0	5	0	0	0

Continued on next page

Table B.7: May 2014 Braun-Blanquet cover species data.

	M1	M2	M3	M4	M5	M6	M7	M8	M9	M10	M11	M12	M13	M14	M15	M16	M17	M18	M19	M20	M21	M22	M23	M24	M25	M26	M27	M28	M29	M30	M31	M32	M33	CE1	CE2	CE3	CE4	CE5	CE6	CO1	CO2	CO3	CO4	CO5
Trigrugo	0	0	0	0	0	0	0	0	0	0	0	0	0	0	0	0	1	0	0	0	0	0	0	0	0	0	0	0	0	0	0	0	0	0	0	0	0	0	0	0	0	0	0	0
Tropmori	0	0	0	0	0	0	2	0	0	0	0	0	0	0	0	0	0	0	0	0	0	0	0	0	0	0	0	0	0	0	0	0	0	0	0	0	0	0	0	0	0	0	0	0
Turnscab	0	0	0	0	0	0	0	0	0	0	0	0	0	0	0	0	0	0	0	0	0	0	0	0	0	0	0	0	2	2	2	2	2	0	0	0	0	0	0	0	0	0	0	0
Urerbacc	0	0	3	0	0	0	2	0	0	0	0	0	0	0	0	0	0	0	0	0	0	0	0	0	0	0	0	0	0	0	0	0	0	0	0	0	0	3	0	0	0	0	0	0
Verbovat	0	2	0	0	0	0	0	0	0	0	0	0	0	0	0	0	0	0	0	0	0	0	0	0	0	0	0	0	0	0	0	0	0	0	0	0	2	0	0	0	0	0	0	0
Waltindi	0	0	0	0	0	0	0	0	0	0	0	0	0	0	0	0	0	0	0	0	0	0	0	0	0	0	0	0	2	0	0	0	0	0	0	0	0	0	0	1	0	0	0	0
Xantwend	0	0	0	0	0	0	3	0	0	0	0	0	0	0	0	2	1	0	0	0	0	0	0	0	0	0	0	0	0	0	0	0	0	0	0	0	0	0	0	0	0	0	0	0

Table B.8

Table B.8: May 2014 maximum plant height species data.

	M1	M2	M3	M4	M5	M6	M7	M8	M9	M10	M11	M12	M13	M14	M15	M16	M17	M18	M19	M20	M21	M22	M23	M24	M25	M26	M27	M28	M29	M30	M31	M32	M33	CE1	CE2	CE3	CE4	CE5	CE6	CO1	CO2	CO3	CO4	CO5
Acalypha	3	0	0	0	0	0	0	0	0	0	0	0	0	0	0	0	0	0	0	0	0	0	0	0	0	0	0	0	0	0	0	0	0	0	0	0	4	4	4	0	0	0	0	0
Acantetr	4	0	0	0	0	0	0	0	0	0	0	6	0	0	4	6	6	0	0	0	0	0	0	0	0	0	6	0	0	0	0	0	0	0	0	0	0	2	0	0	3	2	0	0
Agercony	0	0	0	0	0	0	0	0	0	0	0	0	0	0	0	0	0	0	0	0	0	0	0	0	0	2	1	2	0	2	3	0	3	0	0	0	0	0	0	0	0	0	0	0
Amphpani	0	0	0	0	0	0	0	0	0	0	0	0	0	0	0	0	0	0	5	0	0	0	0	0	0	0	0	0	0	0	5	4	5	0	0	0	0	0	0	0	0	0	0	0
Pthcctnm	1	0	6	0	4	6	5	0	0	0	0	0	0	0	0	0	0	0	0	0	0	0	0	0	0	0	0	0	0	0	0	0	0	2	3	6	5	5	0	0	0	0	0	0
Aphescab	0	6	0	0	0	0	0	0	0	0	0	0	0	0	0	0	0	0	0	0	0	0	0	0	0	0	0	0	0	0	0	0	0	0	0	0	0	0	0	0	0	0	0	0
Bidepilo	0	0	0	0	0	0	0	0	0	0	0	5	0	0	0	0	0	0	0	0	0	0	0	0	0	0	0	0	0	0	0	0	0	0	0	0	0	4	0	0	0	4	6
Blepmucr	0	0	0	2	2	3	0	4	0	3	2	6	6	0	0	0	0	0	0	0	0	0	0	0	0	0	0	0	0	0	0	0	0	2	2	0	0	0	6	0	3	3	0	3
Bromping	5	5	0	5	0	0	0	0	5	5	0	5	5	0	4	5	5	0	0	0	0	0	4	0	0	5	0	0	0	5	0	0	0	5	5	5	5	0	5	0	0	0	0	0
Burssima	0	0	0	0	0	0	0	0	0	0	0	0	0	0	0	0	0	0	0	0	0	0	0	0	0	0	0	0	0	0	0	0	0	0	4	6	0	0	0	0	0	0	0	0
Byrscras	0	0	0	0	0	0	0	0	0	6	0	0	6	6	0	1	0	0	0	0	0	0	0	0	0	0	0	0	0	0	0	0	0	0	0	0	0	0	0	0	2	0	0	0
Byttacul	4	0	2	0	0	3	0	0	0	0	0	0	0	0	0	0	2	0	0	0	0	0	0	0	0	0	0	0	0	0	0	0	0	0	0	0	0	0	6	0	0	6	0	0
Casecory	0	0	1	0	0	0	0	0	0	0	2	0	0	0	0	0	0	0	0	0	0	0	0	0	0	0	0	0	0	0	0	0	0	3	0	0	5	6	0	0	0	3	0	0
Cenchrus	0	0	0	0	0	0	0	0	0	0	0	0	0	4	2	0	0	4	0	3	3	3	4	2	4	5	4	4	4	5	0	0	0	0	0	0	0	0	0	0	0	0	4	0
Cissmicr	0	0	0	6	0	0	0	5	5	0	4	6	6	0	0	0	0	0	4	0	0	0	0	0	0	0	0	0	0	0	0	0	0	0	0	0	0	0	0	0	0	0	0	0
Cissvert	0	1	6	6	4	0	2	0	5	4	5	6	0	2	0	2	6	0	4	0	0	0	2	0	0	4	4	0	0	5	4	5	4	0	0	0	0	0	5	4	0	0	0	0
Cleovisc	1	0	0	3	2	1	0	0	2	0	0	3	3	0	0	0	4	0	0	0	0	0	0	0	0	0	0	0	0	0	4	2	3	0	0	0	0	0	0	0	0	4	0	3
Cochviti	0	0	0	0	0	0	0	0	0	2	0	0	0	0	0	0	0	0	0	0	0	0	0	0	0	0	0	0	0	0	0	0	0	0	6	0	2	0	0	0	0	0	2	5
Dalescan	0	0	6	0	0	2	2	2	5	0	5	2	0	0	4	0	0	0	4	0	0	0	0	0	0	0	0	0	1	5	4	5	4	0	0	0	0	0	3	3	5	5	0	3
Diodia	0	0	0	0	0	0	0	0	0	0	0	0	0	0	1	0	0	1	0	1	0	1	0	0	1	0	2	1	1	1	2	0	0	0	0	0	0	0	0	0	0	0	0	0
Euphcoll	0	0	0	6	4	6	0	0	0	0	0	6	6	0	6	3	6	0	0	0	0	0	0	0	0	0	0	0	0	0	0	0	0	5	0	0	0	0	4	0	0	6	0	0
Fabaflow	0	0	0	0	0	0	0	0	0	0	0	0	0	0	0	0	0	0	0	0	0	0	0	0	0	0	0	0	0	0	4	0	0	0	0	0	0	0	0	3	0	0	0	0
Fabapod	0	0	0	0	0	0	0	0	0	1	0	0	0	0	0	0	0	0	0	0	0	0	0	0	0	0	0	0	0	0	0	0	0	0	0	0	0	1	6	0	0	0	0	0
Glirsepi	0	0	0	0	0	0	0	0	0	0	0	0	2	0	0	0	0	0	0	0	0	0	0	0	0	0	0	0	0	0	0	0	0	6	0	6	0	0	6	0	0	0	0	0
Ipomoea	1	0	4	5	0	0	2	0	0	0	0	0	0	0	0	0	0	0	0	0	0	0	0	0	0	0	0	0	0	0	0	0	0	0	0	0	5	0	6	0	1	1	0	0
Irescale	0	0	1	0	0	1	0	0	4	0	3	5	0	0	0	0	0	0	4	0	0	0	0	0	0	0	0	0	0	0	3	5	0	5	0	0	0	0	0	0	3	6	0	0

Continued on next page

Table B.8: May 2014 maximum plant height species data.

	M1	M2	M3	M4	M5	M6	M7	M8	M9	M10	M11	M12	M13	M14	M15	M16	M17	M18	M19	M20	M21	M22	M23	M24	M25	M26	M27	M28	M29	M30	M31	M32	M33	CE1	CE2	CE3	CE4	CE5	CE6	CO1	CO2	CO3	CO4	CO5
Jatrcurc	0	0	0	0	0	0	0	0	0	0	0	0	0	0	0	0	0	0	0	0	0	0	0	0	0	0	0	0	0	0	0	0	0	0	0	0	4	0	0	0	0	0	0	0
Justcart	0	0	0	0	2	3	2	1	0	0	0	0	0	0	0	0	0	0	1	0	0	0	0	0	0	0	0	0	0	0	2	3	2	0	0	0	0	1	0	3	0	3	0	0
Kallstrm	0	0	0	0	0	0	0	1	0	0	0	0	0	0	0	0	0	0	0	0	0	0	0	0	0	0	0	0	0	0	0	0	0	0	0	0	0	0	0	0	0	0	0	0
Lanturti	0	0	0	0	5	0	0	2	5	0	0	4	0	0	0	0	0	0	0	0	0	0	0	0	0	0	0	0	0	0	0	0	0	0	0	0	0	0	0	0	0	0	0	0
Lasirusc	3	4	0	5	0	0	0	0	0	0	0	0	0	0	0	0	0	0	0	0	0	0	0	0	0	0	0	0	0	0	0	0	0	5	0	5	0	0	5	0	0	5	0	0
Loncmini	0	0	0	0	0	0	0	0	0	0	0	6	0	0	0	0	0	0	0	0	0	0	0	0	0	0	0	0	0	0	0	0	0	0	0	0	0	0	0	0	0	0	0	0
Malvconn	3	2	3	0	0	0	4	0	0	0	0	0	0	0	0	0	3	0	0	0	0	0	0	0	0	0	0	0	0	0	0	0	0	0	0	0	0	0	0	0	3	0	0	0
Maraarun	0	0	0	0	1	2	0	0	0	2	2	3	3	0	2	3	1	0	4	0	0	0	0	0	0	0	0	0	0	0	0	0	0	2	0	0	0	0	0	2	3	0	0	0
Micoarge	0	0	0	0	0	0	3	0	0	0	0	0	0	0	0	0	0	0	0	0	0	0	0	0	0	0	0	0	0	0	0	0	0	0	0	0	0	0	0	0	0	0	0	0
Mimoalbi	0	0	0	0	0	0	0	5	0	3	0	4	0	4	0	0	0	1	0	2	2	0	0	0	0	1	4	0	0	4	4	0	0	0	5	0	0	0	0	0	0	0	5	0
Oecemacu	2	1	1	1	0	0	1	0	0	0	0	0	0	0	0	0	0	0	0	0	0	0	0	0	0	0	0	0	0	0	0	0	0	0	1	0	0	0	0	0	1	2	0	0
Opliburm	0	0	0	0	2	0	0	0	1	1	1	0	0	0	0	0	0	0	0	0	0	0	0	0	0	0	0	0	0	0	0	0	0	0	0	0	0	2	0	2	2	0	0	0
Petialli	0	0	0	0	0	0	2	0	0	0	0	0	0	0	0	0	0	0	0	0	0	0	0	0	0	0	0	0	0	0	0	0	0	0	0	0	0	2	0	0	0	0	0	0
Philjacq	0	5	0	0	0	0	0	0	0	0	0	0	0	0	0	0	2	0	0	0	0	0	0	0	0	0	0	0	0	0	0	0	0	0	0	0	0	0	0	0	0	0	0	0
Pisomacr	0	0	6	0	0	0	0	0	0	0	0	0	0	0	0	0	0	0	0	0	0	0	0	0	0	0	0	0	0	0	0	0	0	6	0	0	0	0	0	0	0	0	0	0
Plumrubr	2	0	0	0	0	0	0	0	0	2	0	0	0	0	2	0	0	0	0	0	0	0	0	0	0	0	0	0	0	0	0	0	0	0	6	0	0	0	0	0	0	5	5
Rauvtetr	0	0	6	0	0	4	3	4	0	0	4	0	0	0	0	0	0	0	0	0	0	0	0	0	0	0	0	0	0	0	0	5	0	0	0	0	0	0	0	5	0	0	0
Ruelblec	0	0	1	0	2	0	0	1	2	0	3	0	0	0	0	0	0	0	0	0	0	0	0	0	0	0	0	0	0	0	0	0	0	0	0	0	0	0	0	0	0	0	0	0
Ruelinun	0	0	0	0	0	0	0	0	0	0	0	0	0	0	0	0	0	0	0	0	0	0	0	0	0	0	0	0	0	0	0	0	0	2	4	0	3	0	3	0	0	0	0	0
Russsarm	0	0	3	4	0	0	0	0	0	0	0	0	0	0	0	0	0	0	0	0	0	0	0	0	0	0	0	0	0	0	0	0	0	5	3	0	0	0	0	0	0	0	0	0
Selagnll	0	0	0	0	0	0	0	0	0	0	0	0	0	0	0	0	0	0	0	0	0	0	0	0	0	0	0	0	0	0	0	0	0	0	0	0	1	0	0	0	0	0	0	0
Sennpall	0	0	2	3	0	6	2	6	5	0	6	0	0	0	0	0	0	0	0	0	0	0	0	0	0	0	4	0	0	5	0	3	0	3	0	0	0	0	5	0	0	3	0	0
Serjgros	2	0	2	2	0	2	0	1	2	0	2	4	0	0	0	0	0	0	0	0	0	0	0	0	0	0	0	0	0	5	0	0	0	4	5	6	0	0	0	0	0	2	0	0
Sidarhom	0	0	0	0	0	0	0	1	1	0	0	0	1	0	0	0	0	0	0	0	0	0	0	0	0	0	0	0	2	0	0	0	0	0	0	0	0	0	0	0	0	0	0	0
Sidaspin	0	4	0	0	0	0	0	0	0	0	0	0	0	0	0	0	0	0	0	0	0	0	0	0	0	0	0	0	0	0	0	0	0	0	0	0	0	0	0	0	0	0	0	0
Smilspin	0	2	4	0	0	0	2	0	2	4	5	6	2	0	0	0	2	0	0	0	0	0	0	0	0	0	0	0	0	0	0	0	0	0	0	0	0	0	0	0	4	0	0	0
Stemmadn	0	6	0	0	4	0	6	0	0	6	0	0	0	0	0	5	0	0	0	0	0	0	0	0	0	0	0	0	0	0	0	0	0	6	0	0	0	0	0	0	0	0	0	0
Tecostan	6	0	6	0	6	0	0	0	0	0	0	0	0	0	0	0	0	0	0	0	0	0	0	0	0	0	0	0	0	0	0	0	0	0	0	0	0	0	0	0	0	0	0	0

Continued on next page

Table B.8: May 2014 maximum plant height species data.

	M1	M2	M3	M4	M5	M6	M7	M8	M9	M10	M11	M12	M13	M14	M15	M16	M17	M18	M19	M20	M21	M22	M23	M24	M25	M26	M27	M28	M29	M30	M31	M32	M33	CE1	CE2	CE3	CE4	CE5	CE6	CO1	CO2	CO3	CO4	CO5
Thevetia	0	0	0	6	4	6	0	0	0	0	0	0	0	0	0	0	0	0	0	0	0	0	0	0	0	0	0	0	0	0	0	0	0	4	3	0	0	0	0	0	0	4	0	3
Trichava	0	0	0	0	0	0	6	0	0	6	0	0	0	0	0	6	0	0	0	0	0	0	0	0	0	0	0	0	0	0	0	0	0	0	0	0	0	0	0	0	6	0	0	0
Trigrugo	0	0	0	0	0	0	0	0	0	0	0	0	0	0	0	0	0	0	0	0	0	0	0	0	0	0	0	0	0	0	0	0	0	0	0	0	0	0	0	0	0	0	0	0
Tropmori	0	0	0	0	0	0	2	0	0	0	0	0	0	0	0	0	0	0	0	0	0	0	0	0	0	0	0	0	0	0	0	0	0	0	0	0	0	0	0	0	0	0	0	0
Turnscab	0	0	0	0	0	0	0	0	0	0	0	0	0	0	0	0	0	0	0	0	0	0	0	0	0	0	0	0	1	1	2	1	1	0	0	0	0	0	0	0	0	0	0	0
Urerbacc	0	0	6	0	0	0	2	0	0	0	0	0	0	0	0	0	0	0	0	0	0	0	0	0	0	0	0	0	0	0	0	0	0	0	0	0	0	6	0	0	0	0	0	0
Verbovat	0	6	0	0	0	0	0	0	0	0	0	0	0	0	0	0	0	0	0	0	0	0	0	0	0	0	0	0	0	0	0	0	0	0	0	0	5	0	0	0	0	0	0	0
Waltindi	0	0	0	0	0	0	0	0	0	0	0	0	0	0	0	0	0	0	0	0	0	0	0	0	0	0	0	0	2	0	0	0	0	0	0	0	0	0	0	2	0	0	0	0
Xantwend	0	0	0	0	0	0	3	0	0	0	0	0	0	0	0	3	2	0	0	0	0	0	0	0	0	0	0	0	0	0	0	0	0	0	0	0	0	0	0	0	0	0	0	0

B.1.3 Environmental data

Table B.9: Environmental data along then transect. Distance= Distance along the transect in m from site 21, Bearing= Bearing from the volcano, Av. Exposure = Average exposure to the volcanic plume based on Gaussian fits to the SO_2 data (from February 2013, December 2013, February 2014, May 2014 and June 2014), Av. Litter = Average leaf litter layer depth in cm (from December 2013, February 2014 and May 2014), Av. Canopy= Average canopy openness (%) estimated from hemispherical photography (from December 2013, February 2014 and May 2014), May pH= Soil pH measured in May 2014 and May Cond= Soil conductivity (EC) measured in May 2014.

	Type	Lat	Long	Bearing	Distance	Av. Exposure	Av. Litter	Av. Canopy	May pH	May Cond
1	Forest	11.9733	-86.1749	209	-1088	0.42	4.33	48	5.03	192
2	Forest	11.9737	-86.1754	212	-1020	0.53	5.11	26	4.72	241
3	Forest	11.9738	-86.1769	217	-883	0.82	2.69	40	4.65	422
4	Forest	11.9741	-86.1780	221	-763	1.15	2.51	28	4.87	357
5	Forest	11.9749	-86.1794	227	-598	1.74	2.27	44	4.41	299
6	Forest	11.9749	-86.1794	228	-590	1.77	3.00	35	4.80	403
7	Forest	11.9750	-86.1797	228	-566	1.88	4.93	37	4.37	465
8	Open	11.9751	-86.1798	229	-549	1.95	1.60	64	4.68	253
9	Open	11.9753	-86.1802	230	-504	2.14	2.16	86	5.13	211
10	Forest	11.9756	-86.1799	231	-508	2.13	2.84	38	4.29	310
11	Open	11.9755	-86.1803	231	-479	2.25	2.13	77	4.73	315
12	Forest	11.9757	-86.1806	233	-440	2.43	3.02	44	4.33	225
13	Forest	11.9762	-86.1812	235	-360	2.80	3.49	58	4.24	228
14	Forest	11.9765	-86.1808	235	-371	2.75	2.16	65	4.02	444
15	Forest	11.9765	-86.1810	236	-347	2.86	1.44	89	3.97	218
16	Forest	11.9766	-86.1815	237	-305	3.06	3.87	45	4.23	410
17	Forest	11.9770	-86.1819	239	-248	3.32	2.36	9	4.73	349
18	Gas	11.9776	-86.1826	243	-144	3.76	0.38	79	4.18	223

Continued on next page

Table B.9: Environmental data along then transect. Distance= Distance along the transect in m from site 21, Bearing= Bearing from the volcano, Av. Exposure = Average exposure to the volcanic plume based on Gaussian fits to the SO_2 data (from February 2013, December 2013, February 2014, May 2014 and June 2014), Av. Litter = Average leaf litter layer depth in cm (from December 2013, February 2014 and May 2014), Av. Canopy= Average canopy openness (%) estimated from hemispherical photography (from December 2013, February 2014 and May 2014), May pH= Soil pH measured in May 2014 and May Cond= Soil conductivity (EC) measured in May 2014.

	Type	Lat	Long	Bearing	Distance	Av. Exposure	Av. Litter	Av. Canopy	May pH	May Cond
19	Gas	11.9778	-86.1832	244	-90	3.96	3.22	95	4.21	438
20	Gas	11.9785	-86.1835	247	-10	4.21	0.22	96	3.75	216
21	Gas	11.9786	-86.1836	247	0	4.24	0.22	98	4.00	129
22	Gas	11.9790	-86.1837	249	49	4.36	0.28	97	4.08	183
23	Gas	11.9794	-86.1842	250	112	4.48	0.96	97	4.01	253
24	Gas	11.9798	-86.1846	252	175	4.54	0.07	96	4.16	81
25	Gas	11.9804	-86.1844	254	222	4.56	0.29	96	4.00	262
26	Gas	11.9805	-86.1852	255	276	4.55	0.50	95	3.74	356
27	Gas	11.9811	-86.1852	257	326	4.51	0.60	94	4.15	419
28	Gas	11.9816	-86.1853	259	377	4.43	0.42	82	4.93	151
29	Gas	11.9819	-86.1851	260	400	4.39	0.48	96	4.28	189
30	Gas	11.9825	-86.1855	262	475	4.21	0.84	89	4.21	274
31	Agri	11.9833	-86.1859	265	578	3.89	0.80	96	4.55	333
32	Agri	11.9841	-86.1864	267	672	3.54	1.20	97	4.64	565
33	Agri	11.9845	-86.1872	269	758	3.19	1.67	95	4.60	519
CE1	Forest	11.9773	-86.1662	195	-1850	0.02	3.33	44	4.68	230
CE2	Forest	11.9757	-86.1664	191	-1849	0.02	3.33	44	4.75	284
CE3	Forest	11.9740	-86.1662	190	-1909	0.02	4.00	32	5.29	223
CE4	Forest	11.9716	-86.1689	182	-1736	0.03	2.33	33	4.79	299
CE5	Open	11.9731	-86.1715	195	-1413	0.13	1.33	35	4.95	168

Continued on next page

Table B.9: Environmental data along then transect. Distance= Distance along the transect in m from site 21, Bearing= Bearing from the volcano, Av. Exposure = Average exposure to the volcanic plume based on Gaussian fits to the SO_2 data (from February 2013, December 2013, February 2014, May 2014 and June 2014), Av. Litter = Average leaf litter layer depth in cm (from December 2013, February 2014 and May 2014), Av. Canopy= Average canopy openness (%) estimated from hemispherical photography (from December 2013, February 2014 and May 2014), May pH= Soil pH measured in May 2014 and May Cond= Soil conductivity (EC) measured in May 2014.

Type	Lat	Long	Bearing	Distance	Av. Exposure	Av. Litter	Av. Canopy	May pH	May Cond
CE6 Forest	11.9729	-86.1736	203	-1224	0.26	2.67	22	5.18	276
CO1 Agri	11.9856	-86.1882	272	916	2.53	1.00	97	4.15	601
CO2 Agri	11.9860	-86.1909	273	1125	1.71	3.67	73	4.36	385
CO3 Agri	11.9874	-86.1917	276	1299	1.15	1.67	45	4.28	291
CO4 Agri	11.9893	-86.1937	280	1592	0.51	1.67	96	4.41	181
CO5 Agri	11.9900	-86.1944	281	1700	0.36	1.00	45	4.48	238

B.2 Data Analysis

B.2.1 Ordination scores

Table B.10: Site scores from CCA for all seasons. D=December 2013, F= February 2014, M=May 2014 and CE and CO are sites where data were collected in May 2014 only.

	CCA1	CC2
D1	-1.09	0.10
D2	-1.44	-1.15
D3	-1.32	0.36
D4	-0.32	0.05
D5	-0.47	-0.04
D6	-0.44	0.55
D7	-0.85	-0.09
D8	0.21	0.85
D9	-0.17	1.08
D10	-0.32	-0.99
D11	-0.33	0.81
D12	0.06	-0.90
D13	0.11	-0.84
D14	1.04	-1.46
D15	0.56	-1.11
D16	-0.29	-1.84
D17	-0.28	-0.91
D18	2.00	-0.56
D19	0.64	1.57
D20	2.48	-2.28
D21	2.51	-2.83
D22	2.81	-1.74
D23	1.76	-1.21
D24	2.50	-2.43
D25	2.36	-1.01
D26	1.54	0.07
D27	1.57	-0.85
D28	1.72	0.17
D29	1.60	0.12
D30	1.26	0.24
D31	1.12	1.69
D32	0.63	2.72
D33	0.89	3.00
F1	-1.18	0.22
F2	-1.51	-1.33
F3	-1.06	0.66
F4	-0.66	0.12

Continued on next page

Table B.10: Site scores from CCA for all seasons. D=December 2013, F= February 2014, M=May 2014 and CE and CO are sites where data were collected in May 2014 only.

	CCA1	CC2
F5	-0.70	-0.10
F6	-0.44	1.20
F7	-0.88	0.03
F8	0.33	1.20
F9	-0.12	0.93
F10	-0.46	-1.31
F11	-0.24	1.24
F12	-0.03	-1.10
F13	-0.08	-0.97
F14	1.07	-1.75
F15	0.73	-1.16
F16	-0.25	-2.04
F17	-0.29	-1.20
F18	1.94	-1.19
F19	0.50	2.83
F20	2.58	-2.55
F21	2.61	-2.83
F22	2.61	-2.10
F23	1.10	-1.13
F24	2.61	-2.10
F25	2.78	-2.03
F26	1.74	-0.20
F27	1.68	-0.76
F28	1.50	0.50
F29	1.62	0.33
F30	1.04	0.03
F31	1.28	2.02
F32	0.70	2.53
F33	0.64	2.82
M1	-1.19	-0.08
M2	-1.46	-1.37
M3	-0.98	0.92
M4	-0.72	0.01
M5	-0.54	0.16
M6	-0.52	0.86
M7	-0.94	-0.06
M8	0.05	1.19
M9	-0.09	0.83
M10	-0.29	-1.29
M11	-0.29	0.84
M12	-0.08	-0.65
M13	-0.36	-0.90

Continued on next page

Table B.10: Site scores from CCA for all seasons. D=December 2013, F= February 2014, M=May 2014 and CE and CO are sites where data were collected in May 2014 only.

	CCA1	CC2
M14	1.22	-1.52
M15	0.59	-1.37
M16	-0.38	-1.82
M17	-0.62	-1.10
M18	2.39	-1.72
M19	0.35	1.73
M20	2.39	-1.72
M21	2.17	-1.86
M22	2.81	-1.74
M23	1.10	-1.13
M24	2.78	-2.03
M25	2.81	-1.74
M26	1.42	-0.63
M27	1.39	-0.35
M28	2.62	-0.50
M29	1.80	0.32
M30	1.16	0.34
M31	1.16	2.10
M32	0.41	2.63
M33	0.96	2.54
CE1	-1.04	-0.08
CE2	-1.03	-0.17
CE3	-1.43	0.07
CE4	-1.63	-0.21
CE5	-1.06	0.35
CE6	-1.01	-0.11
CO1	0.79	1.90
CO2	-0.66	-0.03
CO3	-0.70	0.44
CO4	0.40	-1.59
CO5	-0.56	-0.35

Table B.11: Species scores from CCA for all seasons.

	CCA1	CC2
Acalypha	-1.18	0.18
Acanthocereus tetragonus	0.04	-0.49
Ageratum conyzoides	1.24	0.55
Amphilophium paniculatum	0.78	1.71
Pithecoctenium	-0.95	0.16
Aphelandra scabra	-1.32	-0.32
Bidens pilosa	-0.63	-0.49
Blepharodon mucronatum	-0.32	-0.18
Bromelia pinguin	-0.03	-0.50
Bursera simaruba	-1.44	0.39
Byrsonima crassifolia	-0.03	-0.78
Byttneria aculeata	-0.91	0.18
Casearia corymbosa	-0.76	0.25
Cenchrus	1.53	-0.57
Cissus microcarpa	0.10	-0.09
Cissus verticillata	0.31	0.12
Cleome viscosa	-0.18	0.39
Cochlospermum vitifolium	-0.29	-0.20
Dalechampia scandens	0.24	0.46
Diodia	1.57	-0.40
Eleusine indica	1.10	-0.26
Euphorbia colletiades	-0.22	-0.59
Euphorbia herb	0.09	0.27
Fabaceae vine flower	0.94	1.56
Fabaceae vine pod	-0.43	-0.31
Ficus	-0.18	-0.75
Gliricidia sepium	-1.00	-0.15
Ipomoea	-0.64	0.15
Iresine calea	-0.02	0.81
Jatropha curcas	-1.13	0.20
Justicia carthaginensis	0.08	0.86
Kallstroemia	0.09	0.67
Lantana urticifolia	0.03	0.18
Lasiacis ruscifolia	-1.17	-0.03
Lonchocarpus minimiflorus	-0.05	-1.46
Malvaviscus connicus	-0.95	-0.14
Maranta arundinacea	-0.12	-0.48
Melinis repens	1.92	-1.33
Miconia argentea	-0.30	-0.61
Mimosa albida	0.87	-0.48
Oeceoclades maculata	-1.02	-0.04
Oplismenus burmannii	-0.13	0.32

Continued on next page

Table B.11: Species scores from CCA for all seasons.

	CCA1	CC2
Petiveria alliacea	-0.98	-0.23
Philodendron jacquinii	-0.67	-0.85
Physalis	0.70	2.77
Pisonia macranthocarpa	-1.03	0.55
Pityrogramma calomelanos	1.23	-0.79
Plumeria rubra	-0.38	-0.50
Rauvolfia tetraphylla	-0.21	0.81
Ruellia blechum	-0.24	0.59
Ruellia inundata	-1.29	-0.04
Russelia sarmentosa	-0.84	0.08
Selaginella	-1.34	-0.38
Senna pallida	-0.19	0.59
Serjania grosii	-0.34	0.30
Sida rhombifolia	0.20	0.28
Sida spinosa	-1.55	-0.97
Smilax spinosa	-0.38	-0.44
Spermacoce	0.81	0.12
Stemmadenia	-0.70	-0.65
Tecoma stans	-0.83	0.05
Thevetia	-0.61	-0.18
Trichillia havanensis	-0.49	-0.61
Trigonia rugosa	-1.03	0.48
Tropaeolum moritzianum	-1.05	-0.27
Turneara scabra	1.24	0.88
Urera baccifera	-0.97	0.16
Verbesina ovatifolia	-1.40	-0.41
Waltheria indica	1.17	-0.12
Xanthosoma wendlandii	-0.67	-0.60

B.2.2 May 2014 Ordination

CCA for the three different data types gave very similar results. Small differences were found in the significance of individual species and the exact positioning of the species sites and environmental variables. However, the same environmental gradients were recognized, and this supports the use of the simple presence absence data in Chapter 4.

B.2.2.1 Presence absence

Figure B.2: CCA for all species and sites using presence absence data from May 2014. Sites have been classified by their type using symbols and plant species have been classified by their type using colour. The size of a plant species point is determined by its overall abundance along the transect, with points being used instead of text for less abundant species. Environmental data are displayed in grey.

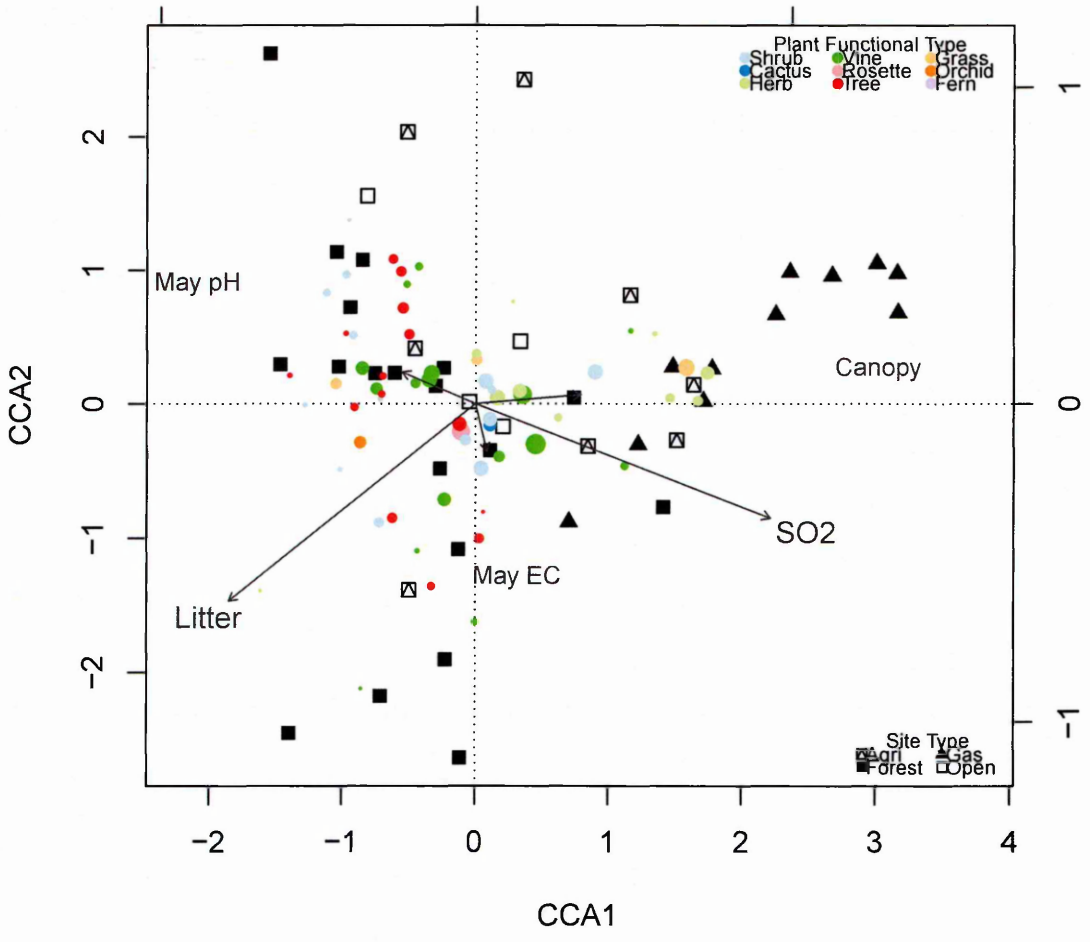

B.2.2.2 Braun-Blanquet classification

Figure B.3: CCA for all species and sites using Braun-Blaunquet cover data from May 2014. Sites have been classified by their type using symbols and plant species have been classified by their type using colour. The size of a plant species point is determined by its overall abundance along the transect, with points being used instead of text for less abundant species. Environmental data are displayed in grey.

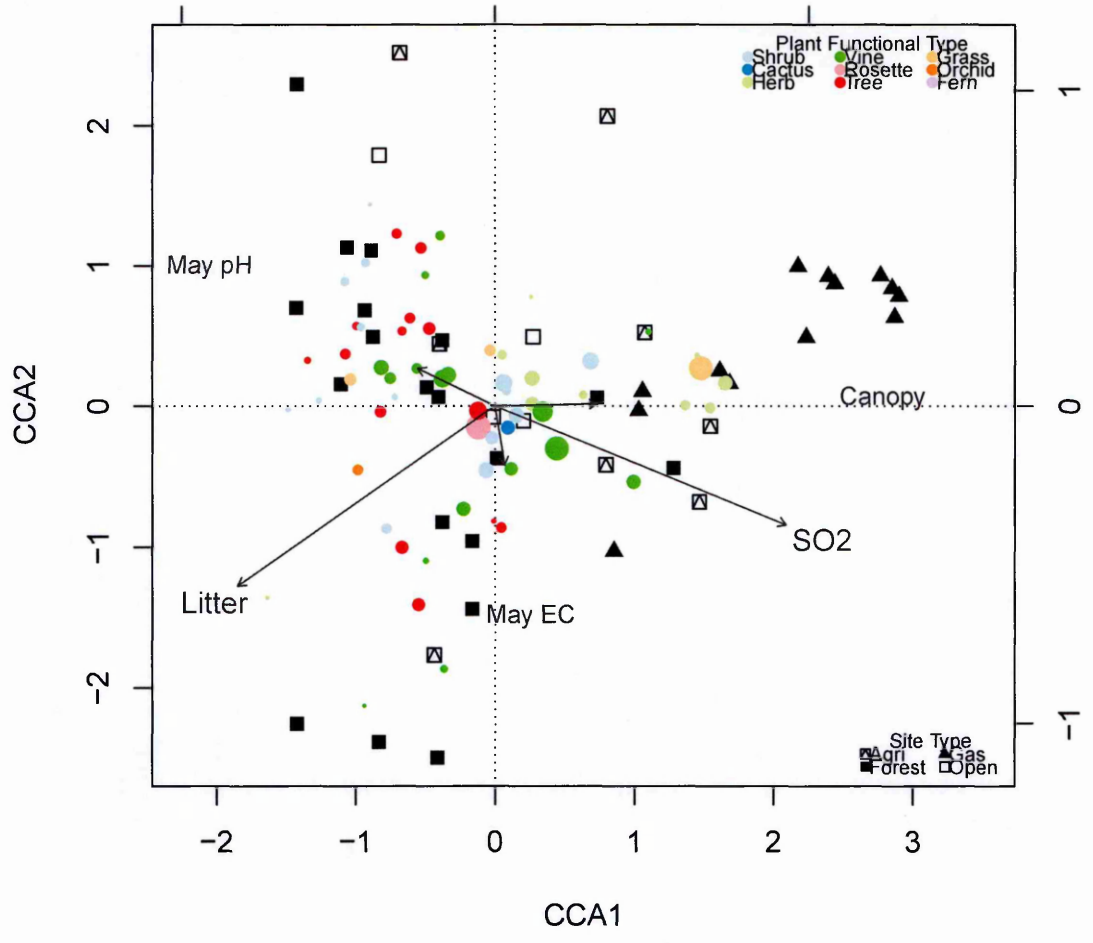

B.2.2.3 Height classification

Figure B.4: CCA for all species and sites using height data from May 2014. Sites have been classified by their type using symbols and plant species have been classified by their type using colour. The size of a plant species point is determined by its overall abundance along the transect, with points being used instead of text for less abundant species. Environmental data are displayed in grey.

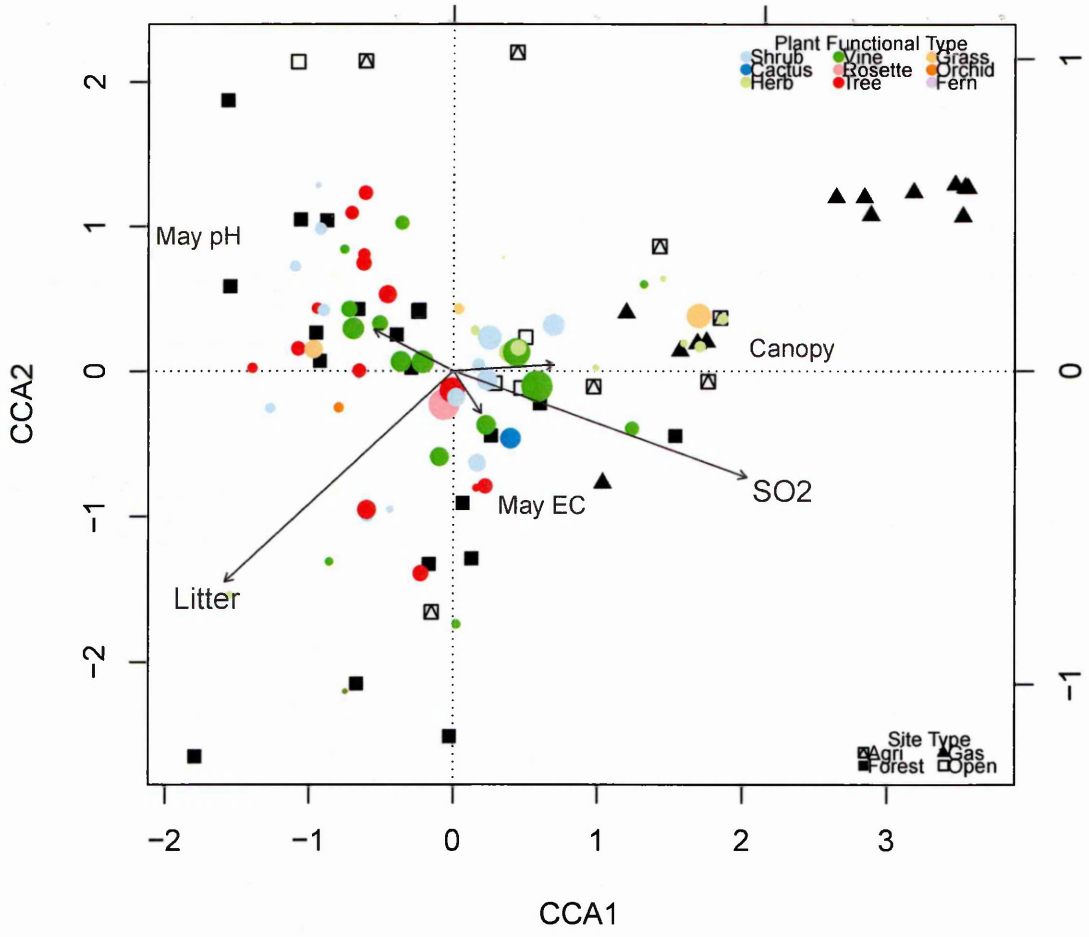

Appendix C

Dalechampia

C.1 *Dalechampia scandens*

Table C.1: Morphological measurements of *D. scandens* (mm) and environmental variables. SO_2 concentrations (at tree height) are measured in $\mu g\ m^{-3}$ and SO_2 deposition (at tree and ground height) is measured in $mg\ m^{-2}\ day^{-1}$. BD= Below the limit of detection.

Lat	Long	Site	Type	LD	LP	BD	BP	G	SL	SO_2	SO_2 tree	SO_2 ground	pH	EC
11.9969	-86.1512	Comalito	Upwind	8	30	9	11	2.7	3.3	BD	2	2	6.6	88
11.9861	-86.1356	Coyotes	Upwind	8	22	12	15	3.1	4.8	BD	2	2	5.6	194
11.9861	-86.1356	Coyotes	Upwind	8	25	16	19	2.9	5.0	BD	2	2	5.6	194
12.0111	-86.1739	Pencas 1	Upwind	17	19	17	19	3.4	5.3	BD	BD	BD	5.5	70
12.0094	-86.1728	Pencas 2	Upwind	12	43	9	12	4.1	4.1	BD	BD	BD	5.4	57
11.9738	-86.1777	4	Part	14	53	10	10	4.0	3.6	191	99	95	5.4	177
11.9751	-86.1799	8	Part	10	36	7	8	2.9	2.7	449	278	214	5.3	213
11.9751	-86.1799	8	Part	22	41	10	11	3.6	5.0	449	278	214	5.3	213
11.9751	-86.1799	8	Part	25	31	10	12	4.1	4.4	449	278	214	5.3	213
11.9751	-86.1799	8	Part	38	50	15	19	2.9	5.1	449	278	214	5.3	213
11.9753	-86.1802	9	Part	16	56	9	11	3.4	3.3	489	308	232	4.8	500
11.9753	-86.1802	9	Part	17	26	9	7	3.5	3.1	489	308	232	4.8	500
11.9753	-86.1802	9	Part	18	37	10	12	3.4	2.9	489	308	232	4.8	500
11.9756	-86.1804	11	Part	13	39	10	10	3.5	4.0	536	345	254	5.4	1824
11.9756	-86.1804	11	Part	17	44	10	12	3.6	4.1	536	345	254	5.4	1824
11.9756	-86.1804	11	Part	23	26	14	14	3.9	5.0	536	345	254	5.4	1824
11.9756	-86.1804	11	Part	36	63	14	17	4.0	4.7	536	345	254	5.4	1824
11.9797	-86.1678	Bat cave	Crater	13	42	12	12	3.0	3.8	614	616	616	4.5	158
11.9797	-86.1678	Bat cave	Crater	16	34	17	17	4.2	5.2	614	616	616	4.5	158
11.9797	-86.1678	Bat cave	Crater	19	43	10	12	2.7	3.2	614	616	616	4.5	158
11.9810	-86.1666	Entrance	Crater	16	34	16	19	4.0	5.1	614	616	616	4.5	158
11.9762	-86.1812	12	Gas	13	29	11	14	2.9	3.8	676	460	321	4.7	397

Continued on next page

Table C.1: Morphological measurements of *D. scandens* (mm) and environmental variables. SO_2 concentrations (at tree height) are measured in $\mu g\ m^{-3}$ and SO_2 deposition (at tree and ground height) is measured in mg m^{-2} day^{-1}. BD= Below the limit of detection.

Lat	Long	Site	Type	LD	LP	BD	BP	G	SL	SO_2	SO_2 tree	SO_2 ground	pH	EC
11.9762	-86.1812	12	Gas	14	38	13	17	3.5	4.6	676	460	321	4.7	397
11.9762	-86.1812	12	Gas	15	11	11	14	3.3	4.7	676	460	321	4.7	397
11.9777	-86.1831	19	Gas	41	44	12	11	3.4	3.7	991	756	485	4.1	325
11.9820	-86.1852	28	Gas	33	68	20	23	3.5	6.0	1016	899	607	4.3	260
11.9824	-86.1855	30	Gas	24	48	13	14	3.7	4.7	954	853	591	4.0	253
11.9824	-86.1855	30	Gas	29	40	14	15	4.0	5.1	954	853	591	4.0	253
11.9824	-86.1855	30	Gas	36	43	14	19	3.6	5.3	954	853	591	4.0	253
11.9833	-86.1860	31	Gas	39	62	13	13	3.6	4.4	820	744	545	4.1	576
11.9833	-86.1860	31	Gas	29	70	8	8	2.6	2.9	820	744	545	4.1	576
11.9833	-86.1860	31	Gas	45	48	12	7	2.9	4.5	820	744	545	4.1	576
11.9841	-86.1864	32	Gas	14	41	18	21	4.2	4.2	699	640	496	4.5	368
11.9841	-86.1864	32	Gas	25	52	13	12	3.5	4.4	699	640	496	4.5	368
11.9841	-86.1864	32	Gas	29	53	17	20	3.6	4.9	699	640	496	4.5	368
11.9844	-86.1872	33	Gas	15	42	18	21	3.8	4.9	604	555	453	4.8	329
11.9844	-86.1872	33	Gas	17	39	13	15	2.9	4.4	604	555	453	4.8	329
11.9844	-86.1872	33	Gas	21	56	8	6	3.1	3.1	604	555	453	4.8	329
11.9844	-86.1872	33	Gas	26	58	12	14	3.4	5.0	604	555	453	4.8	329
11.9844	-86.1872	33	Gas	29	70	15	15	3.8	5.0	604	555	453	4.8	329

C.2 *Byrsonima crassifolia*

Table C.2: Morphological measurements of *B. crassifolia* (mm) and estimated SO_2 concentrations ($\mu g\ m^{-3}$) and deposition rates ($mg\ m^{-2}\ day^{-1}$) for May and June (both at tree height). BD= Below the limit of detection.

Lat	Long	Site	Type	LL	LW	SFL	SL	FL	Tot	May SO_2 (C)	June SO_2(C)	May SO_2 (D)	June SO_2(D)
11.9841	-86.1864	32	Gas	87	42	100	72	28	6	304	358	135	236
11.9823	-86.1853	B64	Gas	71	35	82	50	32	5	420	307	212	195
11.9766	-86.1813	B81	Gas	74	38	98	66	32	9	331	52	132	18
11.9763	-86.1810	B82	Gas	76	36	70	47	23	6	302	43	114	14
11.9755	-86.1799	B83	Gas	93	40	77	56	21	4	219	24	69	6
11.9786	-86.1723	B63	Part	84	40	93	67	26	8	19	1	2	0
11.9882	-86.1920	B67	Part	83	47	60	36	23	7	33	195	5	97
11.9899	-86.1945	B69	Part	71	33	103	68	36	6	7	89	1	32
11.9887	-86.1926	B71	Part	77	39	65	37	27	5	23	164	3	76
11.9862	-86.1889	B93	Part	61	32	59	35	24	5	136	334	42	208
11.9885	-86.1849	B95	Part	80	41	68	44	24	6	102	308	28	185
11.9757	-86.1664	CE2	Part	67	34	94	57	37	6	0	0	0	0
12.0065	-86.1472	B59	Upwind	63	33	80	60	20	7	BD	BD	BD	BD
12.0120	-86.1451	B60	Upwind	68	35	76	58	17	7	BD	BD	BD	BD
11.9967	-86.1519	B84	Upwind	48	24	53	31	22	4	BD	BD	BD	BD
11.9972	-86.1515	B85	Upwind	59	33	59	49	9	8	BD	BD	BD	BD
11.9975	-86.1511	B86	Upwind	68	32	65	46	19	6	BD	BD	BD	BD
12.0014	-86.1573	B87	Upwind	78	45	42	27	15	6	BD	BD	BD	BD
12.0023	-86.1609	B88	Upwind	72	37	81	48	33	6	BD	BD	BD	2
12.0062	-86.1707	B89	Upwind	66	27	74	58	16	5	BD	BD	BD	2
12.0091	-86.1724	B90	Upwind	90	35	53	34	19	8	BD	BD	BD	2